Tissue Manipulation Using Nano-Particles Ferrofluids for Minimal Access Surgical Applications

YU-SHENG LIN

Submitted in accordance with the requirements for the degree of

Doctor of Philosophy

The University of Leeds
School of Mechanical Engineering

September, 2014

Acknowledgements

I would like to express my deepest gratitude to my Ph.D. supervisor, Professor Anne Neville for her constant support and guidance through my Ph.D. study. Her enthusiasm, the effort she put into the research and her patient all together make this thesis possible.

I am grateful to thank two second supervisors, Dr Rupesh Roshan and Dr Tomasz Liskiewicz, who had supported me in daily research and discussions. I also would like to thank all who had helped this work develop well: the great clinical support from Professor David Jayne, Adrian Hood and Jenifer Barrie on the in-vivo study; the great technical support from Dr Peter Culmer and Dr Ali Alazmani in designing the ex-vivo experimental setup using LabVIEW; the technical support from Dr Nagitha Wijayathunga in characterising the particle migration using micro-CT scanner; the great support from Dr Yi-Fan Chou in processing images using Matlab. In addition, I would like to thank my two examiners, Professor Peter Brett and Dr Mark Wilson for the advices to make this thesis become better.

I am indebted to the secretaries and technicians in the Mechanical Engineering Department in the University of Leeds for the assistant and helping the experimental work: Jacqueline Kidd, Fiona Slade, Ron Cellier, Ted Allwood, Graham Blyth, Graham Jakeman, Brian Leach, Mark Batchelor, Antony Wiese and Jane Tillotson.

Besides, I want to thank the colleagues of the Surgical Technology (ST) group, the Institute of Functional Surfaces (iFS) and the former Institute of Engineering Thermofluids, Surfaces and Interfaces (iETSI), in particular, Abinesh Gnanavelu, Alfonso Lopez, Ashley Bell, Ashley Stratton-Powell, Hongyuan Zhao, James Chalder, Joe Lanigan, Karen Mitchell, Laura Sanders, Liuquan Yang, Louise Hunter, Michal Ciolkowski, Nicholas Raske, Wendy Cheong, William Mayfield, Yugal Rai, Yong Hua, Zahra Ehteshami.

Yu-Sheng Lin 25.02.2015

首先我要把完成這份論文的感動送給我的家人: 一直支持著和鼓勵我的父母 妙美和瑛敏, 因為你們的栽培, 讓我能有勇氣和毅力完成這個研究. 另外在學術和生活中不斷地引領著且啟發著我的姐姐 鈺維和哥哥 育宣, 已經在天國的奶奶 林趙菊江, 還有陪伴著我唸書且照顧飲食和健康的女友 玉萍. 謝謝你們.

另外我要感謝一起在英國奮鬥過的朋友們, Tom, 鎮遠和 Iris 夫婦, 逸凡和逸凡媽媽, 安頎 Angy, 大威 David, 國峰, 瓏文, Peppy, 任賢 Lucas, Michelle, 惠瑜 Elsa, 惠芳 Helen, Peter, 政閔和 Anna 夫婦, 庭緯, 懿恬, 逸帆, 淑薰, 啟瑞和毛寶一家人, 敏禎, Vanessa, 芊霓, 肇君, Rachel, Evonne 以及許多來不及列在裡面的朋友們, 謝謝你們.

還有要感謝的是遠在台灣持續給我鼓勵的朋友師長們, 謝謝你們.

林育昇 25.02.2015

Abstract

Nano-scale Iron-Oxide ferrofluids exhibit a special property, ‘superparamagnetism’, that induces an attractive force toward an external magnetic field. The aim of this project is to investigate the use of ferrofluids for tissue retraction during Minimally Access Surgery (MAS). In the in-vivo porcine experiments, 0.3 ml of ferrofluid (200 mg/ml concentration) containing 10 nm particles is injected subserosally into the small bowel, respectively. A 0.6 T magnetic field is created using a combination of 10 mm and 20 mm diameter Neodymium Iron Boron magnets. The vertical retraction distance is measured up to 80 mm and video-recorded. The results demonstrate the capacity of ferrofluid to facilitate the tissue manipulation and analysis of the migration of the particles within the tissue using micro computed tomography (CT). A theoretical model developed to validate the experimental results is also beneficial for predicting retraction force. In conclusion, this feasibility study provides a protocol for systematically using small volumes of ferrofluid, without the need to mechanically grasp the tissue.

Contents

Nomenclature

F_g	Grip force	N
F_t	Pinch force	N
F_h	A force is associated with the movement of the hand	N
F_O	A force exerted on tissue by the movement of the tip generates	N
F_{pullh}	A pull force is generated when surgeons pull the handle away	N
F_{pullO}	Associated pull force on tissue	N
k	Spring constant	$N \cdot m^{-1}$
ΔX	Displacement	m
T	Tesla	Tesla
R	Resistor	Ω
p.d.	Potential difference	V
μ_0	Permeability of air	$H \cdot m^{-1}$
r	Distance of any points in the free space to the centre of the magnet surface	m
$\overrightarrow{\hat{\imath}, \hat{\jmath}, \hat{k}, \mathrm{r}}$	Unit vectors	---
I	Current	A
R	Radius of magnet surface	m
∅	Angle of the projectile vector and radius	degree
H	Magnetic field density	T
H_c	Coercivity	$A \cdot m^{-1}$
μ_r	Relative magnetic permeability	---
F	Magnetic force	$kg \cdot m \cdot s^{-2}$ or N
ΔX	Difference of magnetic susceptibility	Dimensionless

μ_0	Permeability of air	$\mathrm{Wb} \cdot (\mathrm{A} \cdot \mathrm{m})^{-1}$
V_t	Total volume of particles	m^3
B	Magnetic field density	$\mathrm{Wb} \cdot (m^2)^{-1}$ or T
$\nabla \cdot$B	Magnetic field density gradient	$\mathrm{Wb} \cdot (m^3)^{-1}$ or $\mathrm{T} \cdot \mathrm{m}^{-1}$
F	Preload force	N
a	Radius of the cylinder	m
E	Young's modulus	kPa
d	Indentation depth	m

Abbreviation

MAS	Minimal Access Surgery
MIS	Minimally Invasive Surgery
LESS	Laparo-Endoscopic Single-Site Surgery
NOTES	Natural Orifice Transluminal Endoscopic Surgery
UK	United Kingdom
2D	Two-Dimensional
3D	Three-Dimensional
CT	Computed Tomography
CCD	Charge-Coupled Device
FF	Ferrofluid
MRI	Magnetic Resonance Imaging
FEM	Finite Element Method
MAGS	Magnetic Anchoring and Guidance System
EMR	Endoscopic Mucosal Resection
ESD	Endoscopic Submucosal Dissection
SFA	Surface Force Apparatus
AFM	Atomic Force Microscope
MT	Magnetic Tweezers
DNA	Deoxyribonucleic Acid
RNA	Ribonucleic Acid
MUST^{TM}	Modular Universal Surface Tester

DLS	Dynamic Light Scatter
MagRAT	Magnetic Retraction and Adhesion Tissue tester
NeFeB	Neodymium Iron Boron
p.d.	potential difference
PBS	Phosphate Buffered Saline
TEM	Transmission Electron Microscopy
SEM	Scanning Electron Microscopy
S/N	Signal-to-Noise
FEMM	Finite Element Method Magnetics
CAD	Computer-Aided Design

Figures

Tables

Chapter 1 Introduction

This research studies the feasibility of using nano-particle ferrofluid to retract tissue, by taking advantage of magnetic attraction. The contributions made from an engineering perspective are as follows: first, a protocol for testing magnetic retraction using ferrofluids is established, secondly important parameters in the study are optimised, and thirdly, a mechanical design of magnetic configuration is developed. The scientific contributions made include a simple model to predict the magnetic retraction and a characterisation of particle migration within tissue using micro-Computed Tomography (CT). The outcome brought to the clinic is the feasibility of using nano-particle ferrofluid to provide the force required to retract tissue.

This chapter introduces the background of Minimal Access Surgery (MAS). It is going to address the general procedure and equipment, and indicate the challenges due to such a confined working area and tissue manipulation is one of these issues. The importance of this topic is because tissue manipulation is always the first action done with tissue. Therefore, it is soon narrowed down the interest to a problem and aims to test a promising method to facilitate effective tissue manipulation. This chapter is organised as follows. Section 1 introduces the background of MAS. Section 2 illustrates the aims and objectives in this study. Section 3 briefly outlines every chapter.

1.1 Background

MAS is a promising surgical procedure and has been widely used in abdominal surgery. MAS has several significant advantages, such as less incisions size, rapid

patient recovery, reduction of medical care cost and blood loss. Moreover, MAS minimises the percutaneous trauma to the body resulting in less scars on the skin. Hence, MAS improves cosmetic results. The postoperative pain, wound, ileus, and badly abdominal adhesion formation are decreased. (Brown and Irving, 1995, Cuschieri, 1999, Cuschieri and Berci, 1990, Najmaldin and Guillou, 1998).

In brief, open surgery is generally performed via a large incision which allows surgeons to directly access the abdominal cavity, as shown in Figure 1.1 (Right) (Trief and Olk, 2013). This method enables surgeons to manipulate tissue with their hands easily, but patients usually suffer from intense pain and face higher risks of infection after the operation. Recovery time are long and hence healthcare costs are large. MAS on the contrary reduces such pain and risks as it is performed via several short incisions on the belly (about 5 – 15 mm long) to approach tissue for different surgical procedures, as shown in Figure 1.1 (Left). Surgical instruments are inserted through these incisions using an extended shaft and controlled by surgeons outside the abdomen.

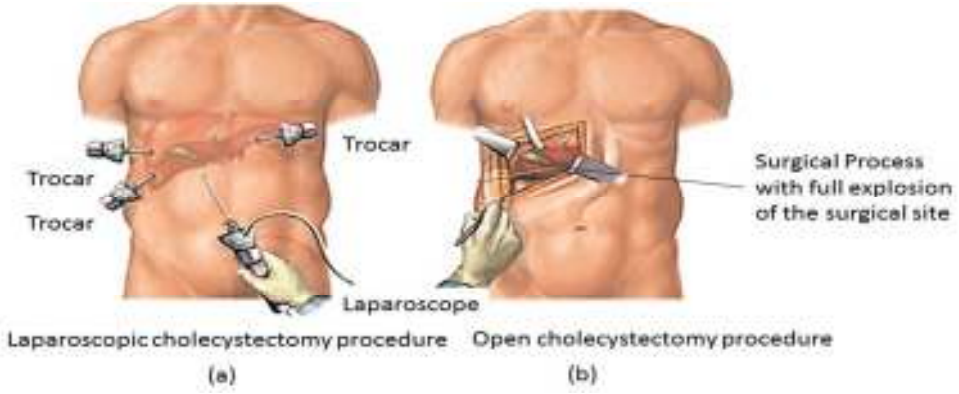

Figure 1.1 Two schematic diagrams showing the differences between (a) the laparoscopic cholecystectomic surgery with three trocars and one laparoscope inserted into the body accessing through small incisions (b) the conventional cholecystectomic surgery with a large incision where organs and tissue are exposed clearly (Trief and Olk, 2013).

Often MAS is also referred to as “Minimally Invasive Surgery” (MIS), which reflects the benefit of the procedure, which lowers the level of invasion to human bodies with an aim to reach various organs and tissue still. Therefore, MAS becomes a popular surgical procedure and gradually replaces the use of open surgery. The history of MAS can be traced back to the civilization in Mesopotamia and ancient Greece (Brown and Irving, 1995). The initial idea was to deliver medicine using a tube and speculum. Afterwards, multi-disciplinary efforts have been invested to improve the efficiency and effect of the procedure and performance. For example, the fibrescope, also known as “cold light system”, was invented to replace previous light source using the concept of transmitting optical images from outside into the cavity by the effect of total internal reflection (Hopkins and Kapany, 1954). The optical fibre of the fibrescope keeps the flexibility of movement and feature of tube can be inserted to improve the light and combined with microscope to explore the abdominal cavity during the surgery (Brown and Irving, 1995, Najmaldin and Guillou, 1998, Aoyama et al., 1996).

In addition to the improvement of operative procedure, CO_2 insufflation was found to be used in the intraoperative endoscopy. It was discovered that CO_2 is more soluble than room air in blood and tissue and can be absorbed to be released by the lungs (Bretthauer et al., 2005, Church and Delaney, 2003, Bretthauer et al., 2003, Bretthauer et al., 2007). This finding solves the problem that most patients feel discomfort while passing the air within the bowel (Ramaraj et al., 2011). Nowadays, the development of Laparo-Endoscopic Single-Site Surgery (LESS) aims to improve the cosmetic results by reducing the numbers of scars.

Moreover, the feasibility of replacing any artificial incision to the natural orifice, called Natural Orifice Transluminal Endoscopic Surgery (NOTES), is under

the investigation (AUSTIN, 2009, Kalloo et al., 2004, McGee et al., 2006, Merrifield et al., 2006, Pai et al., 2006, Pearl and Ponsky, 2007, Shaikh and Thompson, 2010b, Sumiyama et al., 2006, Wagh et al., 2006, Galvao Neto et al., 2009).

Generally speaking, the procedure of the laparoscopic surgery starts with insufflation via an incision made on the abdomen. The insufflator would pump CO_2 into the abdominal cavity to lift up the abdomen in order to provide enough operating space. To create incisions, a long veress needle is stabbed at the abdomen for creating sufficient accessing ports. Immediately after the incisions, trocars are mounted to hold the ports to form accessing paths for the laparoscope and other instruments so that they can be inserted through them without slipping from the abdomen. The trocar therefore works as a sealed valve allowing surgical tools to enter the body.

Various surgical tools are then inserted including a tube camera connecting to the visual system to show the vision inside the abdomen on screen (Cuschieri and Berci, 1990). During laparoscopic surgery, surgeons basically rely on this vision to conduct their operation (see Figure 1.2 (Left)). Other surgical tools used for operative functions, such as forceps, scissors, scalpel blades and retractors have all been re-developed from existing surgical devices used for the open surgery (Cuschieri, 1999). These modified instruments are attached to long and thin sticks in order to be inserted through accessing ports (5-15 mm long) so that surgeons can hold them from outside the abdomen. The shaft has been in place of surgeon's hands (see Figure 1.2 (right)). In a nutshell, surgeons work on the laparoscopic procedure without directly looking at the tissue or touching them with bare hands. The information provided on the screen is indirect.

Figure 1.2 A laparoscopic surgical equipment (a) a surgeon holds a laparoscope with a camera inside the abdomen and monitors the screen during the operation. (b) The long, thin and rigid instruments are used for accessing the abdominal cavity (Galvao Neto et al., 2009).

Over the last twenty years, MAS has been widely used for abdominal surgery. Laparoscopic surgery is the most well-known branch of MAS (Brown and Irving, 1995, Cuschieri, 1999, Cuschieri and Berci, 1990, Najmaldin and Guillou, 1998). In addition to robotic surgery which has been under development (Rentschler et al., 2007, Rentschler et al., 2006, Taylor and Jayne, 2007). MAS has gained rapid popularity as surgical area covers almost all the organs (Comarow, 2002). According to the National Bowel Cancer Audit Annual Report 2013 (p.27), the percentage of laparoscopic surgery used for bowel cancer treatment in the United Kingdom (UK) increased from 25% to 40% between 2008 and 2012 (Figure 1.3) (The Health and Social Care Information Centre, 2012, 2013).

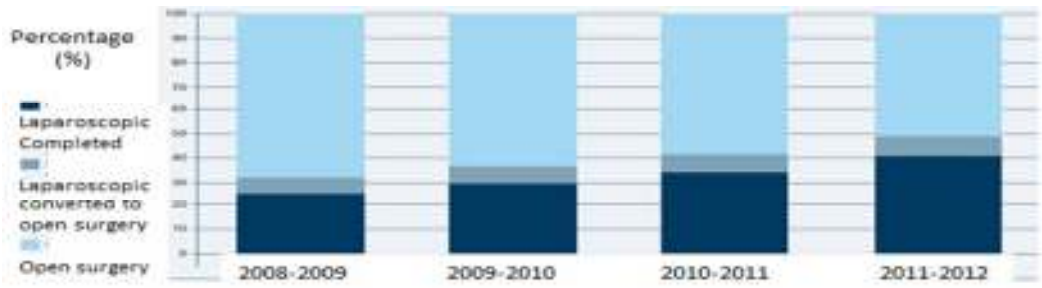

Figure 1.3 The statistics of the percentage of laparoscopic surgery for the bowel cancer treatment during 2008-2012 (The Health and Social Care Information Centre, 2012, 2013).

The number of laparoscopic surgery cases conducted is increased not only in the UK, but also globally. Between 1998 and 2009, the percentage of distal pancreatecomies performed by MAS approaches increased from 2.4% to 7.3% (Tran Cao et al., 2014). The percentage of laparoscopic surgery used for cholecystotomy in Taiwan was 60% in 2005 and increased to 63% in 2007 based on the investigation of the Bureau of National Health Insurance in Taiwan (Lien et al., 2013). Some other earlier reports also show a similar trend of using laparoscopic surgery (Nguyen et al., 2005). This can be observed from the growth of the abdominal surgical instruments market - according to the market research report provided from the organisation "MarketsandMarkets" (Novel Instruments For Minimally Invasive Techniques, 2010), the number of MAS has grown at a 10% annual rate since 2010 whilst the non-MAS only grew 3-5% annually.

Several advantages have contributed to the growing popularity of MAS. For example, MAS minimises the percutaneous trauma to the body, decreases the amount of blood loss and leaves less scars on the skin. In addition to the improvement of the cosmetic results, MAS also relieves the postoperative pain, wound, ileus, and badly abdominal adhesion formation. Since surgeons are not necessarily in direct contact with blood and body fluid, MAS also avoids infection of viral diseases and contamination. Moreover, the less damage done on the body, the quicker the patient would recover. As a result, medical care costs have been reduced (Cuschieri, 1999).

MAS is beneficial to both patients and the medical care systems, therefore it gradually replaces the traditional abdominal surgery, such as cholecystectomy, sympathectomy, cardiomyotomy and antireflux surgery (Cuschieri, 1999). However, there are three major challenges associated with the development of this technique

(Caron, 2012, Philosophe, 2003, Lam et al., 2009). Firstly, the two-dimensional vision makes it difficult for judging the depth of the surgical area and adjusting the depth perception and spatial orientation (Horgan and Vanuno, 2004). Secondly, the lack of the direct haptic feedback whilst using conventional tissue manipulation tools is speculated to be the reason causes involuntary traumas on tissue (Taylor and Jayne, 2007, Culmer et al., 2012). Thirdly, the confined surgical space limits the range of movement of the long-shafted laparoscopic instruments used during a MAS procedure (Mintz et al., 2008).

These challenges lead to the following pitfalls, including an unstable video platform and static two-dimensional (2D) images (Ballantyne, 2002). During the procedure, sometimes the camera would be rotated away from the horizon of the camera holder. The 2D video and the lack of the haptic feedback make it difficult to perceive the depth of the working area (Horgan and Vanuno, 2004). The bad visual information received means potential injury to the vessels and viscera during primary cannula insertion and diathermy burns.

The absence of direct hand manipulation and tactile feedback may also cause damages by accidental tear during grasping tissue (de Visser, 2003a, Alaswad, 2013, Bishoff et al., 1999b, Deziel et al., 1993, Puangmali et al., 2008). De et al. (2007, 2006) presented the consequences of different stresses applied by the multiple compressions during grasping, as shown in Figure 1.4. Such tissue damage has been highlighted as the most serious forms of lesions (Vonck, 2013a) which potentially causes morbidity and mortality in tissue sessions (van der Voort et al., 2004). Besides, the long and straight laparoscopic instruments are limited in their shapes and their motion is constrained by the fixatioin enforced by the abdominal wall trocars and the low level of freedom of the mechanism (Cuschieri, 1999). It is

necessary to avoid placing multiple instruments too close in the operative field as collision of different tools in the patient's abdomen may incur due to the insufficient room for the movement of grasper or sissors jaws, as shown in Figure 1.5 (Najmaldin and Guillou, 1998).

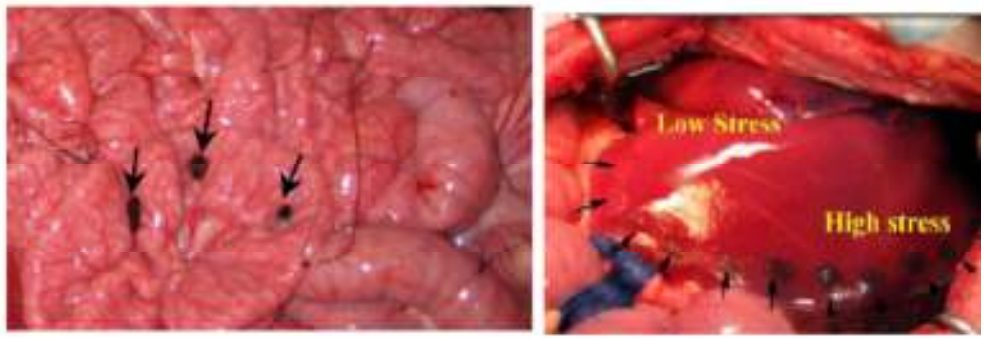

Figure 1.4 The accidental damage caused by an inappropriate stress during grasping bowels (pointed out by the arrows). The graspings resulted from different of stress levels are presented (De et al., 2007).

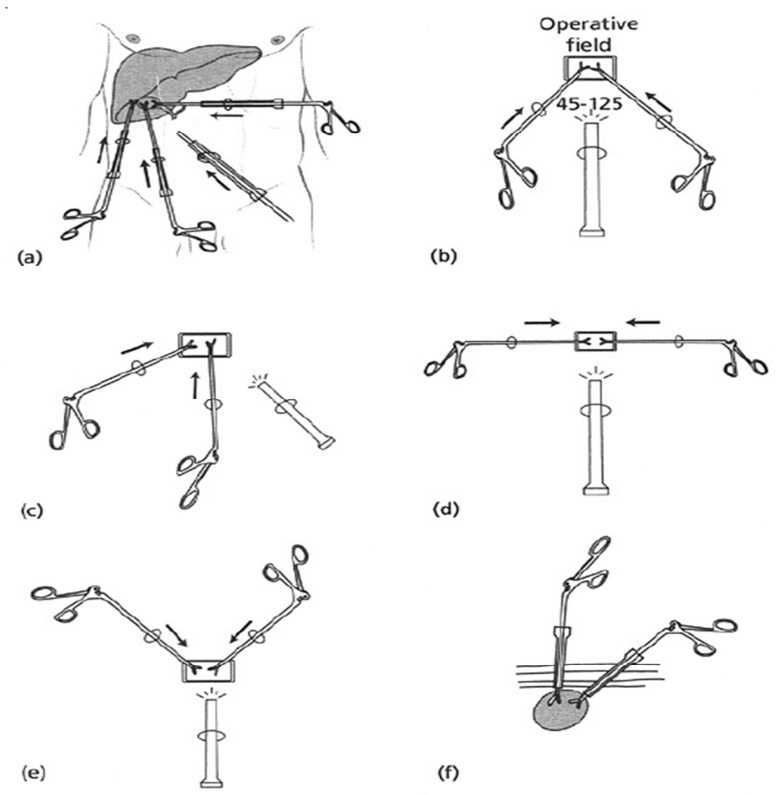

Figure 1.5 The management of the position when a second or multiple instruments are inserted in order to keep enough space for ensuring the flexibility of surgical work (Najmaldin and Guillou, 1998).

The challenge posed by the constrained space is much clearer in other MAS procedures such as single-site surgery. Single-site surgery has to accommodate multiple equipments all at the same time through the same accessing port so the procedure becomes much more complicated (McGee et al., 2006). The design of the instruments has to work around the constraints of the operating area during a normal operation (Galvao Neto et al., 2009). The dimension of the instruments has to be minimised and the functions are combined together, see Figure 1.6 (Shaikh and Thompson, 2010b). The same situation can be observed in robotic surgery, the need for reducing the sizes of surgical equipments presents a technical challenge (Taylor and Jayne, 2007). It is also economically challenging because the development and maintenance costs are expensive (Hashizume and Tsugawa, 2004). Therefore, there is an urgent need for finding out cheaper and more efficient ways of conducting MAS. And it is in this sense that this research project contributes to the field.

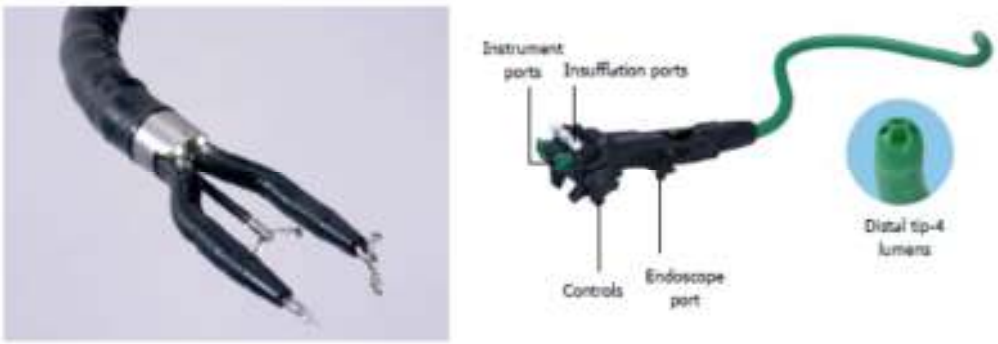

Figure 1.6 The latest development of an articulating instrument for the single-port surgery (Shaikh and Thompson, 2010b).

These challenges in carrying out MAS are currently being overcome by providing appropriate training to surgeons. The more skilled and experienced the surgeon, the better the performance they can have with the instruments (Vonck, 2013b). However, not every surgeon is that skilled and experienced. This presents another disadvantage of a laparoscopic procedure, which requires a higher level

technical expertise and longer training in order to manoeuvre the MAS surgical instruments (Yamauchi et al., 2002).

In order to shorten the training period and to assist surgeons to work confidently and easily, the instruments have been under rapid development from different aspects. For example, imaging techniques such as computed tomography (CT) and magnetic resonance imaging (MRI) systems, are important developments for surgeons to manoeuvre from outside the abdomen without any need of invasion (Cuschieri, 1999). Such X-Ray and MRI are well-established methods in diagnostics and biopsies using radioactivity and magnetic interaction to navigate the operative field and target organ (Kaiser et al., 2011). Besides, surgical robots are currently under the development to assist operations (Diodato Jr et al., 2004, Hashizume and Tsugawa, 2004). Robotic surgery can provide the real time images and manipulate tissue for biopsy (Rentschler et al., 2006). The systems are manipulated from outside the body and have the advantages of precision, miniaturisation and smaller incisions to decrease blood loss (Estey, 2009). However, there is often a challenge is that the robotic arm which often long and bulky in order to allow flexible range of motions and load multiple instruments. The articulating segment technology is currently being invented to manipulate tissue and also accommodated laparoscopic instruments with more flexibility in movements (Dhumane et al., 2011, Puangmali et al., 2008), as shown in Figure 1.6.

Tissue manipulation has been considered an important part of MAS procedure as it is always the first thing to do after approaching intra abdomen. The conventional tools for tissue manipulation use grasping forceps, which applies a mechanical pinch force from a grip action onto the object. The shape of a grasp

forceps normally looks like a jaw attached onto the tip of a long shaft, as shown in Figure 1.7 (Najmaldin and Guillou, 1998).

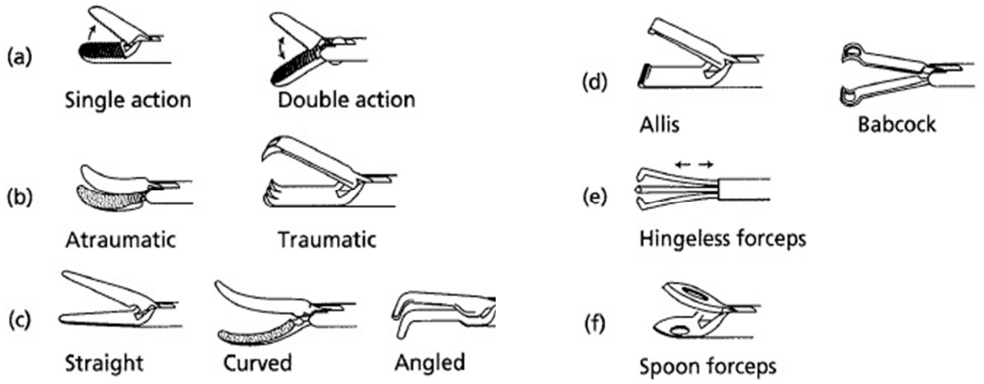

Figure 1.7 The conventional jaws of a grasping forceps (Najmaldin and Guillou, 1998) which provides a mechanical force to lift up tissue when it clips on them.

However, the contact of the pinch force provided by the jaws has been found to relate the accidental damages to tissue due to the lack of haptic feedback (de Visser, 2003a, Alaswad, 2013, Bishoff et al., 1999b, Deziel et al., 1993, De et al., 2007, De et al., 2006). Recently, some alternative instruments have been developed in order to replace the conventional jaws by retraction, using novel methods such as vacuum pressure (Vonck, 2013b, Vonck et al., 2010, Vonck et al., 2011, Vonck et al., 2012) or magnetic retraction (Best et al., 2011, Best and Cadeddu, 2010, Cadeddu et al., 2009, Dominguez et al., 2009, Kume et al., 2008a, Kume et al., 2008b, Cantillon et al., 2013, Park et al., 2007, Raman et al., 2009, Ryou and Thompson, 2009, Schlager et al., 2010, Scott et al., 2007, Shaikh and Thompson, 2010a, Uematsu et al., 2010, Wang et al., 2010b, Wang et al., 2012, Wang et al., 2009, Wang et al., 2008, Zeltser et al., 2007, Zeltser and Cadeddu, 2008, Tortora et al., 2013). These methods will be discussed in a great detail in the next chapter about how these instruments to manipulate tissue.

1.2 Aims and Objectives

The aim of the work presented in this thesis is to investigate the feasibility of using nano-scale ferrofluids, a state-of-the-art magneto-rheological fluid in medical applications, to facilitate tissue manipulation. The literature review, in Chapter 2, introduces some alternative methods for tissue manipulation. These unconventional methods, different from the traditional pinch force, show the potential of magnet-powered devices for tissue manipulation. However promising, such a method is still in its infancy stage and needs more research to explore how it can work with different materials and where it can be applied to.

Overall, this study explores how ferrofluids interact with different physical properties and how they behave in different environments. A systematic procedure is established through the ex-vivo tests, in-vivo tests, particle characterisation and theoretical model. By the end, the database established from the quantitative study can become a protocol for this field.

The objectives of this study are:

- To conduct a parametric study of the ferrofluids in terms of the performance of retraction and adhesion force
- To optimise the retraction and adhesion force and find an appropriate ferrofluid for surgical use
- To identify the mobility of ferrofluids within a tissue and the co-relationship of adhesion force
- To demonstrate the feasibility of ferrofluids for tissue manipulation in the in-vivo experiment
- To analyse the interaction force from a theoretical perspective

- To suggest a specific surgical protocol that may use these fluids in laparoscopic surgery procedure

1.3 Overview of the Thesis

Chapter 1

Chapter 1 introduces the background of MAS and outlines the motivation behind and aims and objectives of this research project, which experimented and tested the feasibility of using nano-scale particles suspended in a ferrofluid to retract tissue during the process of tissue manipulation, taking advantage of magnetic applications. It talks about why the entire project studies the feasibility of a general MAS procedure and medical equipment used, then identifies the challenges found in practice, such as a confined working area during a surgery and tissue manipulation.

Chapter 2

Chapter 2 reviews the current applications in the field of MAS in particular the methods used for tissue manipulation, including conventional graspers, articulating segment technology and magnetic retraction. This review helps to grasp the state of the art of all the relevant instruments and demonstrate the relevance of this research project to the cutting edge development.

Chapter 3

Chapter 3 reviews the literature of the experimental setup and the protocol to measure different types of adhesion. This chapter also introduces the method applied in this study.

Chapter 4

Chapter 4 introduces the experimental setup in this study during both the ex-vivo and in-vivo procedures. The experimental conditions are also introduced in terms of the parametric studies.

Chapter 5

Chapter 5 presents the results of the retraction and adhesion force measurements from the ex-vivo experiments. The parametric study can suggest the suitable condition of ferrofluids to manipulate tissue demonstrating ex-vivo and in-vivo.

Chapter 6

Chapter 6 presents the characterisation of ferrofluids particles in terms of their abilities of displaying density distribution within an injected volume. The characterisation is conducted using the micro CT scanner.

Chapter 7

Chapter 7 presents a theoretical analysis from the magnetic interaction aspect. The magnetic interaction causes the primary retraction and adhesion force. The theoretical model in this study is based on magnetostatic equation and solved by Finite Element Method (FEM). This model not only verifies the experimental results but also can be used to predict the performance of FFs for tissue manipulation based on the studied parameters.

Chapter 8

Chapter 8 discusses the findings, the limitations of the study and the potential in tissue retraction.

Chapter 9

In this concluding chapter, the entire study is reviewed as a protocol of using ferrofluids in manipulating tissue. It is also suggested some recommendations for the future work in this field.

Chapter 2 Literature Review of Techniques Used for Tissue Manipulation

One of the principal challenges in MAS, as already addressed in Chapter 1, is operating surgical instruments in a confined environment during a complicated procedure. Several tasks are normally involved during a MAS operation; laparoscopic surgeons need to grasp, handle and manipulate soft tissue or organs by means of so called grasping forceps. The performance of surgeons using grasping forceps is called “safe grip” (de Visser, 2003b, Kemner, 1999), an action of which surgeons apply a sufficient force to manipulate tissue. During the action, surgeons need to prevent inadvertent damage caused by the act of grasping. A risk of instrument collision may occur when multiple instruments are applied simultaneously (Najmaldin and Guillou, 1998). In turn, training for surgeons who use MAS approaches becomes complicated and difficult (Yamauchi et al., 2002). Nowadays, there is a converging trend of including different methods as a means of manipulating tissue to improve a MAS training procedure (Cuschieri and Berci, 1990).

This chapter reviews the techniques used for tissue manipulation, including conventional grasping forceps and cutting-edge tools currently under development for MAS, such as magnetics, vacuum pressure and a specific procedures of tissue retraction. It is organised as follows. Section 1 introduces the conventional graspers for open surgery and MAS. Section 2 introduces the developing tools used in tissue manipulation. Section 3 summarises all methods mentioned in Chapter 2.

2.1 Conventional Graspers for Open Surgery and MAS

The history of grasping forceps development in MAS has been fairly recent. It is helpful to introduce the tool used in open surgery first before arriving at the more recent development of the MAS tools because many of these modern MAS tools are modified, improved and transformed from the concepts and designs of conventional tools normally used in open surgery.

There are lots of different designs of grasping forceps. Not all can be introduced here. Figure 2.1 (Fine Science Tools GmbH, 2014) shows some classical conventional grasping forceps used in open surgery, including teeth forceps, smooth forceps, Allis forceps and a modified Hemostatic forceps called Kocher forceps. It can be seen in the figure that grasping forceps normally consist of two lines of tines to hold tissue or organs together. In addition, grasping forceps have either teeth or smoothly serrated on the tips to prevent tissue from slipping (Wéber et al., 2008).

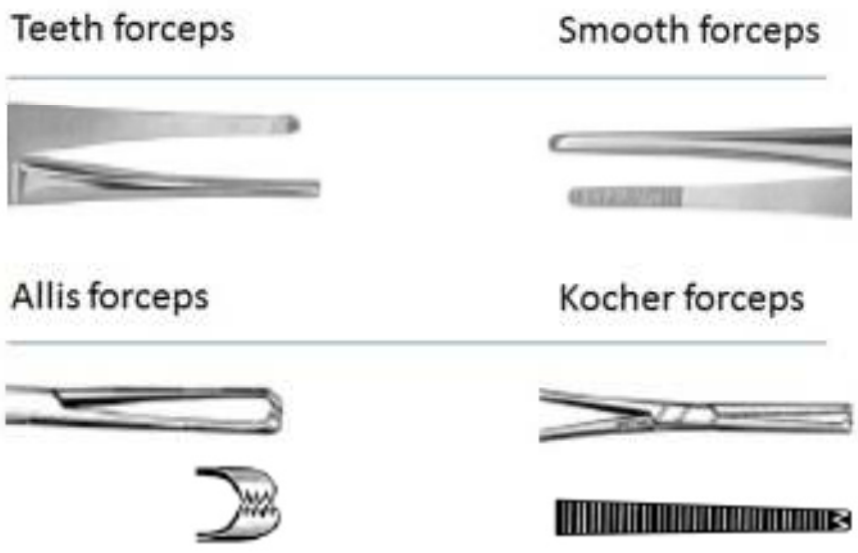

Figure 2.1 Figures of different classical conventional forceps, including enlarged pictures of tips (Wéber et al., 2008, Fine Science Tools GmbH, 2014). Grasping involves applying a pinch force on both sides of the tissue then combines a pull force in order to lift the tissue up (de Visser, 2003b).

Figure 2.2 shows an experimental set-up to evaluate the compression of tissue under different pinch forces (Heijnsdijk, 2004). This schematic force diagram also shows that a pinch force is applied by pressing the tines and a pull force is replaced by a spring effect. Forceps should be held like a pencil and they grip when compressed between thumb and index finger (Boros et al., 2006). The pinch force can be adjusted by pressing at different positions along the tines to transform the compression on the tip of the teeth.

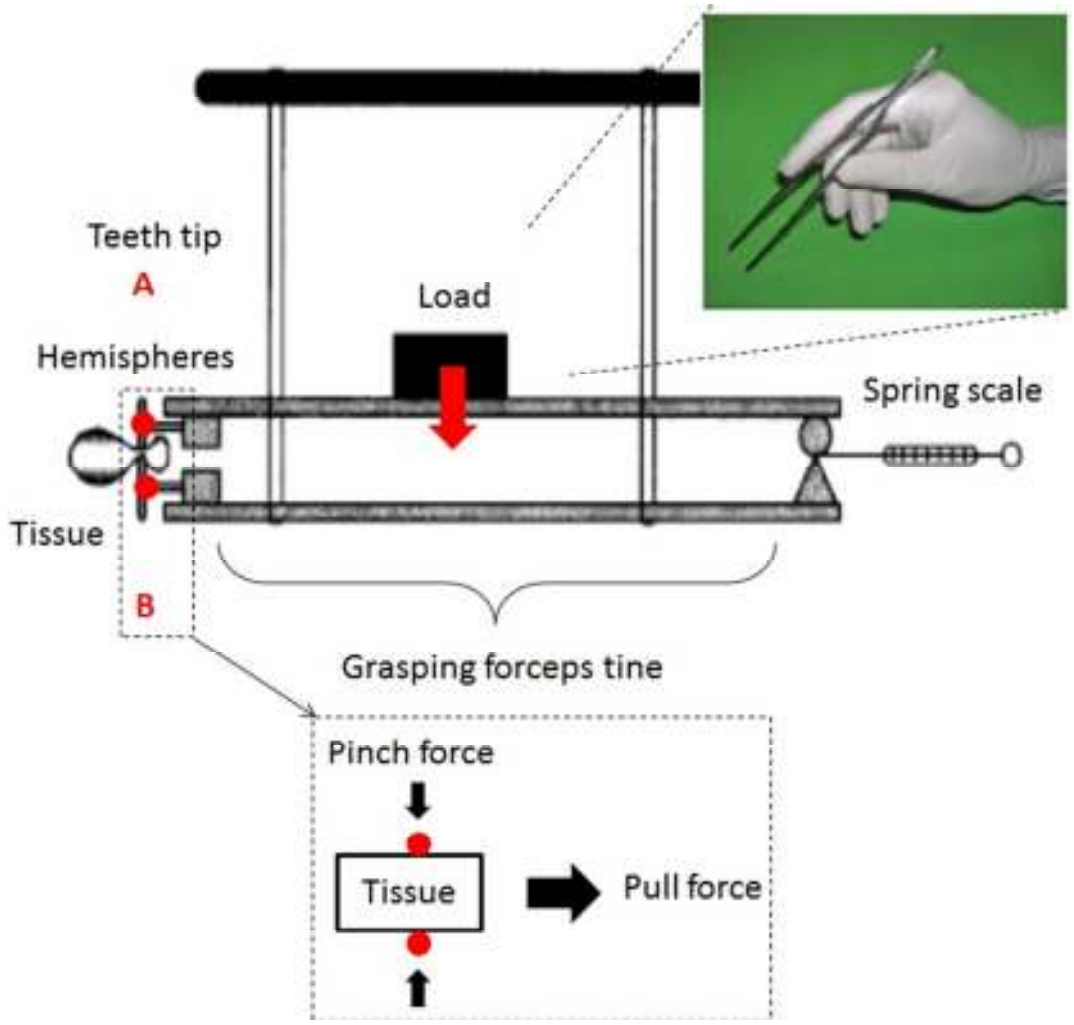

Figure 2.2 A schematic diagram showing pinch forces and pull forces for tissue manipulation in laparoscopic grasping forceps (Heijnsdijk, 2004).

The difference between the grasping forceps for traditional open surgery and those for MAS is principally a modified handle with a long, thin and rigid shaft

which allows the forceps to be manoeuvred through incisions that are no more than 5 mm large, as shown in Figure 2.3 (Lobe, 2003). The instrument comprises a handle and a shaft, which are both available with various tips and can be reusable or disposable.

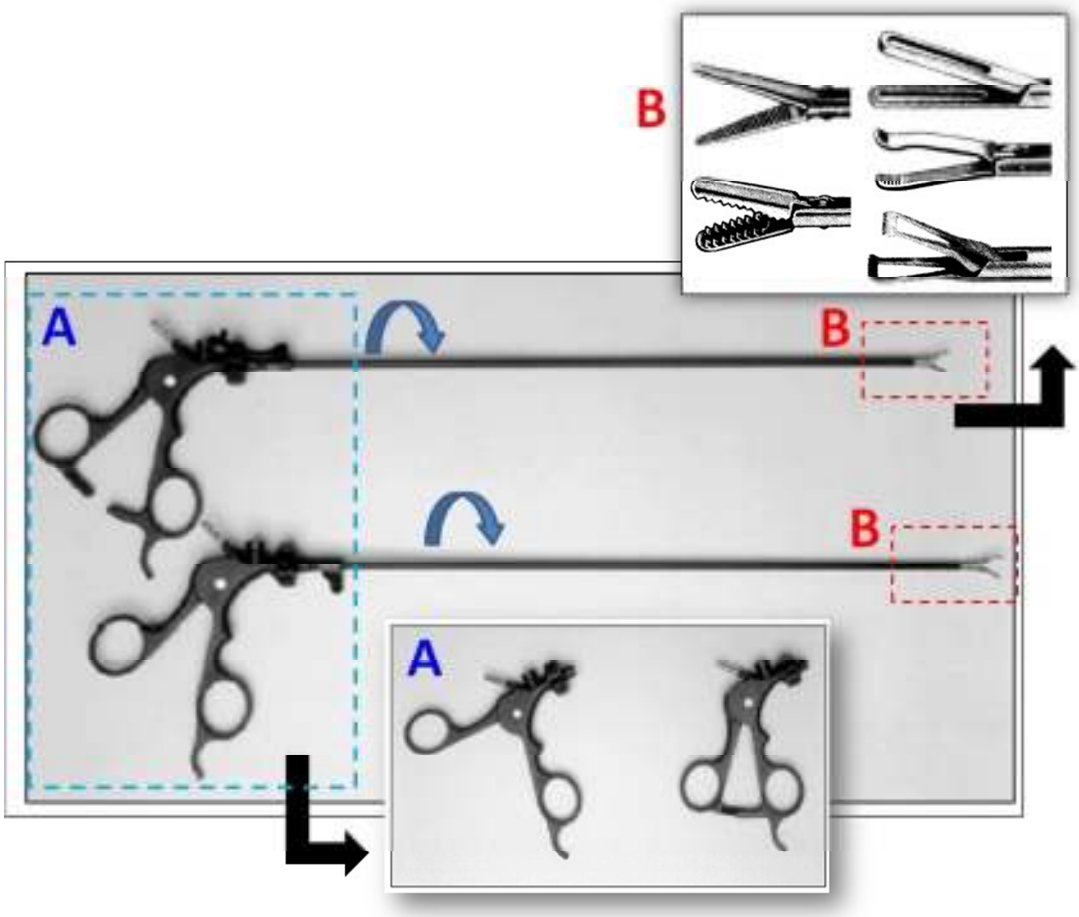

Figure 2.3 Figures of typical laparoscopic graspers which may be disassembled to handles, marked as A, and shafts with variable tips attached, marked as B (Lobe, 2003).

Although the concepts of laparoscopic graspers being quite similar to the conventional graspers, to manoeuvre, the implementation for MAS is different and some more factors that might interfere or interrupt the procedure have to be considered. Figure 2.4 (Westebring-van der Putten, 2011) is a schematic graph of a laparoscopic grasper showing a force diagram. During the operation, several forces

are involved, including a grip force (F_g) occurred when surgeons control the handle to open and close the jaw, a pinch force (tip force) (F_t) generated at the contact point with tissue. A force is associated with the movement of the hand (F_h), and a force exerted on tissue by the movement of the tip generates (F_O). A pull force is generated when surgeons pull the handle away (F_{pullh}) and an associated pull force on tissue (F_{pullO}).

These interference factors are supposed to oppose each other and should have the same magnitude. However, Westebring-Van der Putten (2011) noticed that these interference factors are not simply equal because pinch force is not equal to tip force due to the instruments mechanism. The pull forces are not equal as there is a friction force between the trocar and shaft. Two movement forces are not equal as there is a scaling factor and a resistance of the abdominal wall.

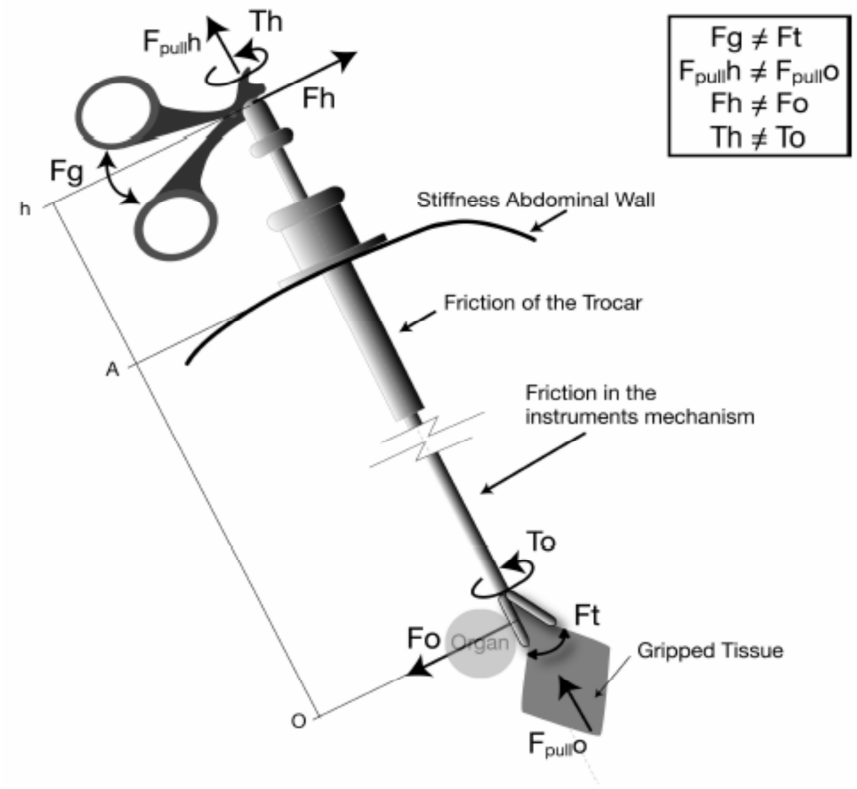

Figure 2.4 A schematic figure of a laparoscopic grasper with its force diagram (Westebring-van der Putten, 2011).

Prior to this study, Gupta et al. (1996) investigated the relationships between grip forces, pinch forces found in using laparoscopic forceps and surgical forceps. They concluded that pinch forces in laparoscopic surgery were significantly smaller than grip forces provided by surgeons' hands. In contrast, pinch forces were significantly greater than grip forces when surgeons controlled grasping forceps in an open surgery.

As such, forces applied in laparoscopic surgery are dramatically different from those in open surgery. Without a three-dimensional (3D) constructive vision and haptic feedback, the difficulty of the operation is seen to increase while surgeons apply a grip force to manipulate grasping forceps (de Visser, 2003a). Surgeons have to rely on 2D visual clues showing the level of tissue deformation to tell how much force applied (Culmer Peter, 2012). This kind of indirect information causes clinical problems, such as tissue damage resulted from inappropriate force in the instrument-tissue interaction (Rodrigues et al., 2012, Bishoff et al., 1999a). It has been reported that using grasping forceps or scissors is one of the common complications of such surgical injuries in laparoscopic surgery (van der Voort et al., 2004). The exampled figures (De et al., 2007, De et al., 2006) have been shown in Figure 1.4.

An ideal grasping action is considered as an act of holding tissue securely without damaging it. To achieve this goal, it requires practice and skill of controlling the forces and the tools. Because the tips of graspers are so small that the pressure at the tips is magnified, too much pressure can lead to tissue damage and too little pressure can cause the tissue to slip out of grasp. A pull force would be associated with a slip force due to the action-reaction law (Kemner, 1999, de Visser, 2003a). If a pull force is much greater than a pinch force, slip effect would happen. On the other hand, if a pinch force is much greater than a pull force, tissue would be

damaged. The relationship of pull forces and pinch forces forms an area called “safe grip”, as shown in Figure 2.5 (de Visser, 2003a).

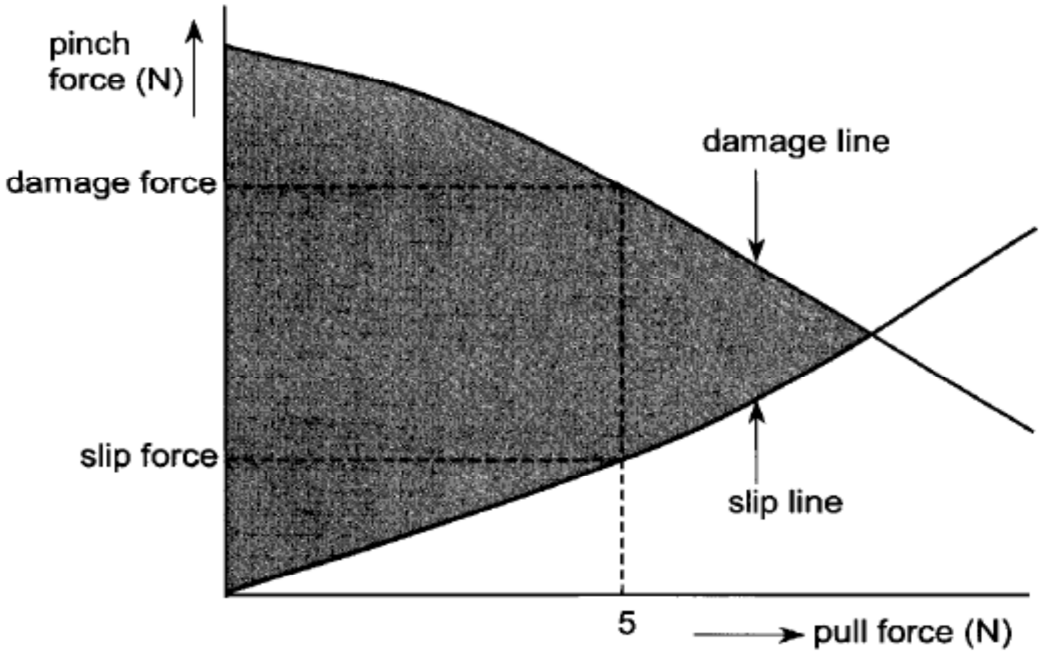

Figure 2.5 A safe grip diagram showing how tissue would be damaged and slip (de Visser, 2003b).

Although Figure 2.5 does not show a force value on axis, it has been suggested that safe grip standard would change according to different types of tissue or organs (de Visser, 2003b). Each tissue type was found to have its own individual range of acceptable maximum forces before visible tissue damages are observed (Rodrigues et al., 2012). For example, an average pinch force of approximately 2.5 N and 5 N maximal to the colon stretches the mesocolon sufficiently for dissection in a laparoscopic procedure (de Visser, 2003b). Tolendo et al. (1999) presented an average pinch force of 9 N but did not report the reaction of the tested organ.

The new-generation grasping forceps and instruments are equipped with multiple articulations in order to have more freedoms in the orientation, as shown in Figure 2.6 (Diodato Jr et al., 2004). This type of articulated grasping forces is

designed in particular for robotic surgery and single site surgery as these procedures occupy even less accessible space (Dhumane et al., 2011).

Figure 2.6 Figures of articular grasping jaws for the robotic surgery (Diodato Jr et al., 2004).

The instruments are forced to minimise the dimensions and combine all functions together to reduce the numbers of instruments during the surgery, as shown in Figure 2.7. The concept of grasping forceps is the same as that of laparoscopic grasping forceps, but the dimension of grasping forceps is reduced so a challenge to the technique is whether pinch force is sufficient on the working site.

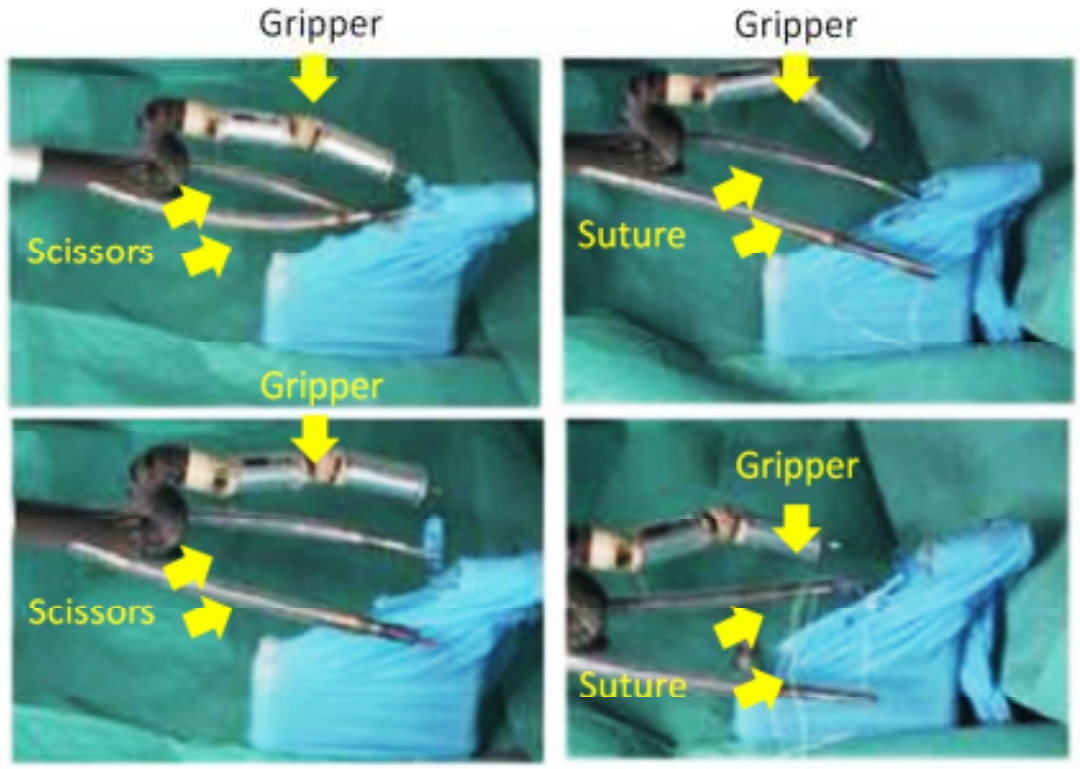

Figure 2.7 Two demonstrations of multiple functions of robotic articulating instruments show the surgical steps: i) using one gripper to hold and one pair of scissors for dissection, and ii) using one gripper and two needle holders for suturing (Shang et al., 2012).

2.2 Alternative Methods for Tissue Manipulation in MAS

It has been often speculated that clinical problems may occur when inappropriate grip forces are applied due to a lack of haptic feedback. Different types of tissue have their own acceptable maximum forces tolerance before visible tissue damage can be noticed. The core of the technical challenge here is if surgeons can grip with a constant force during the entire operative duration or not. An instrument has to enable surgeons to apply consistent grip force and control it easily.

This technical challenge has also made MAS training more complicated. To address the challenge, alternative methods have been explored for tissue manipulation with more comprehensible techniques and more consistent forces.

These methods include vacuum pressure and magnetic retraction, as shown in Figure 2.8.

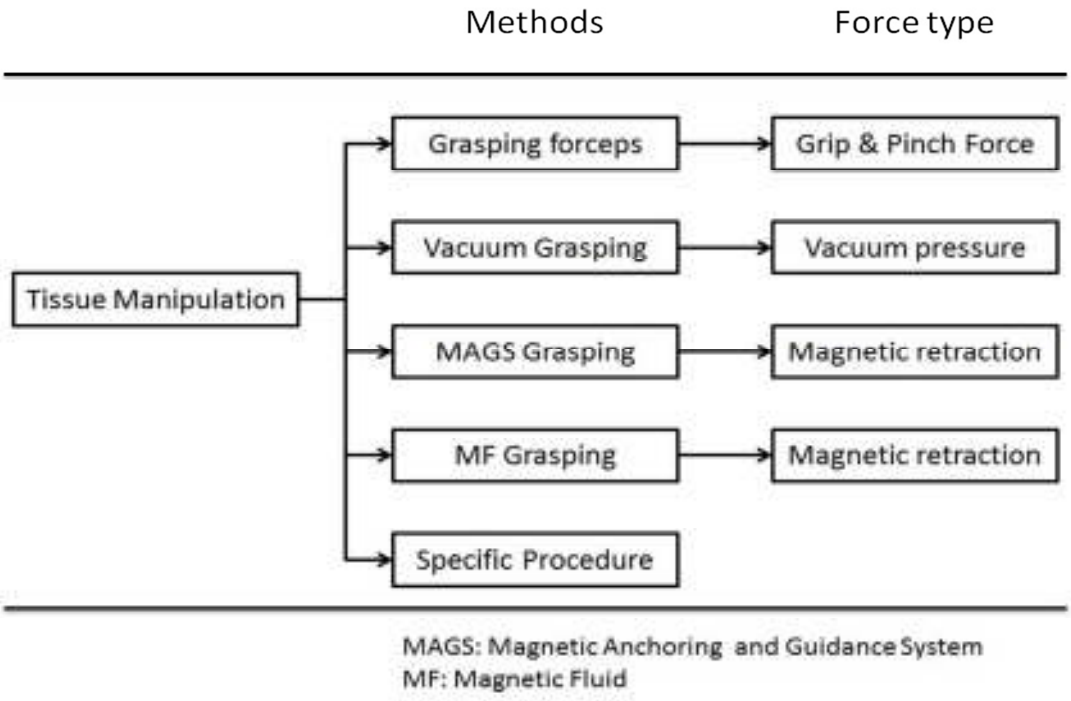

Figure 2.8 The methods and associated force types for tissue manipulation.

2.2.1 Vacuum Grasping

Vonck (2010, 2011, 2013b, 2012) introduced a method for manipulating the bowel tissue by means of vacuum pressure. The bowel tissue is delicate and flexible with a natural lubricant on the tissue surface. Many cases if bowel injury in laparoscopic surgery are caused by grasping (Bishoff et al., 1999b, de Visser, 2003a, Deziel et al., 1993, Rodrigues et al., 2012, van der Voort et al., 2004). A device has been created with a desirable nozzle connected to an air tube so as to provide vacuum pressure to suck tissue up, as shown in Figure 2.9 (Vonck, 2013b).

Figure 2.9 shows that the pressure applied on the area of tissue acts as an instant maximum pull force, which is expected by subtracting from the leakage effects, which occurs when tissue fails to close the inner wall of the nozzle. It has

been reported that a challenge in this application as the pull force is not constant due to the leakage effect and the result may lead to tissue slipping away (Vonck, 2013a). Therefore, the design of the nozzle shape becomes important in order to stabilise the pull force.

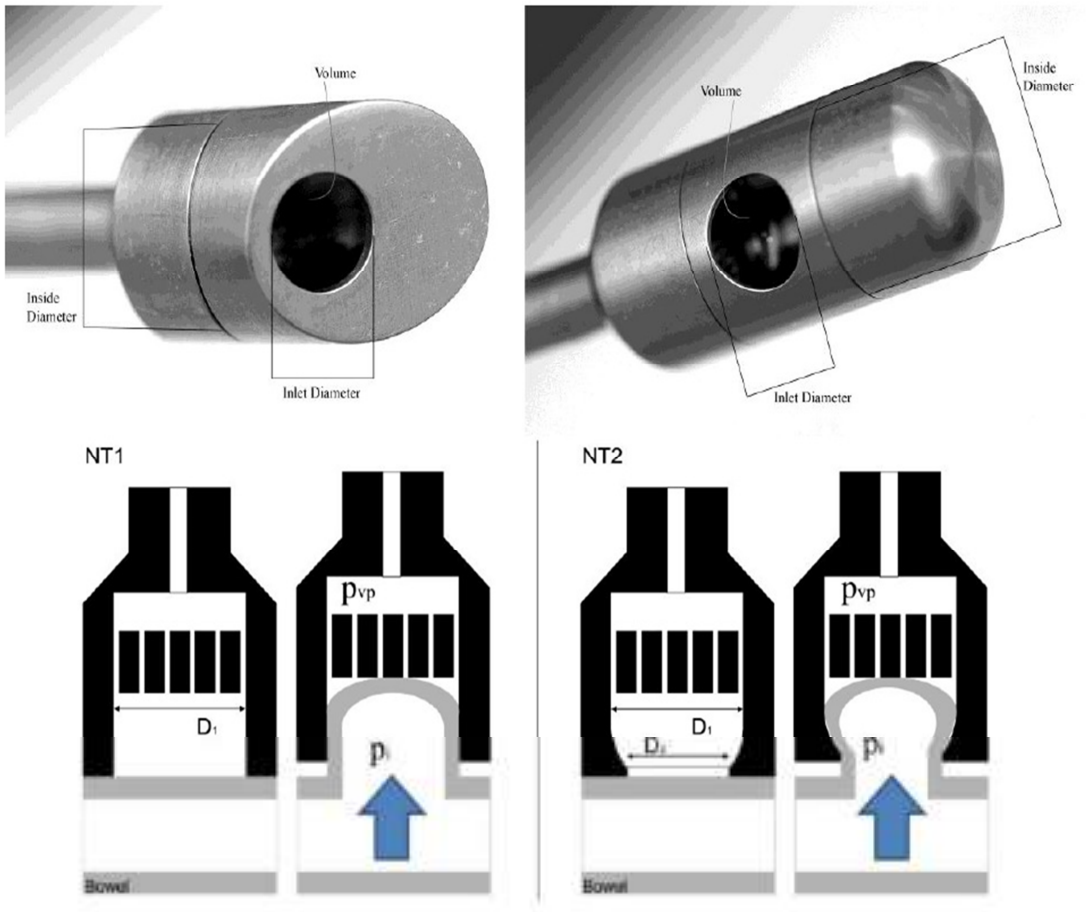

Figure 2.9 Schematic representations and figures of vacuum nozzles showing pull forces and the leakage problem occurring when tissue slipping away (Vonck, 2013b).

Vonck (2013b) also conducted in-vivo tests executed in open surgery and the results showed a retraction height of 20 cm after sucking up the bowel tissue, as shown in Figure 2.10. The force applied caused few damages such as small and moderate haemorrhages. It has been reported that a pressure level of 20 and 60 kPa (the maximum pull force about 5 N) caused tissue damages with a visible

ecchymoses. The nozzle prints caused by the sucking pressure would disappear after 10 minutes. In addition to the the leakage of the sucking pressure, potential tissue injury is another challenge of this application.

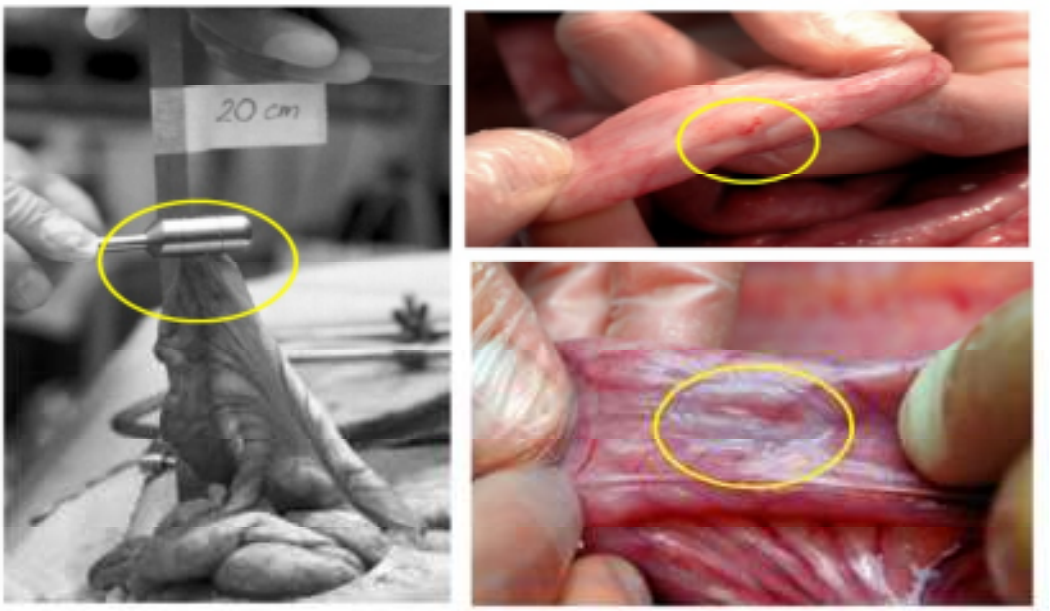

Figure 2.10 Figures showing the vacuum pressure is provided by the nozzle held by hand. The ecchymoses and the vacuum print can be observed in the circular marks on the right-hand side (Vonck, 2013b).

2.2.2 Magnetic Anchoring and Guidance System (MAGS) Grasping

Apart from vacuum pressure, which is often used in the industry to retract objects, magnetic force has also been widely used to pull and attract things without a need of physical contact. The utilisation of magnetism in medical applications have been included diagnostic applications, therapeutic applications, tissue movement and removal of ferromagnetic materials (Driller and Frei, 1987).

An example of the application of magnetism is “Magnetic Anchoring and Guidance System” (MAGS) for tissue manipulation (Best et al., 2011, Best and Cadeddu, 2010, Cadeddu et al., 2009, Dominguez et al., 2009, Kume et al., 2008a, Kume et al., 2008b, Park et al., 2007, Raman et al., 2009, Ryou and Thompson,

2009, Scott et al., 2007, Shaikh and Thompson, 2010a, Uematsu et al., 2010, Zeltser et al., 2007, Zeltser and Cadeddu, 2008). This method applies a magnetic force to pull soft tissue or organs. The magnetic force is generated by external and internal magnets where are placed outside and inside the abdomen, a configuration is shown in Figure 2.11.

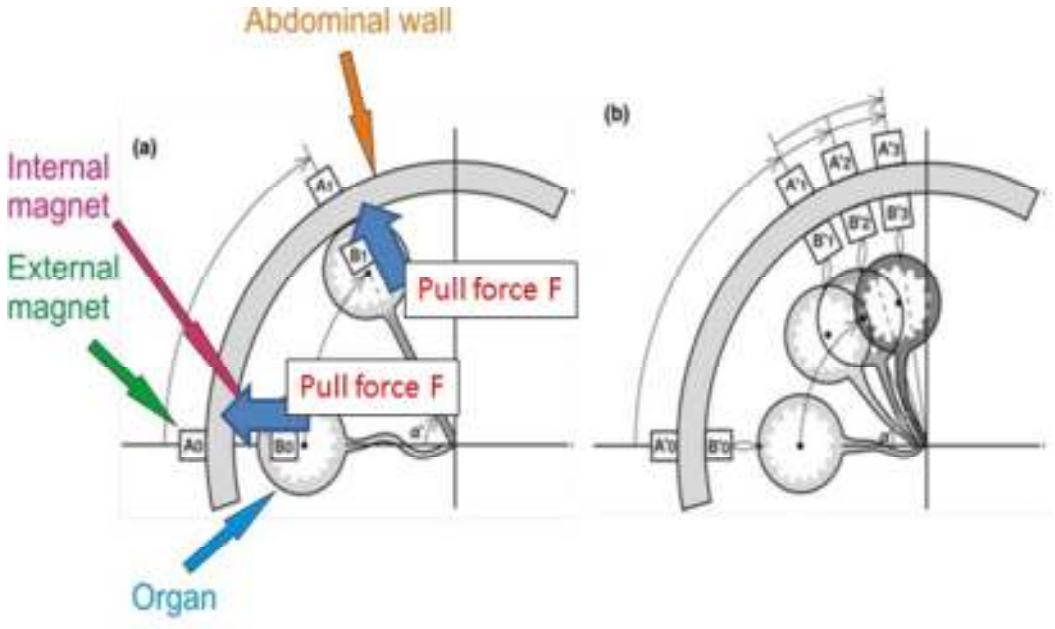

Figure 2.11 A schematic diagram showing the magnetic retraction of MAGS. The internal magnet can be attached to different positions of tissue or organs for tight or flexible retraction: a) the gall bladder is strained tightly by a pull force b) the gall bladder is remotely controlled by moving the external magnets (Kume et al., 2008a).

With an internal magnet attached on tissue, MAGS can be used to remotely control tissue manipulation by adjusting the position of the external magnets. The pull force remains consistent to hold tissue firmly when the retraction is being formed. In general, the way to attach tissue is to grip tissue. Although few studies have been focused on quantifying grip forces, the magnitude of pull force has been investigated as a function of distance between external and internal magnets (Best et al., 2011). Park et al. (2007) presented a force and distance curve showing that this

relationship is a reversed exponential curve. That said, the closer distance it gets, the stronger force will be, as shown in Figure 2.12.

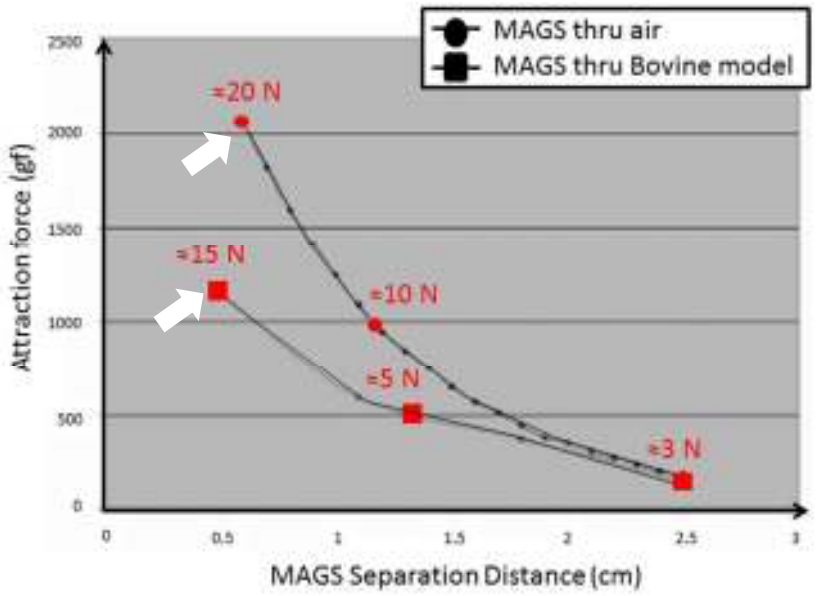

Figure 2.12 The retraction force-distance of the MAGS is measured against a separation of 5 mm at the arrows in the figure (Park et al., 2007).

The results showed that the maximal pull force against 5 mm was 20 N in air without any shield and 15 N with a shield of bovine model. As such, there is a "safe range" to lift up 300 g from a distance of 25 mm inside the bovine model and a maximal pull force that can afford 1200 g. There have been a few ex-vivo and in-vivo tests conducted based on the idea of manipulating tissue with a weight within the safe range by using the same configuration of magnets sets (Best et al., 2011, Best and Cadeddu, 2010, Cadeddu et al., 2009, Park et al., 2007, Zeltser et al., 2007, Zeltser and Cadeddu, 2008). However, the magnetic intensities of the magnets sets have not been extensively described.

To prepare MAGS set-up, the internal magnets need to be inserted through an access port and be attached the tissue or organs in a traditional laparoscopic procedure (Raman et al., 2009). It has been suggested that multiple internal

magnetic sets can be inserted through the same access port. In this way, the numbers of access port can be reduced (Zeltser et al., 2007, Zeltser and Cadeddu, 2008).

The in-vivo studies using MAGS as a means of tissue manipulation to conduct the listed procedures in MAS are summarised in Table 2.1. It can be seen that MAGS relies on permanent magnets. This is mainly because the dimensions of electro magnets need to be much larger than those of permanent magnets. Since this is opposite to the concept of minimising access ports, it is a challenge to work with electro magnets (Cantillon et al., 2013).

Table 2.1 Summary of the in-vivo tests involving MAGS as a means for tissue manipulation. (The laparoscopic surgery is denoted as LS and the Natural Orifice Translumenal Endoscopic Surgery is denoted as NOTES).

Author	LS / NOTES	Position	Tester	Permanent magnet	Electric magnet
Park et al. (USA) 2007	LS	Abdomen	Swine	√	X
Scott et al. (USA) 2007	NOTES	Cholecystectomy	Swine	√	X
Zeltser et al. (USA) 2007	LS	Nephrectomy	Swine	√	X
Kume et al. (Japan) 2008	LS	Cholecystectomy	Swine	√	X
Kume et al. (Japan) 2008	LS	Peritoneal cavity	Swine	√	X
Cadeddu et al. (USA) 2009	LS	Nephrectomy	Human	√	X
Dominguez et al. (Argentina) 2009	LS	Cholecystectomy	Human	√	X
Uematsu et al. (Japan) 2010	LS	Cancer therapy	Human	√	X

It has been argued that MAGS can successfully grip tissue and organs firmly to assist a resection (Kume et al., 2008a, Kume et al., 2008b, Dominguez et al., 2009, Uematsu et al., 2010), as shown in Figure 2.13.

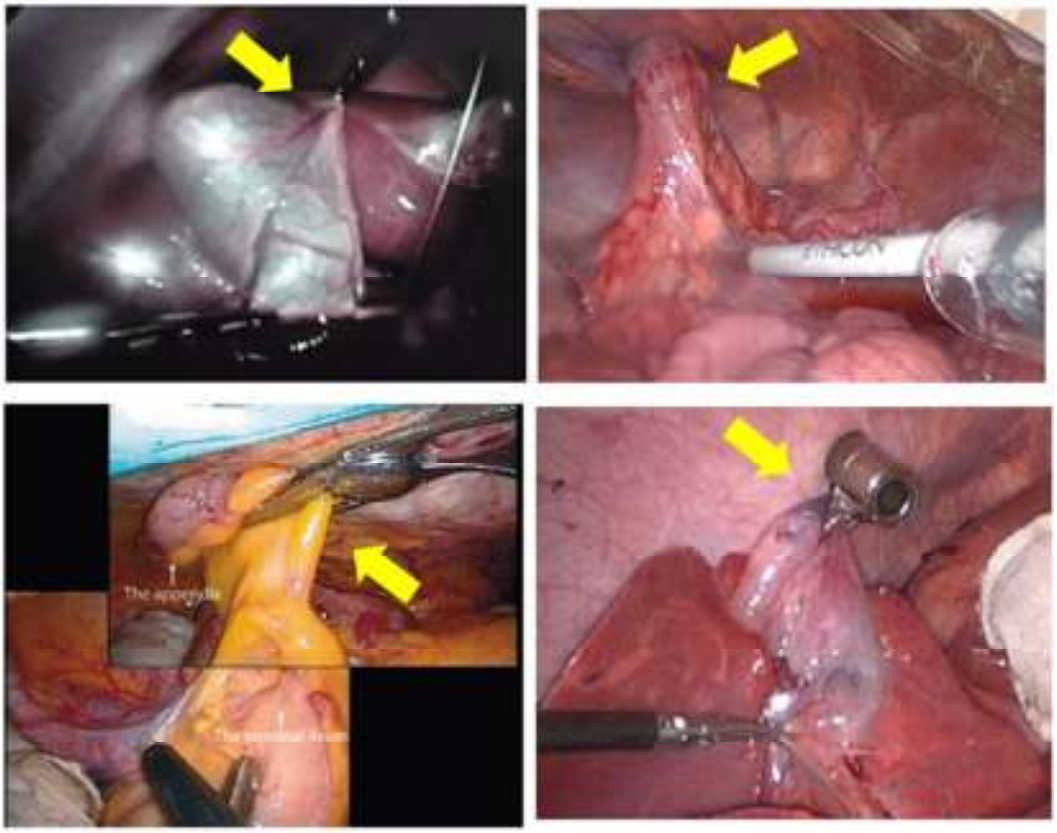

Figure 2.13 The images showing how the internal magnets are attached on tissue and organs to assist a surgical procedure (Kume et al., 2008a, Kume et al., 2008b, Dominguez et al., 2009, Uematsu et al., 2010).

The challenges in MAGS include magnet collision when multiple magnets are used. The strong attraction forces make it difficult to separate these magnets so magnets collision may occur. It has been suggested that to prevent the magnets from collision with a distance between each (Best et al., 2011). Besides, the existing method for internal magnets to be attached on tissue normally requires a grip force, shown as the arrows pointed in Figure 2.13, and a grip effect on tissue denotes a risk of tissue damage like those done by conventional graspers (Dominguez et al., 2009).

In addition to these involuntary injuries, the force controller has improved the MAS procedure and plays an important role in this method.

2.2.3 Magnetic Fluid Grasping

Not only the MAGS uses magnetic force as a means for tissue manipulation, but also the magnetic fluid can be used in this application. Magnetic fluid is composed of ferromagnetic particles stably suspended in a carrier liquid and can be easily magnetised in the presence of a magnetic field (Odenbach, 2004, Shinkai, 2002, Silva et al., 2012, Vékás, 2008).

Wang et al. (2008, 2009, 2010b, 2012) introduced a concept of generating a pull force when a magnetic fluid is exposed to an external magnetic field. As such, the particles inside the magnetic fluid would move toward the magnets and the movement can then pull the tissue if a magnetic fluid is attached to them. The material involved in their studies was stainless steel particles (MP-SS410), with an average particle size of 15μm, suspended onto a carrier fluid such as cyanoacrylate liquid in order to avoid particles aggregations when placed in a homogeneous magnetic field (Wang et al., 2008). After the preparation, there are two ways for the magnetic fluid to be attached to the tissue: glue (Wang et al., 2008) and injection (Wang et al., 2010b, Wang et al., 2009), as shown in Figure 2.14.

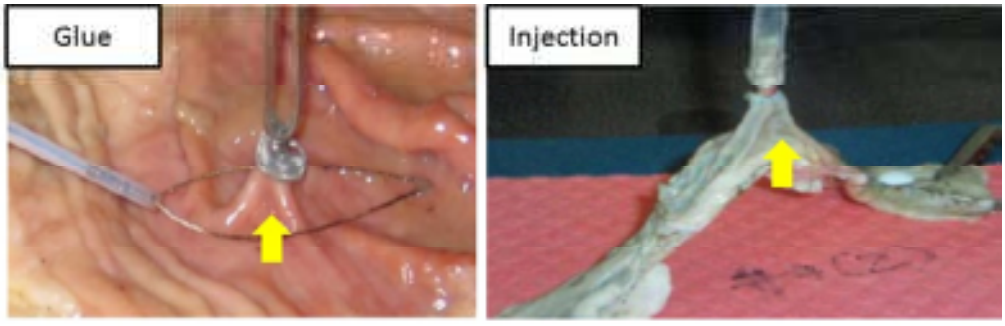

Figure 2.14 Images showing two implementations of magnetic fluid, one by gluing onto a tissue surface (Wang et al., 2008) and the other by injecting into a tissue layer (Wang et al., 2009) for manipulating tissue, respectively.

Gluing tissue may seem to be more reliable because it involves no direct interaction with tissue cells. However, it has been found that the adhesives can sometimes fail to attach to moist tissue surfaces (Wang et al., 2008). The injection method has less interference from the natural surface lubricant. In the studies Wang et al. conducted, permanent magnets (NdFeB) were used.

In these operations, magnetic retraction force was seen as the pull force (Wang et al., 2010b, Wang et al., 2012, Wang et al., 2009, Wang et al., 2008). The magnitude varied due to several factors, including the distance between the implemented magnet and magnetic fluid, volume and concentration of the magnetic fluid and the strength of the magnetic field. The force and the distance graph shows a reverse exponential curve, as shown in Figure 2.15 (Wang et al., 2009). The result showed the closer the distance between the implemented magnets and the magnetised tissue, the stronger the retraction force. It has been reported that a1 sufficient force up to 10 mm by a volume of 50 µl MP-SS410 fluid with a concentration of 2000 mg/ml would provide a maximum force of 3.45 N to pull a tested bowel tissue.

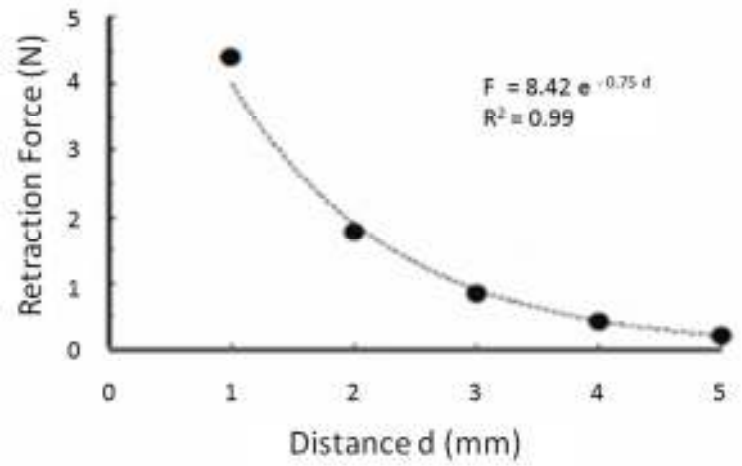

Figure 2.15 This figure showing the intensity of retraction force at the distance of the implemented magnets to the magnetised tissue (Wang et al., 2009).

Magnetic fluid grasping although having shown potential in a number of publications still faces quite a few challenges, including how to implement biocompatible adhesives to glue tissue surfaces without the peeling off effect. Also leakage problems can occur when high concentrations and large volumes are injected. Particles can also aggregate in a homogeneous magnetic field. There is difficulty of manufacturing a magnetic fluid with higher concentration of particles (>750 mg/ml) (Wang et al., 2009, Wang et al., 2008).

Moreover, using magnetic stainless steel materials such as SS-410 in tissue has a few concerns of biocompatibility and toxicity for a long-term effect (Bailey et al., 2005). Even though stainless steel materials have already been widely used in the application of hip replacement, the implant materials are required restrictively to contain non-magnetic feature in order to prevent any interactions of ferro- or ferri-magnetic behaviour from a magnetic field (Jindal, 2012). Although it was suggested that holding tissue has less interaction with tissue and the particles could be removed when sweeping later by magnets (Wang et al., 2009).

2.2.4 Specific Procedures for Tissue Manipulation

In addition to physical forces for tissue manipulation, two specific procedures have been introduced to manipulate tissue: Endoscopic Mucosal Resection (EMR) and Endoscopic Submucosal Dissection (ESD) (Kantsevoy SV et al., 2008, Hyun et al., 2006, Jung and Park, 2013, Lenz et al., 2010). The concepts of EMR and ESD are to inject an alkaline solution into mucosal or submucosal tissue layers on the stomach or oesophagus in order to raise the lesion for dissection (Kantsevoy SV et al., 2008). It is separated from the deep muscle layer, as shown in Figure 2.16 (Olympus, 2014). This is a specific procedure to raise the lesion to a sufficient height for removal without a serious damage.

The procedures do not involve new implements to grasp tissue, neither do they apply physical force to tissue. It is only recommended for a specific purpose at an early stage of tumour resection. The advantages of adopting these procedures are quicker recovery (hence no overnight stay in the hospital) and smaller wounds.

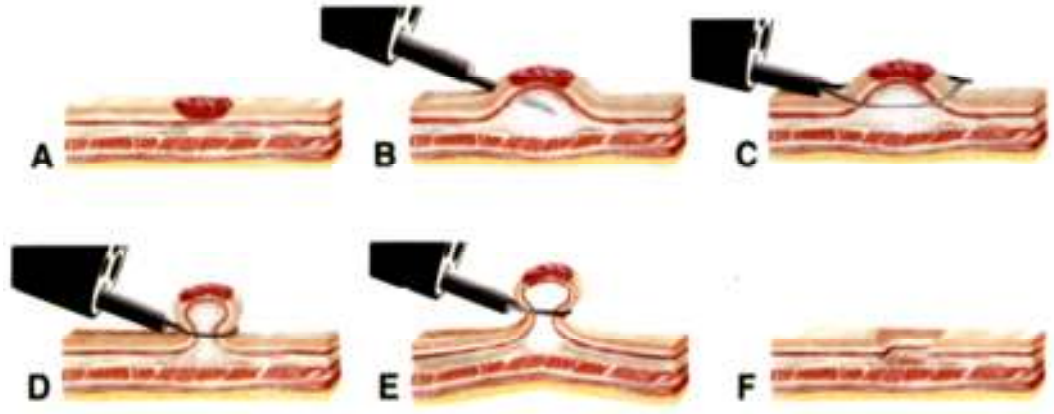

Figure 2.16 A schematic figure showing the procedure of EMR, which starts a procedure of injection at the cancer site in order to create a tissue deformation and then uses the snare to reset the mucosa or submucosa. (Soetikno et al., 2003).

2.3 Conclusions

In summary, the clinical challenges introduced in this chapter relate to involuntary tissue injury which often occurs in laparoscopic surgery due to a lack of haptic feedback during a surgery. Grip forces can be executive when using conventional grasping forceps. In addition, every tissue has a different reference to the maximal grip force before tissue damage occurs. Inconsistent grip force can lead to tissue slippage. Although skills and experiences of surgeons can prevent inadvertent damage, risks still exist when these procedures are conducted. Technological advancement therefore should mitigate some of these issues.

To overcome the challenges of inconsistent grip forces, a concept has been proposed to provide a comprehensive pull force to replace conventional pinch force.

The existing methods include vacuum grasping, MAGS grasping, magnetic fluid grasping and other specific procedure. Although all of these demonstrate promising performance in grasping tissue, there exist limitations for each implementation, as summarised in Table 2.2. The specific procedures of EMR and ESD can be applied to raise the lesion for dissection, which causes a minor wound on tissue layers. However, their challenges are providing not sufficient height and avoiding liquid dispersion during the operation.

Table 2.2 A list of current limitations in existing grasping methods**.**

Implements	Limitations
Vacuum grasping	• Tissue damage as small and moderate haemorrhages • Air leakage causes tissue to slip • No adaptable technical support yet
MAGS grasping	• Magnets collision when applying multiple magnets • Difficulty in separating the strong attraction forces • Tissue damage when implementing internal magnets on tissue • No force controller during retraction • Inadvertent tear may occur when a strong attraction force is applied • No adaptable technical support yet
Magnetic fluid grasping	• Difficulty in implementing biocompatible adhesives • Leakage problem may occur when high concentration and large volumes of the fluid are injected • Particles aggregation may occur in a homogeneous magnetic field • Synthesis of magnetic fluids are with higher concentration (>750 mg/ml) • Biocompatible and toxic concern for a long-term effect using magnetic Stainless Steel materials • No adaptable technical support yet

MAGS was firstly introduced to use magnetic force in tissue manipulation remotely. However, the strong attraction force leads to a difficulty in separation when magnetic collision occurs. Magnetic fluid has shown an ability to provide sufficient force in tissue manipulation, but there exists little investigation into its effects in existing literature. This implementation requires advanced technical supports to resolve existing challenges in pull force analysis, materials selection, experimental repeatability, system design, practical and in-vivo studies etc.

This research aims to investigate the feasibility of a new material, nano-particles magnetic fluid (ferrofluids) and its performance in tissue manipulation. The outcome will improve our understanding of force spatial map from an engineering perspective and an empirical experiment based on ex-vivo test of grasping tissue.

Chapter 3 Literature Review on Approaches for Adhesion Force Measurement

This research aims to investigate the feasibility of using ferrofluids as a means for tissue manipulation. Ferrofluids are used to magnetise tissue locally to allow a pull force to replace the pinch force produced by conventional graspers to grip tissues. As discussed in the literature review in Chapter 2, it is important to have a good understanding of the forces involved during tissue manipulation in laparoscopic surgery. In order to illustrate the force enabled by ferrofluids, this chapter will survey the existing literature on methods and apparatus used to measure the extent of different types of adhesion from an engineering perspective, e.g. wet adhesion, magnetic adhesion for retraction. This chapter is organised as follows. Section 1 will introduce an existing physical model of tissue retraction and the objective add-in after the entire study. Section 2 will review the existing methods and apparatus in adhesion measurement. Section 3 will review the mechanism of retraction methods. Section 4 will identify the magnetic adhesion and associated applications. Section 5 will give a summary of the literature review for the experimental design.

3.1 Adhesion Principle Involved in Tissue Manipulation

The model developed by Wang et al. that analysed pull force generated from magnetic fluids, as shown in Figure 3.1. This physical model presented an external magnetic field generated by a magnetic probe (permanent magnet) to induce a magnetic interaction force to manipulate the magnetised tissue. In contrast to the conventional grasping forceps, there were no grip forces or pinch forces involved in

this process. The principle of retraction was using magnetic interaction force to pull a certain loading of tissue during tissue manipulation.

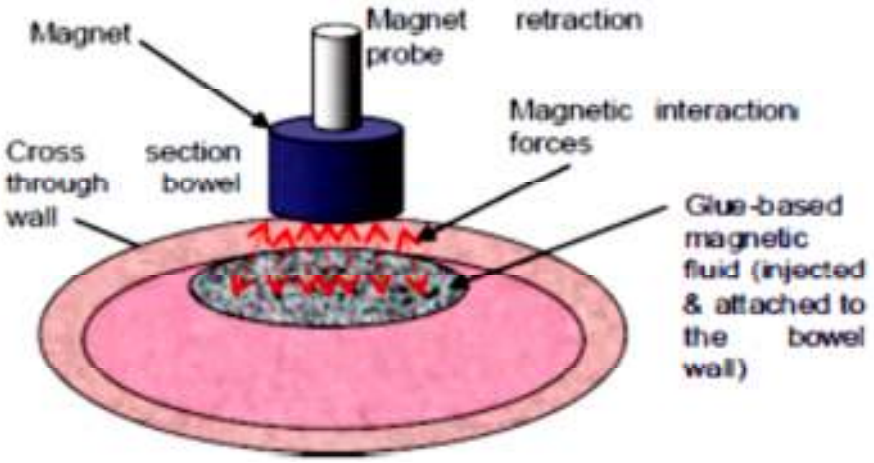

Figure 3.1 Schematic graph explaining force involved in magnetic fluid grasping (Wang et al., 2010b).

This model is useful for understanding the mechanism of using ferrofluids as a means of tissue manipulation. Furthermore, the mechanism observed in the study has made the model expanded a little bit with regard to tissue surface adhesion involved in tissue manipulation. When testing a plain tissue without magnetising tissue, an intensity observed from tissue surface is so called tissue surface adhesion.

In addition to the process of the tissue retraction, an interaction force is observed when the magnetised tissue is retracted by the magnetic probe before getting in contact. From the retraction to detachment, the measured intensity of detachment is larger than the retraction. Therefore, the physical model is expanded with tissue surface adhesion including interactions exerted between soft tissue and flat plane surface. The measured intensity is also defined as magnetic retraction and magnetic adhesion. This research contributes to this by including tissue adhesion and magnetic adhesion in a modified model as shown in Figure 3.2.

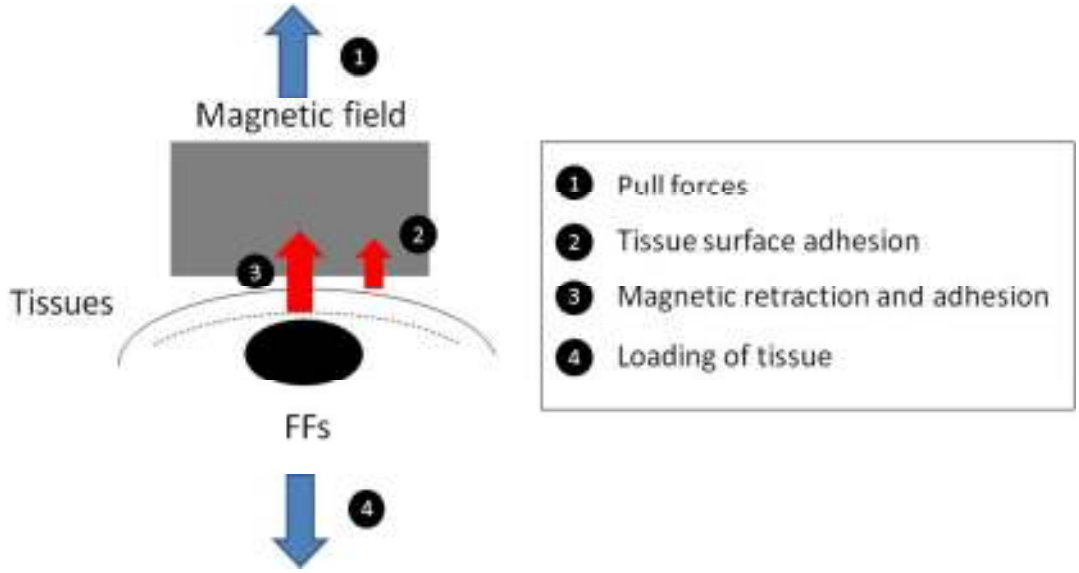

Figure 3.2 A modified model presenting a force diagram involved in tissue manipulation using ferrofluids. The investigations in this study are based on this model to clarify the measurement from an engineering approach.

3.2 Adhesion Measurement from an Engineering Perspective

The use of retraction is through the adhesion by a contact between the retractor and object. In this section, a range of methods and apparatus are reviewed from an engineering perspective for adhesion of surface contact. Several methods have been used to measure adhesion force when two surfaces make contact (Pocius, 2002, Pizzi and Mittal, 2003, Lacombe, 2006). For example, Lacombe (2006) introduces pull-off tests, indentation tests, self-loading tests, tensile tests, scratch tests and peel tests.

Adhesion forces occur in both normal and lateral directions before the contact is fully ruptured. Methods such as pull-off tests, indentation tests, tensile tests (Shao et al., 2009, Shao and Stewart, 2010) and self-loading tests measure the normal adhesion which is perpendicular to the contact surface. The mechanism of pull-off tests and indentation tests requires a probe to be placed upon the substrate (Lacombe, 2006). The procedure is to apply a contact at the substrate and pull the

substrate off opposite to the direction of the applied force. In this way, the adhesion force can be captured while a backward motion pulls the substrate away. There are some examples shown in session 3.3 and 3.4.

Based on this approach of pull-off and indentation, the literature shows that some factors can affect adhesion force, e.g. surface roughness (Gay, 2002), preload forces for a contact (Autumn and Peattie, 2002, Greiner et al., 2007, Liang et al., 2000, Long and Hui, 2009, Roshan et al., 2011), surface orientation (Rabenorosoa et al., 2009). Due to different textures of surfaces which are composed of different materials, some rough, some smooth, the magnitude of adhesion force varies as well. The existing literature suggests that soft substrates usually give higher adhesion force than hard substrates when making contact with a rigid material. This is due to its feature of highly deformable surface (Gay, 2002), as shown in Figure 3.3. One can see that the surface pressure increases when the contact area is enlarged.

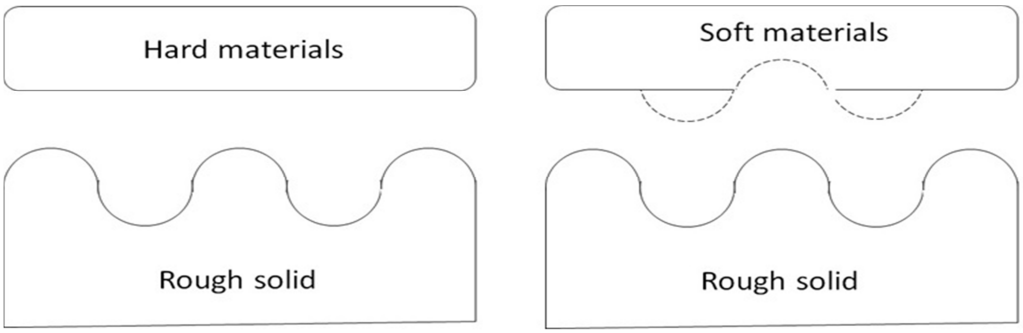

Figure 3.3 Different levels of surface deformation show different types of adhesion between the hard and soft substrates during an indentation (Gay, 2002).

After experimenting various contact angles between the substrate and the indenter, Rabenorosoa et al. (Rabenorosoa et al., 2009) found that a maximal adhesion force can occur when the contact angle is zero. This means the indent surface is perpendicular to the substrate. The results also showed that whilst the contact angle has a significant influence on the pull-off force, the preload force did

not. Therefore, the effect of preload force on the adhesion force is fairly consistent in the research (Autumn and Peattie, 2002, Greiner et al., 2007, Liang et al., 2000, Long and Hui, 2009, Roshan et al., 2011).

The mechanism of tensile tests and self-loading tests is set up with one end fixed and the other end attached with a load to the substrate. The load generates a pull force in order to stretch the substrate. The substrate may be deformed or displaced during loading, and an adhesion force is obtained until the contact is taken off.

Apart from normal adhesion, shear adhesion is another category that has been investigated, such as through peel tests and scratch tests (Lacombe, 2006). Shear adhesion is different from the perpendicular direction of its orientation as parallel to a lateral movement towards the substrate, as shown in Figure 3.4. In general, the mechanism of scratch tests is to ensure a contact is attached to a substrate using a probe (Lacombe, 2006). While moving the probe laterally to the substrate surface, a shear adhesion force occurs. This method is often used on hard substrates (Lacombe, 2006) because plastic deformation is often extruded and makes it technically difficult to measure when a soft material is scratched and deformed, as shown in Figure 3.4. Achanta (2008) studied a ball-on-flat contact by reciprocating sliding using the Modular Universal Surface Tester (MUST) rig. The motion of a reciprocating sliding caused a shear adhesion effect and the magnitude of the shear adhesion was investigated over a range from micro- up to milliNewtons.

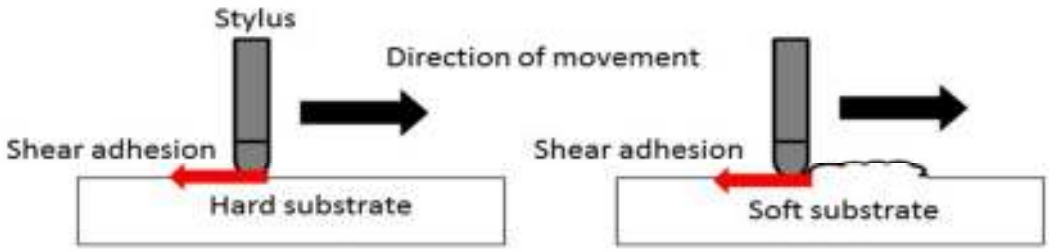

Figure 3.4 A comparison between conducting a scratch test on a hard and a soft substrate. The deformation of the soft material increases the difficulty of using this method (Lacombe, 2006).

Except scratch tests, peeling mechanism is also used to investigate shear adhesion force (Lacombe, 2006). The apparatus requires a thread attached on one end of the substrate and pulled while the substrate is slid via a connected thread to ensure both slide and pull motions travelling with the same speed, as shown in Figure 3.5.

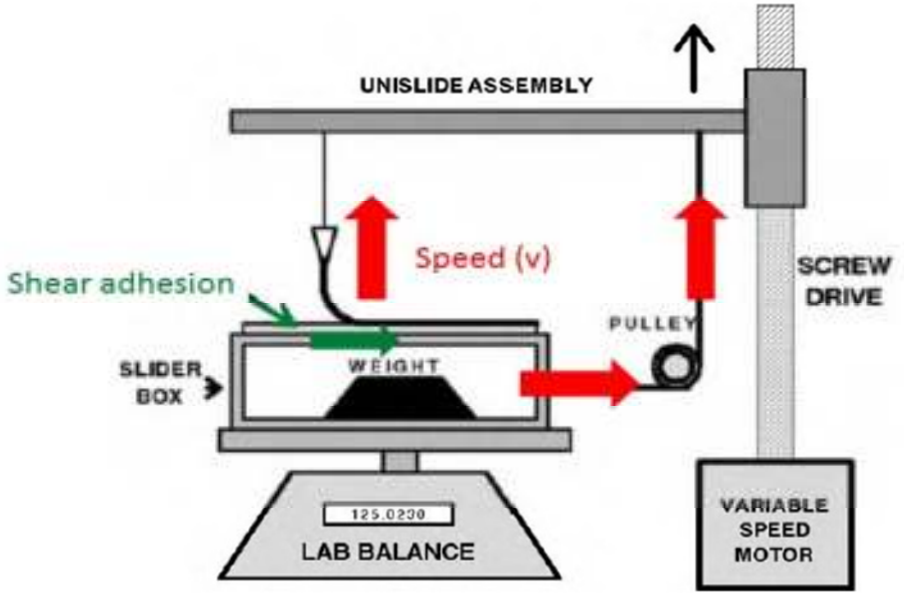

Figure 3.5 A schematic diagram showing a peel tester with a load cell for measuring the variation of force. This apparatus has a feature that both slide and pull motion travel with the same speed (Lacombe, 2006).

3.3 Review of Adhesion for Retraction

While a surface contact generates an adhesion force on tissue, several natural matters have been attracted huge attentions of their adhering and pulling powers. For example, insects and animals like geckos (Autumn and Peattie, 2002, Huber et al., 2005, Lee et al., 2007, Liang et al., 2000, Sangbae et al., 2008, Stark et al., 2013, Geim et al., 2003), tree frogs (Federle et al., 2006, Roshan et al., 2011) beetles (Eisner and Aneshansley, 2000, Cheung et al., 2005) all have the abilities to attach themselves to dry or wet surfaces. That means that a sufficient adhesion force can withdraw the pulling from the gravitational force generated by the weight. The adhesion force is generated by the texture of the foot toes that has nano or micro-structured pillars, as shown in Figure 3.6.

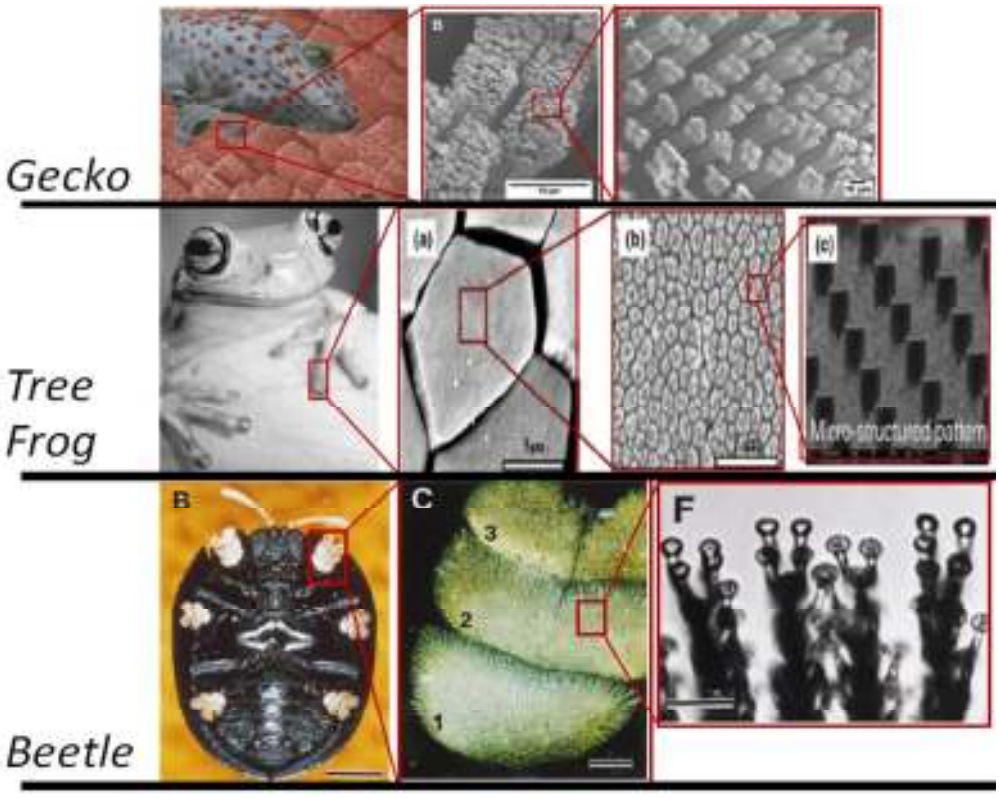

Figure 3.6 A collection of morphology of gecko, tree frog and beetle foot toes showing the micro-structured surfaces with pillared fibres (Eisner and Aneshansley, 2000, Roshan et al., 2011, Huber et al., 2005, Stark et al., 2013).

This kind of pillared fibre can also be seen in other biomaterials (Schliemann and Goodman, 2011). The mechanism of an adhesion force was considered to be generated by the combination of capillary and van der Waals forces (Taylor et al., 2010, Menon et al., 2007). The adhesion feature is currently applied in many biomimetic materials for the development of climbing robots (Menon et al., 2007, Cheung et al., 2005, Filippov et al., 2011, Gebeshuber et al., 2005, Murphy et al., 2006, Sangbae et al., 2008, Style et al., 2013).

The performance of adhesion against the pulling from gravity is often investigated from an engineering perspective using microrheology apparatuses, which have been developed to measure the small scale of contact as a function of micro-nanoNewtons, such as Surface Force Apparatus (SFA) and Atomic Force Microscope (AFM) (Lin and Valentine, 2012a, Lin and Valentine, 2012b, Gavara and Chadwick, 2010). The procedure is to use a cantilever which carries a tip to work as an indenter under either a single contact or semi-contact (frequent contact), and to probe onto the substrate (Gavara and Chadwick, 2010). The results from the microrheology tools are used not only to study the topography of the surface but also to obtain the stress and strain curve, similar to the pull-off and indentation tests. The tips are normally selected to form a contact as cylinder-cylinder or sphere-planar for a point or line contact, resulting in no requirement of a precisely relative angular position for calibrations. Otherwise, the adhesion force on the rough surfaces is strongly reduced compared to that on the flat one (Lorenz et al., 2013). AFM is normally used for measuring micro-scale matter as the resolution of AFM is normally as high as nano- to micrometres. However, the width of the scanning area is usually less than 100 μm, and this makes it difficult to characterise a large area surface. The advantage of using AFM is to detect the atomic force such as molecular

repulsive forces, Van der Waal's forces and capillary forces for the scale like biomimetic materials, as shown in Table 3.1.

Table 3.1 Adhesion tests of biomimetic materials, for example gecko pads, frog tree pillars and beetle fibres using apparatus of AFM.

Material	Method of measurement	Description
Gecko pads versus a needle tip (Huber et al., 2005, Geim et al., 2003)	Microrheology indentation method (AFM)	Using AFM to provide a contact of indentation using the needle tip. The measurement was conducted using a single spatula during perpendicular pull.
Biomimetic adhesive of hybrid gecko and mussel versus a needle tip (Lee et al., 2007)	Microrheology indentation method (AFM)	Using AFM to provide a contact of indentation using the needle tip. The measurement was conducted on a single pillar area.
Gecko adhesion in shear direction versus wet and dry surface (Stark et al., 2013)	Microrheology indentation method (AFM)	Testing adhesion force between the gecko hair-like surface and a flat surface in shear direction under different wettability.
Beetle bristles versus flat surface (Eisner and Aneshansley, 2000, Cheung et al., 2005)	Pull-off method	The apparatus consists of a platform to contact with the beetle bristles and measures the adhesion force while increasing the load to pull off the contact.
Biomimetic adhesive pad like tree frog with pillars versus wet and dry surface (Roshan et al., 2011)	Indentation method (MUST rig)	Testing adhesion force between the tree frog pillar-like surface and a peritoneal tissue surface in normal direction.

Adhesion force has been studied using pull-off tests and indentation tests. However, few literature is directly related to the adhesion force between a flat surface like magnet and soft tissue. Soft tissue is normally covered with body lubricant and considered as wet surface. The wet adhesion is normally investigated using a dome shape indenter during pull-off tests so as to avoid the disturbance from the influence of the surface texture and the orientation (Derks et al., 2003, Lindner et

al., 2005, Nase et al., 2008, Poivet and et al., 2003, Poivet et al., 2004, Banks and Mill, 1953, Francis and Horn, 2001). The wet surface forms a liquid bridge, which provides an attractive effect. This phenomenon is shown clearly in Roshan et al.'s study about the pillar-like adhesive pad probed on the rat peritoneum (Roshan et al., 2011). Before the indenter was brought into contact with the substrate (see Figure 3.7), the liquid adhesion was observed to speed up the indenter in contact with the wet surface, behaving as if what is called the "snap-in" effect (Taylor et al., 2010, Taylor et al., 2009).

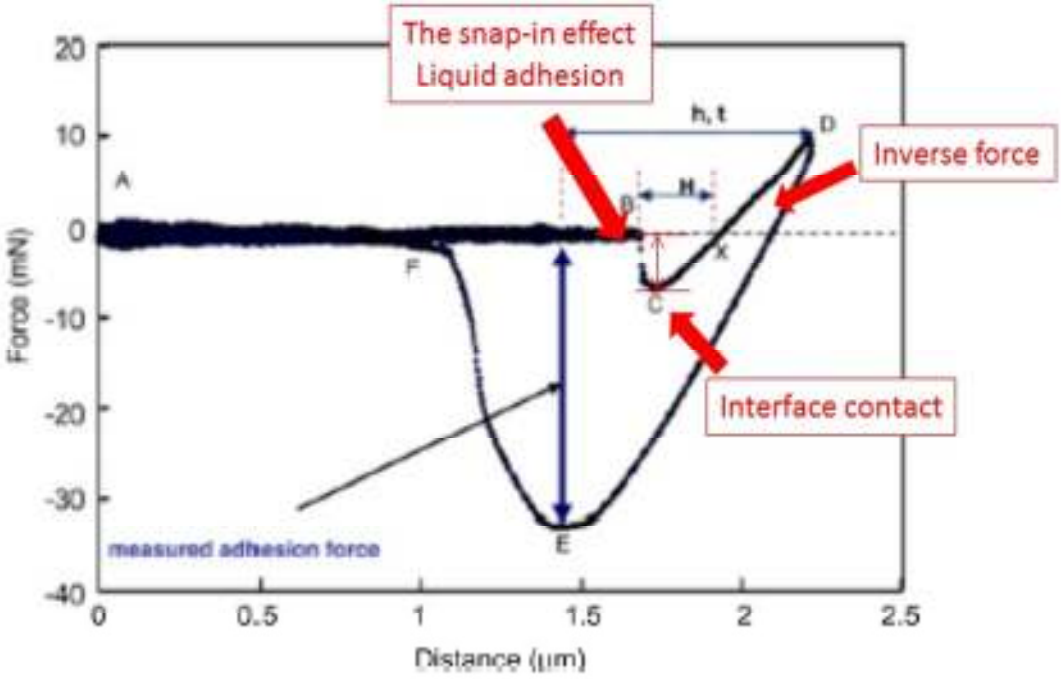

Figure 3.7 A figure showing the force-distance curve with a clear wet adhesion force which speeded up the contact as the snap-in effect is in action. It also shows that the maximal adhesion force is significantly larger than the wet adhesion force (Roshan et al., 2011).

When the interface was compressed and then detached, there was an adhesion force observed. The wet adhesion force was broken when the interface was squeezed and an inverse force occurred. The magnitude of wet adhesion was investigated over the range within 10 mN.

3.4 Magnetic Adhesion

Unlike the capillary and van der Waals forces which always exist when objects interplay with one another, magnetic adhesion only occurs when a ferromagnetic substrate is exposed to a magnetic field where a magnetic force is generated (Menon et al., 2007). In contrast to van der Waals forces, that require the contact of two surfaces, magnetic forces do not require any contact of media as they can be remotely applied without a physical contact. The magnetic force is able to retract ferromagnetic substrate, for example, and it has been used in MAGS, magnetic tweezers (MT).

Although magnetic adhesion has the ability to attract substrates remotely, the power is not infinite and relies on the distribution of magnetic field. MAGS is the application of magnetic adhesion for tissue manipulation in MAS. It uses the external permanent magnets to attract the internal magnets which are attached to tissue or soft organs. The performance is often investigated using the pull-off method to measure the maximal retraction force versus distance from the magnetic resources (Best et al., 2011). The measurement is conducted while the opposite polar surfaces of magnets move towards each other and induce an adhesion force, as shown in Figure 3.8.

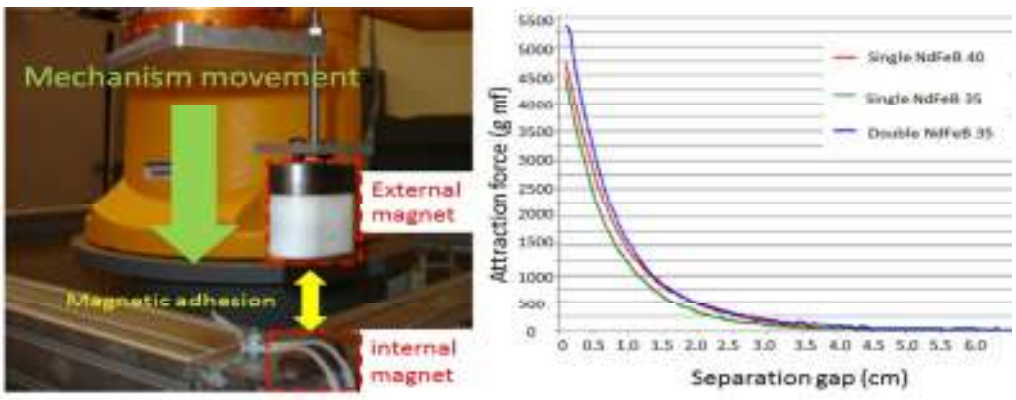

Figure 3.8 Adhesion measurement of retraction force between the external and internal magnets (Best et al., 2011).

The result shows that the decrease of distance will lead to the increase of adhesion force (Park et al., 2007, Best et al., 2011). In addition to afore mentioned, the components in the apparatus have to be non-magnetic otherwise there will be a significant effect in the accuracy.

When the internal magnet is replaced by a single metallic bead, the magnetic adhesion force can pull the metallic bead. An application called MT is incorporated into the optical microscope or fast camera to visualise samples. An active AFM with magnetic assembly is an example of this technique used to separate the Deoxyribonucleic acid (DNA) and Ribonucleic acid (RNA) while the magnetic bead is attached to tissue cells (Neuman and Nagy, 2008). A necessary force as pico- to nanoNewtons is required to pull the magnetic bead in order to separate the contact with tissue cells (Lipfert et al., 2009), as shown in Figure 3.9. There is a negative co-relation between the magnetic force and the distance between the magnetic field source and the substrate. The shorter the distance, the stronger adhesion force will be. (Lin and Valentine, 2012a, Lin and Valentine, 2012b).

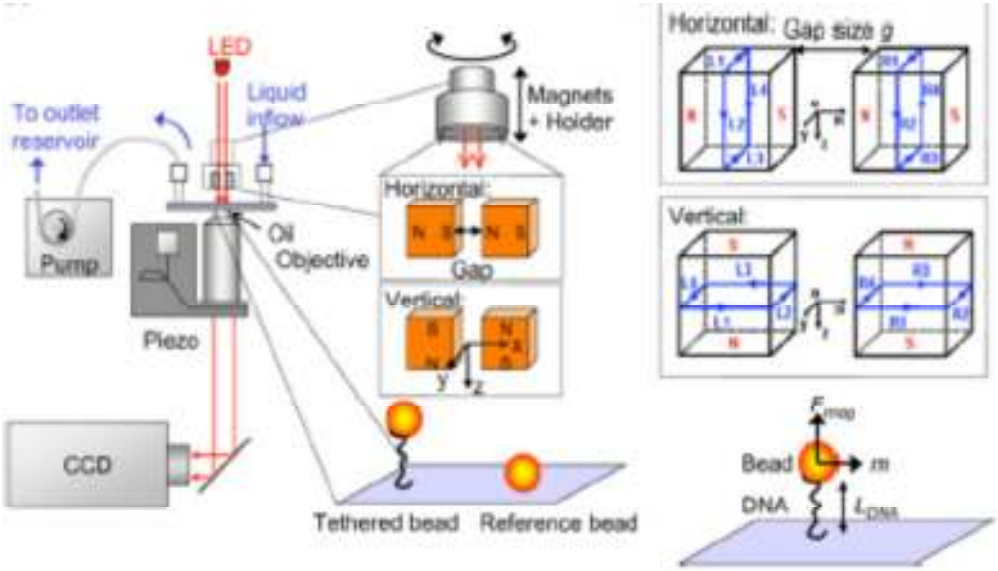

Figure 3.9 A MT apparatus which includes a CCD camera for visualising the real time separation showing the magnetic retraction occurs at the bead and substrates by the pull of magnetic adhesion (Lipfert et al., 2009).

The resource of magnetic field is either generated from electromagnets or permanent magnets and has often been used for pulling purposes (Wang et al., 2010b, Wang et al., 2009, Wang et al., 2008). There are the pros and cons with the electromagnets and permanent magnets. The main advantage of using electromagnetic configuration is its ability to provide various magnetic field patterns (Lira and Miranda, 2009a, Lira and Miranda, 2009b, Mahle et al., 2008, Muller et al., 2006, Miranda and Oliveira, 2004). However, the field strengths generated from electromagnets are much lower than those generated by permanent magnets under the condition of the same size. The electromagnet is also easier to apply torque due to its low field strength. To pursue a stronger magnetic field strength, Lin and Valentine demonstrate that strength can be increased as a combination of permanent magnets stack being added up (Lin and Valentine, 2012a, Lin and Valentine, 2012b).

Another magnetic adhesion applied in tissue manipulation using magnetic fluid has been investigated using the tensiometer (Wang et al., 2010b, Wang et al., 2012, Wang et al., 2009, Wang et al., 2008). The tensiometer is employed in the tensile methods to measure the relationship of load and displacement, as shown in Figure 3.10.

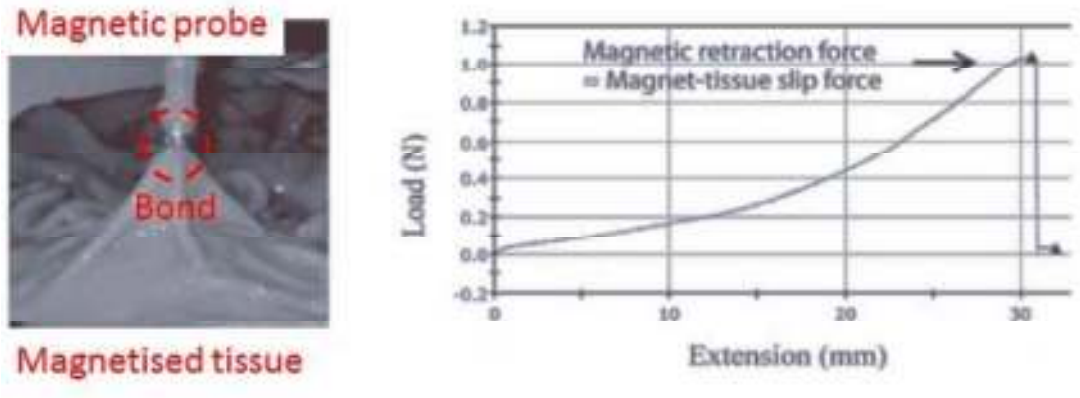

Figure 3.10 The experimental measurement of adhesion between a magnetic probe and magnetised tissue using a tensiometer. The load-extension curve indicated the rupture point of the adhesion (Wang et al., 2008).

The procedure was first to magnetise tissue via injecting or gluing magnetic fluids to tissue. The magnetic adhesion has been found increasing when the magnetic field strength increases as well as when the distance between the magnetic resource and the substrate decreases. The magnetic adhesion of Wang's studies was investigated over a range from 1 to 5 Newton.

3.5 Conclusions

In summary, the literature survey in this chapter can be summarised to a diagram of force range with regard to tissue adhesion. The comparison in Figure 3.11 shows the force range of different adhesions: for example surface adhesion is about 10 – 80 mN, wet adhesion is about 6 – 60 mN, magnetic adhesion in MAGS for solid magnets is about 250 – 50000 mN, magnetic adhesion for magnetic tweezer is about 300 pN – 1 μN and magnetic adhesion for magnetic fluid is about 1 – 5 N.

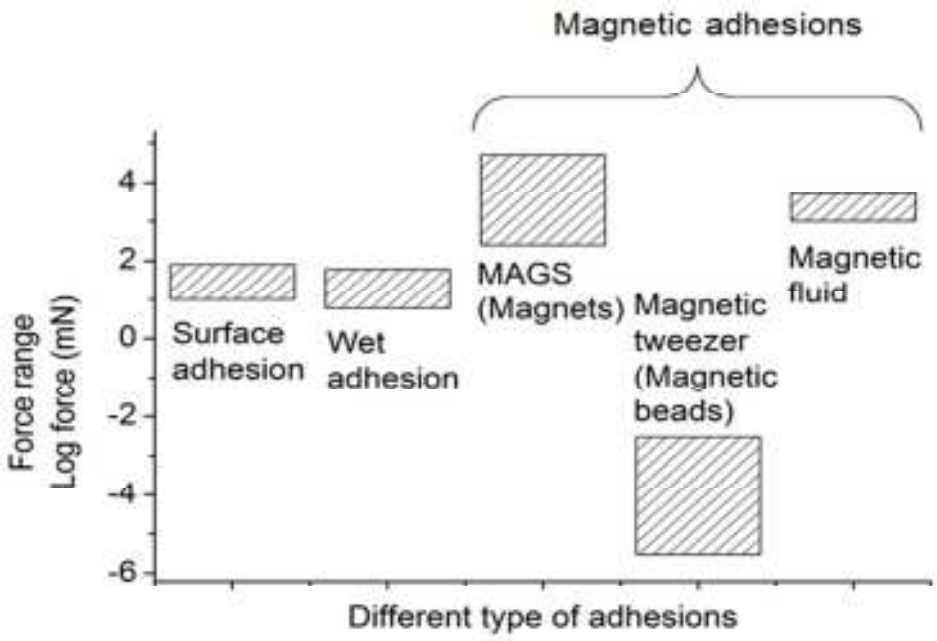

Figure 3.11 A comparison graph showing the force range for different types of adhesions.

It is found that few literature is directly linked to tissue adhering with ferrofluids. Hence, an experimental protocol is organised by the expanded physical model in order to study the feasibility of ferrofluids to facilitate effective tissue manipulation.

In the literature review, experimental methods are often using pull-off tests and indentation tests for the normal direction adhesion. In addition to a specific testing environment of the magnetic adhesion, the components on this apparatus have to be non-magnetic. So the AFM and the MUST^{TM} rig are not used but a self-developed testing rig of a combined approach of pull-off tests and indentation tests is developed.

The specification of this self-developed testing rig is according to the discussion in this chapter with regard to the force range.

Chapter 4 Methodology for Tissue Manipulation Measurement

This thesis has employed both ex-vivo and in-vivo methods to model the process of manipulation in order to investigate the feasibility of using magnetic adhesion force to replace the conventional mechanical clipping method as a means of retraction in the Minimal Access Surgery (MAS). The methodology of the investigation is illustrated in this chapter.

This chapter is organised as follows. Section 1 presents the experimental setup of the existing apparatus – MUST^{TM} tester for ex-vivo adhesion measurements in tissue retraction. Section 2 presents the instrumentation of a developed experimental tester MagRAT tester to overcome the challenges occurred in the MUST^{TM} tester during the magnetic measurements in retraction. Section 3 presents the information of those experimental materials used in magnetic tissue tests, including ferrofluids and animal tissue. Section 4 presents a study of the particle size suspended in the ferrofluids by using the dynamic light scatter (DLS)Nanosizer. Section 5 presents a study of the particle density distributions in the magnetised tissue test by using the micro CT scanner. Section 6 presents an experimental design to analyse the parametric results for optimisation by using the Taguchi method. Section 7 presents the experimental arrangement of the in-vivo experiments in tissue retraction.

4.1 Instrumental Adhesion Measurements – MUST^{TM} Tester

The adhesion measurements are conducted using two different apparatuses. The first apparatus is an existing tester, the Modular Universal Surface Tester

(MUST^{TM}), manufactured by Falex Tribology N.V. (FALEX TRIBOLOGY, 2014), which has allowed Taylor (2009) and Roshan (2011) to measure the molecular adhesion interaction between a pillar surface and rat peritoneum. This device equips a two-dimension motion module at the bottom and a sensor system on top of the module, as shown in Figure 4.1.

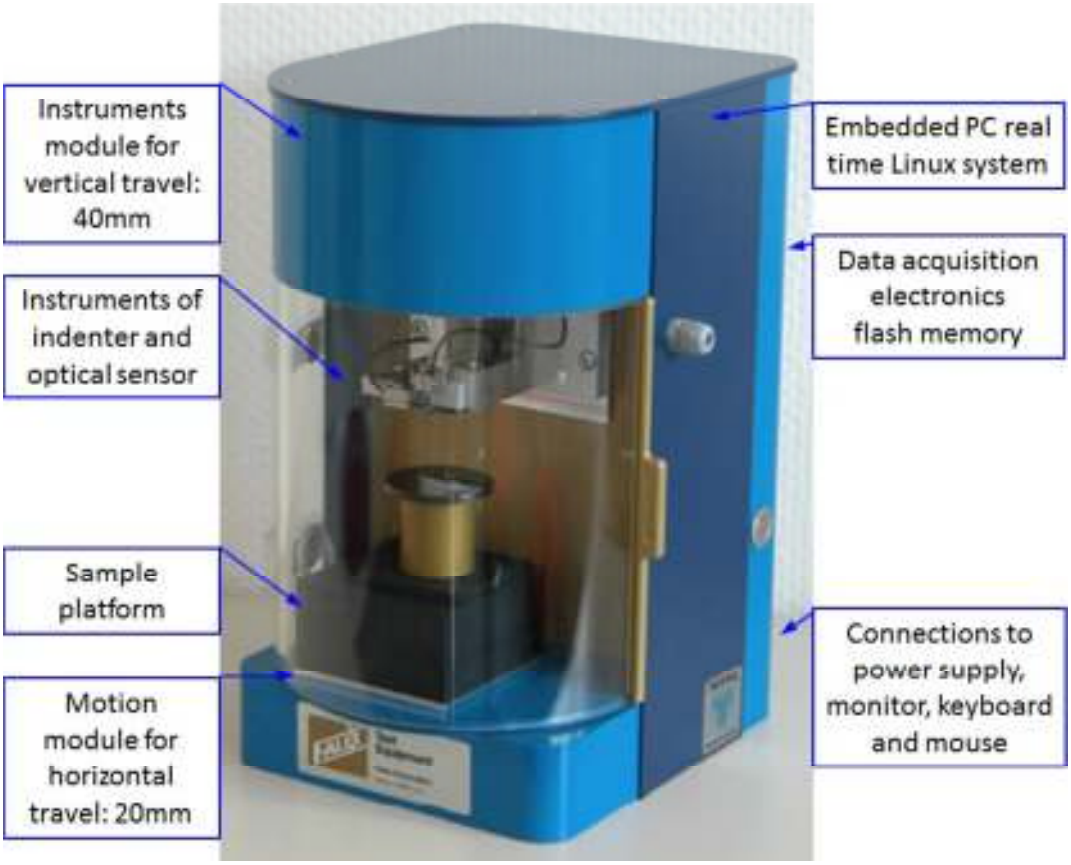

Figure 4.1 The appearance of MUST^{TM} tester (FALEX TRIBOLOGY, 2014) showing the device with a plastic door to prevent vibration and light emission. This device has its own operation system and a data acquisition of 10 N. There is a 2 axis motion basement and a vertical motion carrying an indenter and sensors.

4.1.1 A Sensoring System (Optical Fibre and Cantilever)

MUST^{TM} tester has a sensor system to detect the displacement and force. The sensor system is equipped with an optical-fibre to sense a reflection light from a

mirror which is attached to a cantilever, another component of the sensor system. The intensity of the reflected light can be converted into an electric signal by optoelectronic transducers. When there is a deformation of the cantilever due to an applied force, this electric signal obtained can be calculated based on the resultant displacement. The sensitive resolution of this optical sensor is 20 nm. The calibration of the intensity of the optical sensor is a function of distance, as shown in Figure 4.2.

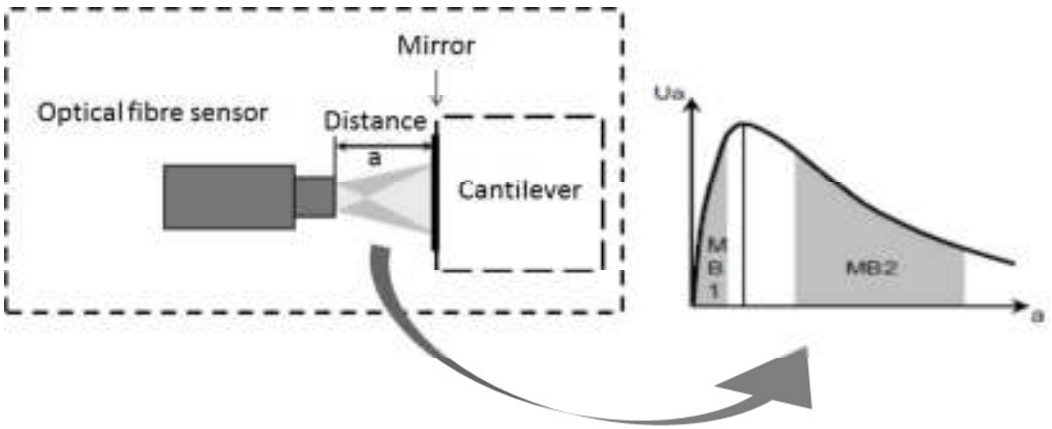

Figure 4.2 A schematic diagram showing the optical fibre sensor opposite to a mirror attached to one side of the cantilevers. There is a gap between the sensor and the mirror. The intensity of the reflected light varies depending on the distance. And, the relationship between the intensity of lights and the distance shows a peak value as a critical distance, used for the calibration.

The intensity increases with the decrease of the distance between the sensor and the mirror until a critical distance is reached. If the distance is shorter than the critical distance, the intensity will decrease. As such, to identify the critical position of the optical fibre which separates the measurement ranges as MB1 and MB2 (see Figure 4.2) called “peak finding”. The peak finding is conducted on site where the MUST tester shows a reading of a signal on screen. The result showed that varying the distance between the optical fibre sensor and the mirror would deliver different outcomes, and an appropriate value was selected between 4500 and 5000.

Calibration of the optical fibre sensor is important for the start of every experiment because systematic errors may occur due to deformation exerted on the setup of the cantilever and vibration.

On the other hand, the sensor system enables the mechanism to measure the deflection of contact using a pair of steel cantilevers which work as a spring. A schematic graph is shown in Figure 4.3 where the probe in contact with the surface makes the cantilever deflect. This deflection Δd is recorded by the optical-fibre. The deflection is over a range of micrometres and the force is over a range of milliNewtons.

Figure 4.3 The sensor system including a pair of cantilevers to show the level of deflection, which is captured by the optical-fibre sensor. A probe is attached on the cantilever and operated towards substrates (FALEX TRIBOLOGY, 2014).

To investigate the relationship of the force and deformation of the cantilever, we need to understand the stiffness of the cantilever. When the cantilever is considered as a spring, the stiffness coefficient can be obtained according to the Hooke's law. The following equation represents the relationship between the deformation and force exerted with spring constant k being the coefficient of stiffness.

$$\text{Tension} = k \cdot \Delta X$$

The calibration of the cantilevers is conducted directly on the MUST^{TM} tester when the peak finding for optical fibre sensor was already completed in advance. The experimental procedure started with adding loads on one side of cantilevers. If a false value of the stiffness coefficient (k) is set at 1 mN/μm, the results of the displacement (ΔX) should be the same as a tension applied.

The graph below shows a positive coefficient linear relationship between the applied load and the deflection. The gradient fitted represents the stiffness coefficient, see Figure 4.4. The stiffness coefficient used in the study is 0.4 mN/μm and a desired force range of the cantilevers is up to 1 N.

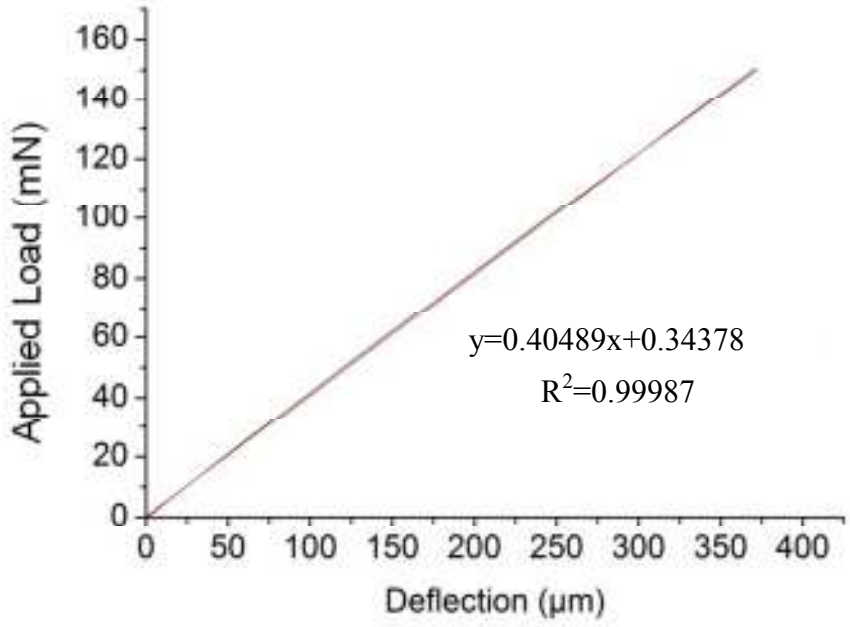

Figure 4.4 A positive coefficient linear relationship of the applied load and the deflection of the cantilever. The linear line represents the stiffness of the cantilever.

4.1.2 Motion Modules (Instrumental Module and Movable Module)

The MUST^{TM} tester consists of two motion modules, which are the instrumental module for vertical travel and the motional module for horizontal travel,

as shown in Figure 4.1. The instrumental module affords the sensor system to be configured during an experiment for the purpose of measurement. The movable module is a reciprocating device which has a stroke length of 20 mm. When an experiment starts, the movable module drives the sample platform to contact the sensor system. Figure 4.5 shows the configuration of the sensor system and the movable module for adhesion measurement, during which the movable module brings the tissue sample to make contact with the indenter, and then pulls away.

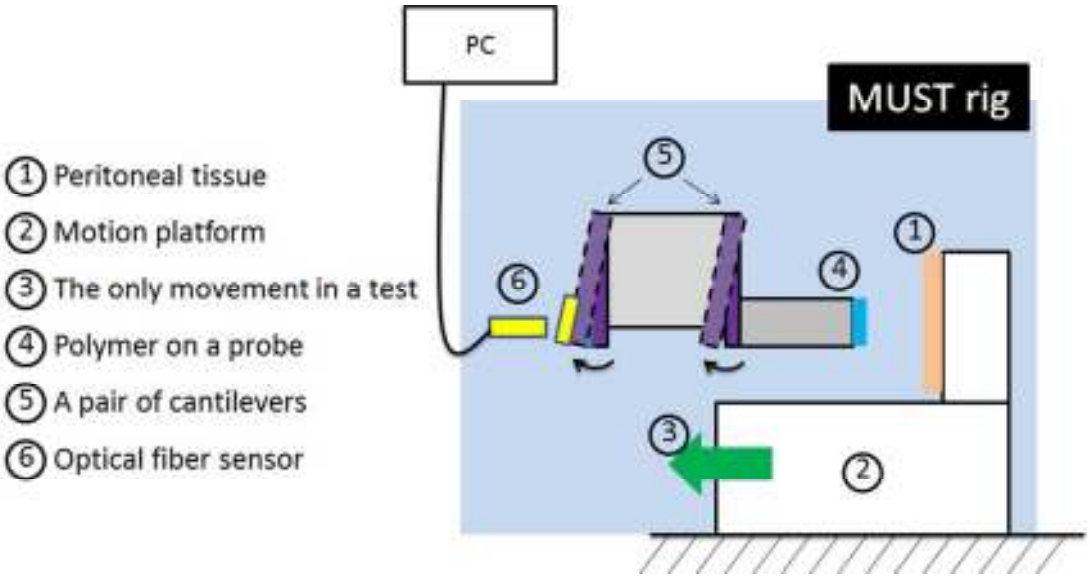

Figure 4.5 A schematic diagram of operating MUST^{TM} during a test.

4.1.3 Configurations

The configuration of the MUST^{TM} tester is to hang the indenter onto the cantilever either horizontally or vertically downwards to the sample. However, the configuration cannot be placed as in the setup of laparoscopic surgery. In addition to the setup, there is a clear bending effect, which influences the accuracy of the cantilever significantly due to the heavy indenter, as shown in Figure 4.6. Besides, the MUST^{TM} tester is not a proper device for measurement in a magnetic field because some components are prone to being magnetised (e.g., steel screws and

slide table). In order to present a more accurate result of magnetic retraction, an advanced setup called MagRAT tester was assembled.

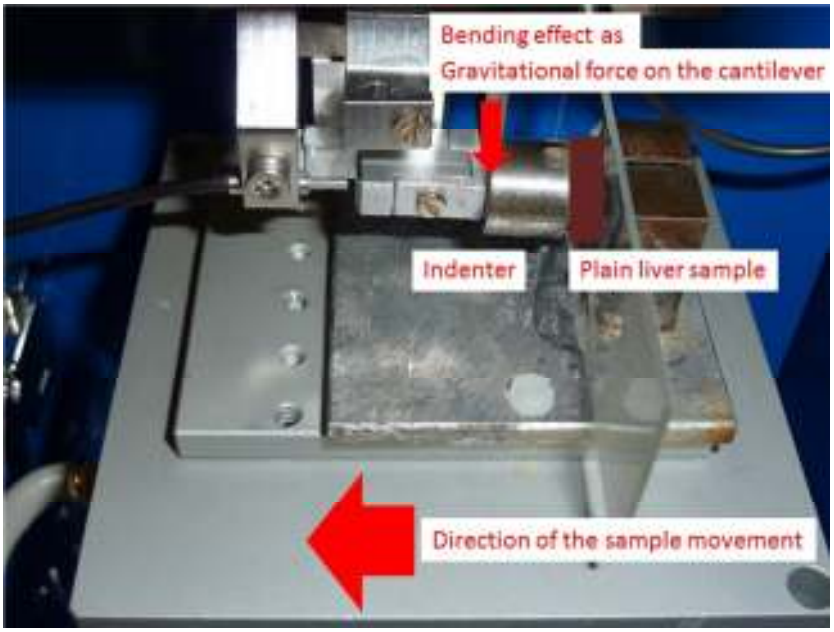

Figure 4.6 This photo shows the general setup of a MUST^{TM} tester with an indenter attached to the cantilevers. It clearly illustrates a bending effect when a heavy indenter renders an initial deformation and a torque.

4.2 Instrumental Adhesion Measurement – The MagRAT Tester

4.2.1 Configurations

A customised tissue tester, Magnetic Retraction and Adhesion Tester (MagRAT), was designed to simulate the entire procedure of tissue manipulation from conducting the injection to retraction. The tester is more flexible to overcome the magnification issue. It also costs less compared to other available modular testers currently on the market. Therefore, MagRAT was assembled with non-magnetic materials most of which were manufactured of aluminium in house at our workshop.

A preliminary adhesion measurement to test the feasibility of retraction was conducted using ferrofluids and a force module with a rolling mechanism. The rolling mechanism turned a torque into a linear motion so that it could manoeuvre a probing test onto the magnetised tissue manually, as shown in Figure 4.7. A flexible scale ruler was attached to the stroke to show the distance between the magnetised tissue and the magnetic probe.

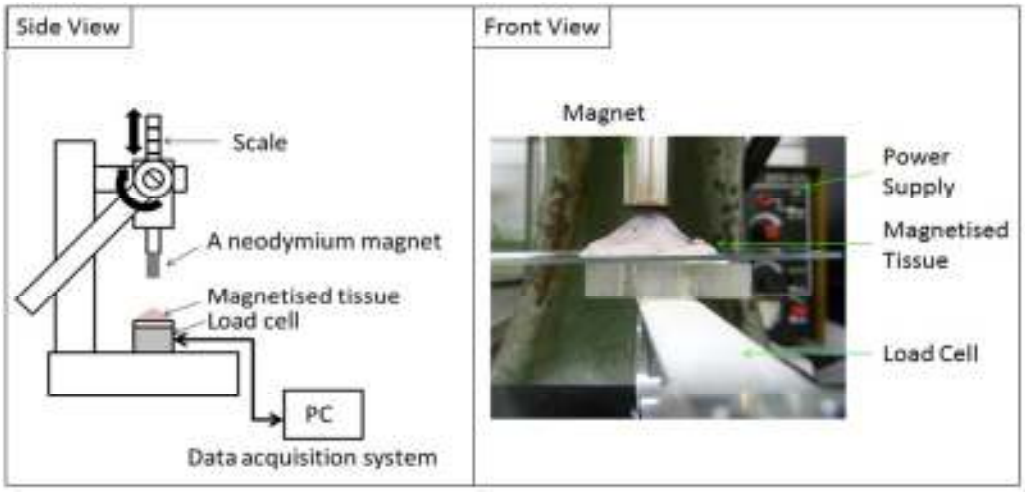

Figure 4.7 A schematic graph of an earlier version of MagRAT, which turned torque into a linear motion to control the magnetic retraction manually. The retraction experiment was conducted using a load cell to measure the force variation of the interaction.

4.2.2 A Force Sensor

The force sensor for the retraction experiment is a beam-shape load cell LCAE-600G, provide by Omega Engineering Inc.® (2013-2014), The load cell is connected to a power supply and a data acquisition system, NI-USB 6008 (National Instruments®, 2014), to record the dynamic force measurement. Its specification can measure up to 0.6 kgf with a resolution of ±10% of full scale output. The material was made of aluminium.

The adhesion result is expected to be less than 1 N within the specification (0-6 N). However, to reduce the number of errors of a scale difference from the equipment, the accuracy and background information about the sensor performance have to be altered during the calibration through several mathematical translations (Al Khaburi, 2010). The signal captured is controlled within ±1 Volt. The calibration procedure is a series of loading tests and is repeated for 5 times in order to get an overall error of the nonlinearity of 2.2 %, and the calibration diagram is shown in Figure 4.8. The potential difference has been rescaled and zeroed.

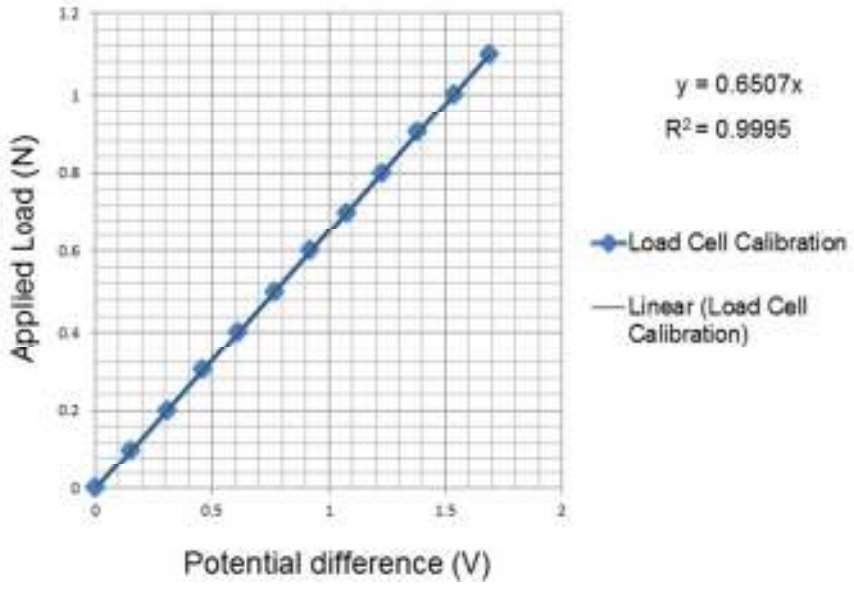

Figure 4.8 A load cell calibration diagram showing the calibrated range between 0 and 1.1 N.

4.2.3 Motion Modules

An advanced version of the MagRAT tester improves the functionality of automatic control from an earlier device with a motional module, as shown in Figure 4.9. The motional module includes two linear slides of T-LSR075B, provided by Zaber Technologies Inc.® (2014) to control the majority of the motions of tissue indentation. Each linear slide is driven by a step motor with a resolution of 0.49 μm, accuracy of 15 μm and a backlash less than 7 μm. The dimension of each is about

200 mm height and 65 mm width with a travel distance of 75mm. There is a maximum travelling speed could reach 20 mm/s, but in this study the travelling speed is set at 1 mm/s to allow the clearance of the magnetic effect on force measurement.

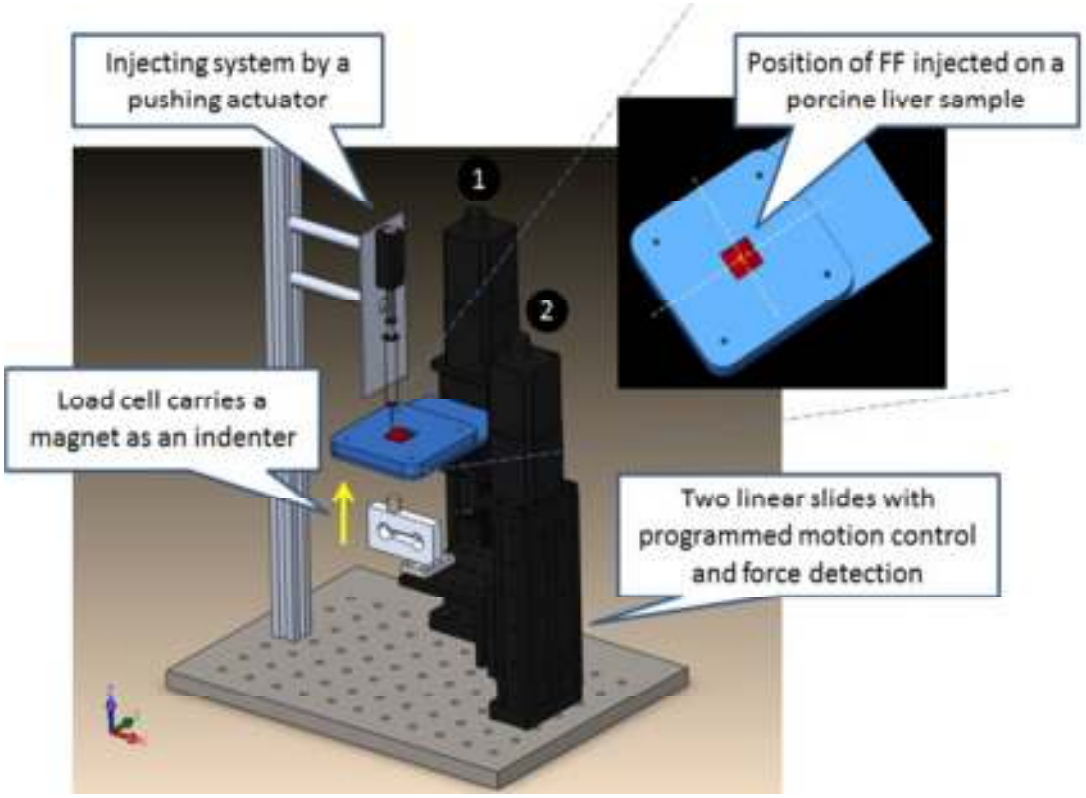

Figure 4.9 A schematic graph of an improved version of the MagRAT tester. There are two vertical linear slides which provide two parallel movements to conduct the indentation and pull-off tests.

The configuration shown in Figure 4.9 is for the normal indentation test, where one linear slide carries a tissue clamping plate for tissue to be magnetised and the other one carries the force sensor mentioned in session 4.2.2. Both linear slides in this configuration move vertically. The tissue clamping plate is placed in the middle of the injection system and the magnet on the force sensor. When one linear slide moves to conduct the injection or indentation procedure, the other stands by.

Figure 4.10 shows a different configuration of MagRAT tester which aims to test the shear adhesion. One vertically standing linear slide carries a force sensor and a magnet to provide an external magnetic field. The other is placed horizontally with a tissue clamping plate to conduct a lateral movement.

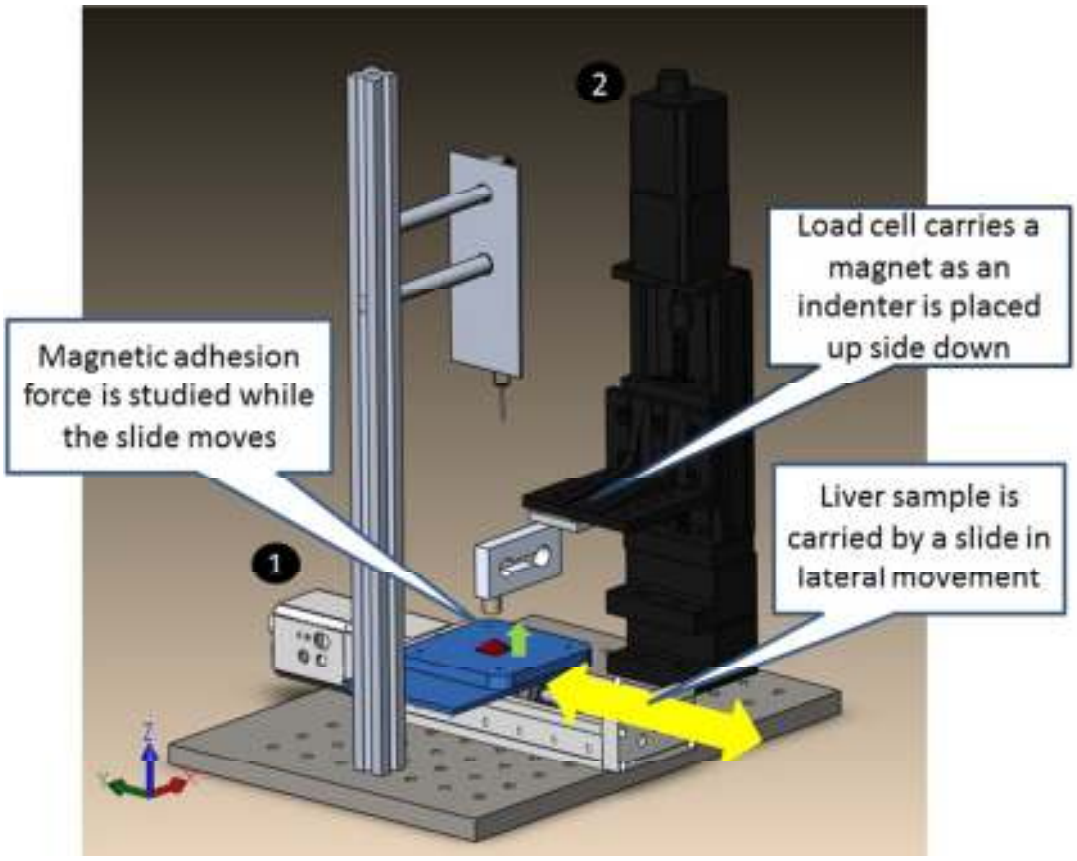

Figure 4.10 A schematic graph of different modes of MagRAT tester for shear adhesion measurement. Instead of two parallel movements, a tissue clamping plate that moves horizontally is set up to scan across the magnetic probe.

4.2.4 Magnetic Inducers

There are three different magnetic inducers made of Neodymium iron boron magnets (NeFeB). They are used to provide an external magnetic field for the retraction. All of them are in cylindrical shape and the geometries are listed: (M_A) 10 mm height and 20 mm diameter width, (M_B) 10 mm height and 10 mm diameter width and M_C is a combination of M_A and M_B.

The magnetic inducer is attached to the force sensor. The centre of the magnetic inducer is placed right under the tissue sample and aligned with the square hole of the clamping plate for a physical contact of indentation so as to retract tissue.

4.2.5 HIRST Gaussmeter

The magnetic flux is generated from the entire contact area of the magnetic inducers (M_A)(M_C) 78.5 mm^2 and (M_B) 314 mm^2. The magnetic field strengths are measured by using a portable hall-effect Gaussmeter GM08, provided by HIRST Magnetic Instruments Ltd.® (2004) with an accuracy of ±1%. The device is mounted on the side of MagRAT and the sensor is placed perpendicularly next to the magnetic inducer. When the adhesion measurement is ongoing, the magnetic inducer would move towards the sensor and the dynamic magnetic field strength would be recorded in terms of the function in light of the distance between the magnetic inducer and magnetised tissue, shown in Figure 4.11.

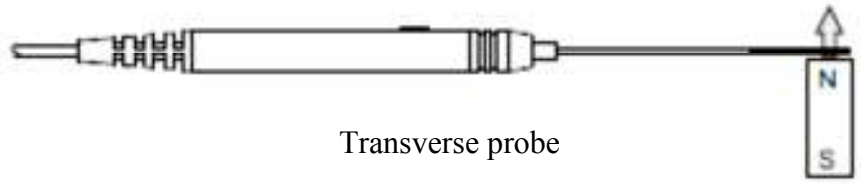

Figure 4.11 The GM8 Gaussmeter is attached to a transverse probe and the tip of the probe has a sensor detecting the magnetic field strength.

4.2.6 Instrumental an Injection Module

In order to make a customised tester to simulate the entire tissue manipulation procedure, MagRAT is used to improve the injection module, which allows tissue to be magnetised automatically and accurately. The injection module involves two steps: inserting the needle into tissue sample, and injecting ferrofluid through a

syringe. In the beginning of the injection procedure, a ferrofluid was filled with syringe and tissue samples (porcine liver, in this case) was cut into a 3 cm by 3 cm square and placed on a tissue clamping plate, which is clamped sandwiched between the upper and underneath plates, as shown in Figure 4.12. There is a square hole in the middle of each of the upper and underneath plates for injecting the ferrofluid and performing indentation tests, respectively.

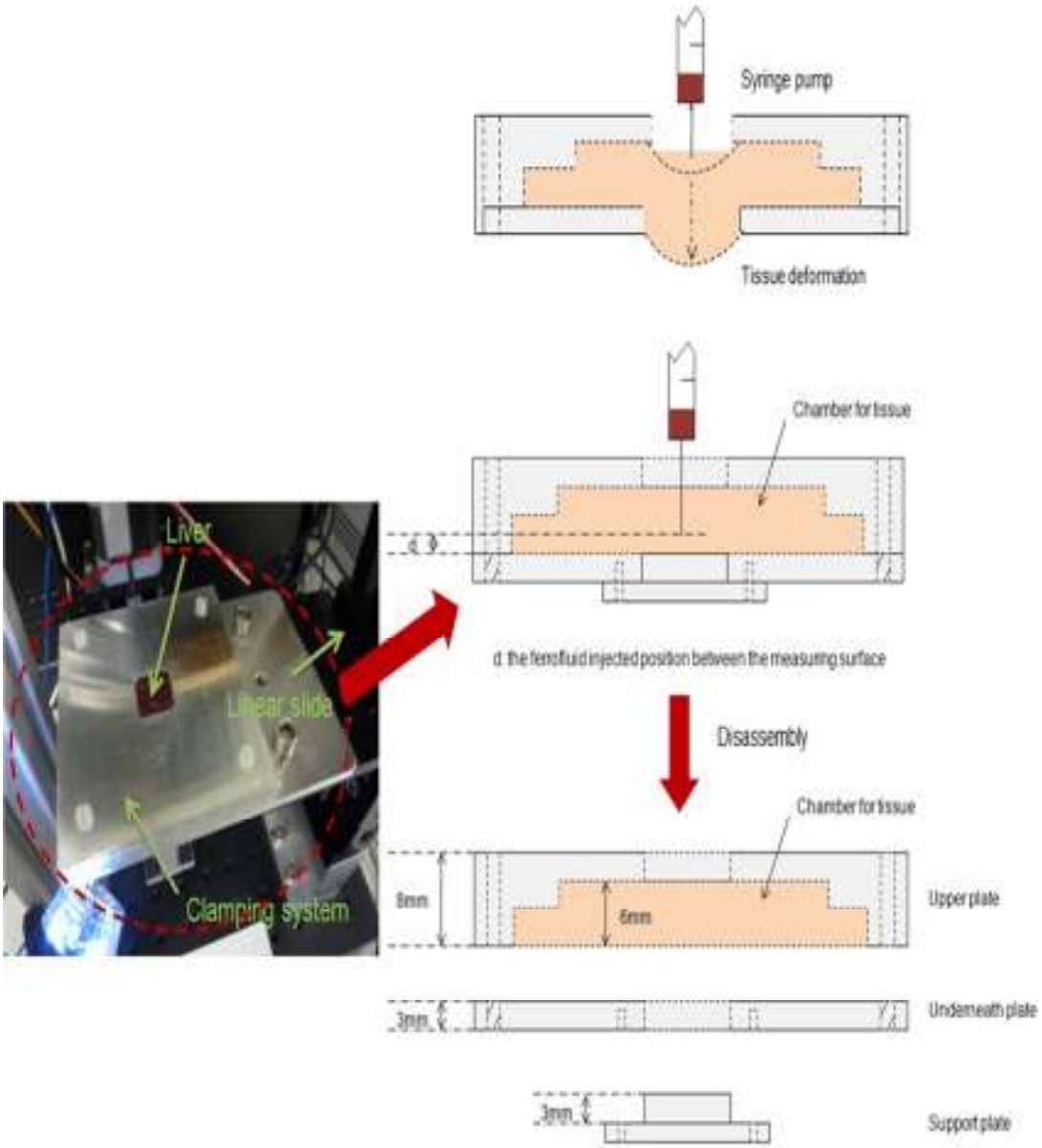

Figure 4.12 The photo and explosion graphs of clamping plates with a tissue sample in the square hole for injection and indentation. The top graph represents the difficulty of using the injection module due to tissue deformation. Hence, the support plate shown in the other graphs solves the issue of deformation.

Tissue deformation during the injection procedure in ex-vivo tests used to be an issue due to the pressure exerted on surface which would lead to an uncertainly depth of injection. The injected position of the injection is therefore one of the experimental parameters. In order to achieve an accurate injection, a solution is designed so as to attach another small flat plate to support tissue. This support plate is removed right after the injection.

A L12 linear actuator, provided by Firgelli Technologies Inc.® (2011) works as a syringe pump to push the syringe and lead an injection of ferrofluids. It has a 50 mm long stroke with a constant actuated speed of 1 mm/s. Tissue is pierced by a needle with a constant speed of 1 mm/s.

4.2.7 Sensor of the Injection Module

The injection module includes a sensor to detect the contact of the needle and the tissue surface. This is essential for providing a reference to the injected depth. The concept of the sensor is based on an electrical conductivity method to detect an electric circuit from the tissue. The electric current is supplied by a power supplier through the electrodes. As Figure 4.13 shows, a 1 kΩ external resistor (R1) is connected to the tissue, considered as an internal resistance of tissue (R2). There are two electrodes are attached to the tissue surface and the needle, respectively and wired to the data acquisition system. The configuration of the experimental arrangement is a series-circuit.

The contact of the tissue surface and the needle is like a switch (S1). When the surface is in contact, it forms a close circuit. The injection module is programmed to detect a 5 Volts potential difference (p.d.) to control the injection process. During

the process, the movement of the piercing needle starts when the p.d. is detected by the data acquisition system. The injection depth is defined from the contact.

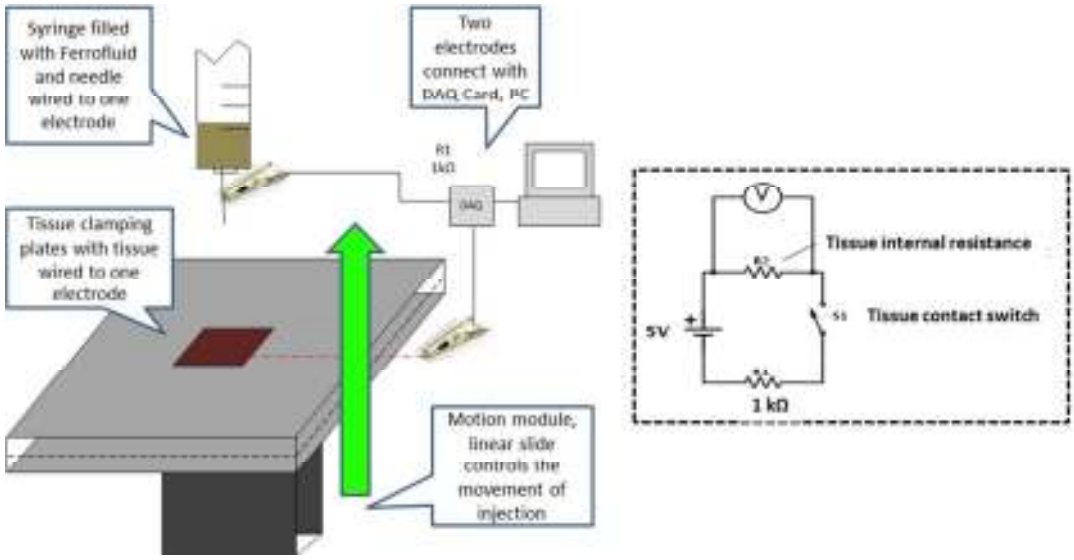

Figure 4.13 The electric conductivity method for the injection module works as a sensor to control the injection procedure. There are two resistances in the series circuits to make tissue contact work as a switch.

4.2.8 Procedures of Adhesion Measurement

The tissue manipulation procedure which utilises the MagRAT tester for experimental simulation involves two main processes: 1) an injection of FFs and 2) indentation for force measurement. The motions for the processes are programmed using LabVIEW® program with a user interface, which can be configured to execute a specific procedure, as shown in Figure 4.14. The main program includes different modularised sub programs for injection and force measurement to differentiate individual procedures.

Regarding the experimental procedure of injection, the ferrofluid under test is filled into a syringe on the injection module and a tissue sample is prepared and placed on the clamping plates. The clamping plates are fixed onto one linear slide, which would move toward to the needle. To initiate the injection module, a command would need to be given from the computer program.

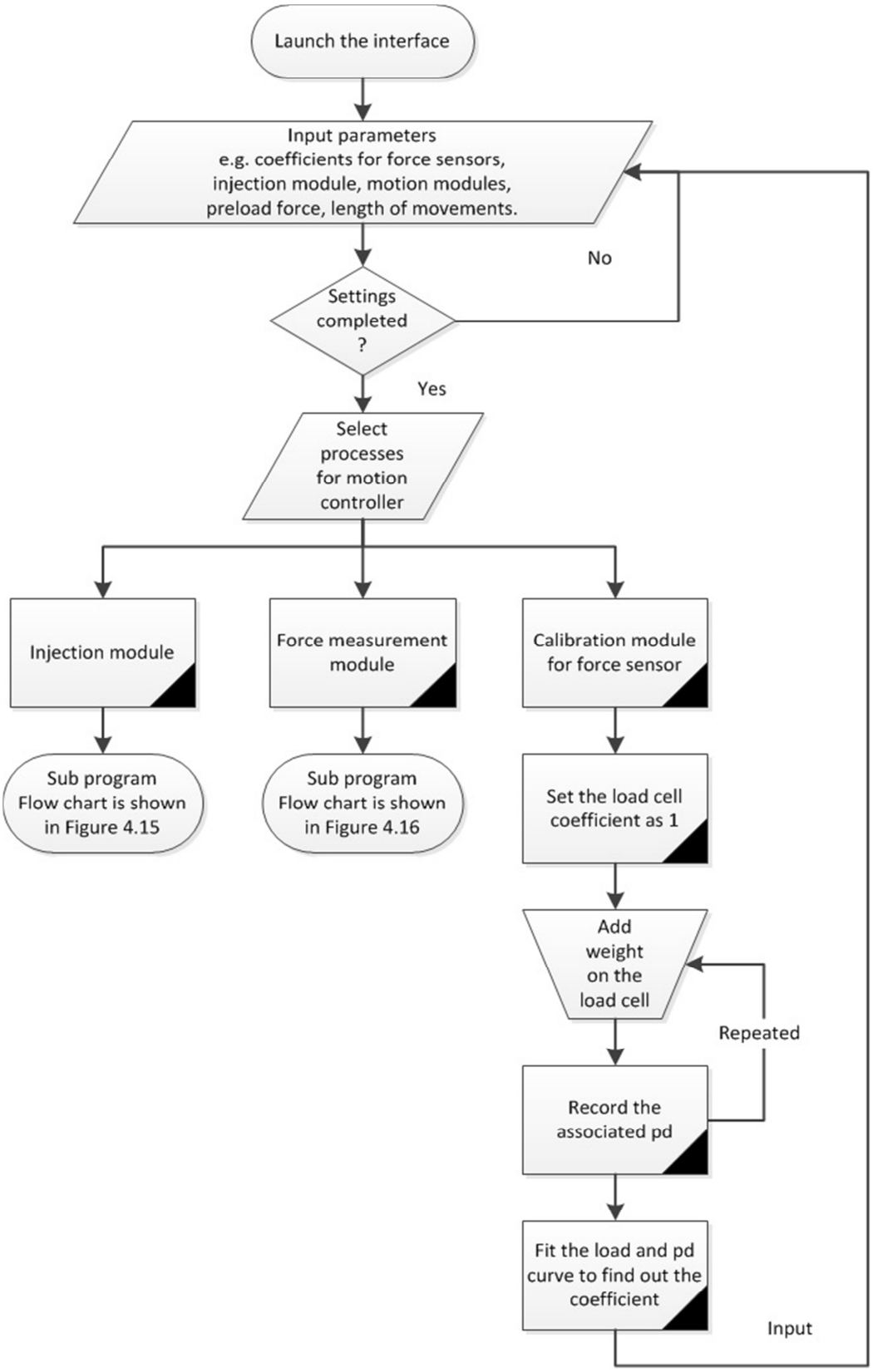

Figure 4.14 A flow chart of the design of the MagRAT tester which includes two main procedures and one calibration for a force sensor.

The steps of the entire injection procedure are shown in the flow chart (see Figure 4.15) and described below. Firstly, the linear slide drives the clamping plate to touch the tissue, and then the tissue is pierced by the needle for a given depth when the electrical conductivity method detects the contact of the clamping plate and the tissue (see section 4.2.7). Secondly, the syringe pump is actuated to complete the injection at the desired depth. The last step of the injection procedure is to bring the tissue platform back to the initial position for the force measurement.

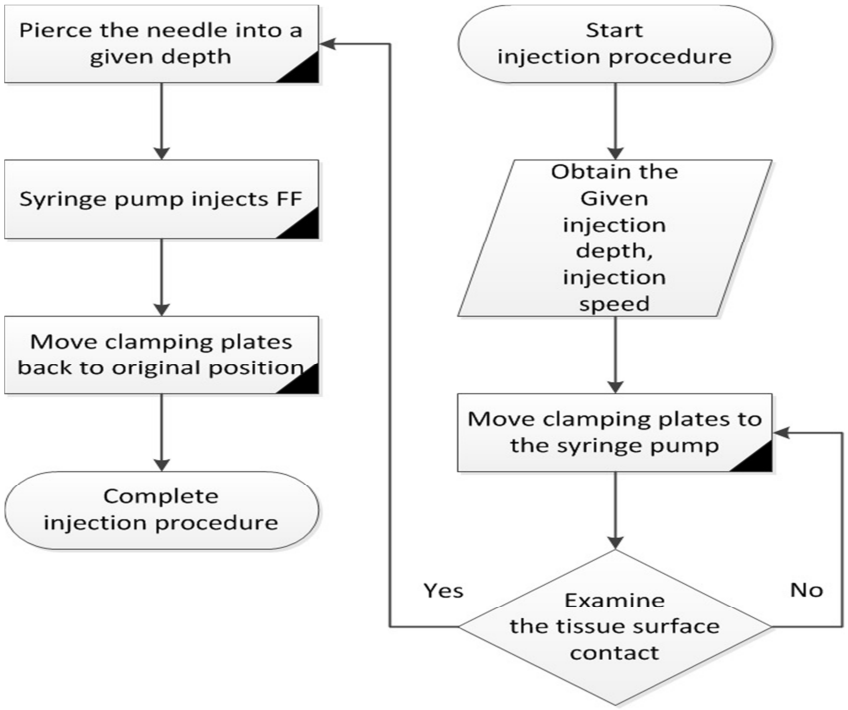

Figure 4.15 A flow chart of the programmed injection procedure which begins with preparing an experiment and ends when the injection is completed. The entire procedure is controlled by the computer program automatically with some given parameters, e.g. depth and speed.

The program for the force measurement is divided into two different modes for different adhesion measurement, normal adhesion and shear adhesion, as shown in Figure 4.16.

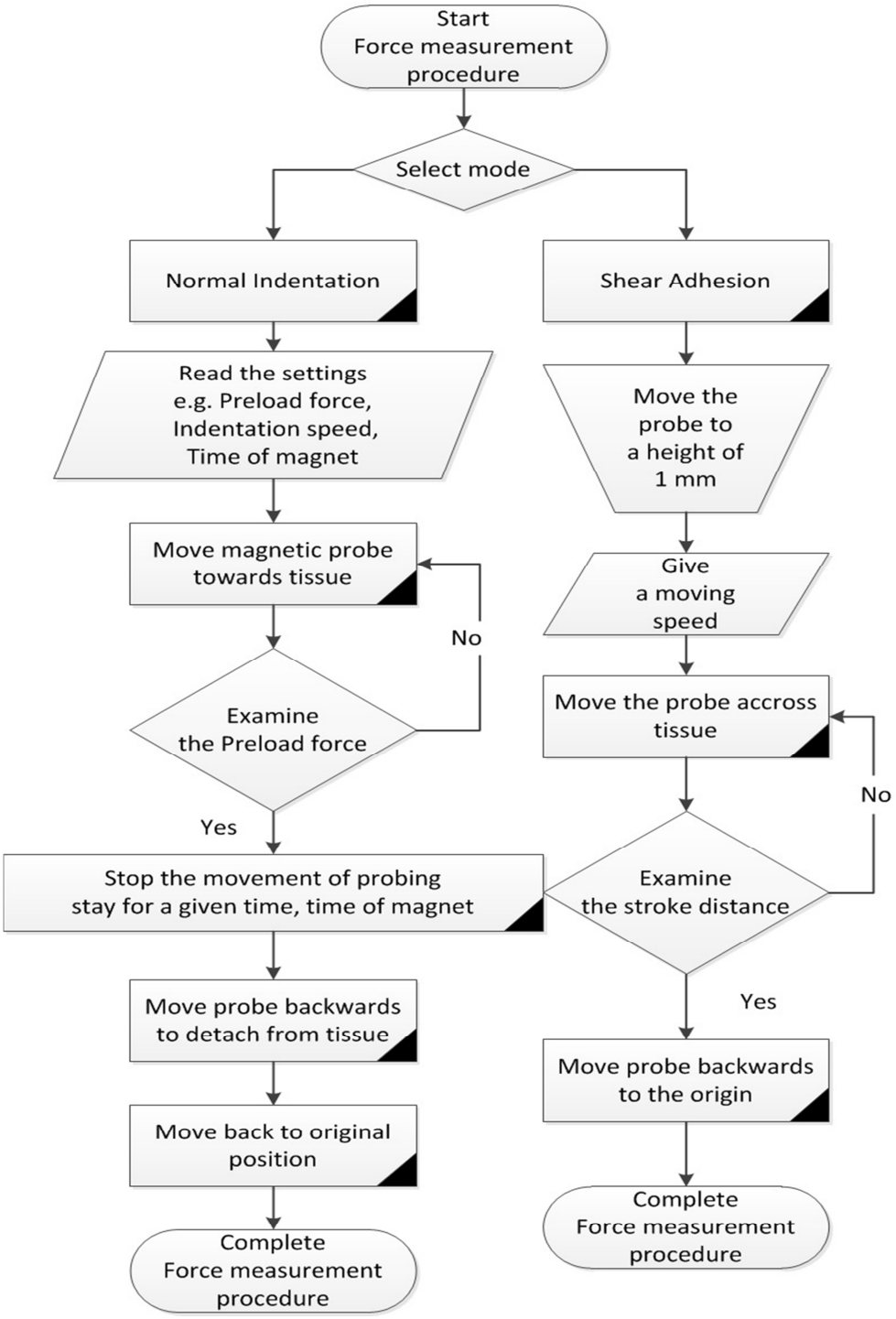

Figure 4.16 A flow chart of force measurement for two different adhesion modes: normal and shear.

Normal adhesion can be defined by measuring the pull-off force from a contact between the magnetic probe and the magnetised tissue. The procedure is a combination of pull-off tests and indention tests. It starts from probing tissue perpendicularly, as shown in Figure 4.9. In the force measurement, the magnetic

probe is commanded to move towards to the tissue first. The forward movement brings the device to contact the tissue surface until the force reaches a pre-decided value of 20 mN, as the preload. The movement stops immediately at the preload, and stays at that position for a given time. During this period, the magnetic probe is in contact with the tissue. Therefore, it is named “the time of the magnet”.

Afterwards, the magnetic probe is detached from the tissue and moves back to its original position. The normal adhesion measurement can be repeated for 100 cycles in each configuration. Shear adhesion happens when an adjusted scratch test is performed. The procedure is to move the magnetic probe for a distance of 1 mm height from the magnetised tissue, and stays at that position.

In the shear experiment, the slide, carrying the tissue clamping plate, moves in with reciprocating motion underneath the magnetic probe, as shown in Figure 4.10. The slide moves back to initial position to complete one cycle of the track. The shear adhesion measurement can be repeated for 100 cycles at each track.

4.2.9 Procedures of Tissue Retraction Examination

In order to examine the retraction of tissue manipulation using ferrofluids, the optimised testing environments are selected from the ex-vivo force measurement. The procedure is as the same as the preparation of force measurement and the test is conducted using the MagRAT tester. Testing samples are three sections of the porcine colon. The content of colon is cleaned in advance and then is prepared into three sections with the weights of 120, 90 and 30 g. The experiment only presents the ability of retraction. The retracted distance is measured using a vernier-caliper. The results evidence how much load the tested environment could achieve.

4.3 Sample Specification

In the ex-vivo tests, tissue samples, e.g. rat peritoneum, porcine liver and colon, have been tried at different stages. At the preliminary stage, rat peritoneal tissue is harvested through the dissection procedure at the Central Biomedical Services at the University of Leeds, as shown in Figure 4.17. The dimensions of the peritoneal tissue are trimmed to a size around 25-30 mm height and 15-20 mm width. The thickness is very thin, only 1-2mm. The rats used for the experiments are easy to feed and grow up quickly. Tissue is immersed in Phosphate Buffered Saline (PBS) solution prior to the experiments so that a consistent pH value of 7.4 can be maintained. The osmotic concentration and ion concentrations of PBS buffer solution work on most of the tissue (isotonic). The tissue is glued to a glass slide in the force measurement.

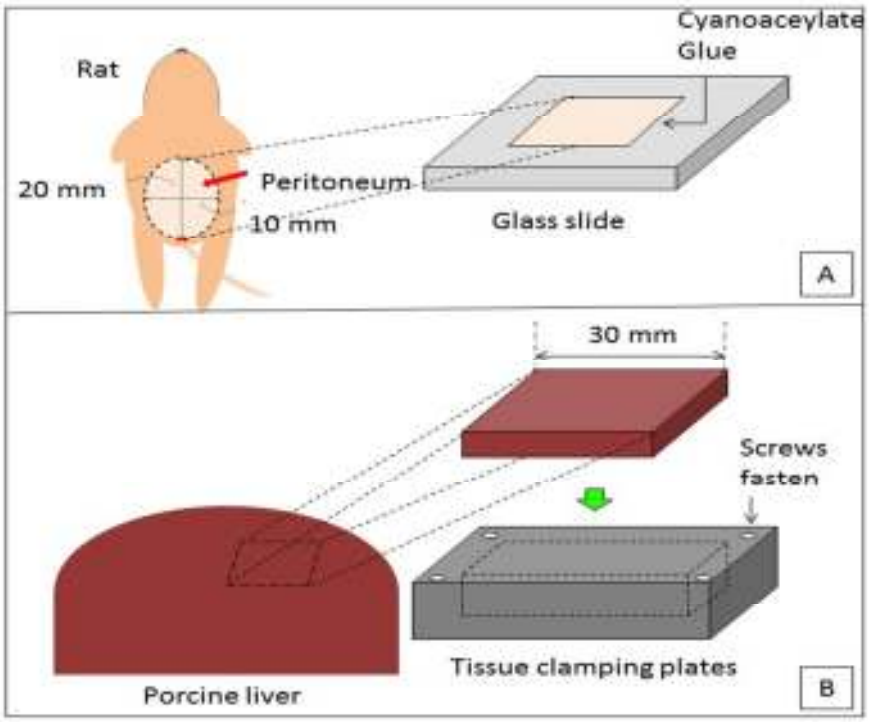

Figure 4.17 Procedures of preparing the tissue samples of rat peritoneum and porcine liver, all the samples were prepared in-situ and cut using the scalpel.

However, it is difficult to study the injection position without a precise depth control. Therefore, instead of using rat peritoneum as tissue samples, porcine liver is used because it is more rigid and thicker which makes the injection easier. Liver sample is delivered from the abattoir and is cut from the surface into square pieces of 30 mm by 30 mm, as shown in Figure 4.17. Then the liver sample is fastened using some screws onto the clamping plate for the force measurement.

To demonstrate the ability of retraction in the ex-vivo experiment, porcine colon is used for the tissue manipulation. The colon sample is chopped into several pieces, each of which weight about 300 g, 450 g, 600 g and 1 kg. During the demonstration, the colon sample is placed on a flat table and indented by the magnetic probe in order to present the feasibility for retraction.

Ferrofluids are already widely used in mechanical and medical applications due to their unique fluidity and magnetism. They are composed of magnetite particles (Fe_3O_4), suspended with a carrier fluid. The sizes of their particles are within the nano-scale to ensure the particles are stable in the fluids and are superparamagnetic in nature. The importance of this magnetism is that superparamagnetic particles can only be magnetised in a magnetic field. In other words, they do not present magnetism in the absence of magnetic fields.

The ferrofluids used in this work are selected from the existing biomedical applications (Odenbach, 2004, Shinkai, 2002, Silva et al., 2012). The particles are normally covered with hydrophilic polymers which protect them from aggregation by foreign ions (Lin et al., 2005). Furthermore, the particles are coated with different surfactants which allow them to interact with specific molecules. Table 4.1 shows the ferrofluids chosen to study different properties, e.g. concentration, particle sizes and coated surfactants of the particles.

The effect of particle sizes of the available range from 10, 50, 100, 200 to 1000 nm are investigated to understand their effects. A home-made magnetic fluid with an average size of 45 μm is used to verify the difference of force performance. The size of a particle is defined by an average size provided by the companies without taking the thickness of surfactant layer into account. However, the particle size varies and the basis might aggregate. The size distribution is characterised in session 4.4.

Table 4.1 Specifications of ferrofluid chosen in this study, 1 denotes the sample provided by Chemicell™ (2010); 2 denotes the sample provided by micromod© (2014); 3 denotes the sample provided by Liquids Research Ltd (2014).

Denotation	Functional coating	Particle size (nm)	Concentration (mg/ml)	Application
UCC- [1]	None	50, 100, 200	25, 100, 200	Absorption of biomolecules (Cationic charged)
NP-IO- [2]	None	200	200	
AMINE- [1]	Amine silane	50	25	Coupling of biomolecules
DXS- [1]	Chitosan	50	25	Linear, biodegradable polymer
DEAE- [1]	Starch	50	25	Binds cells, bacteria, viruses
SIMAG- [1]	Polymer	1000	25	
UCC- [3]	None	10	25, 100, 200	
UCC-isoparaffin [3]	None	10	25, 100, 200	

4.4 Particle Sizing Measurement

A dynamic light scattering (DLS) instrument – Zeta NanoSizer, provided by Malvern® (2014), is used to characterise the average nano-particle sizes and the numbers of the size distribution of the testing ferrofluids. DLS is the technique

currently used for measuring particle sizes ranging from nano-meters to microns. The equipment is equipped with a laser to the cuvette contained with the sample. A detector is placed at a certain angle to record the scattered light intensities over a time series, as shown in Figure 4.18 (Chicea et al., 2012). The measurements are done at room temperature 20°C and the following parameters are used for size estimation: refractive index of Fe_3O_4 and water are 2.42 and 1.33, respectively. The absorption coefficient of Fe_3O_4 is 0.01. All the tested ferrofluids are diluted into a series of concentration of 1, 0.5 and 0.1 wt%, respectively.

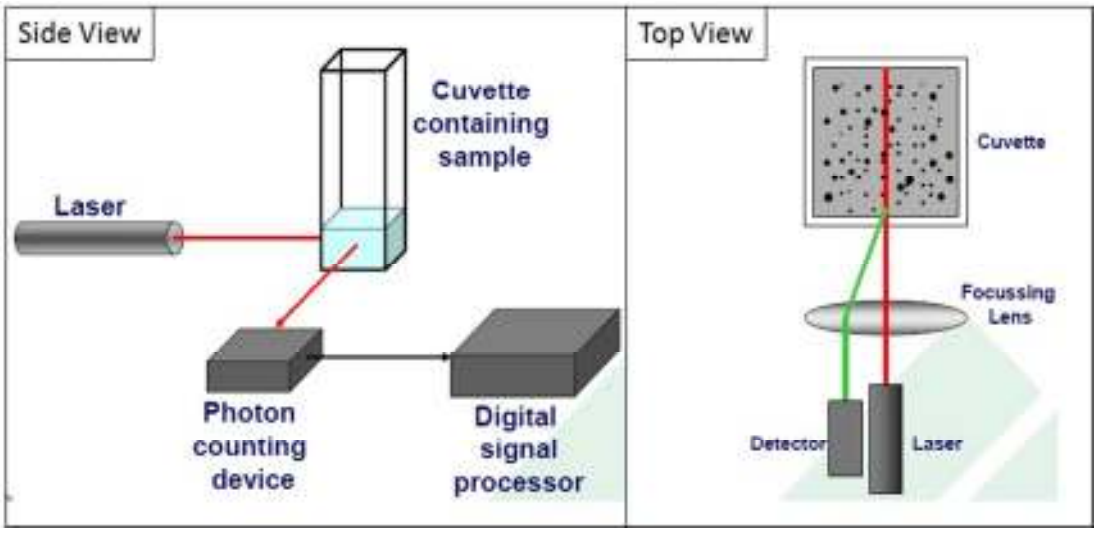

Figure 4.18 This schematic graph representing the configuration of the particle sizing measurement using the Malvern DLS nanosizer. The scattered laser lights of the particles are collected by the detector (Malvern®, 2014).

4.5 Particle Density Distributing Measurement

To study the influence of the retraction from the migration of particles, a micro CT scanner is used to characterise the particles density distribution of a magnetised tissue after the magnetic retraction in the ex-vivo tests. There are several microscopic methods available to characterise the particles, e.g. Transmission Electron Microscopy (TEM) and Scanning Electron Microscopy (SEM). However, a

significant issue associated with the injection is that the transparent lights have caused difficulty in penetrating a depth over 100 µm. CT is equipped with a rotating X-ray tube, which can ionise the atoms and molecules of the materials and allow the radiation to pass through to generate images from different directions, as shown in Figure 4.19. Different materials can be distinguished because they have different attenuation coefficients.

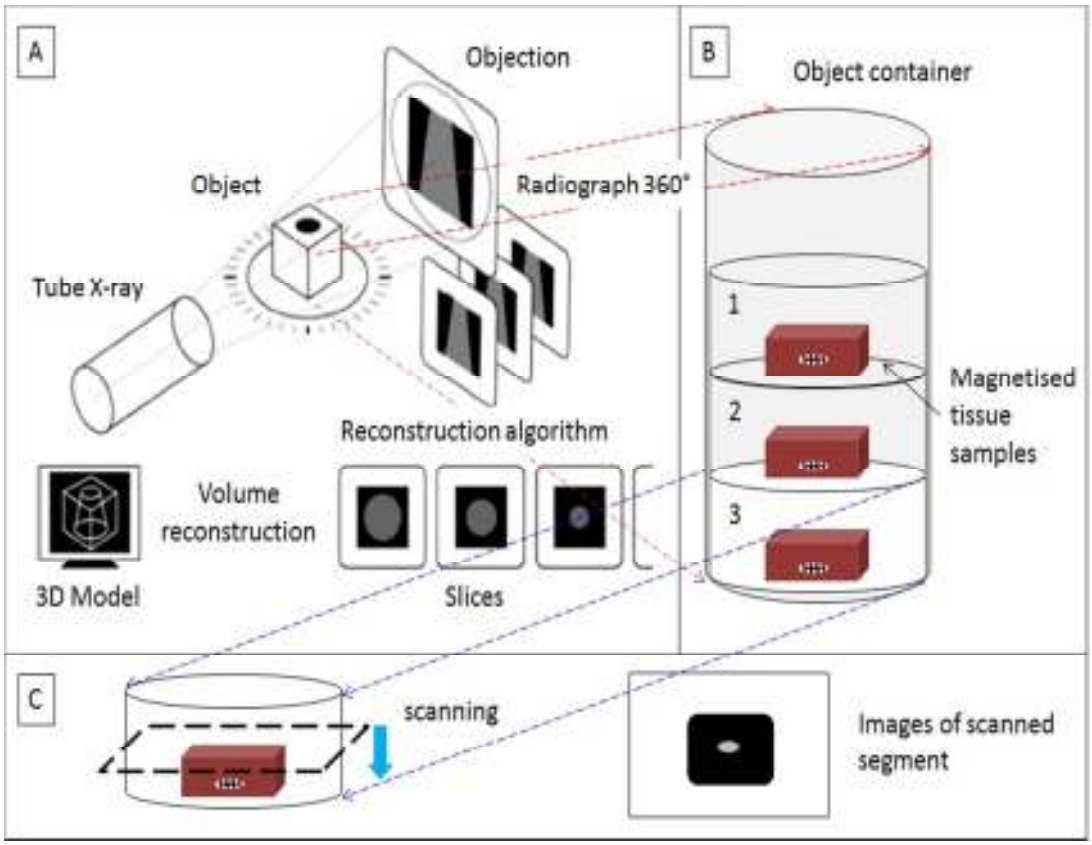

Figure 4.19 (A) The principle of Computed Tomography (micro CT) (Wang et al., 2010a). (B) The configuration of the object tissue samples in a container filled with wool fibre. (C) The object is scanned and represented as a series of segment showing the density of metallic particles.

The experimental setup is shown in Figure 4.19, where the magnetised tissue is placed in separate Petri dishes. The reason for putting them in different containers in series carefully is to avoid dis-alignment. Wool fibres are used to fill up the empty space in the container to fix the position of the tissue.

The finest resolution of the voxel in the experiment is 6.2 μm, which is still much larger than all the other particles in the tested ferrofluids in nano-scale. However, each segment still reveals the information of the density of the particles distribution through image analysis, conducted by a Matlab® program to convert the segments into grey scale so as to identify the contrast between bright and dark. The results will be presented in Chapter 6.

4.6 Taguchi Method for Parametric Analysis

In order to optimise the testing conditions from the ex-vivo results and apply the magnetic retraction on the in-vivo tests, the parametric study is evaluated by an experimental design using Taguchi Method. The Taguchi method is widely used to compare the effects of multiple parameters during their interactions (Grieve et al., 1998) from a combination of the statistics and engineering perspectives.

Traditional experimental design for comparing four independent parameters at three different levels requires a large number of individual experiments (81 experiments) and the numbers can be expanded to 405 if each experimental setup is repeated 5 times. Normally, the traditional experimental design is time-consuming, requires a long process of tissue processing and costs expensive to carry out.

Therefore, the Taguchi method is introduced as an alternative approach to experimental design to determine parameters affecting the performance of retraction. Besides, the statistical analysis of Taguchi method can also evaluate the significant levels of each parameter to convenient for optimisation of the experimental configurations.

Taguchi (1993) defined those experimental parameters which could be designed in the experiment as internal parameters, and those unable to be designed in the experiment as external parameters. In this study, the particle size, concentration and volume of the ferrofluids as well as the magnetic field strength are the internal parameters. The external parameters include the mechanical properties of soft tissue, e.g. stiffness, weight and the duration of operations.

The Taguchi method then uses an orthogonal array to distribute the internal parameters used in the study, as shown in Table 4.2. The distribution of the parameters has to be arranged in a balanced manner. The reason for balancing is to have an equal number of levels within each column (Morsi et al., 2004).

Each orthogonal array is identified by the form $L_A(B^C)$. *A* represents the number of experiments conducted using this design. B denotes the number of investigated levels within each column. *C* identifies the number of columns available representing parameters used in the experiment.

For example, as shown in Table 4.2, the orthogonal array $L_9(3^4)$ requires 9 experiments to investigate 4 different parameters, each of which is set at 3 predetermined levels. The design of the array enables the effect of each parameter to be separated from one another so as to ensure the statistical independence. The size of the comparable experiments is reduced from a hundred to nine and the effects of the interactions between the parameters are examined.

Table 4.2 $L_9(3^4)$ Taguchi matrix with four parameters and three levels.

Experiment	Parameter 1	Parameter 2	Parameter 3	Parameter 4	S/N
1	1	1	1	1	S/N_1
2	1	2	2	2	S/N_2
3	1	3	3	3	S/N_3
4	2	1	2	3	S/N_4
5	2	2	3	1	S/N_5
6	2	3	1	2	S/N_6
7	3	1	3	2	S/N_7
8	3	2	1	3	S/N_8
9	3	3	2	1	S/N_9

In the analysis of the Taguchi method, the means, variances and signal-to-noise (S/N) ratio are calculated from the experimental results to determine the influence of the parameters on the performance. The S/N ratio, defined as the standard deviation of the performance parameters for each experiment divided by the total number of experiments, provides a measure of the impact of noise factors on performance. Therefore, an optimised testing environment is found and then applied in in-vivo experiments.

$$\frac{S}{N}=-10\log_{10}V$$

In which the variance, V, is given by

$$V=\frac{1}{N}(Y_1{}^2+Y_2{}^2+Y_3{}^2+\ldots+Y_N{}^2)$$

Where N is the number of noise factors and Y_i is the result from each test.

4.7 In-vivo Experimental Arrangement

Six white pigs weighing 25-30 kg are brought in from the Leeds University Farm seven days before the procedure. They are starved for 14 to 16 hours prior to the sedation. For the sedation procedure, an intramuscular injection of Stresnil (Azaperone, Janssen Animal Health, UK) of 40 mg/ml at a dose of 2.25 mg/kg and an intramuscular injection of Hypnovel (Midazolam, Roche, UK) 5 mg/ml at a dose of 0.32 mg/kg are used. The animals then are left in a quiet, dark area for twenty minutes before being transported to the induction room.

The induction procedure involved inserting a 22G intravenous cannula into a marginal ear vein that is secured by an adhesive tape. The induction agent is Rapinovet (Propofol, Schering-Plough Animal Health, UK) 10 mg/ml at a dose of 4 mg/kg. After the animal is induced, it is intubated and applied with general anaesthesia using inhaled Isoflurane at 2-4% in oxygen. The animal is placed on its back so that its abdomen is prepared with cleansing solution and draped.

The in-vivo experiment is performed through a midline laparotomy. Ferrofluids, selected from the optimisation study, are injected into the mucosa layer of the colon wall manually by surgeons. The volume of injections are 0.1, 0.2, 0.3 ml respectively on each single location. The surgeons hold several different magnetic probes to induce the magnetised location. The performances of different configurations are examined if the retraction is successful. Every experimental configuration is repeated three times in both vertically and horizontally movements. The retraction height is measured using a scale ruler.

Chapter 5 Results from the Tissue Retraction Experiments

The ex-vivo and in-vivo experiments are conducted to explore the feasibility of using ferrofluids to manipulate tissues. The measurement focuses on two aspects: 1) the capability of adhesion and retraction forces of ferrofluids, 2) the requirement of experimental environment to retract tissues. This chapter presents the results of ex-vivo and in-vivo tissue retraction experiments. It is structured as follows. Section 1 presents the results of adhesion measurement obtained from the ex-vivo experiments based on various variables of ferrofluids, e.g. with and without coating surfactant, particle size, concentration, volume, preload, magnetic field strength, duration of time of magnetisation and shear effect. Section 2 presents the characterisation of the sizes of those particles suspended in ferrofluids. Section 3 presents the study of optimisation of the experimental environment and the influence of each parameter. Section 4 presents an in-vivo study of the tissues retraction in the pig model. The optimised parameters are applied to the ex-vivo and in-vivo tissue tests in order to demonstrate the capability of manipulating tissues using magnetic retraction. Section 5 gives a summary of the measurement done in this chapter.

5.1 Ex-vivo Experiments

5.1.1 Adhesion Force Profile

The typical force-time profile from the adhesion measurement is shown in Figure 5.1, where the Y axis represents the retraction and adhesion force and the X axis represents time elapsed. Time is recorded when the force measurement started.

Therefore, the entire motion of a single cycle during the retraction simulation can be explained by the profile in sequence.

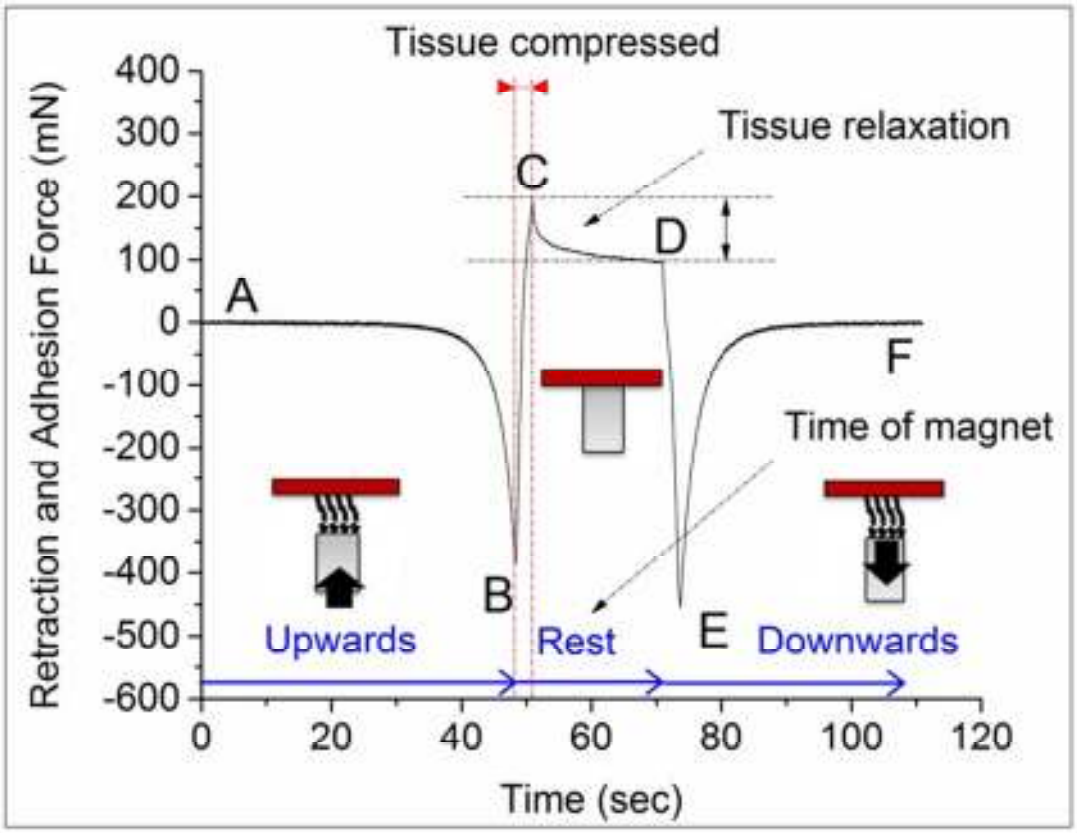

Figure 5.1 A typical force-time profile of a full cycle of tissue manipulation.

Point A is the beginning of every force measurement, starting right after the injection. Period AB records the response while the magnetic probe moves towards the magnetised tissue. Point B shows a maximum retraction force occurring when the probe is in contact with the tissue. Period between the point B and C shows that the probe continues to squeeze the tissue until the interaction force reaches a pre-defined load, which is the point where C shows a maximum preload applied on the interface. The probe is allowed to be in contact with the tissue during period CD, defined as “time of magnetisation”. After this period, the magnet is moved backward to measure the adhesion force (period DE). At point E, the probe is completely

detached from the tissue and the maximum adhesion force will be recorded. Lastly the probe is moved back to the initial position after the period EF.

5.1.2 A Test of Plain Tissues

Figure 5.2 shows the adhesion measurement of the plain porcine liver tissue. The graph only shows two peaks representative of the values of the preload and maximum adhesion force, respectively. There is no retraction shown in the graph before the contact of the probe with tissue. The force response goes up directly to a preload level without any magnetic retraction.

Refering to the figure that the maximum adhesion force occurs when the tissue is fully detached from the contact of the probe. This can be considered as a part of the retraction at point X marked on the figure, which matches the physical model in section 3.1.

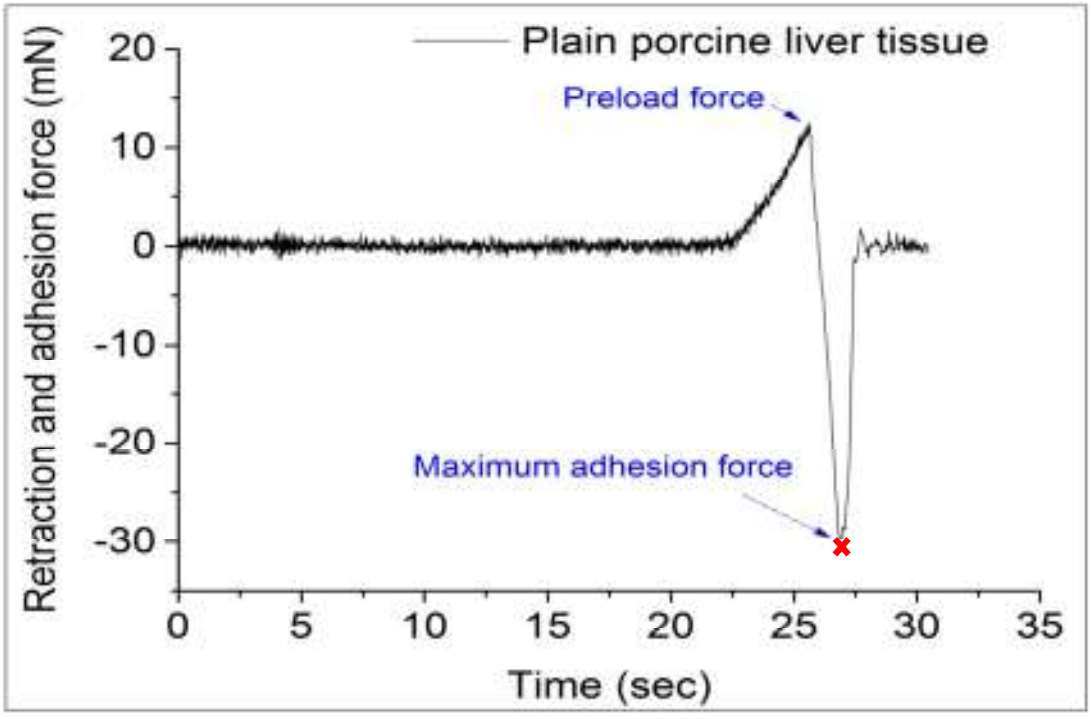

Figure 5.2 Initial force-time response for a plain tissue indentation with a preload force of 15 mN and a maximum adhesion force of 30 mN.

5.1.3 Tests of Various Ferrofluids and Magnetised Tissues

The tested ferrofluids have been described in section 4.3. In the following results, the ferrofluids are denoted by the coating with the particle size, as shown in Table 4.1.

The tested ferrofluids can be separated into the suspensions with coated and non-coated particles. To distinguish the original performance in retraction of the coated and non-coated ferrofluids, the experiments were conducted using the samples applied onto tissue as well as samples without tissue in order to reflect the reality of retraction effect. The tests of the ferrofluid tested in the containers are called “pure ferrofluids tests”. Those “magnetised tissue tests” are with the ferrofluids injected into tissues.

The magnitude of the maximum adhesion force for each 0.1 ml coated ferrofluids exposed to a 0.6 T magnetic field is shown in Figure 5.3. The tested concentration is 25 mg/ml. Compared to the magnetised tissue tests, the adhesion force in the pure ferrofluids tests is significantly greater. In the pure ferrofluid tests, the case of ferrofluid with particles coated with aminosilane (AMINE) shows a very similar value in the different particle size of 50 and 100 nm as 21.72±2.6 mN and 20±2.88 mN.

When the particle size is as the same (50 nm) with different coating materials, dextransulfate (DXS) and diethylamine ethyl starch (DEAE), the results show 12.93±1.55 mN and 15.95±0.8 mN in retraction. The largest particle size of 1 μm coated with silica presents a maximum adhesion force of 23.39±0.92 mN. The magnetised tissue tests show very little retraction effect which only occurs between 0 to 4 mN, less than 1 gram force.

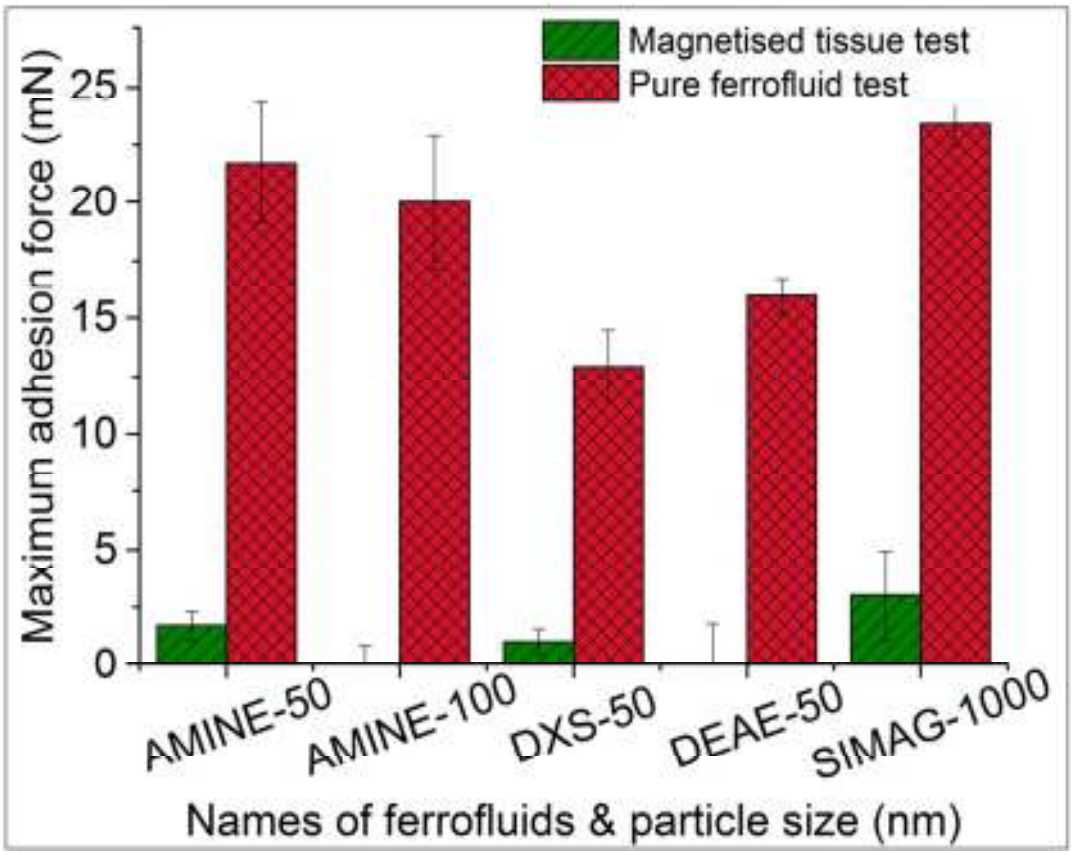

Figure 5.3 Performance of coated FFs in retraction. The coated materials include aminosilane (AMINE), diethylamine ethyl starch (DEAE), dextransulfate (DXS), silica (SIMAG). The notations are labelled with its particle size (nm). The tests of the ferrofluid tested in the containers are called "pure ferrofluids tests". Those "magnetised tissue tests" are with the ferrofluids injected into tissues. The testing environment is a volume of 0.1 ml ferrofluids with a concentration of 25 mg/ml exposes to a 0.6 T magnetic field.

On the other hand, Figure 5.4 shows the magnitude of the maximum adhesion force of 0.1 ml non-coated ferrofluids in an experimental environment of a 0.6 T magnetic field with dfferent particle sizes, 10, 50, 200 nm. The experimental concentration is increased to 200 mg/ml. The results from the pure ferrofluid tests with a particle size of 200 nm are very similar to 135.36±1.92 and 135.4±1.7 mN.

It can be concluded that ferrofluids from two different providers with the same particle size have a similar capability of attraction. The adhesion force increases with the decrease of particle sizes. The ferrofluid with a particle size of 10 nm

within a carrier fluid of iso-paraffin shows the highest adhesion force of 356.79±4.63 mN.

Compared to the pure ferrofluid tests, the results from the magnetised tissue tests decrease but the maximum adhesion force is consistently observed to be higher given the smaller particle sizes. The two ferrofluids with the finest particle size of 10nm in this study show 114.61±30.6 and 149.49±22.52 mN in retraction, which fall into a range of 11 to 15 gram force.

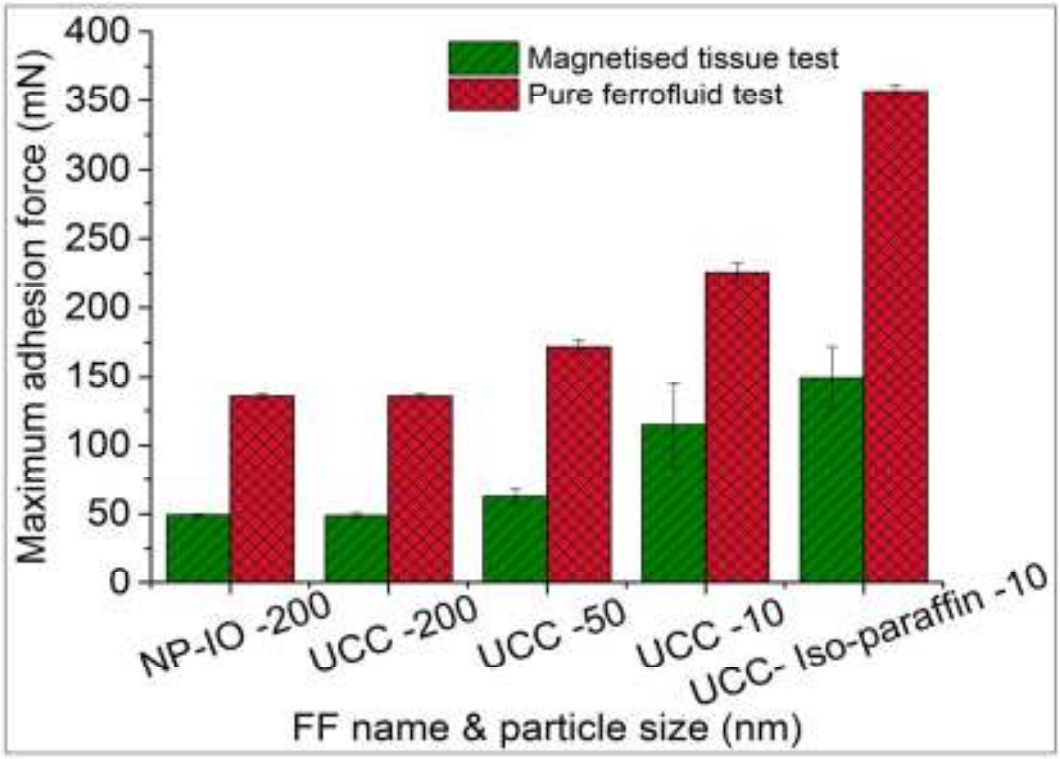

Figure 5.4 Performance of non-coated ferrofluids with various particle sizes of 10, 50, 200 nm. The testing environment is that a volume of 0.1 ml ferrofluid with a concentration of 200 mg/ml exposes to a 0.6 T magnetic field. The tests of the ferrofluid tested in the containers are called “pure ferrofluids tests”. Those “magnetised tissue tests” are with the ferrofluids injected into tissues.

It is compared between Figure 5.4 and Figure 5.5. When these non-coated ferrofluids are diluted from a concentration of 200 mg/ml to 25 mg/ml using the distilled water, the adhesion force is reduced proportionally nearly 0.125 times, as

shown in Figure 5.5. The adhesion force in the magnetised tissue test of non-coated ferrofluids is between 5 to 20 mN. The results are more significant compared to the coated ferrofluids of 0 to 4 mN.

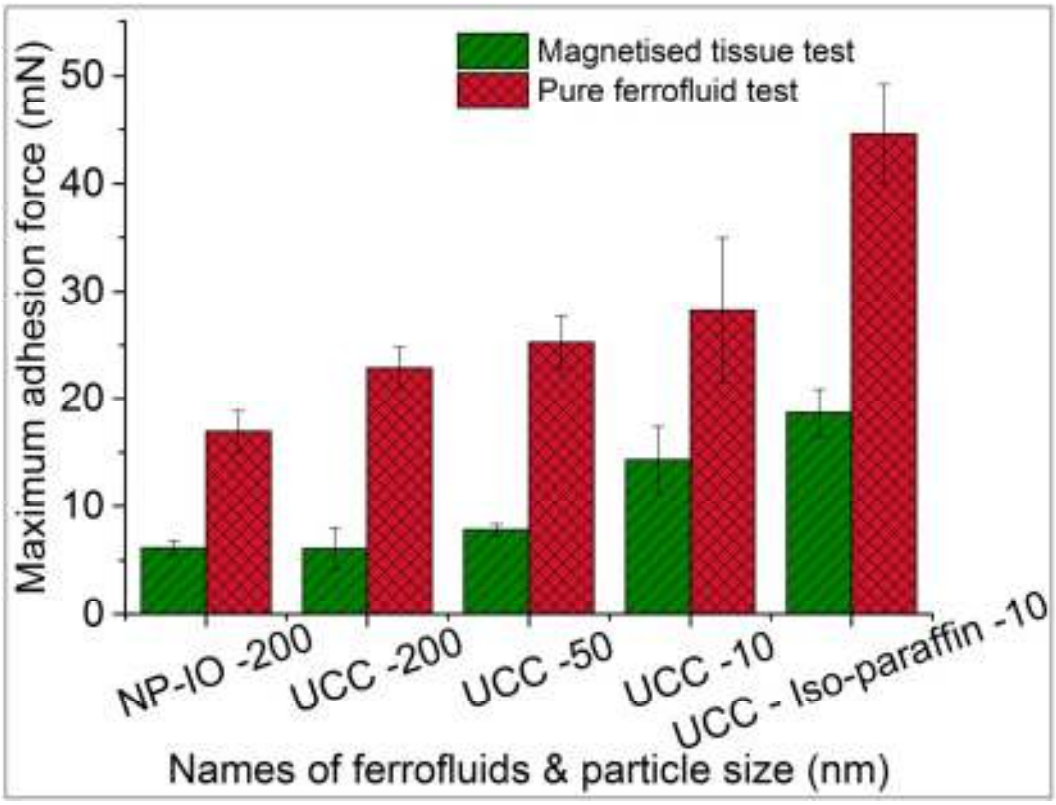

Figure 5.5 Performance of non-coated ferrofluids with various particle size of 10, 50, 200 nm. The testing configuration is that a volume of 0.1 ml ferrofluid with a concentration of 25 mg/ml exposed to a 0.6 T magnetic field. The tests of the ferrofluid tested in the containers are called "pure ferrofluids tests". Those "magnetised tissue tests" are with the ferrofluids injected into tissues.

A further study of an increased injection quantity of 0.3 ml, the largest available quantity of the injection without the issue of leaking from the magnetised tissue is shown in Figure 5.6 about the performance in retraction with a concentration of 200 mg/ml exposed to a 0.6 T magnetic field. The results show that the greater adhesion force consistently occurs in the case of smaller particles. And, the adhesion force in the pure ferrofluid tests is always greater than that in magnetised tissue tests as expected.

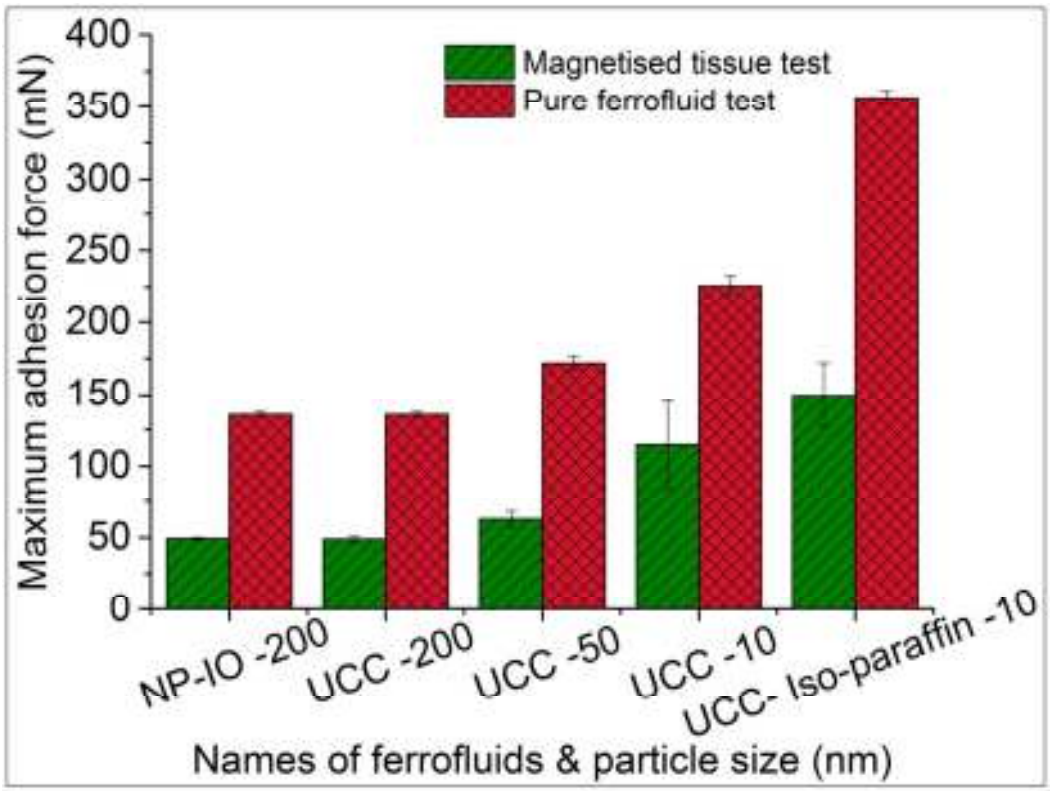

Figure 5.6 Performance of non-coated ferrofluids with various particle sizes of 10, 50, 200 nm. The testing configuration is an increased quantity of 0.3 ml ferrofluid with an increased concentration of 200 mg/ml exposed to a 0.6 magnetic field. The tests of the ferrofluid tested in the containers are called "pure ferrofluids tests". Those "magnetised tissue tests" are with the ferrofluids injected into tissues.

In addition to the comparison between the magnetised tissue tests and pure tests, a force difference between ferrofluid injected in the tissue and ferrofluid stored in a container can be observed. There is a consistent difference around 50 mN to a maximum 100 mN. This conclusion can potentially assist any future tests with tissue by simply doing pure tests.

Figure 5.7 shows a summary of maximum adhesion force with regard to the non-coated ferrofluids in order to investigate the effect of injection volume of ferrofluid on the performance in retraction. It can be seen in the figure that the higher injection volume leads to a higher adhesion force in retraction. The best adhesion force obtained in this study is 518 mN which occurs in the configuration of

a volume of 0.3 ml ferrofluid with a carrier fluid of iso-paraffin with 10nm particle size and a concentration of 200 mg/ml exposed to a 0.6 T magnetic field. The outcome is almost double the force provided by a 0.2 ml ferrofluid. However, the maximum force of 0.2 ml ferrofluid is just 1.37 times greater than the case in 0.1 ml ferrofluid. This figure shows a positive correlation between the maximum adhesion force and injection volume.

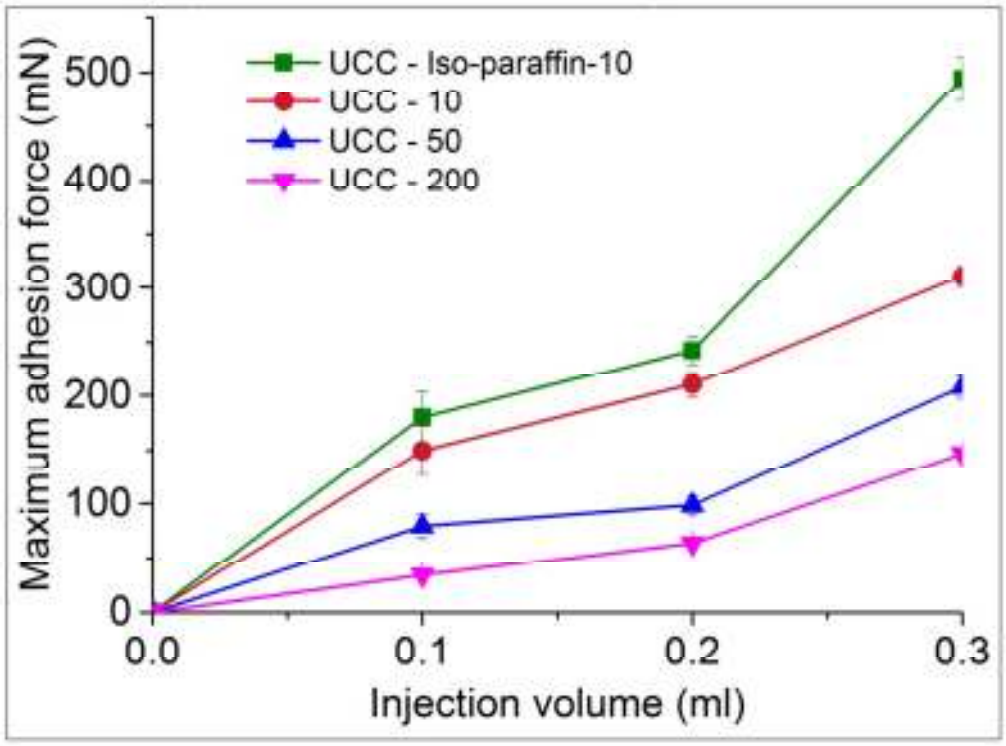

Figure 5.7 Performance of non-coated ferrofluids with various injection quantities of 0.1, 0.2, 0.3 ml. The testing configuration is the ferrofluids with a concentration of 200 mg/ml exposed to a 0.6 T magnetic field. This diagram showing the positive correlation between the injection volume and maximum adhesion force.

5.1.4 Effect of Operation - Preload

Preload force is the intensity of the force as the the rigid magnetic probe is brought into intimate contact with magnetised tissue. The investigation of the effect of preload force in retraction was taken in the magnetised tissue test with a

configuration of a 0.1ml non-coated ferrofluid (UCC) with the concentration of 200 mg/ml and the particle size of 200 nm. The tested values are 100, 125 and 225 mN. Figure 5.8 shows that the adhesion force remained the same value, which does not change with the increase of preload.

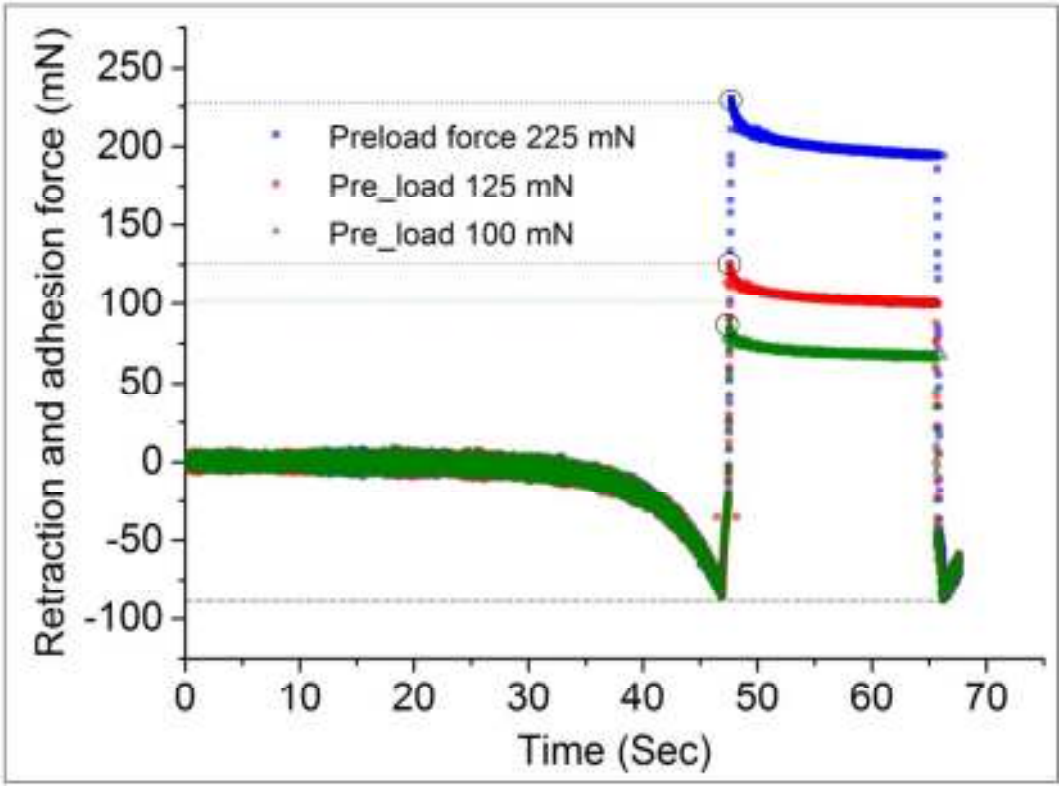

Figure 5.8 Initial force-time profile for the investigation of preload force, showing three different preload forces of 100, 125 and 225 mN. The trends of retraction and adhesion force are almost overlapped for the preload.

5.1.5 Effect of Magnetic Field Strength

Three magnetic inducers are used in this study to provide different magnetic field strengths. Their geometries are shown in Figure 5.9. The magnetic field strength is measured in terms of the gap distance from the surface, as described in section 4.2.4.

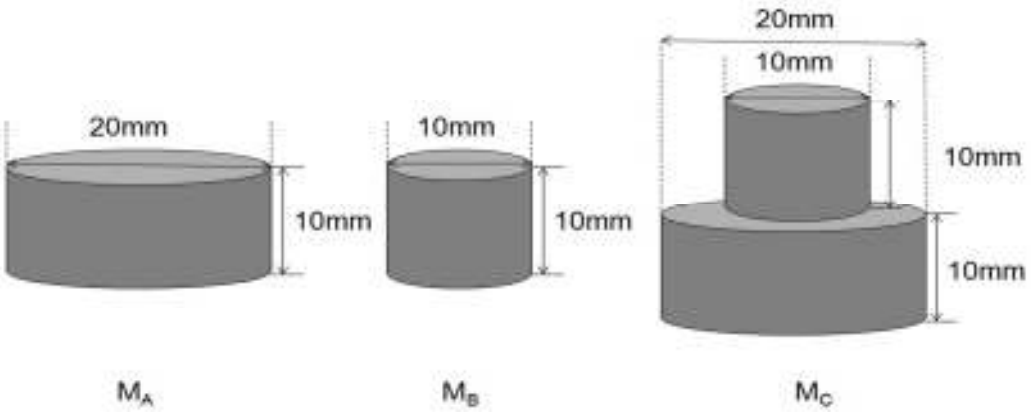

Figure 5.9 Geometry of three magnetic configurations.

Figure 5.10 shows the magnetic response measured from the central position of the diameter and the maximum magnetic field strengths of three magnetic inducers are around 0.4, 0.5 and 0.6 Tesla, respectively.

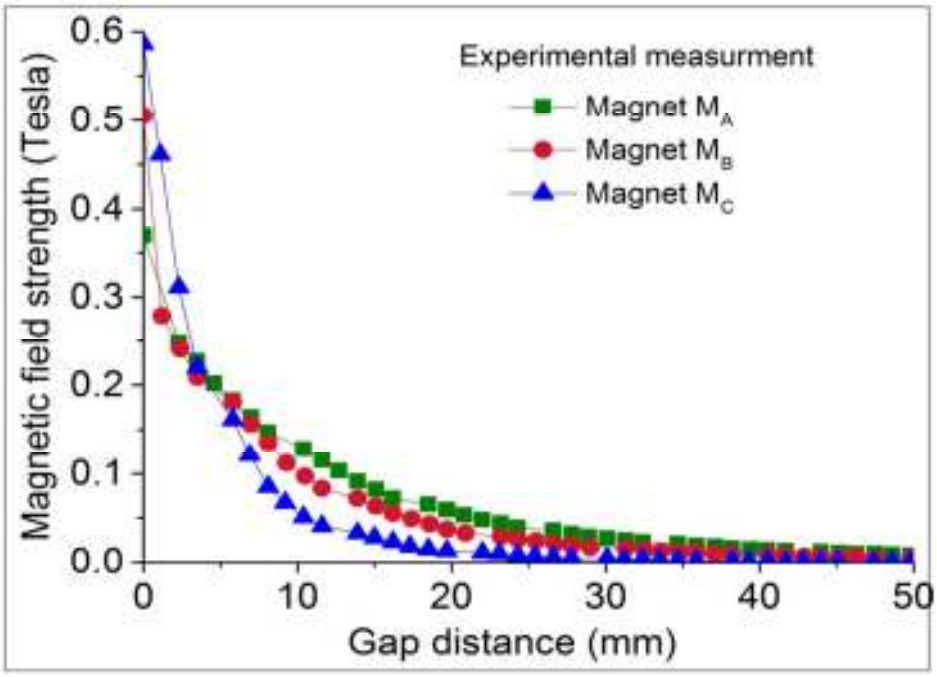

Figure 5.10 Initial magnetic field strengths of three magnetic inducers versus gap distance.

The effect of the magnetic field strength in retraction is investigated in the magnetised tissue test, which the tested environment is 0.3 ml ferrofluid with 200 mg/ml concentration. The initial adhesion force responses are shown in Figure 5.11,

Figure 5.12, Figure 5.13 and Figure 5.14 in terms of different non-coated ferrofluids. It is clear that there is a positive correlation between the magnetic field strength and the adhesion force.

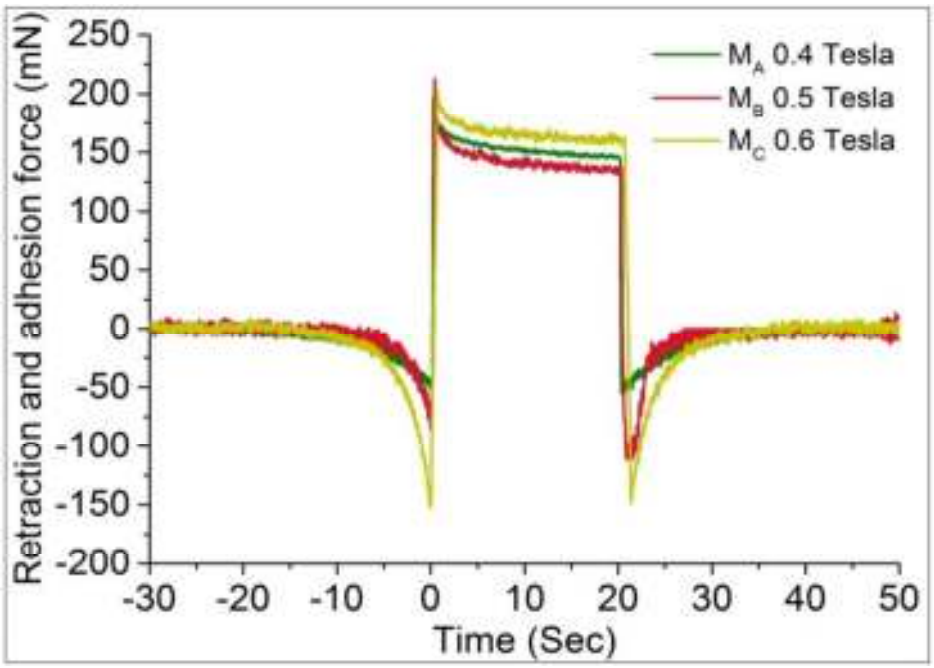

Figure 5.11 Initial force-time profile for the investigation of magnetic field strength, showing three different magnetic inducers of 0.4, 0.5 and 0.6 T. The tested non-coated ferrofluid is with the particle size of 200 nm.

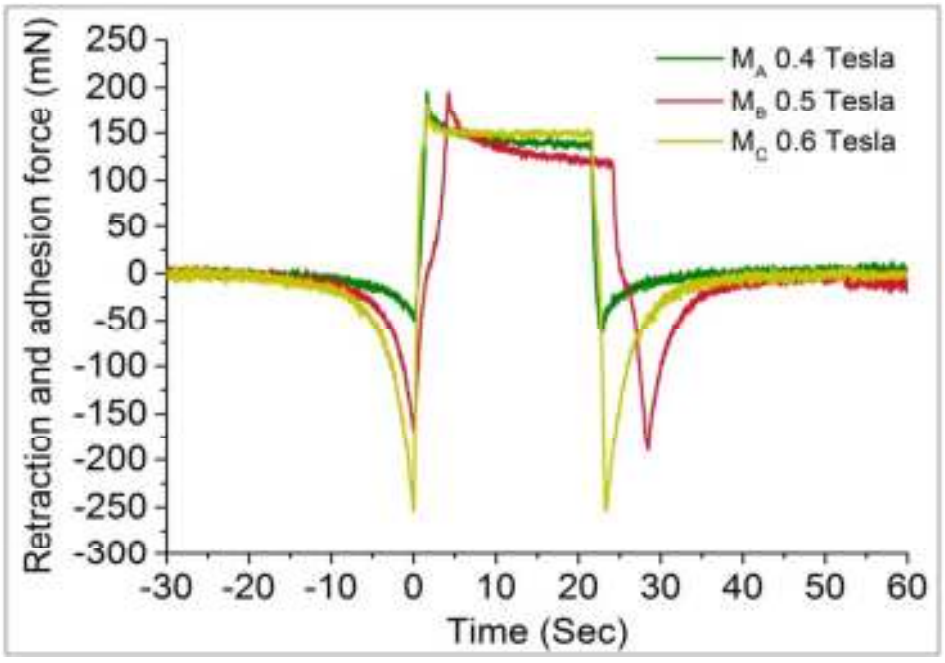

Figure 5.12 Initial force-time profile for the investigation of magnetic field strength, showing three different magnetic inducers of 0.4, 0.5 and 0.6 T. The tested non-coated ferrofluid is with the particle size of 50 nm.

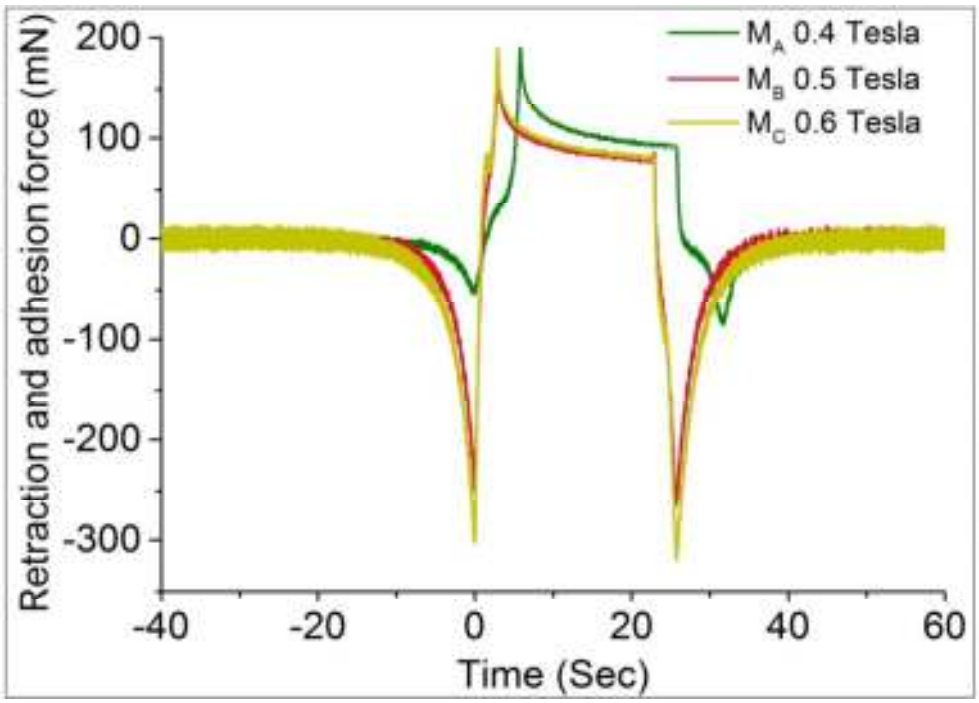

Figure 5.13 Initial force-time profile for the investigation of magnetic field strength, showing three different magnetic inducers of 0.4, 0.5 and 0.6 T. The tested non-coated ferrofluid is with the particle size of 10 nm.

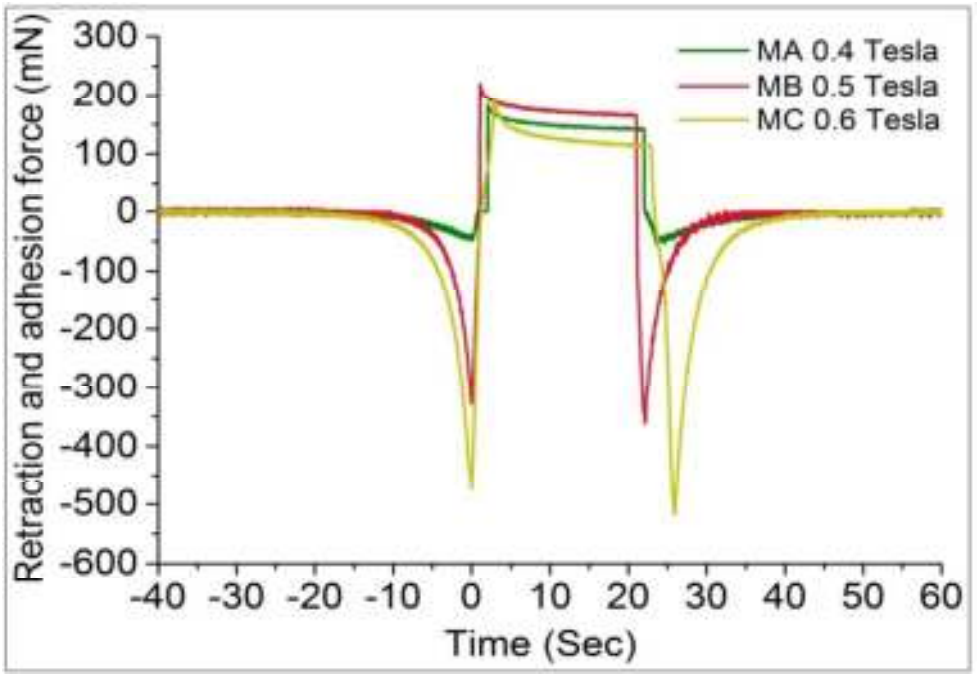

Figure 5.14 Initial force-time profile for the investigation of magnetic field strength, showing three different magnetic inducers of 0.4, 0.5 and 0.6 T. The tested non-coated ferrofluid is with the particle size of 10 nm in a carrier fluid of iso-paraffin.

5.1.6 Effect of Duration of Magnet Contact

The act of tissue manipulation is normally considered as the first direct contact with the tissue. The length of contact time varies from operation to operation, some as short as a few minutes and others may take hours. In this study, the investigation of time of magnetisation in retraction is conducted by different contact time of 20, 60, 120 and 600 seconds. The experiments of the magnetised tissue tests are with an experimental environment of a 0.1ml non-coated ferrofluid (UCC) with the concentration of 200 mg/ml and the particle size of 200 nm, as shown in Figure 5.15. The initial retraction force keeps the same in all experimental environments of 52 mN, which represents the same response in retraction before the contact. However, the maximum adhesion force is gradually increased with time after the first contact with the magnet.

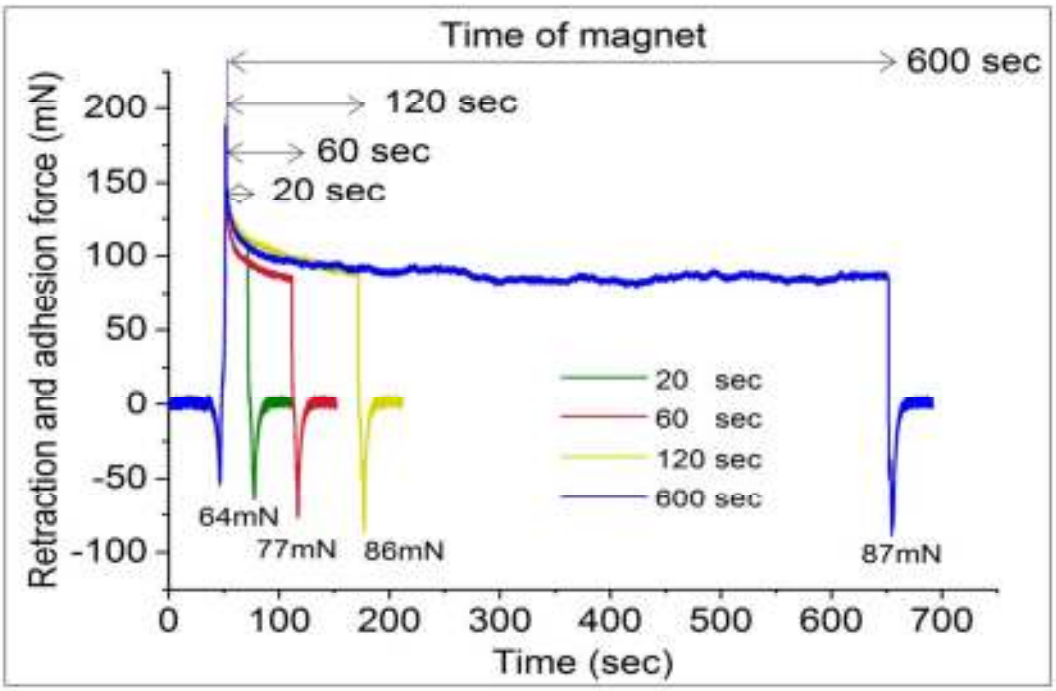

Figure 5.15 Initial force-time profile for the investigation of effect of time of magnetisation, showing four different durations, 20, 60, 120, 600 seconds. The testing configuration is the magnetised tissue test of 200 nm particle size with a concentration of 50 mg/ml exposed to a 0.6 T magnetic field.

5.1.7 The Operation – Indentation Cycles

Multiple manipulations may occur in a single operation. Although the significance of the first cycle of tissue-based diagnosis is usually considered to contains the most direct information of tissue, e.g. elasticity and viscoelasticity etc. However, the robustness of the retraction performance is a topic during the multiple manipulations.

The effect is evaluated by repeating each testing configuration for one hundred times. The experimental environment uses 0.3 ml ferrofluid with 200 mg/ml concentration exposed to a 0.3 T magnetic field and a time of magnet of 20 seconds. The result is shown in Figure 5.16. The adhesion force increases gradually with the cycles and one can clearly observe an ascending trend in the case of non-coated ferrofluid with 10 nm particle size in the carrier fluid of iso-paraffin. The results are the same as the conclusion in section 5.1.6 that the more the exposure to the magnetic field, the better the adhesion force.

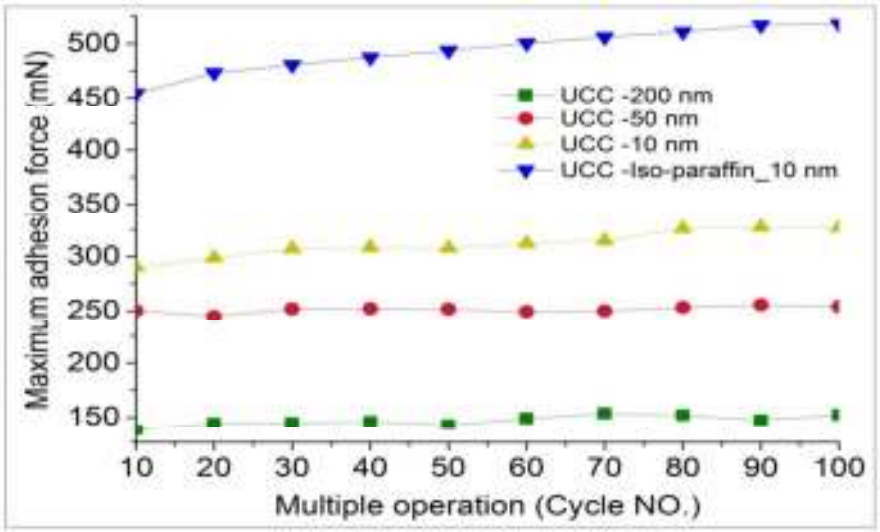

Figure 5.16 Multiple indentation tests in the tests of non-coated ferrofluids with different particle sizes. The performance of retraction is very robust without dropping as the cycles continue. Each experimental configuration repeats for 100 times.

5.1.8 Shear Adhesion

The drag ability in this magnetic retraction method is investigated in the shear adhesion. Referring to the experimental setup for shear adhesion measurement in Figure 4.10, the shear adhesion is investigated by a scratch test in the magnetised tissue tests using non-coated ferrofluids to understand the roadmap of retraction.

The experiment investigate 5 trajectories to present the force distribution surrounding the magnetised tissue.

Figure 5.17, Figure 5.18 and Figure 5.19 show the spatial maps which combine the shear adhesion in the lateral direction and the maximum adhesion in a normal adhesion. The area of scan tracks is within a 20 mm range of the magnetised tissue. This spatial map provides an information of the force responded to the magnetic field surrounding the magnetised tissue.

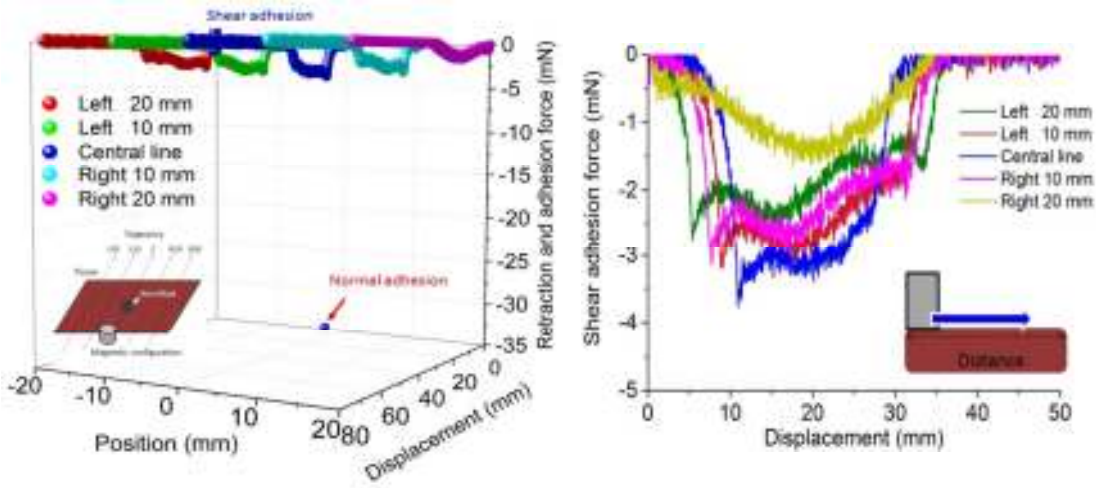

Figure 5.17 Initial force-time profile for the investigation of shear adhesions, showing five different scan tracks separated by the interval of 10 mm. The testing configuration includes a magnetised tissue test of a volume of 0.1 ml with 200 nm particle size and a concentration of 200 mg/ml exposed to a 0.6 T magnetic field.

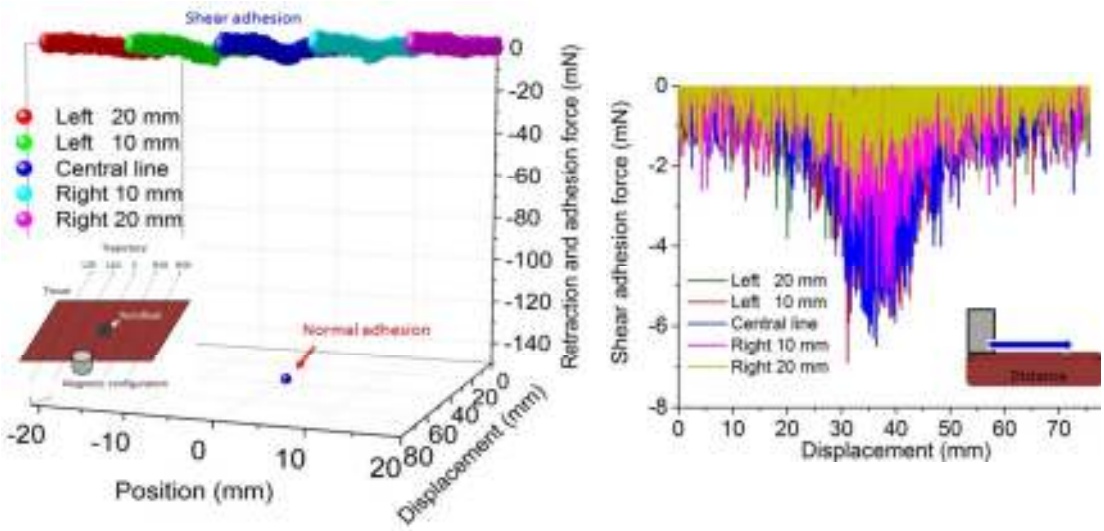

Figure 5.18 Initial force-time profile for the investigation of shear adhesions, showing five different scan tracks separated by the interval of 10 mm. The testing configuration includes a magnetised tissue test of a volume of 0.1 ml with 10 nm particle size and a concentration of 200 mg/ml exposed to a 0.6 T magnetic field.

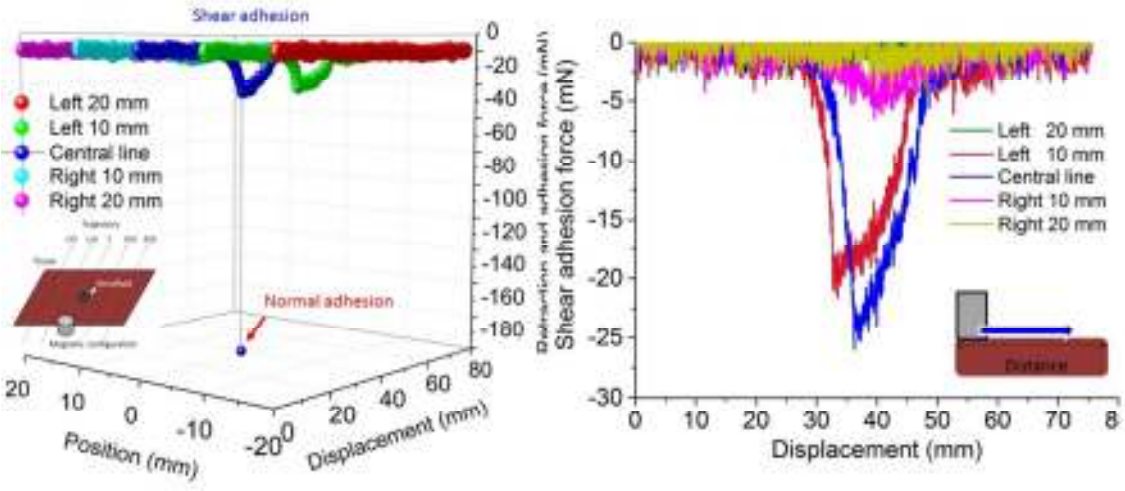

Figure 5.19 Initial force-time profile for the investigation of shear adhesions, showing five different scan tracks separated by the interval of 10 mm. The testing configuration includes a magnetised tissue test of a volume of 0.1 ml non-coated ferrofluid in the carrier fluid of iso-paraffin with 10 nm particle size and a concentration of 200 mg/ml exposed to a 0.6 T magnetic field.

The testing environment features an injected volume of 0.1 ml with the concentration of 200 mg/ml and exposes to the magnetic field strength of 0.6 T and is carried out on different particle sizes of 10 nm and 200 nm.

It can be seen in the spatial maps, the normal adhesion is always significantly stronger than the shear adhesion. Also, the greater normal adhesion is, the higher shear adhesion will be. The stronger shear adhesion occurs near the injection site. The force responded area is about 20 mm x 20 mm.

However, the maximum shear adhesion obtained in this study is 40 mN. It can be concluded that the retraction can be broken if the lateral force is over the maximum shear adhesion. The shear adhesion is relevant to the drag motion in retraction.

5.1.9 Retraction Effect

In terms of the adhesion measurement, the best performance of adhesion amongst all the magnetised tissue tests in this study is the non-coated ferrofluid with the particle size of 10 nm in the carrier fluid of iso-paraffin and the concentration of 200 mg/ml exposed to the 0.6 T magnetic field. The evaluations of performance in retraction of the tested environments are summarised in Table 5.1.

The tissue retraction is then examined by three different injection volumes of 0.1, 0.2 and 0.3 ml. Table 5.1 shows the result when the tissue can be retracted in the case of 0.2 and 0.3 ml. The retracted distance from the magnetised site stays the same at 20 mm and 25 mm when the weight of the tissue is over 33 g, as shown in Figure 5.20.

Table 5.1 An examination of ex-vivo tests in tissue retraction of the porcine colon.

Non-coated Ferrofluid UCC			
Testing environment			
FF particle size (nm)	10		
FF concentration (mg/ml)	200		
FF quantity (ml)	0.1	0.2	0.3
Magnetic field intensity (T)	0.6		
Ex-vivo results from force measurement (Ex-vivo)			
Maximum adhesion force (mN)	150	330	520
Tissue retraction examination (In situ, real tissue)			
Weight of colon section (g)	124	124	124
Result of retraction	No	Yes	Yes
Retraction distance (mm)		20	25
Weight of colon section (g)	90.81	90.81	90.81
Result of retraction	No	Yes	Yes
Retraction distance (mm)		20	25
Weight of colon section (g)	33.03	33.03	33.03
Result of retraction	No	Yes	Yes
Retraction distance (mm)		Lift up	Lift up

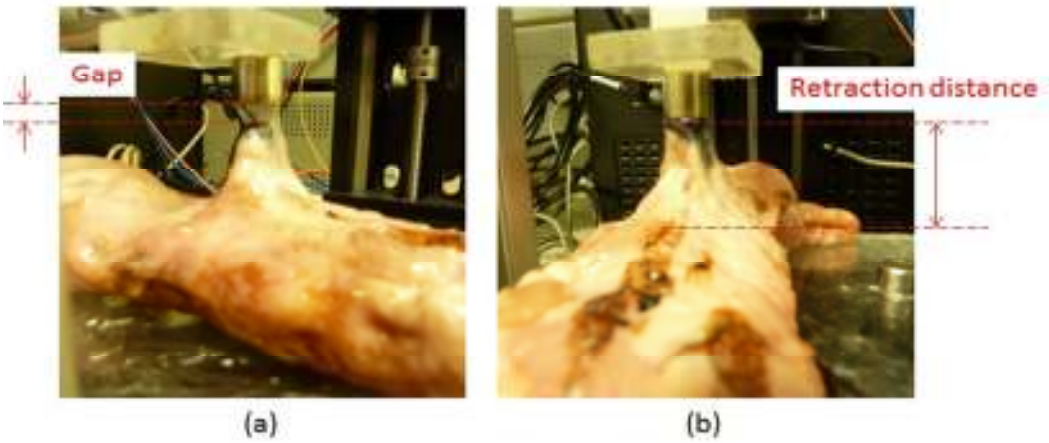

Figure 5.20 (a) The retraction occurs while the magnetised tissue is exposed to the external magnetic field at a distance before the contact. (b) Demonstration of a magnetised tissue adhered to the magnet and the retraction distance, as shown from the tissue surface to the magnetic probe.

The figures evidence that the upper layer of porcine colon is lifted up from the magnetised site, however, the tissue is dropped immediately once the maximum adhesion force can no longer afford to hold the over weights of 120 and 90 g. If the weight is lower than the allowance adhesion force, a process can be completed, as shown in Figure 5.21 where the retraction of the entire section of porcine colon with a weight of 33 g is captured. The retraction lasts for at least 10 minutes from the beginning to the end of the experiment.

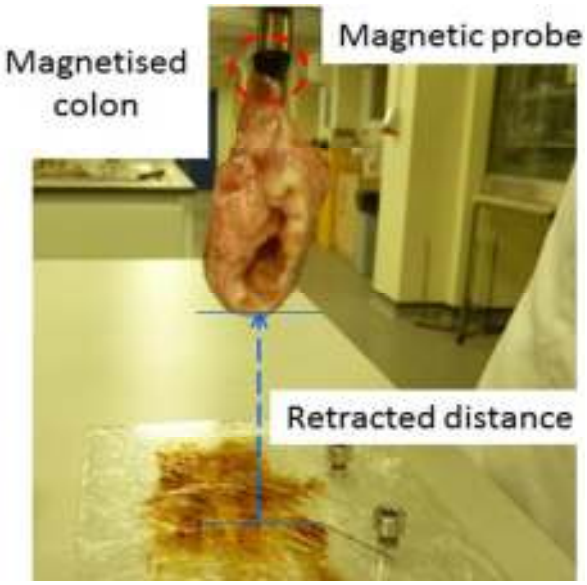

Figure 5.21 Demonstration of retracting a section of a magnetised porcine colon.

5.2 Results of Particle Sizing

This section investigates the particle sizes of the tested ferrofluids with the specified particle sizes. This investigations provides a size distribution of particles suspended in ferrofluids, also characterises if particles are aggregated.

The size of those particles in the suspensions is approached through the particle sizing experiments by averaging three different diluted concentrations from the tested ferrofluids. The results are summarised in Table 5.2 showing the

inequality between the averaged particle size in the experiments and the initial particle size in the specifications. The captured particle size ranges up to 1000 nm but the majority of the intensity locates at between 50 and 120 nm, which can be seen in the initial particle size and intensity profile in Figure 5.22 and Figure 5.24. Figure 5.23 shows the test of an initial particle size of 10 nm (cf. Figure 5.22).

Table 5.2 Table of an averaged particle size of the tested ferrofluids with coated and non-coated particles.

Sample coating	Specification concentration (mg/ml)	Diluted concentration (mg/ml)	Specified particle size (nm)	Experimental size (nm)	Averaged size (nm)
Non	200	10	10	40.68	43.75
		5		40.25	
		1		50.34	
Non (iso-paraffin)	200	10	10	86.53	66.88
		5		57.82	
		1		56.3	
Non	25	10	50	55.69	57.35
		5		57.01	
		1		59.35	
Starch	25	10	50	84.35	80.67
		5		80.67	
		1		77	
Amine silane	25	10	50	83.12	80.59
		5		80.65	
		1		78.01	
Chitosan	25	10	100	92.17	93.35
		5		95.76	
		1		92.14	
Non	200	10	200	110	105.1
		5		101.5	
		1		103.8	
Non	100	10	200	121	119.23
		5		119.6	
		1		117.1	
Non	25	10	200	125.1	120.3
		5		120.3	
		1		115.5	

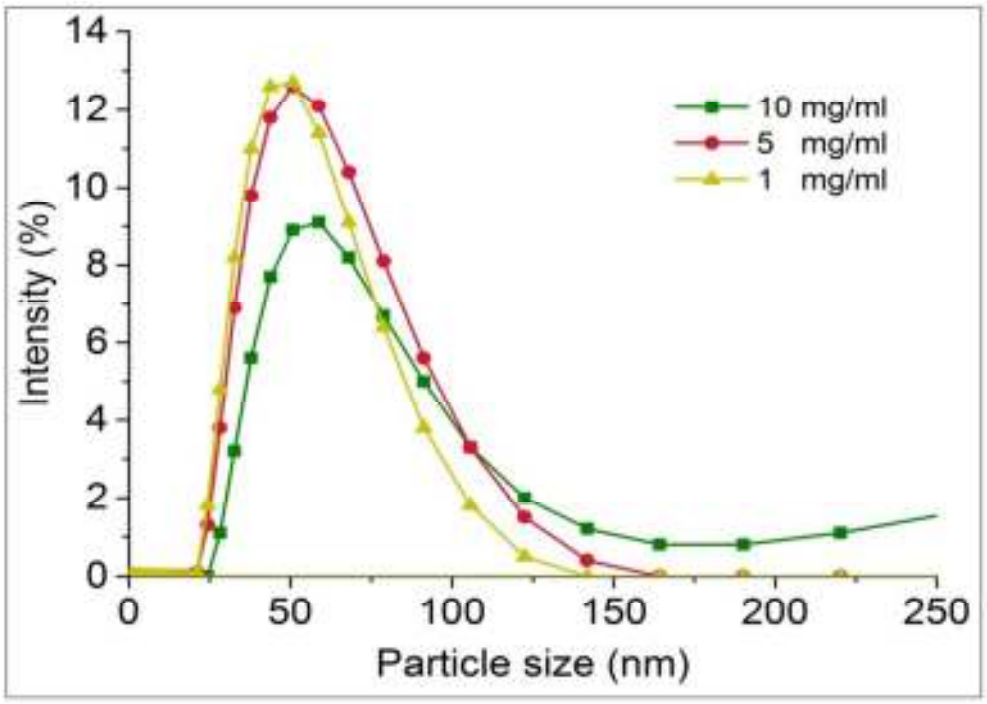

Figure 5.22 Initial particle size and intensity profile of the ferrofluid UCC-10-Iso-paraffin. The specified particle size is 10 nm, but the majority of the intensity is around 50 nm.

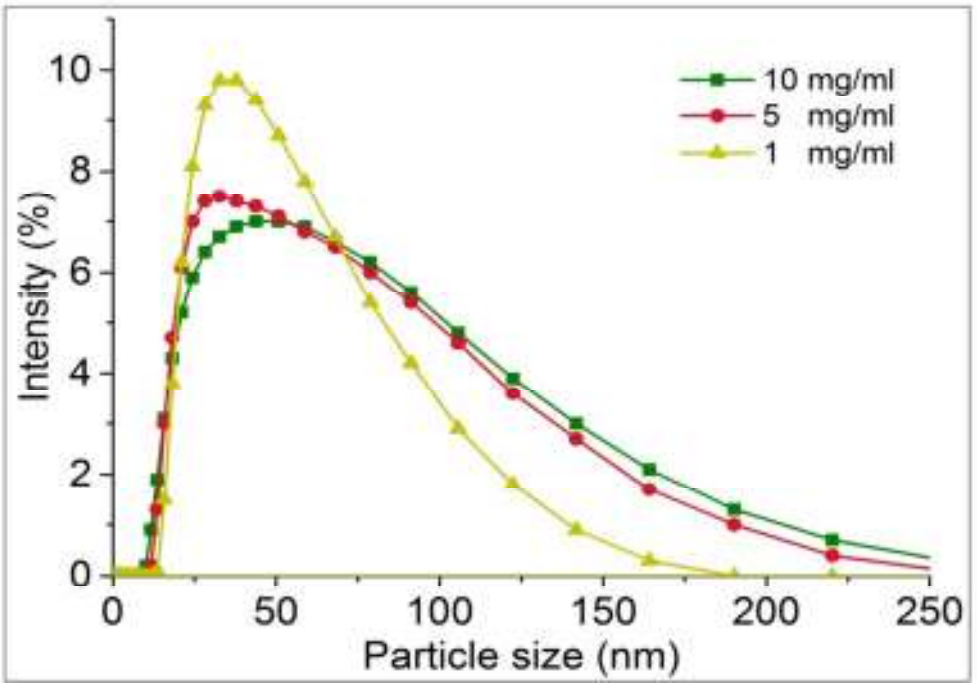

Figure 5.23 Initial particle size and intensity profile of the ferrofluid UCC-10. The specified particle size is 10 nm, but the majority of the intensity is around 48 nm.

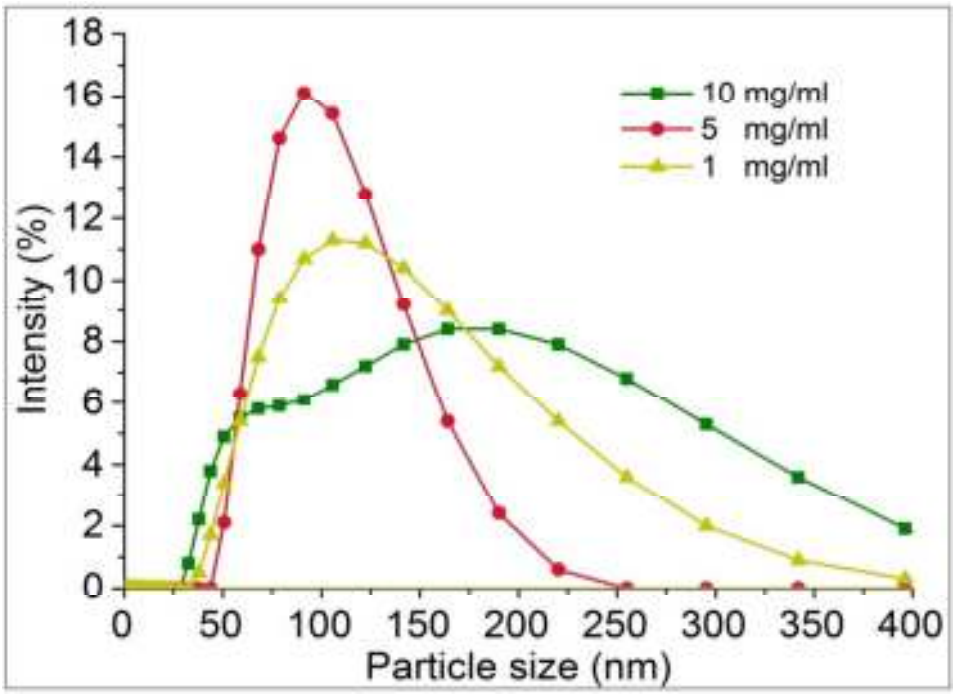

Figure 5.24 Initial particle size and intensity profile of the ferrofluid UCC-10-Iso-paraffin. The specified particle size is 200 nm, but the majority of the intensity is around 120 nm.

The investigation into sizing particle experiments illustrates that the averaged particle size is not the same as what is specified originally. The majority of the particles sizes within the range of between 80 and 120 nm. Hence a specification of 100 nm is very close to the experimental result.

The specification of 50 nm is also very close to the experimental result but the sizes of the coated particles are larger than the specified ones. The specification of lager and smaller size of 200 nm and 10 nm are either more or less than the experimental results. Table 5.2 also shows that the particles of the same sample size in the specification of 200 nm with different concentrations have a similar size.

It can be seen in Figure 5.24 that there are two peaks in the concentration of 10 mg/ml. Normally the distribution is a single peak, but this pheonomenon observed seems the particle agglomeration in the higher concentration.

5.3 Taguchi Method for Parametric Study

The effect of several different parameters on the performance of adhesion measurements in retraction have been examined by using the orthogonal array experimental design proposed by Taguchi. The parametric study with four main internal parameters and three associated levels have been investigated with a $L_9(3^4)$ experimental matrix. Referring to the introduction in section 4.6, the parameters and levels are filled into the array with the predefined order. Then the results of maximum retraction force and maximum adhesion force are obtained from the ex-vivo adhesion measurements given the experimental environments. These results collected are shown in Table 5.3.

Furthermore, the means, variances and S/N ratios are calculated in Table 5.3. Once the S/N ratios are analysed for each parameters and levels, the results are used to find the impact for each parameter. Tests in three different levels of each parameter are averaged by the number of the tests, as shown in Table 5.4. The S/N ratio indicates that the smallest ratio has the best performance. In this study, a lower level of particle sizes leads to better performance in retraction, in addition to the studies of other parameters of concentration, volume, magnetic field strength, a higher level of each shows that better performance in retraction can be found.

The importance of each parameter is evaluated by the difference of main effect. The main effect, defined as the high level S/N subtract the low level S/N, shows the variation of the performance. Generally, that the larger the main effect of the parameter, the more influence is has on the result.

$$\text{main effect} = |\text{S/N:maximum} - \text{S/N:minimum}|$$

Table 5.3 Results of $L_9(3^4)$ Taguchi study of the ex-vivo adhesion measurements. (The colour of background showing the value from different source, predefined value, experimental result and calculation, respectively).

Experiment	Particle size (nm)	Concentration (mg/ml)	Volume (ml)	Magnetic Field strength (T)	Maximum retraction force (mN)	Maximum adhesion force (mN)	Mean adhesion force (mN)	Variance	S/N ratio (%)
1	10	25	0.1	0.4	2.17±2.82	3.51±3.11	2.84	8.51	-9.30
2	10	100	0.2	0.5	83.41±6.1	88.26±5.44	85.84	7373.53	-38.68
3	10	200	0.3	0.6	302±9.72	319.15±7.3	310.58	96530.36	-49.85
4	50	25	0.2	0.6	21.14±1.1	21.16±1.15	21.15	447.32	-26.51
5	50	100	0.3	0.4	24.92±4.9	32.27±5.42	28.6	831.18	-29.2
6	50	200	0.1	0.5	55.7±10.8	63.4±12.1	59.55	3561.03	-35.52
7	200	25	0.3	0.5	10.71±0.8	13.91±0.77	12.31	154.10	-21.88
8	200	100	0.2	0.4	17.09±0.7	18.67±0.69	17.88	320.32	-25.06
9	200	200	0.1	0.6	50.64±1.4	49.35±1.12	50.00	2499.92	-33.98

Table 5.4 A table showing the main effects of the S/N with regard to different parameters and levels.

Level	Particle size (nm)	Concentration (mg/ml)	Volume (ml)	Magnetic field strength (T)
1 (Minimum)	-32.61	-19.23	-26.27	-21.18
2	-30.41	-30.98	-29.92	-32.02
3 (Maximum)	-26.97	-39.78	-33.64	-36.78
Main effect	5.64	20.55	7.37	15.59

A comparison of four parameters tested is presented in Figure 5.25. It can be seen that these four parameters all affect the retraction performance. However, compared to the particle size and volume, the parameters of concentration and magnetic field strength are much more significant ones in the retraction performance in this study.

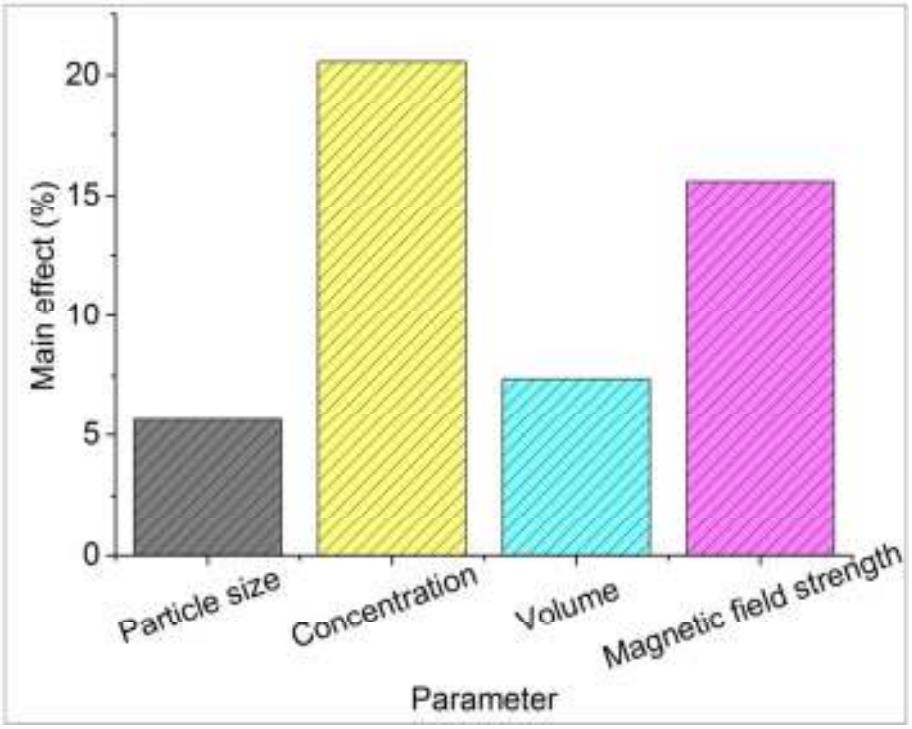

Figure 5.25 A diagram showing the influence of different parameters on the performance in retraction.

It can be seen in Table 5.3 that Experiment no.3 gave the lowest S/N ratio and the highest retraction and adhesion forces. The testing environment includes the smallest particle size, the highest concentration, the highest volume and the strongest magnetic field strength. The factors chosen satisfy the best values suggested by the main effects shown in Figure 5.25. Therefore, this is the optimised testing environment in this study.

5.4 In-vivo Experiment

The optimised tested environment is then applied to the in-vivo tests on alive animals. Figure 5.26 shows the preliminary result of the experiment of retracting magnetised tissues of the peritoneum, conducted by the laparoscopic procedure with a magnet attached to the tool. The result shows a little retraction from the magnetised site. The tested ferrofluid is the non-coated sample with the particle size of 200 nm with the concentration of 200 mg/ml exposed to the magnetic field strength of 0.5 T.

Figure 5.26 The in-vivo experiment of tissue retraction by a laparoscopic procedure showing a peritoneal tissue being pulled up by a magnet on the screen.

A second in-vivo experiment is conducted using the optimised testing environment from the ex-vivo experimental database. The optimised environment refers to the non-coated particles with higher volume, higher concentration and smaller particle sizes exposed to the magnetic field with stronger strength. The in-vivo tests are based on such optimised parameters of a magnetic field strength of 0.6 T conducted in the pig model. The evaluation of the successful retraction is recorded shown in Table 5.5.

Table 5.5 The evaluation sheet of the in-vivo experiments of retracting porcine bowel using the optimised ferrofluids from the ex-vivo tests. (√ denotes successful retraction; X denotes failed retraction**)**

Evaluation sheet						
Target	Porcine bowel					
Magnetic field strength (T)	0.6					
Injection site	Single spot			Two spots		
Volume (ml)	0.1	0.2	0.3	0.1	0.2	0.3
UCC - 10nm iso-paraffin	X	X	√	X	√	√
UCC - 10nm	X	X	X	X	X	X
UCC - 50nm	X	X	X	X	X	X
UCC - 200nm	X	X	X	X	X	X

The ferrolfuid is injected into the bowel layer at a single spot in the beginning of the test, as shown in Figure 5.27. During the injection, it has been observed that the ferrofluid came off from the injected site if the injection is closer to the injected position. This issue of sucking off is avoided when the length of needle is changed from a short to a longer. Therefore, it is important in the protocol to use a long

needle to perform the injection in order to keep the ferrofluid away from the injected site. In so doing, it can also avoid leaks from the injected site when the injected quantity increases.

The evaluation sheet shows that the successful retraction only occurs when the sample is with a particle size of 10 nm in the carrier fluid of iso-paraffin and injected quantity of 0.3 ml. A slight response to the injected quantity of 0.2 ml ferrofluids can be observed, as shown in Figure 5.28. The complete retraction of the bowel section is demonstrated in the environment of injected quantity of 0.3 ml, as shown in Figure 5.29.

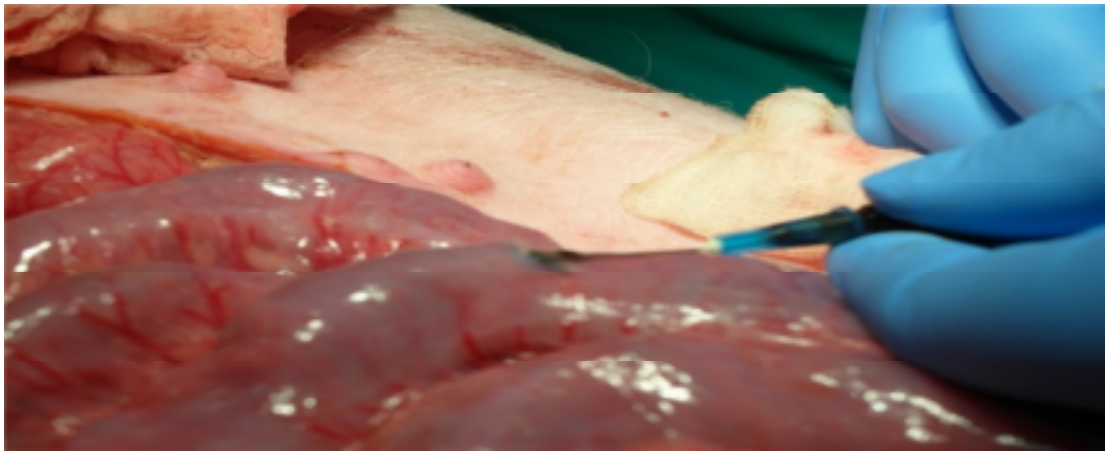

Figure 5.27 A ferrofluid is being injected via a laparotomy procedure to the mucosa layer of a pig bowel. (the in-vivo tests were conducted by Professor David Jayne and Adrian Hood, I was in charge of deliverying the kits)

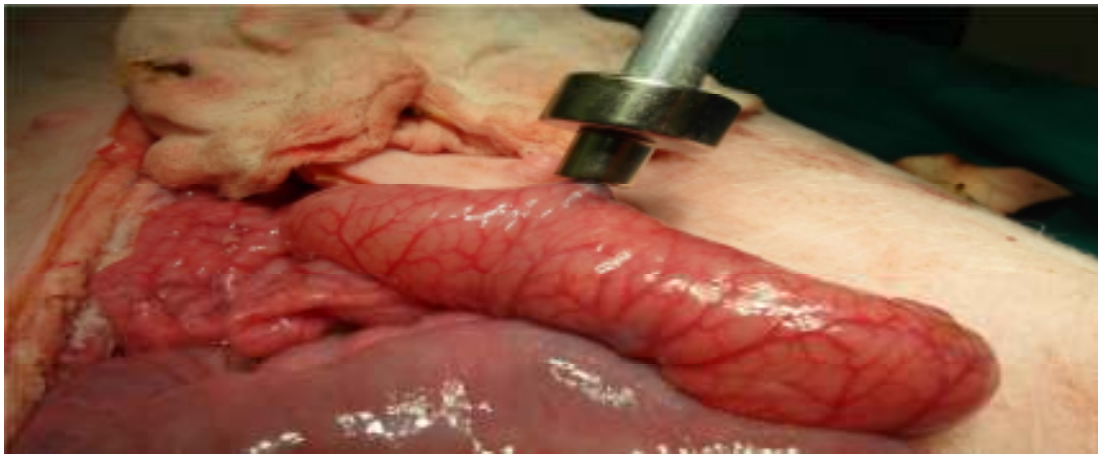

Figure 5.28 A magnetised tissue with an injected quantity of 0.2 ml is responding to the magnets, but the section remains difficult to be pulled up.

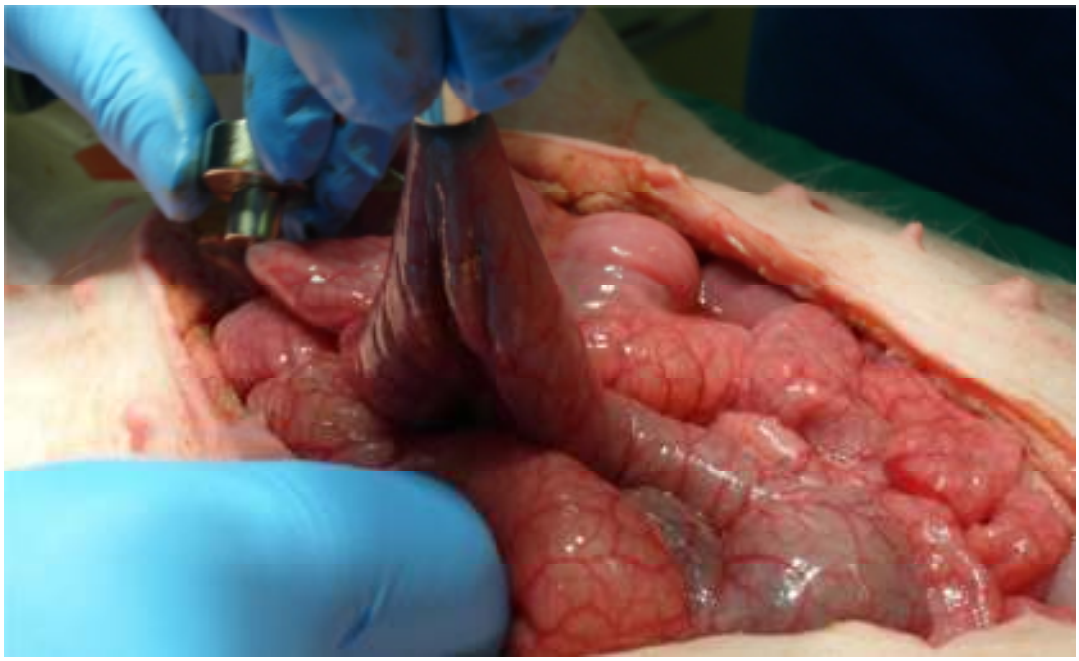

Figure 5.29 The magnetised tissue is retracted by the magnet when the injected quantity is increased to 0.3 ml. It can be seen that the magnetised site is adhered to the magnet firmly.

Figure 5.30 and Figure 5.31 show the retraction of the bowel section with two magnetised sites. The retraction was firmly attached to both magnetised sites and the maximum retracted distance is measured at 80 mm height.

Figure 5.30 Two magnetised sites, one with 0.3 ml and the other 0.2 ml ferrofluids. The section of the bowel is being retracted.

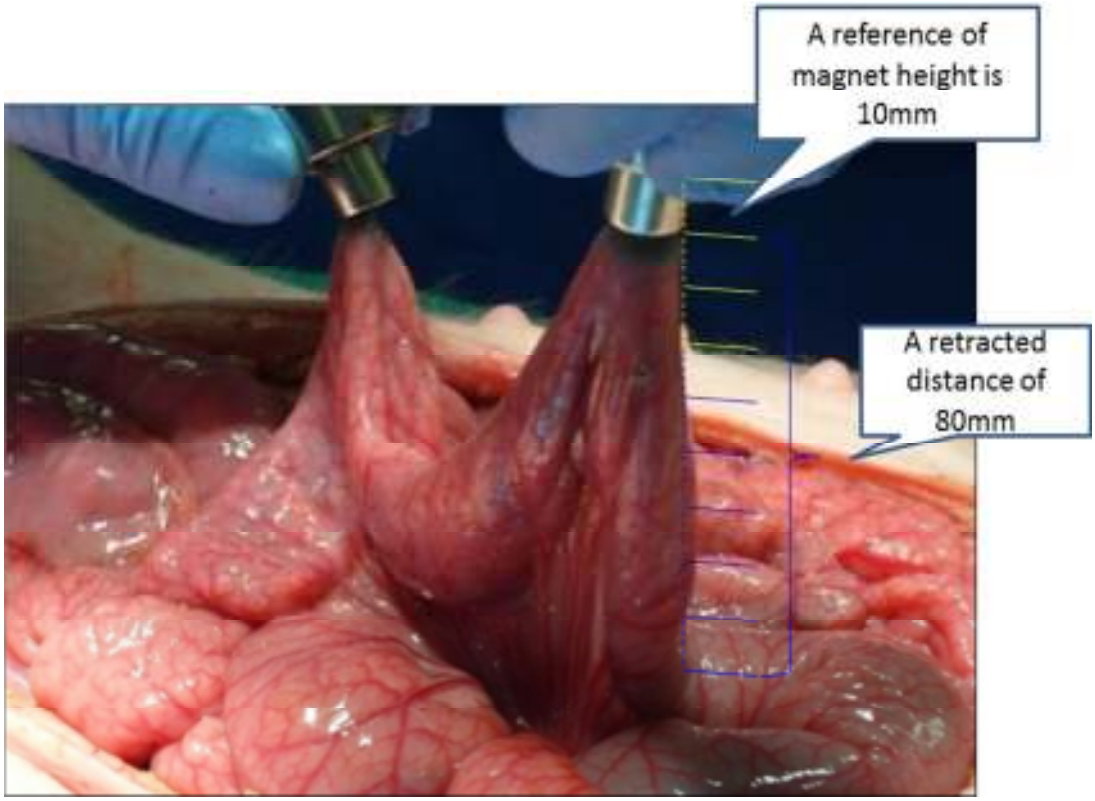

Figure 5.31 A section of the bowel being retracted by two magnetised sites both with an injection quantity of 0.3 ml.

The retraction has been video recorded so the manipulation can be investigated closely by repeatedly watching the videos and slowing down the procedure. Figure 5.32 shows the captured images (a two-second clip) of the magnetised tissues being dragged to the screen in the direction of right then back to left until it is being dropped.

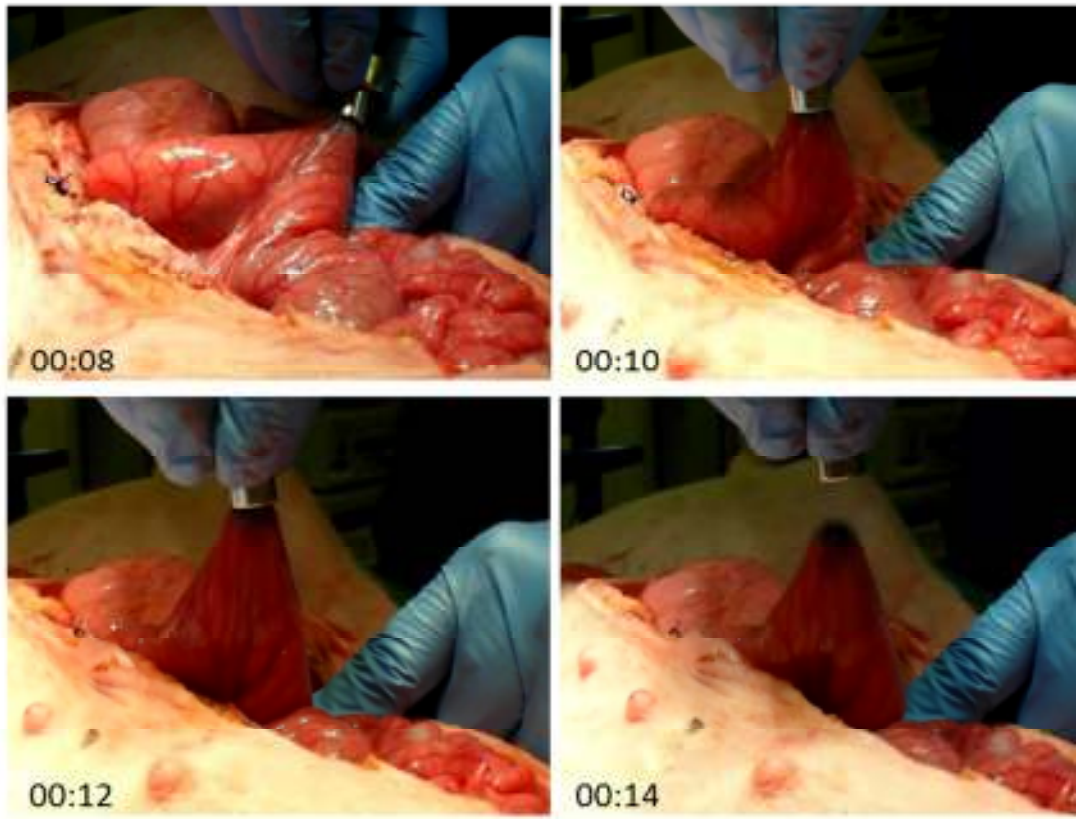

Figure 5.32 The continuing recording of the tissue manipulation by the magnet on a single magnetised site.

It can also be observed that the ferrofluid is being concentrated while the magnetised site is exposed to the magnetic field. When the magnet is removed, the ferrofluid soon disperses, as shown in Figure 5.33. This result represents the mobility of the injection.

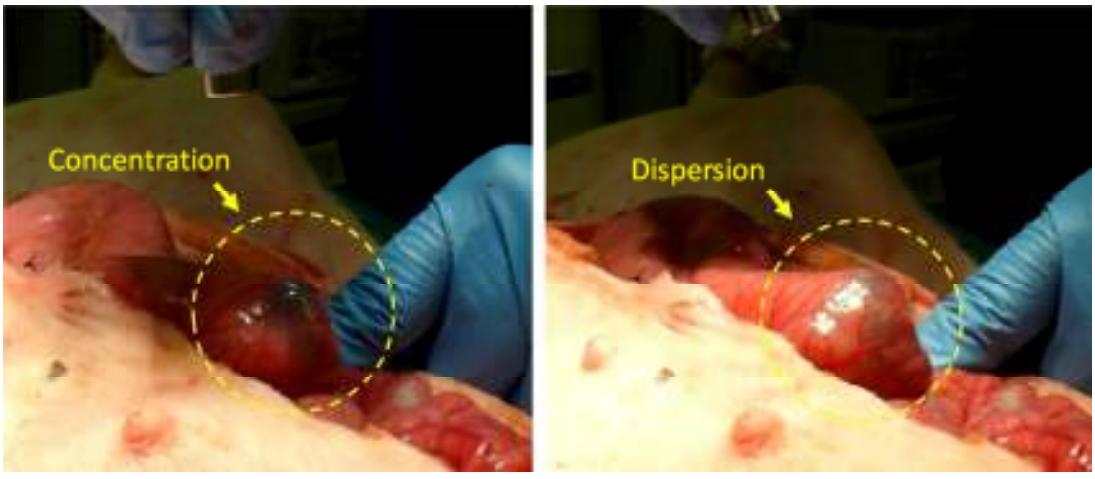

Figure 5.33 The continuing recording shows that ferrofluid is concentrated under the magnetic effect and disperses without the magnetic field.

5.5 Summary

In summary, this chapter has presented the ex-vivo and in-vivo experiments with regard to the tissue retraction. The capability of tissue retraction is quantitatively measured by two devices, the MUST^{TM} rig and a self-developed tissue tester. Several parameters have been investigated, including the particles with coating or without coating, size of particles, volume and concentration of ferrofluids as well as the magnetic field strength and operation duration and cycles.

The tissue tester studied three different force quantities: 1) Tissue surface adhesion, 2) Magnetic tissue retraction 3) Magnetic shear adhesion. Tissue surface adhesion is tested from the intensity to detach from the tissue surface.

Regarding the magnetic tissue retraction, the results show the adhesion measured is positive correlative to the volume, concentration of the ferrofluids and magnetic field strength. The non-coating ferrofluids shows better adhesion than the coating ferrofluids in the same volume and concentration. The tests in duration and operation cycles show that the robustness of the magnetic retraction.

In addition to the capability in dragging tissue, a spatial map of adhesion force is integrated with the magnetic shear adhesion measured. The spatial map shows that the adhesion decreases dramatically in the lateral movement.

Excluding the force measurement, some other characterisations are also presented in this chapter. The magnetic field strength of three different magnetic configurations are presented and the accumulated configuration provides the strongest magnetic field strength. The particle size of testing ferrofluids is also obtained by using Nanosizer. The results show the difference between the specified particle size and the characterised particle size.

The parametric study is further investigated using the Taguchi method. The result shows that the volume of ferrofluid plays the most important roles. The second significant parameter is the magnetic field strength.

The optimised testing environments are then applied in the ex-vivo demonstration and in-vivo tests. The feasibility with regard to manipulating tissue is evidenced that the magnetic retraction using ferrofluids can retract the bowel to a height of 8 cm for laparoscopic surgery. The ex-vivo demonstration has also shown that the testing colon section is lifted, which equals to the gram-force.

Chapter 6 Characterisation of Particle Distribution in Tissue

The ex-vivo and in-vivo experiments introduced in the previous chapter have demonstrated the capability of ferrofluids to facilitate effective tissue manipulation. While the quantitative adhesion tests have demonstrated that retraction is feasible, the results do not provide any information about what is happening beneath the tissue. Microscopy methods offer only very limited penetration through tissue for particle characterisation. Depths beyond 100 μm are not possible. In order to better understand particle migration within the tissue, an alternative method using micro-CT has been applied to study the distribution of particles. More information on particle distribution is yielded through a quantitative analysis of micro-CT images.

The experimental setup is explained in section 4.5. Samples for the migration tests are prepared just after the ex-vivo tests and sent into micro-CT scanner. The preparation time is normally less than 10 minutes. This chapter presents the characterisation of the particle density of a distance of 2 mm between the tissue surface and the injection position. This chapter is organised as follows. Section 1 illustrates the idea of image processing of the original images and trimmed images gathered from the micro-CT scanner. Section 2 presents the results of density distribution in relation to different parameters. Section 3 further analyses the proportion of the normalised particle density between each single segment and the entire segments in order to present how the parametric effects affect the particles in migration. Section 4 summarises the study of particle density characterisation.

6.1 Imaging Processing

As introduced in section 4.6, a self-developed image processing has been programmed by Matlab® program. The procedure begins with reading a micro-CT image on a computer, as shown in Figure 6.1. The region of characterisation is fixed to a 1.2 cm by 1.2 cm square. The image is rendered as an RGB image showing three colour components in the array. The RGB image is further converted to GREY scale that contains elements with values between 0 and 255 in the array, which identifies 0 as the black and 255 as the white. In so doing, the particles can be determined by a contrast of black and white pixels.

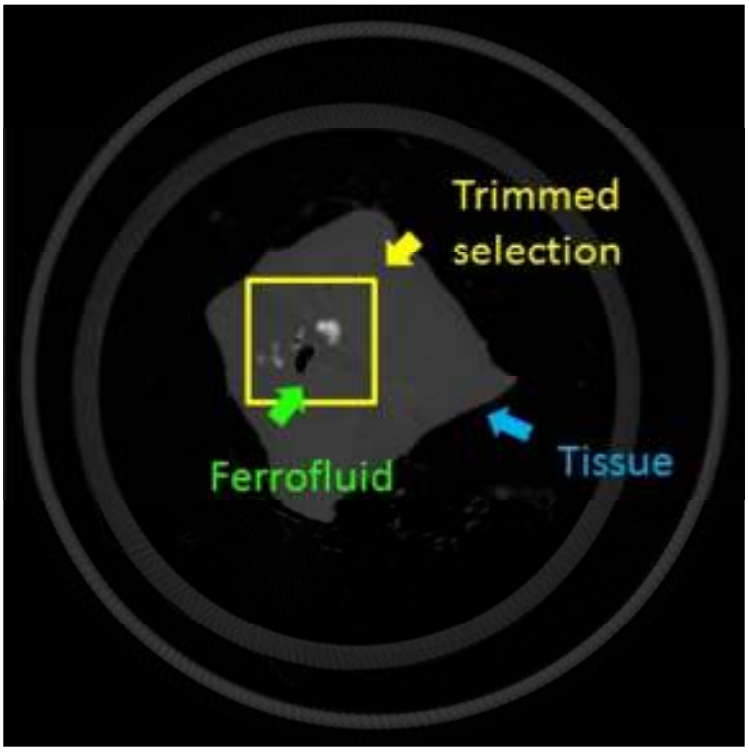

Figure 6.1 An initial micro-CT image showing a segment of the magnetised tissue with ferrofluids surrounding the hole inside tissue. The trimmed area is a fixed area used to study the distribution of particle density.

An indicator called particle density can be identified by the ratio of bright pixels and overall pixels. Once all the images are studied, the distribution of particle density can be displayed. A flow chart representing the entire process is shown in

Figure 6.2. On the right-hand side of Figure 6.2 is a schematic diagram of the original image and the trimmed image.

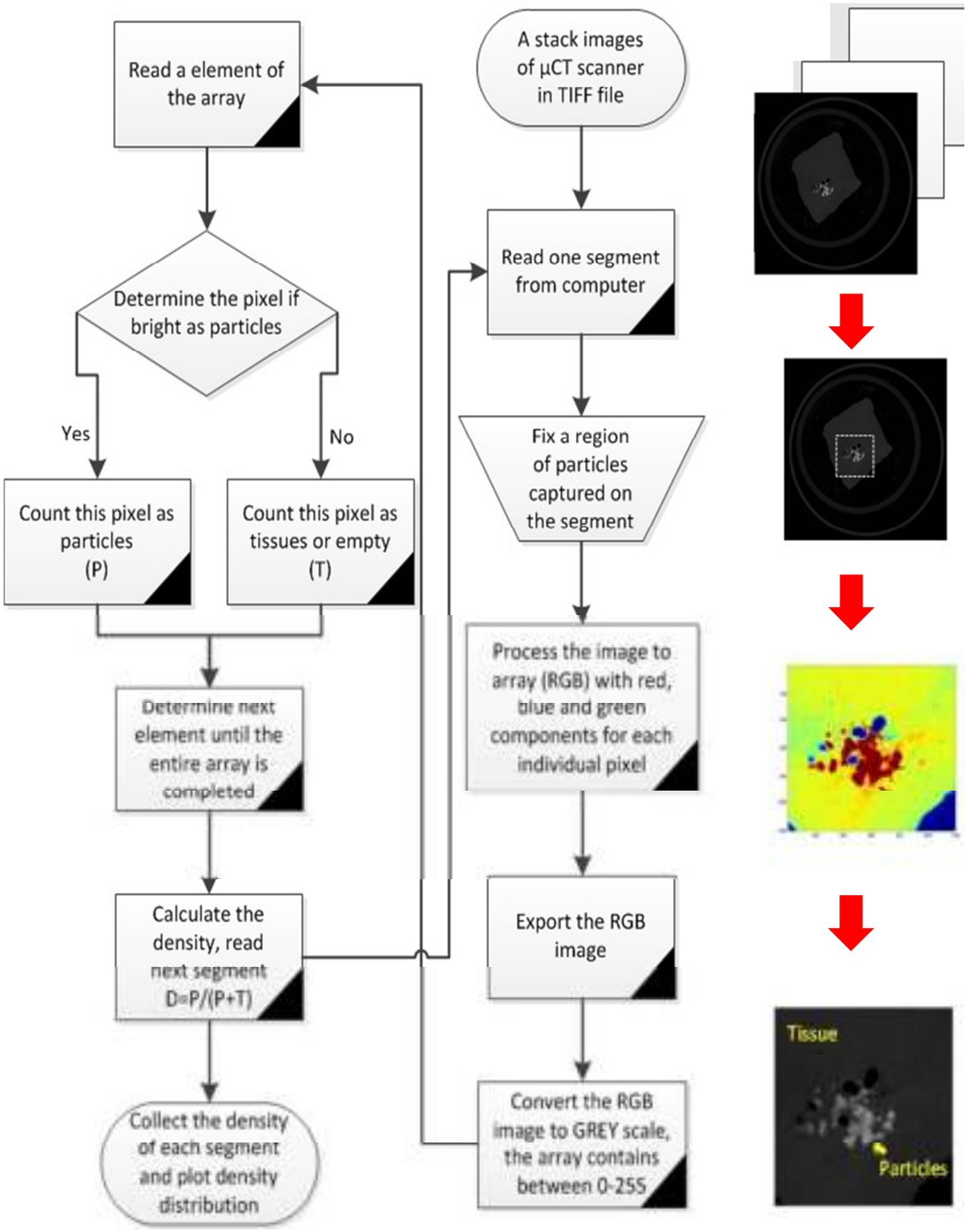

Figure 6.2 A flow chart of the image processing of micro-CT images.

A stack of micro-CT images, especially those with low resolution, requires a lot of memory and capacity of computing power for the analysis and storage.

Therefore it is very difficult to process all the images of the entire tissue. The thickness of the entire tissue is usually fixed as 10 mm, but the characterised thickness in this study is fixed at 2 mm only so as to ensure the tissue responds well to the magnetic field. Each segment has been trimmed to a square shape. All the segments can be reconstructed to a 3-D image, which allows a display of how particles distribute within the tissue, as shown in Figure 6.3. Nonetheless, high reconstruction causes the process very long time for a single scan.

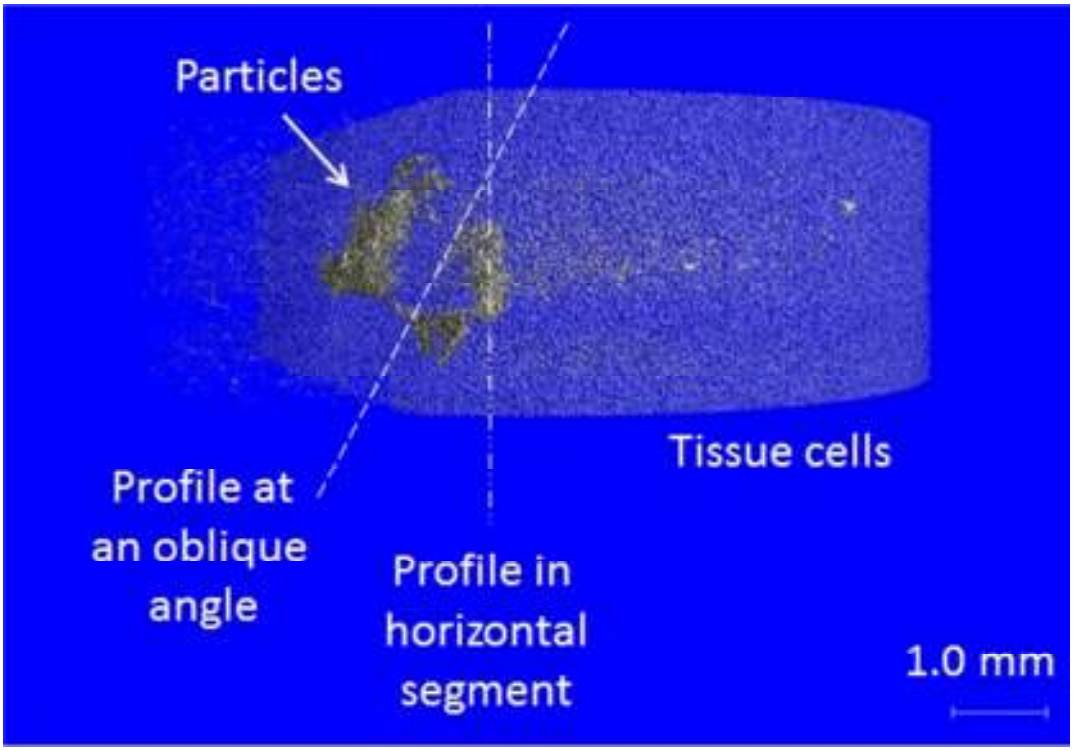

Figure 6.3 A 3D reconstructed image showing the particles distribution within a magnetised tissue sample. It can be seen that the segments normally provided by the horizontal profile, however, an interesting finding can be seen in the profile at an oblique angle.

All the images used in the investigation of density distribution are profiled by the vertical line as shown in Figure 6.3. If the profile is taken at an oblique angle, the score of needle made by the injection and ferrofluid surrounding the hole can be seen in the image, as shown in Figure 6.4.

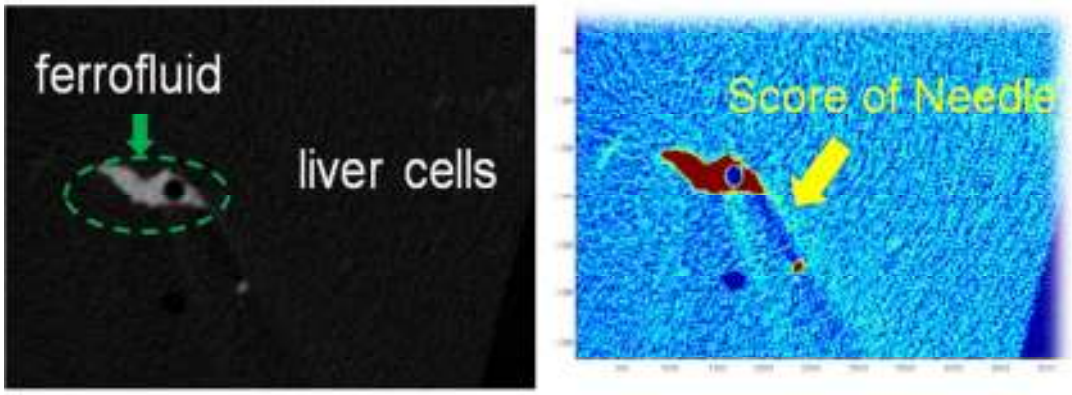

Figure 6.4 GREY-scale and RGB images from a micro-CT scanner showing the needle score by the injection and the ferrofluid surrounding the hole.

6.2 Distribution of Particle Density

Particle density can be obtained by analysing the contrast of particles and tissue of each segment, as shown in the following equation. It is a non-dimensional unit as it represents the ratio of the specific pixels to the entire pixels in the region. The distribution presents the particle density within a depth of 2 mm from the surface of the magnetised tissue, when the particle migration tests were conducted just after the ex-vivo tests. The investigation of density distribution is then applied to study the parametric effects which affect the retraction. Four internal parameters are compared in this study: (i) concentration, (ii) volume, (iii) magnetic field strength and (iv) particle size.

$$\text{Particle density} = \frac{\text{Pixels of particles}}{\text{Total pixels}}$$

Firstly, Figure 6.5 shows a comparison in terms of density distribution of three different concentrations under the testing environment of 50 nm particle size, a magnetic field strength of 0.6 T and an injection volume of 0.1 ml. The horizontal axis indicates depth from the tissue surface. It can be seen that the higher the concentration, the denser the particles are near the magnetised tissue surface.

The injection has been controlled at a distance of 1 mm height from the magnetised tissue surface. The case of 25 mg/ml concentration delivers the majority of particles at the area at between 1 and 2 mm. The case of 100 mg/ml concentration also has the majority of particles at the area between 1 and 2 mm, but there is also a small portion of particles at the area near 0.5 mm. The case of 200 mg/ml concentration has a contrasting result as the majority gathers between 0 and 1.5 mm, closer to the tissue surface. The results can be explained as particles migrate from the injection site during tissue manipulation. The higher concentration has more particles attracted by the magnetic field.

According to the parametric study in the ex-vivo adhesion measurements, the higher concentration has the higher adhesion force. When the higher concentration of ferrofluid is within the tissue, the more particles migrate near the tissue surface.

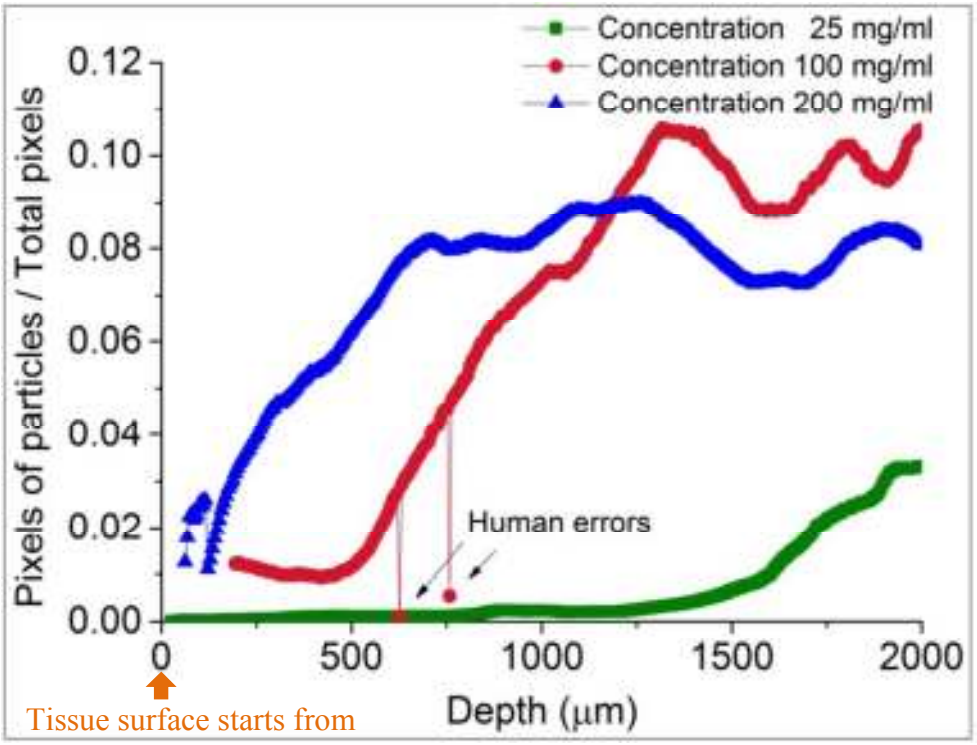

Figure 6.5 A diagram showing the effect of three different concentrations, 25, 100, 200 mg/ml in the characterisation of particle migration. The X axis is the segments within 2 mm and Y axis is the distribution of particle density.

Secondly, Figure 6.6 shows a comparison in terms of density distribution of three injection volumes, 0.1, 0.2, 0.3 ml under the testing condition of the particle size of 200 nm, the same concentration of 200 mg/ml and a magnetic field strength of 0.6 T.

Even if the particle density is a relative value, it is fair to say that a higher volume has a higher particle density. The highest intensity in this study is in the case of a volume of 0.3 ml. The distribution of particle density has two peaks of that in the case of 0.2 ml injection volume. The particle densities distribute denser near the surface (less than 1 mm) as well as deeper than 1 mm.

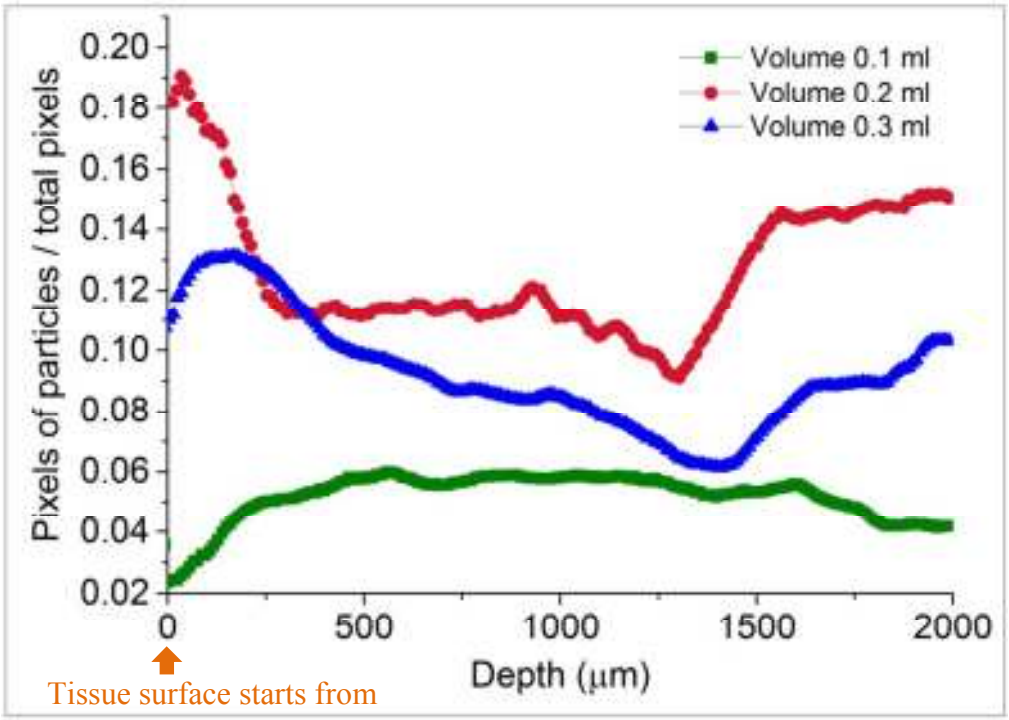

Figure 6.6 A diagram of distribution of particle density showing the effect of three different injection volume, of 0.1, 0.2, 0.3 ml in the characterisation of particle migration within 2 mm.

Thirdly, Figure 6.7 shows a comparison in terms of density distribution of three different magnetic field strengths used in the retraction measurements, 0.4, 0.5, 0.6 T under the testing condition of the particle size of 200 nm, the same concentration of 200 mg/ml and an injection volume of 0.1 ml.

It can be seen that a larger intensity occurs at the depth between 200 and 1250 µm from the magnetised tissue surface in the case of magnetic field strength of 0.6 T. In the case of magnetic field strength of 0.5 T, there is a smaller intensity at the depth of 500 µm. However, the majority of cases with regard to intensity distributes beneath a depth of 1500 µm. In the case of the magnetic field strength of 0.4 T, most particles only gather beneath a depth of 1500 µm.

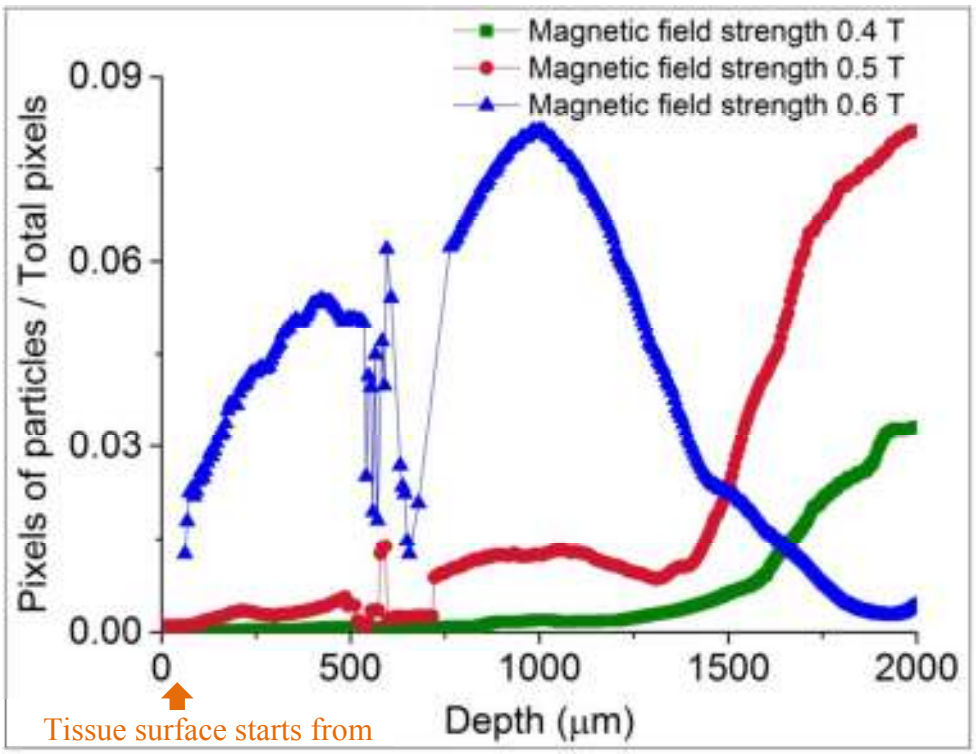

Figure 6.7 A diagram of distribution of particle density showing the effect of three different magnetic field strengths used in the retraction measurements of 0.4, 0.5, 0.6 T in the characterisation of particle migration within 2 mm.

Lastly, Figure 6.8 shows a comparison of density distribution in terms of different particle sizes of 10, 50, 100 and 200 nm under the testing environment of the concentration of 200 mg/ml, an injection volume of 0.1ml and a magnetic field strength of 0.6T.

The distribution of particle density in the case of particle size of 10 nm clearly shows contrasting denser near the magnetised tissue surface and the injection site.

However the distributions in other cases show quite uniform, the particles are slightly more surrounding the injection site.

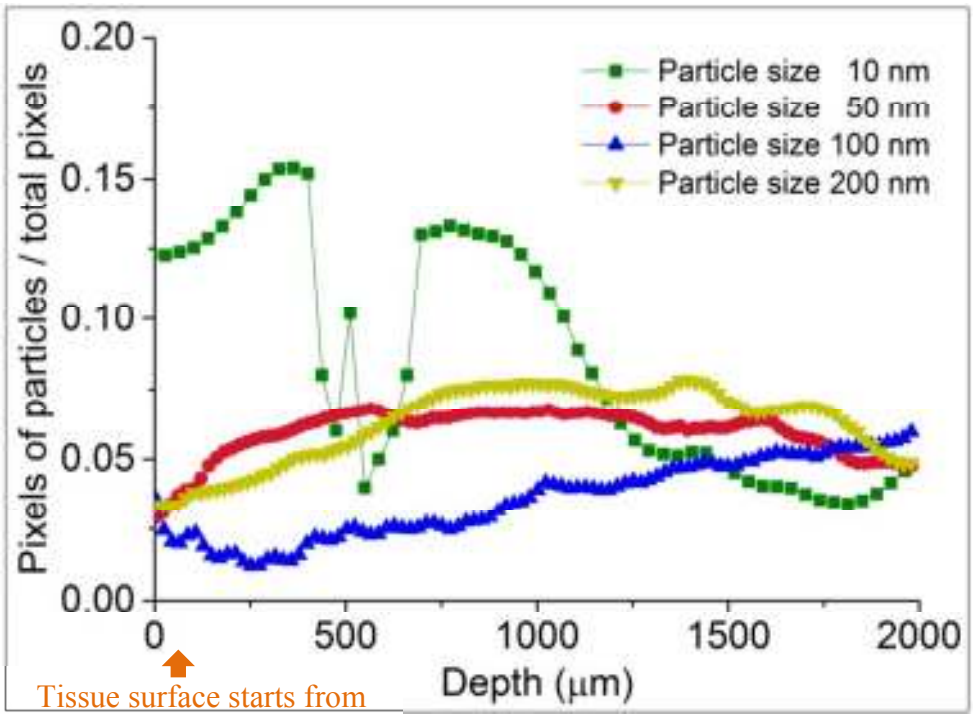

Figure 6.8 A diagram of distribution of particle density showing the effect of different particle sizes of the tested ferrofluids, 10, 50, 100, 200 nm in the characterisation of particle migration within 2 mm.

6.3 Proportion of Particle Density

Section 2 has presented the initial results of particle distribution using a relative density of bright pixels of particles to the total pixels (representing tissue and particles) obtained in every segment.

Section 3 presents a normalised distribution of particle density. Since the characterisation area has been fixed within a depth of 2 mm, particle density can be normalised by the overall density, identify as density proportion, as shown in the following equation. The trend of the proportion aims to show the variation of particle distribution due to the particles migration.

$$\text{Particle density proportion} = \frac{\text{Particle density of a specific segment}}{\text{Sum of the particle density}} \times 100\%$$

The distribution of particle density in Figure 6.5 is analysed and shown in Figure 6.9. The distribution clearly shows that the majority of the particles distribute in the deeper location in the case of concentration of 25 mg/ml. With the increase of the concentration, particles distribution becomes denser and particles gradually move closer to the magnetised tissue surface in the case of concentration of 100 and 200 mg/ml. This distribution satisfies the discussion in the section 6.2 which suggests the particles seem to migrate to the surface after the retraction.

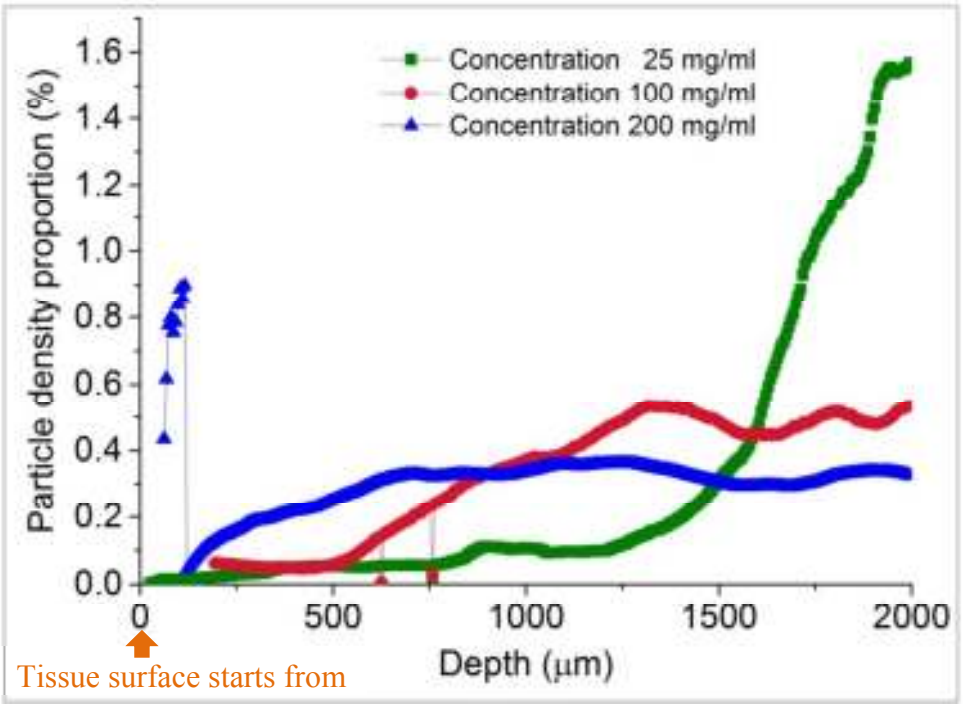

Figure 6.9 A diagram of distribution of particle density proportion showing the effect of three different concentrations, 25, 100, 200 mg/ml in the characterisation of particle migration within 2 mm.

The initial result shown in Figure 6.6 indicates that higher density is captured when a higher volume of ferrofluid is injected as expected. In addition to the distribution, Figure 6.10 clearly shows that in both the cases of a volume of 0.2 and 0.3 ml, the peaks have been observed near the magnetised tissue and the injection

site. On the other hand, the distribution of volume of 0.1 ml appears to be very stable at the injection position but the portion near the magnetised tissue surface appears to be few. The proportion distribution seems to be proportionate and satisfies the discussion in section 6.2, which has explained the valley found in the middle of the curves due to the particles migrating to the surface after the retraction. The particles are retracted closer to the magnetised tissue surface.

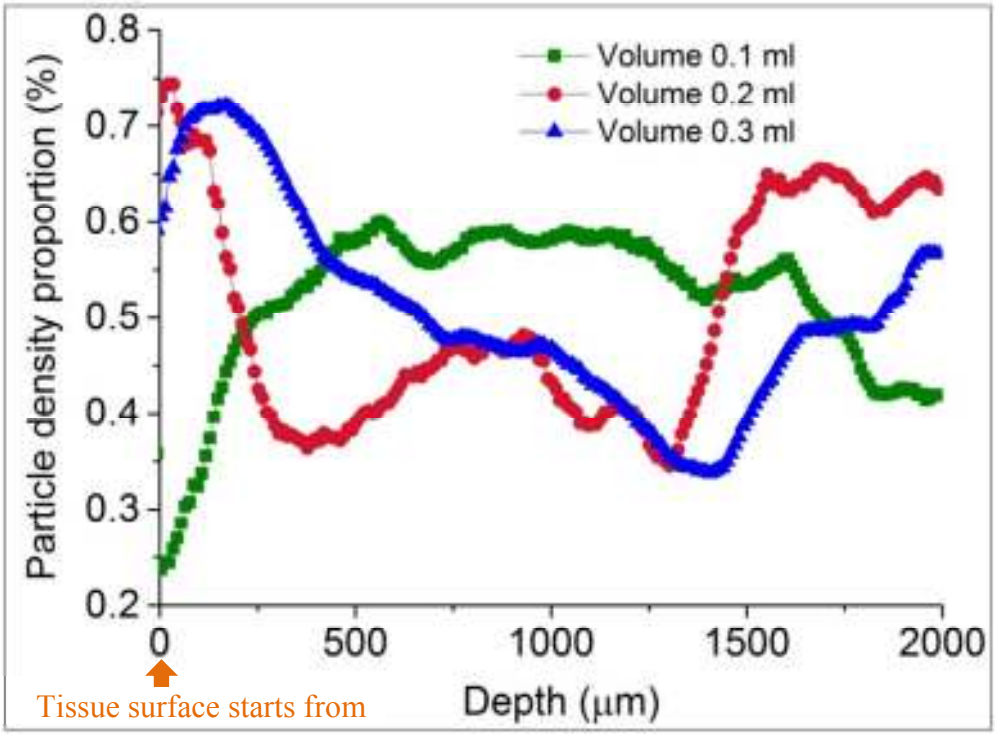

Figure 6.10 A diagram particle density proportion distribution showing the effect of three different injected volumes, 0.1, 0.2, 0.3 ml in the characterisation of particle migration within 2 mm.

Thirdly, Figure 6.11 shows a comparison of the distribution of the density proportions with respect to different magnetic field strengths under the testing condition of the particle size of 200 nm, the same concentration of 200 mg/ml and an injection volume of 0.1 ml. It can be seen that a lower magnetic field strength has resulted in denser particles at the depth of 2 mm. With the increasing the magnetic field strength, the portion moves slightly closer to the magnetised tissue surface.

Hence, the distribution of the proportion satisfies the discussion in section 6.2 which has stated that the particles seem to migrate to the surface due to stronger magnetic attraction.

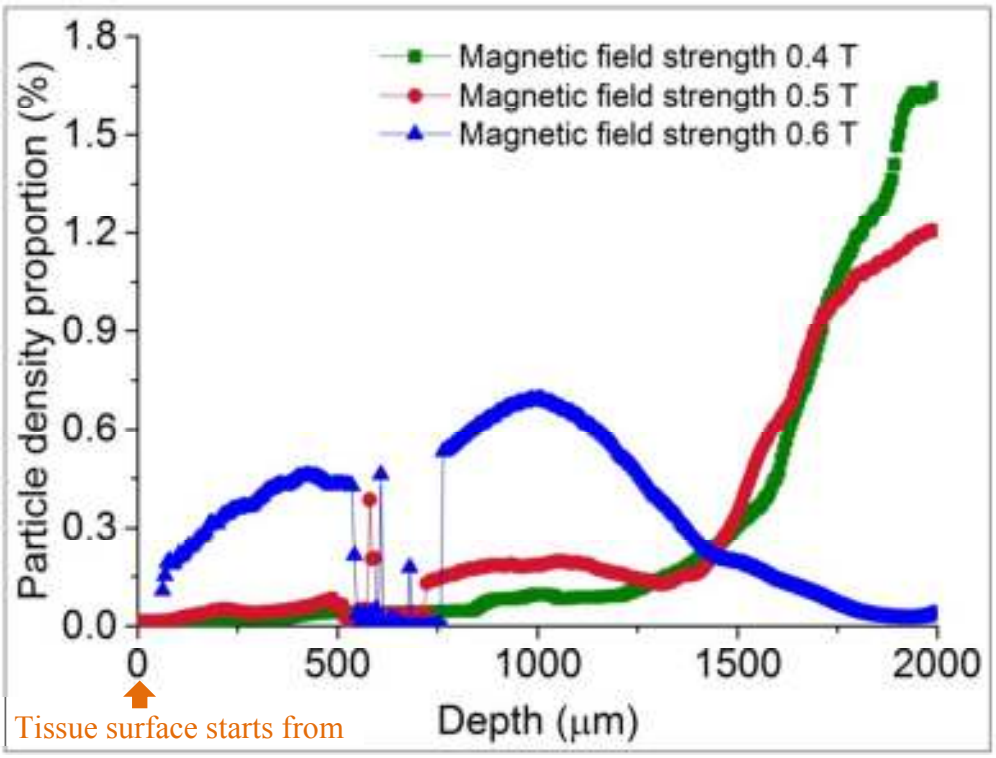

Figure 6.11 A diagram showing the effect of three different magnetic field strengths used in the retraction measurements, 0.4, 0.5, 0.6 T in the characterisation of particle migration within 2 mm.

Lastly, Figure 6.12 shows a comparison of distribution of the proportion with respect to different particle sizes. As described in section 6.2, the distribution of density proportion of the particle size of 10 nm also clearly shows that more particles gather near the injection and magnetised tissue surface. The variation may be not very significant in the tests of particle sizes, however, it can still be seen that the density proportion particles gradually move towards the magnetised tissue surface when their sizes reduce. This result satisfies the parametric study in the ex-vivo experiments where ferrofluid with smaller particle sizes has stronger adhesion force.

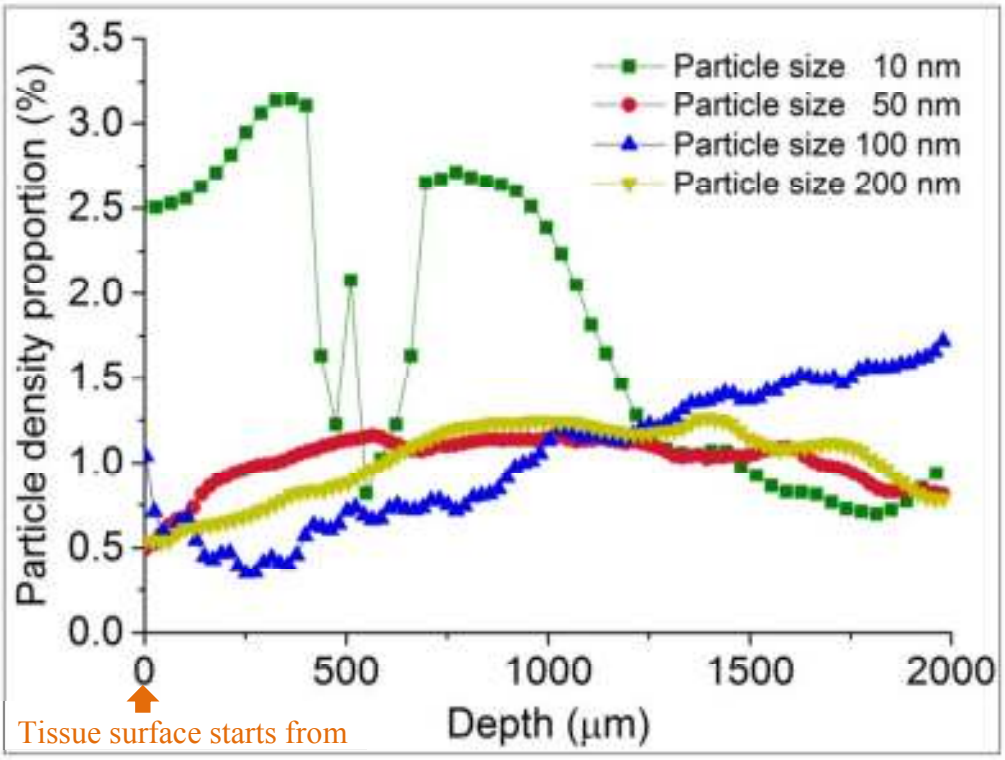

Figure 6.12 A diagram particle density distribution showing the effect of different particle sizes of the tested ferrofluids, 10, 50, 100, 200 nm in the characterisation of particle migration within 2 mm.

In the investigation in Figure 6.12, the particle size of 10 nm has the majority of particle density near the tissue surface. On the contrary, the tests of other particle sizes, such as 50 nm, 100 nm and 200 nm have the uniform distributions. There seems to have a size critia for particles migration. Therefore, the hypothesis of that the smaller particles are more available to migration by the magnetic retraction is discussed.

In terms of the smaller size of particles, the literature evidenced that the more number of particles can be stably suspended in the carrier fluid during the manufacture process (Vékás, 2008, Lin et al., 2005). And the number of particles directly affects the volume of magnetic material. Regarding the next chapter of the theoretical study of force prediction (see section 7.3.1), magnetic retraction force has a positive correlation with the volume of magnetic material. The volumes of the

magnetic material given the different particle sizes of ferrofluids in the same concentration and injection volume are summarised in Table 6.1. It can be seen that the ferrofluid with smaller size of particle has the largest amount of volume. The largest volume of ferrofluid provides the strongest retraction force as expected.

Table 6.1 A table showing the total volume of magnetic particles given different sizes of particles in ferrofluids.

Specified particle size (nm)	Averaged particle size (nm)	Concentration (mg/ml)	Injection volume (ml)	Volume of magnetic material (m^3)
10	40.25	25	0.1	5.43e-09
50	59.35	25	0.1	2.00e-09
200	121	25	0.1	2.87e-10

6.4 Summary

In summary, this chapter has focused on how the particles distribute using the micro-CT scanner. Previous literature has indicated that difficulty in characterisations of particles within tissue. This chapter has presented that particle distribution being successfully captured after the retraction.

Although the resolution of the voxel of the micro-CT scanner is 6.2 μm, which is much larger than the size of particles in nano-scale, the characterisations can show the contrast of ferrofluid particles and tissue in every segment. After processing these images, the results are then visually presented in diagrams with a relative density showing the locations where the particles gather.

Therefore, a self-developed image processing program has been introduced how the segments are transformed from RGB into Grey scale images. However, one

of the disadvantages of this characterisation method is the long duration time during the scanning. Besides, the data requires large the storage space in computer.

A few suggestions from this study to accelerate the scanning and to reduce the data size: 1) Control the characterisation zone, e.g. fix within a respond area of 2 mm depth, 2) Conduct the resolution study, e.g. voxel resolution of 6, 10, 20, 30 μm, 3) Fill the empty using fibres to fix the tissue during the scanning, the rotation during the scanning has affected the results.

The results of the particle distribution have presented that higher density near the tissue surface when the testing environment in high concentration, high volume and strong magnetic field. There are two diagrams showing the particle distribution: 1) particle density, 2) normalised density proportion.

In addition to the correlation between the particle distribution and interaction force, the conclusions are compared according to the results of ex-vivo adhesion measurements, as summarised in Table 6.2. It can be therefore concluded that the more particles distribute near the tissue surface, the stronger interaction force generates.

Lastly, the variation of particle distribution between different concentrations has been observed the most prominent, and variation between different magnetic field strengths is the second most significant. The variations between volumes and particle sizes are less significant in the observation of distribution of particle density. The conclusion of the significant effect from these experiments is fairly same as the conclusion by the Taguchi study in section 5.3.

The outcome in this chapter has not only overcomed the challenge to capture the particle migration within tissue but also highlighted the information linking with how to deploy the approach. The particle position data is extremely significant for

informing the clinical design, for example: the injection behaviour, ferrofluids concentration, particle size, dispersion level, needle depth and time perspective etc. The further study of working protocol and particle effect upon tissue can be referred to the method and results of this characterisation.

Table 6.2 The correlation summarised between particle distribution and interaction force with regard to the parametric study.

Particle distribution	Parameter study	Interaction force
High density occurs near tissue surface when high concentration	Concentration	Increases with the concentration increases
High density occurs near tissue surface when high volume	Volume	Increases with the volume increases
High density occurs near tissue surface when high magnetic field strength	Magnetic field strength	Increases with the magnetic field strength increases
Only a contrasting result in the case of 10 nm, the other distributions are uniform	Particle size	Increases with the particle size decreases

Chapter 7 Theoretical Analysis of Retraction and Adhesion Force

The capacity of ferrofluids to provide adhesion performance in tissue retraction has been studied by both ex-vivo and in-vivo experiments in Chapter 5. A spatial map of both the normal adhesion and shear adhesion in tissue retraction has also been established in the ex-vivo measurements. In the in-vivo study, the magnetic retraction has the potential for manipulating porcine bowel tissue.

In order to develop a protocol of the full understanding in using ferrofluids to manipulate tissue, a theoretical model is developed to improve the experimental design. A theoretical method can also assist in the design of a magnetic probe.

Besides, experimental measurements of a tiny amount of ferrofluids are costly. A theoretical model can improve the experimental design from an economic aspect. The testing environment can be simulated before manufacturing.

The theoretical model is developed through two different methods; a combination of a theoretical equation of magnetic interaction and the finite element method (FEM) of a magnetic field. The simulated results are integrated by the force equation to obtain the magnetic retraction force. This chapter is organised as follows. Section 1 reviews similar studies of modelling magnetic responses. Section 2 illustrates the simulation of modelling a magnetic field. Section 3 further shows the simulation of the adhesion which occurs both with and without contacting the magnetised tissue surface. Section 4 summarises this theoretical model.

7.1 Introduction

As described in a modified physical model in section 3.1, the behaviour of tissue retraction using nano-particle ferrofluids is a complex interaction which is associated with a number of physical, mechanical phenomena such as magnetic interaction, particle interaction and tissue surface adhesion.

According to section 3.5, the intensities of the magnetic response and tissue surface adhesion are within the range of a hundred to a thousand million-Newton forces, much stronger than the particles interaction of the van der Waals force. Given this, the theoretical model in this study is simplified to a combination of the magnetic interaction within tissue and the tissue surface adhesion.

There are similar approaches to simulating magnetic forces of the magnetic applications. For example, Lin and Valentine (2012a, 2012b) modelled the magnetic field of a ring-shaped NdFeB magnet using a computer software, called Finite Element Method Magnetics (FEMM). Their theoretical model could predict an associated force in order to separate DNA/RNA form a particle and could design a magnetic tweezers with a stronger magnetic field strength.

The theoretical method is particular useful in designing a complex magnetic configuration. For example, Hatch (2001) developed a theoretical model to simulate the complicated configuration of multiple permanent magnets before the configuration can be manufactured. Souza et al. (2010) observed that the geometry of tissue culture based on magnetic cell levitation would be similar to the geometry of human tumour xenografts. Based on this finding, they established a theoretical model using FEMM to study the magnetic field strength and the magnetic force on the path of nanoparticles in a mimic hydrogel.

Generally speaking, the models of bar, cylinder shaped magnet can be simplified as they have a symmetric feature. This is the advantage of a theoretical model for helping a design with a complicated configuration. In terms of the existing research in tissue retraction, Wang et al. (2009, 2010b) also established a theoretical model using a software package - COMSOL to simulate the magnetic interaction force of magnetic fluids in order to predict the adhesion force for tissue manipulation.

As said earlier, it is thought that a theoretical model will benefit the future experimental design by providing more efficient and economical solutions to estimating the maximum force.

Figure 7.1 shows how tissue retraction can be examined through a combination of experiments and simulations. Finite Element Method (FEM) is used to model the magnetic field generated by several accumulated cylinder shaped magnets in a spatial map.

The simulated fields are validated with the experimental results in section 5.1.5. Then, the magnetic retraction force against different tested parameters is calculated. The simulated results are again validated through ex-vivo experiments. Finally, the simulation model is established based on the validated results.

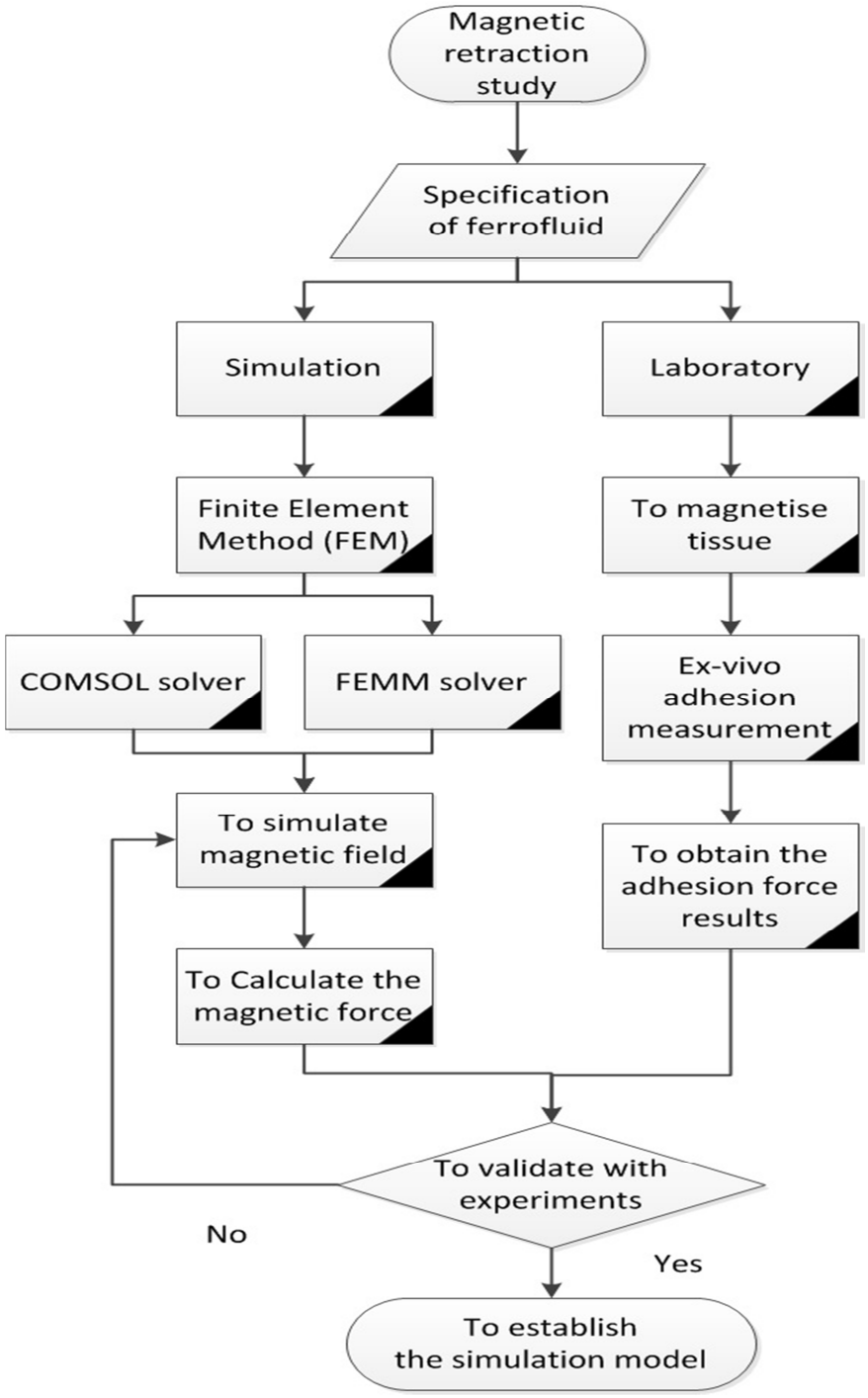

Figure 7.1 A flow diagram showing the integration of theoretical and experimental procedures in this study.

7.2 Theoretical Model of Cylinder Shaped Magnets

7.2.1 Theoretical Model of Magnetic field

In the review of the engineering problems with permanent magnets, which were normally assumed as a magnetostatic problem because the magnetic field does not change with time (Petit et al., 2011, Shliomis, 2003).

Besides, to simulate a cylinder shaped permanent magnet, the model is simplified as a circular current loop electromagnet, as shown in Figure 7.2.

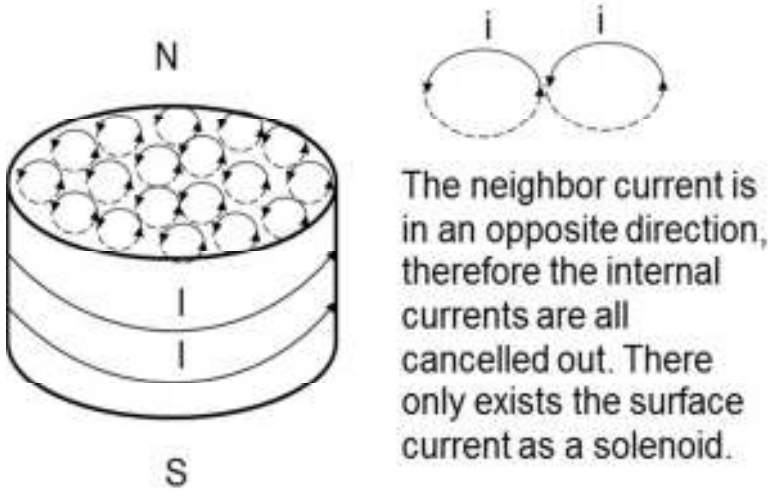

Figure 7.2 A schematic diagram showing a model of the cylinder permanent magnet. The external current is surrounded as the circular current loops and the internal current is cancelled out by its neighbour current due to an opposite direction.

The magnetic field can be defined by the Biot-Savart law which is valid in a magnetostatic field with a steady current. This law proposes that the magnetic field strength relates to three parameters: (i) magnitude, (ii) direction and (iii) length of the electric current, which can be seen in Equation 7.1. In addition, the simulation is based on another two assumptions that magnetic field is uniform and the existing current only surrounds the surface therefore it is a circular current loop. The internal current can be cancelled out due to the opposite direction of the neighbour current.

$$dB=\frac{\mu_0}{4\pi}\frac{Id\vec{s}\times\hat{r}}{r^2}$$ Equation 7.1

Equation 7.1 is the Biot-Savart law, which can estimate the magnetic field strength at a position from the source. μ_0 represents the permeability of air, a constant value of $4\pi * 10^{-7}$ H/m. I is the current and $d\vec{s}$ is a short length of the wire, r is a distance of any points in the free space to the centre of the magnet surface, and $\vec{r}$ is the unit vector.

In section 4.2.4, three magnetic configurations used in this study have been described and the associated magnetic field strengths are investigated between the magnet surface to a vertical distance of 50 mm, as shown in Figure 5.9.

In order to simulate each magnetic field of the cylinder shaped magnetic configurations, a model of a circular current loop is sketched as shown in Figure 7.3, representing the surface of the magnetic configuration

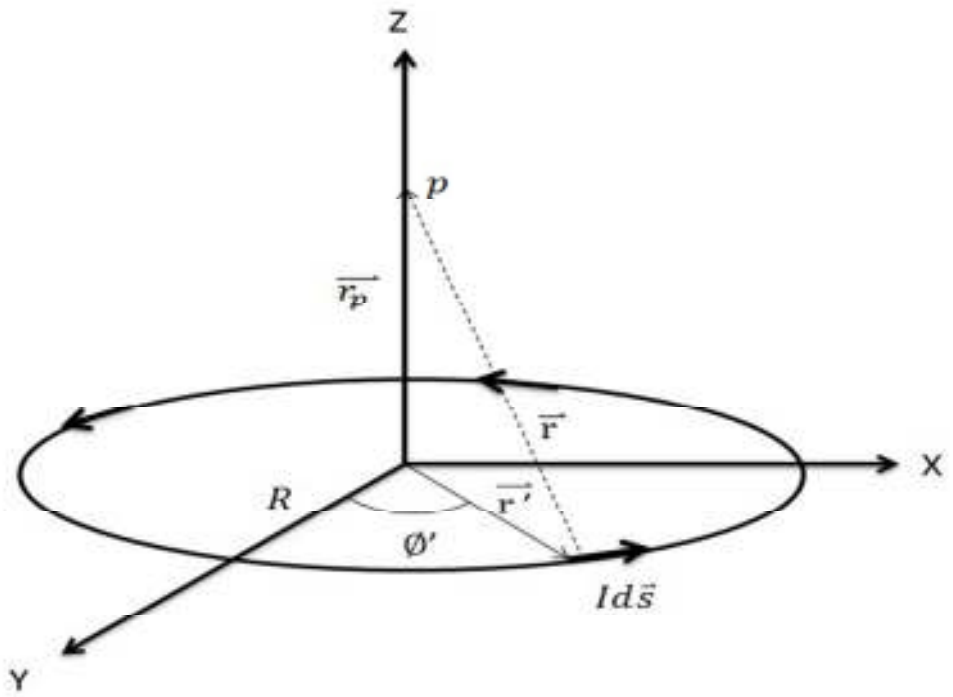

Figure 7.3 A magnetic field generated by a circular current loop which performs as the surface of a cylinder permanent magnet (Liao et al., 2004).

The magnetic field in the circular current loop can be referred to the textbook excerpted by Liao et al. (2004) and the magnetic field strength is expressed in the following expressions.

In a 3D model, $\hat{\imath}, \hat{\jmath}, \hat{k}$, are the unit vectors of X, Y, Z axes, respectively. $\emptyset$ is the angle and R is the radius of the wire.

In the X-Y plane,

$$\vec{r}'=R\left(\cos\emptyset\hat{i}+\sin\emptyset\hat{j}\right) \qquad \text{Equation 7.2}$$

A small current is assumed to flow through the wire changing with the angle and it is represented as,

$$Id\vec{s}=I\left(\frac{d\vec{r}}{d\emptyset'}\right)d\emptyset'=IRd\emptyset'(-\sin\emptyset\hat{i}+\cos\emptyset\hat{j}) \qquad \text{Equation 7.3}$$

If a particle is placed in a distance of z from the centre, the position vector of this particle can be represented as,

$$\vec{r_p}=z\hat{k} \qquad \text{Equation 7.4}$$

The vector $\vec{r}$ is combined by $\vec{r_0}$ and $\vec{r}'$, and the distance of r is obtained.

$$\vec{r}=\vec{r_p}-\vec{r}'=\left(-R\cos\emptyset\right)\hat{i}+(-R\sin\emptyset)\hat{j}+z\hat{k} \qquad \text{Equation 7.5}$$

$$|\vec{r}|=r=\sqrt{\left(-R\cos\emptyset\right)^2+(-R\sin\emptyset)^2+(z)^2}=\sqrt{R^2+z^2} \qquad \text{Equation 7.6}$$

In addition, the small current are expressed as,

$$Id\vec{s}=I\left(\frac{d\vec{r}}{d\emptyset'}\right)d\emptyset'=IRd\emptyset'\left(-\sin\emptyset\hat{i}+\cos\emptyset\hat{j}\right) \qquad \text{Equation 7.7}$$

So that a cross product are expressed as,

$$d\vec{s}\times\vec{r}=\begin{vmatrix} \hat{i} & \hat{j} & \hat{k} \\ -R\sin\emptyset d\emptyset' & R\cos\emptyset d\emptyset' & 0 \\ -R\cos\emptyset & -R\sin\emptyset & z \end{vmatrix}$$

$$=(Rz\cos\emptyset d\emptyset')\hat{i}+\left(R^2\sin^2\emptyset d\emptyset'\right)\hat{k}+\left(R^2\cos^2\emptyset d\emptyset'\right)\hat{k}+(Rz\sin\emptyset d\emptyset')\hat{j}$$

$$=R(z\cos\varnothing d\varnothing')\hat{i}+R(z\sin\varnothing d\varnothing')\hat{j}+R^2 d\varnothing'\hat{k} \qquad \text{Equation 7.8}$$

$$\text{The unit vector of } \hat{r}=\frac{\vec{r}}{r}=\frac{\vec{r_p}-\vec{r}'}{\left|\vec{r_p}-\vec{r}'\right|} \qquad \text{Equation 7.9}$$

Hence, the Biot-Savart law is expressed as,

$$dB=\frac{\mu_0}{4\pi}\frac{Id\vec{s}\times\hat{r}}{r^2}=\frac{\mu_0}{4\pi}\frac{Id\vec{s}\times\vec{r}}{r^3}=\frac{\mu_0 I}{4\pi r^3}\left(R(z\cos\varnothing d\varnothing')\hat{i}+R(z\sin\varnothing d\varnothing')\hat{j}+R^2 d\varnothing'\hat{k}\right)$$

$$=\frac{\mu_0 I}{4\pi(R^2+z^2)^{\frac{3}{2}}}\left(R(z\cos\varnothing d\varnothing')\hat{i}+R(z\sin\varnothing d\varnothing')\hat{j}+R^2 d\varnothing'\hat{k}\right) \qquad \text{Equation 7.10}$$

And the magnetic field strengths of each direction are integrated as,

$$B_x=\int_0^{2\pi}\frac{\mu_0 IR}{4\pi\left(R^2+z^2\right)^{\frac{3}{2}}}(z\cos\varnothing)d\varnothing'=0$$

$$B_y=\int_0^{2\pi}\frac{\mu_0 IR}{4\pi(R^2+z^2)^{\frac{3}{2}}}(z\sin\varnothing)d\varnothing'=0$$

$$B_z=\int_0^{2\pi}\frac{\mu_0 IR^2}{4\pi(R^2+z^2)^{\frac{3}{2}}}\,d\varnothing'=\frac{2\pi\mu_0 IR^2}{4\pi(R^2+z^2)^{\frac{3}{2}}}=\frac{\mu_0 IR^2}{2(R^2+z^2)^{\frac{3}{2}}} \qquad \text{Equation 7.11}$$

According to Equation 7.11, the magnetic field strength at a distance of z from the surface of magnet can be predicted. Figure 7.4 presents a normalised diagram of magnetic field strength between the distance of z to the surface, calculated using Matlab® software.

The ratio of the magnetic field strength between the gap distances from the centre of the circular current loop is obtained based on the theoretical model. It can be seen that the magnetic field strength is strong near the magnet surface and the diagram is as the same as shown in Liao et al. (2004). However, this theoretical model found the magnetic field strength along the vertical direction z axis. Therefore, next Section 7.2.2 introduced another method to simulate the magnetic field strength by Finite Element Method software package – FEMM.

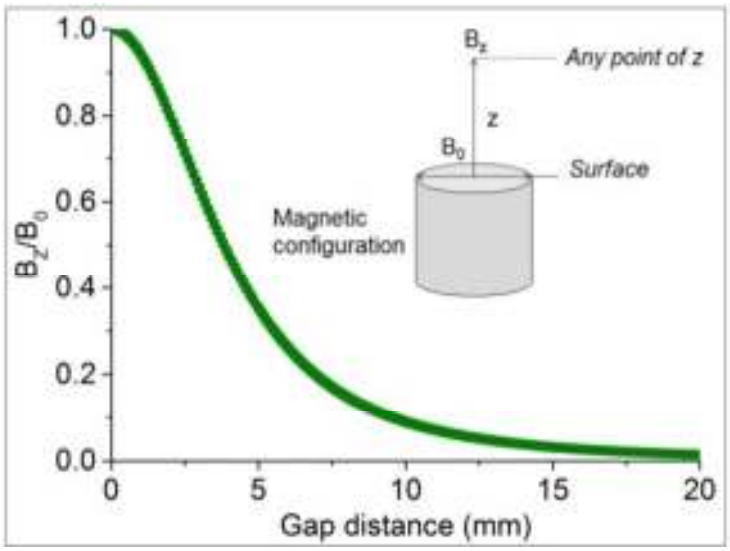

Figure 7.4 A normalised diagram showing the magnetic field strength from the centre of circular current loop to a distance of 20 mm height.

7.2.2 2D FEMM Modelling of Magnetic Field

This section introduces a method of using the Finite Element Method Magnetics (FEMM) to model the field magnitude at any spatial location of the three different configurations of cylinder shaped permanent magnets.

FEMM is a free software to solve low frequency electromagnetic and magnetostatic problem particularly (Meeker, 2011). It contains three parts – a CAD interface to sketch the geometry of problem, a triangle mesh method to conduct finite element method and solvers for specific problems, such as magnetic, electrostatic, heat-flow and current flow problems. Briefly, FEMM formulates a physical problem in a 2D axisymmetric model with the electromagnetic relative equations and solves using finite element method. The equations include Maxwell's formula and a constitutive relationship between magnetic field density (H) and magnetic flux density (B). The magnetic flux density is composed of the magnetic field lines, also known as magnetic field strength.

$$\nabla \times H = J$$

$$\nabla \cdot B = 0$$

$$B = \mu(H) \qquad \text{Equation 7.12}$$

In this study, the problem definition is identified as following features.

- Magnetostatic problem
- Axisymmetric
- All units in millimetres
- Zero frequency (Time independence)

The NdFeB permanent magnets is identified by knowing two properties, coercivity (H_c) and relative magnetic permeability (μ_r), to establish similar magnetism and field.

H_c is an intensity to demagnetise the magnetic field of a specific material to zero. Permanent magnets have high coercivity so that they are also known as magnetically hard material.

This quantity was experimentally measured by a B-H analyser or magnetometer. According to the information provided in Table 7.1, the H_c of material N35, used in this study, was about 867000 A/m (eMagnetsUK, 2010).

Table 7.1 Magnetic properties of NdFeB materials (eMagnetsUK, 2010).

Minimum Values

Material		Br		Hc (Hcb)		Hci (Hcj)		(BH)max	
		mT	G	kA/m	Oe	kA/m	Oe	kJ/m3	MGOe
N27		1,030	10,300	796	10,000	955	12,000	119	25
N30		1,080	10,800	796	10,000	955	12,000	223	28
N33		1,130	11,300	836	10,500	955	12,000	247	31
N35		1,170	11,700	867	10,900	955	12,000	263	33
N38		1,210	12,100	899	11,300	955	12,000	287	36
N40		1,240	12,400	923	11,600	955	12,000	302	38
N42		1,260	12,600	923	11,600	955	12,000	318	40
N45		1,320	13,200	875	11,000	955	12,000	342	43
N48		1,380	13,800	836	10,500	875	11,000	366	46
N50		1,400	14,000	796	10,000	875	11,000	382	48
N52		1,430	14,300	796	10,000	875	11,000	398	50

Permeability indicates a level of the material ease with the magnetic field. It is often identified as the ratio of induction and conduction, as such, magnetic flux density (B) to the conducted magnetising field (H). Hence it is represented by the following equation.

$$\mu = \frac{B}{H} \qquad \text{Equation 7.13}$$

Likewise, the relative permeability (μ_r) is the ratio of the material's permeability to the permeability in the air, $1.26*10^{-6}$ H/m, which can be written as the following equation.

$$\mu_r = \frac{\mu_{material}}{\mu_{air}} \qquad \text{Equation 7.14}$$

In this study, the μ_r of a N35 magnet obtained is 1.05, higher than the permeability of air. The permeability of N35 material is $1.32*10^{-6}$ H/m.

The geometries of the magnetic configurations used in this study have been mentioned in section 4.2.3. The model developed in FEMM is built up following the real dimensions of three different configurations: (M_A) 10 mm height and 20 mm

diameter width, (M_B) 10 mm height and 10mm diameter width, (M_C) a combination of (M_A) and (M_B).

In addition to the model, the cylinder shaped model is drawn in an axisymmetric system as a rectangular block, as shown in Figure 7.5(a). A cylinder can be therefore formed when the block rotates. Once the geometry is established, triangle mesh is generated to the model and the corners where supposed to have more magnetic field lines are particularly emphasised, as shown in Figure 7.5(b).

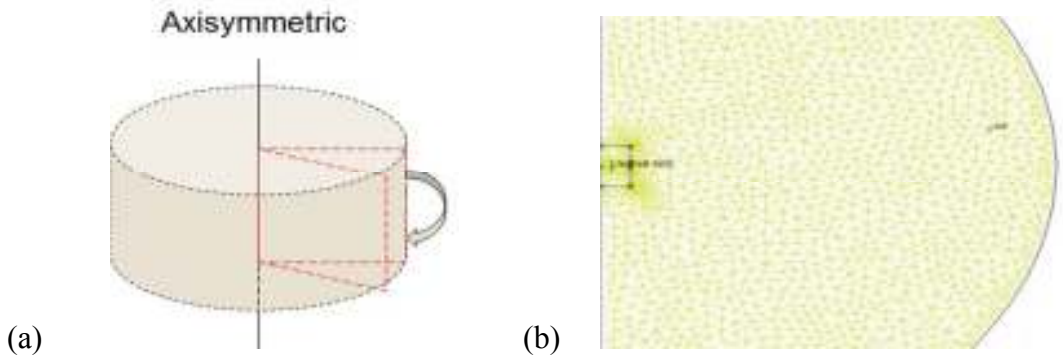

Figure 7.5 (a) A schematic diagram showing that the axisymmetric sketch can be simplified as a rectangular block (b) The meshed diagram showing a magnet in a surrounding air space.

Figure 7.6 shows the gradient of magnetic field strengths of three different magnet configurations used in tissue retraction from the simulated results. The result is associated with magnetic lines. It can be seen that magnetic field strength is increased in the configuration of a combination of two magnets in terms of shapes accumulated. In addition, the magnetic field lines at the edge of magnet are clearly denser which indicated that strength is stronger there. The magnetic field strength at a very short distance from the surface is averaged to a magnitude of each represented configuration as 0.4, 0.5 and 0.6 T, respectively.

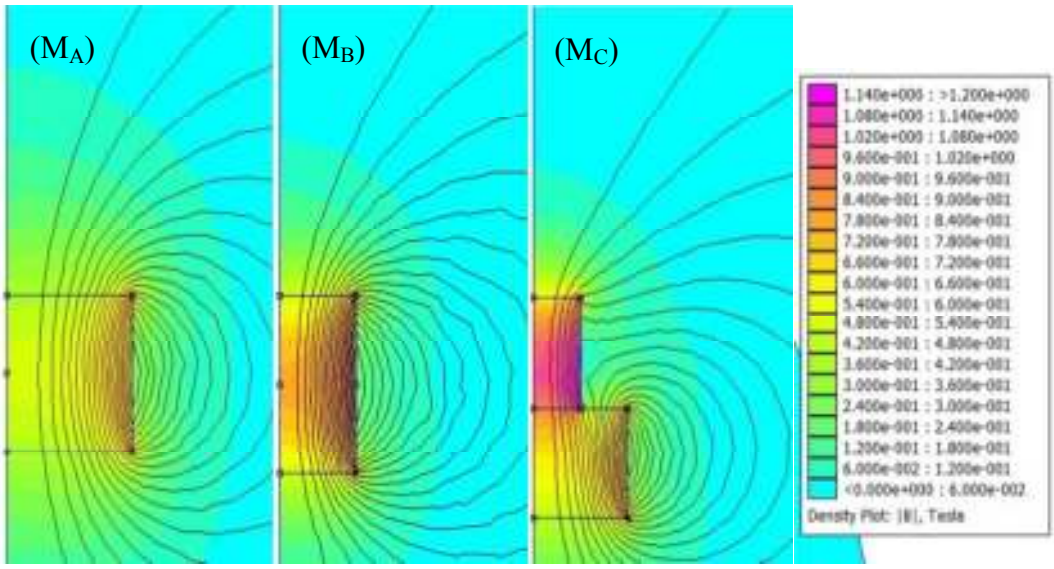

Figure 7.6 Simulated results of three magnetic configurations used in the experimental study showing the intensity distribution of magnetic field and associated lines.

The gradients of magnetic field strengths along the vertical direction (B_Z) upon the surface in three different magnet configurations are presented in Figure 7.7. The field strength is a function of distance and is in particular greater when the distance of z is short, as expected in the experimental measurement of magnetic fields.

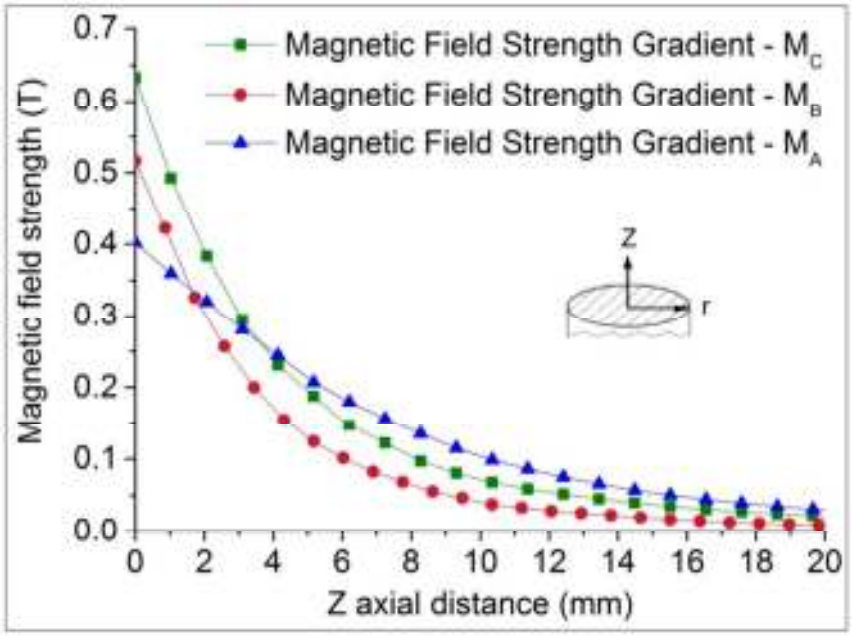

Figure 7.7 A diagram showing the strength distribution of three magnetic fields along the vertical direction Z axis.

The simulated strength gradients are verified by the experimental result in section 5.1.5 obtained by the Gaussmeter. Both the experimental and simulated result are presented in Figure 7.8. The comparison between the experimental and simulated result shows a very similar relationship of three different magnetic fields. The strongest magnetic field strength occurs in the configuration M_C. Although the configuration M_A has the weakest magnetic field strength, its magnetic response at far distance shows higher than the other configurations.

Overall, this simulation models satisfy all the experimental results. The slight difference of magnitude is caused by the different selected location from the magnet surface. The simulation is obtained at the exactly central position of the magnet. However, the sensor of the Gaussmeter is 4 mm width, which differs from the exact location so that there is an error between the experiment and simulation.

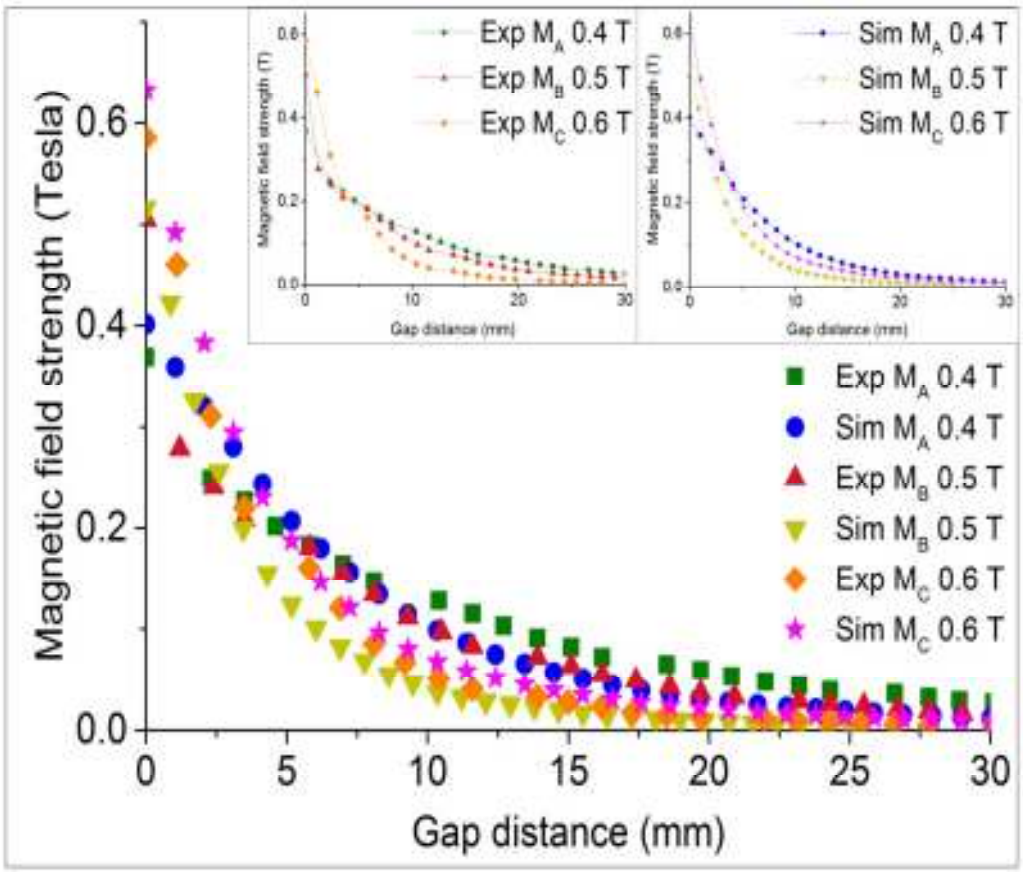

Figure 7.8 A comparison showing results between the simulation using FEMM and experiment of the three different magnet configurations.

7.3 Estimation of Magnetic Force

7.3.1 Force Model

Section 2 has shown the methods to simulate the magnetic field. This section continues the theoretical model to calculate the retraction forces following the simulated field strengths.

As described in the physical model in section 3.1. The mechanism of tissue retraction should be divided into two magnitudes as the retraction force and adhesion force. When the magnetised tissue is exposed to the magnetic field, there is a retraction force, mainly caused by the magnetic interaction. On the other hand, when the magnetised tissue is in contact with the magnet, there is a combination of the magnetic interaction as well as tissue surface adhesion. The surface adhesion is obtained from the adhesion measurement of the plain tissue, as mentioned in section 5.1.2.

According to the survey of magnetic application (Pamme and Manz, 2004, Hatch and Stelter, 2001, Pamme, 2006), magnetic force (F_{mag}) is proportional to the magnetic field strength (B) and the gradient of the magnetic field strength ($\nabla \cdot B$) of the external applied field. Besides, F_{mag} is also proportional to the volume of conducted material (V), and the difference of magnetic susceptibility between the particle and the fluid, ΔX.

$$F_{mag} = \frac{\Delta X \cdot V_t}{2X_0} \nabla(B^2) \qquad \text{Equation 7.15}$$

This equation is expressed as,

$$F_{mag} = \frac{\Delta X \cdot V_t}{\mu_0} (\vec{B} \cdot \nabla)\vec{B} \qquad \text{Equation 7.16}$$

In addition to the coefficients, the magnetic susceptibility varies with different type of tissue and media. The magnitude can be referred to the study in the MRI

application. Vignaud et al. (2005) studied the magnetic susceptibility of tissue with blood and parenchyma roughly in the range from -8.8×10^{-6} to -9.1×10^{-6}. In addition, the magnetic susceptibility of air is about $+0.37\times10^{-6}$. The magnetic susceptibility of magnetite (Fe_3O_4) is about 6000×10^{-3} (Grant and West, 1965). The overall difference of magnetic susceptibility can be estimated by a linear equation which includes the injected magnetic particles, similar to a series resistance. Therefore, the ΔX of tissue is about

$$\Delta X=X_{air}-(X_{particle}+X_{tissue}) \qquad \text{Equation 7.17}$$

There are two ways to determine total volume of material (V_t) in this study. Firstly, volume of a single particle (V_p) times by the number of particles while the exact numbers are provided by the specimen sheet. Alternatively, total volume can be worked out by the basic relationship of concentration, injected quantity and density. For example the density of magnetite is 5.17 g/cm^3. The total volume is a product of concentration and quantity then divided by the density. The number of particles can be found by dividing by the volume of a single particle.

The shape of particles was assumed as a uniform sphere although each particle might be not always the same. The volume of a single particle (V_p) was estimated by the sphere volume equation, which with a radius of half particle size.

$$V_p=\frac{4}{3}\times\pi\times r^3 \qquad \text{Equation 7.18}$$

After the introduction of the magnetic force equation, a study of the agreement of all units used in the equation is derived as following. The units are summarised in Table 7.2.

Table 7.2 A unit table of the parameters used in force equation.

Symbol	Definition	SI Unit
F	Force	$kg \cdot m \cdot s^{-2}$ or N
ΔX	Difference of magnetic susceptibility	Dimensionless
μ_0	Permeability of air	$Wb \cdot (A \cdot m)^{-1}$
V_t	Total volume of particles	m^3
B	Magnetic field density	$Wb \cdot (m^2)^{-1}$ or T
$\nabla \cdot B$	Magnetic field density gradient	$Wb \cdot (m^3)^{-1}$ or $T \cdot m^{-1}$

$$F_{mag}=\frac{\Delta X \cdot V_t}{\mu_0}(B \cdot \nabla)B$$

$$\Rightarrow \frac{kg \cdot m}{s^2}=\frac{1}{\frac{Wb}{A \cdot m}} \cdot m^3 \cdot \frac{Wb}{m^2} \cdot \frac{Wb}{m^3}=\frac{A \cdot Wb}{m} \qquad \text{Equation 7.19}$$

Referring to the definition of Tesla (T),

$$1T=1\frac{N}{A \cdot m}$$

$$\Rightarrow \quad 1N=1T \cdot A \cdot m$$

$$\Rightarrow \quad 1\frac{kg \cdot m}{s^2}=1\frac{Wb}{m^2} \cdot A \cdot m=1\frac{A \cdot Wb}{m} \qquad \text{Equation 7.20}$$

The expressions above show that all the units in the equation in a balance state. The units of these parameters are all in SI units. The magnetic force is then estimated by solving the force equation using Matlab® program.

$$F_{mag}(z)=\frac{\Delta X \cdot V_t}{\mu_0}(\vec{B}) \cdot (\frac{\partial B}{\partial x}\hat{i}+\frac{\partial B}{\partial y}\hat{j}+\frac{\partial B}{\partial z}\hat{k}) \qquad \text{Equation 7.21}$$

The product of two vector terms, the gradient and the magnetic field, become the scalar terms representing a magnetic field strength at a location along the vertical direction (z axis).

7.3.2 Numerical Parametric Study

The magnetic retraction force is predicted by the force model mentioned in section 7.3.1. The simulation is modified with a coefficient R in the force model as the following equation. Table 7.3 summaries the parameters used in the equation, including the density of the magnetite (Fe_3O_4), the difference of magnetic susceptibility between air, tissues and particles, and the magnetic permeability of air.

$$F_{mag}(z)=R\cdot\frac{\Delta X\cdot V_t}{\mu_0}(\vec{B})\cdot(\frac{\partial B}{\partial x}\hat{i}+\frac{\partial B}{\partial y}\hat{j}+\frac{\partial B}{\partial z}\hat{k}) \quad \text{Equation 7.22}$$

Table 7.3 The parameters used in force equation.

Parameter	Magnitude
Density of Fe_3O_4 (kg/m^3)	5.17e+03
Difference of magnetic susceptibility	6000e-03
Permeability of air ($Wb\cdot(A\cdot m)^{-1}$)	4πe-07

Table 7.4 presents the control variables in the parametric studies. The simulation includes three different particle sizes of 10, 50 and 200 nm, three different magnetic field strengths of 0.4, 0.5 and 0.6 T, three different volumes of 0.1, 0.2 and 0.3 ml and three different concentration of 25, 100, 200 mg/ml.

The predicted results are verified by the ex-vivo experiments. A validation is studied of the size applied in the theoretical model to represent particles suspended in ferrofluids. Referring to the particle size characterised in section 5.2, every ferrofluid has a specified size and an averaged size. These two particle sizes are applied in the numerical study to compare which size is suitable for the simulation, as shown in Figure 7.9.

Table 7.4 A table showing the parameters of different ferrofluids used in the numerical study. The estimated single volume and total volume of the particle(s) were marked by *.

Ferrofluids specification size (nm)	10	50	200
Numbers (/g)	1.13+017	1.3e+016	2.2e+014
Size characterisation diameter (nm)	40.25	59.35	121
Size characterisation radius (nm)	20.13	29.68	60.5
1st Quantity (ml)	0.1	0.1	0.1
Concentration (mg/ml)	200	200	200
Numbers	2.34e+015	2.6e+014	4.4e+012
Volume of single particle (cm^3)*	3.42e-17	1.10e-16	9.28e-16
Volume of total particles (cm^3)*	7.72e-02	2.85e-02	4.1e-03
2nd Quantity (ml)	0.2	0.2	0.2
Concentration (mg/ml)	200	200	200
Numbers	4.68e+015	5.2e+014	8.8e+012
Volume of single particle (cm^3)*	3.42e-17	1.10e-16	9.28e-16
Volume of total particles (cm^3)*	1.54e-01	5.69e-02	8.2e-03
3rd Quantity (ml)	0.3	0.3	0.3
Concentration (mg/ml)	200	200	200
Numbers	7.02e+015	7.8e+014	1.32e+013
Volume of single particle (cm^3)*	3.42e-17	1.10e-16	9.28e-16
Volume of total particles (cm^3)*	2.31e-01	8.54e-02	1.22e-02

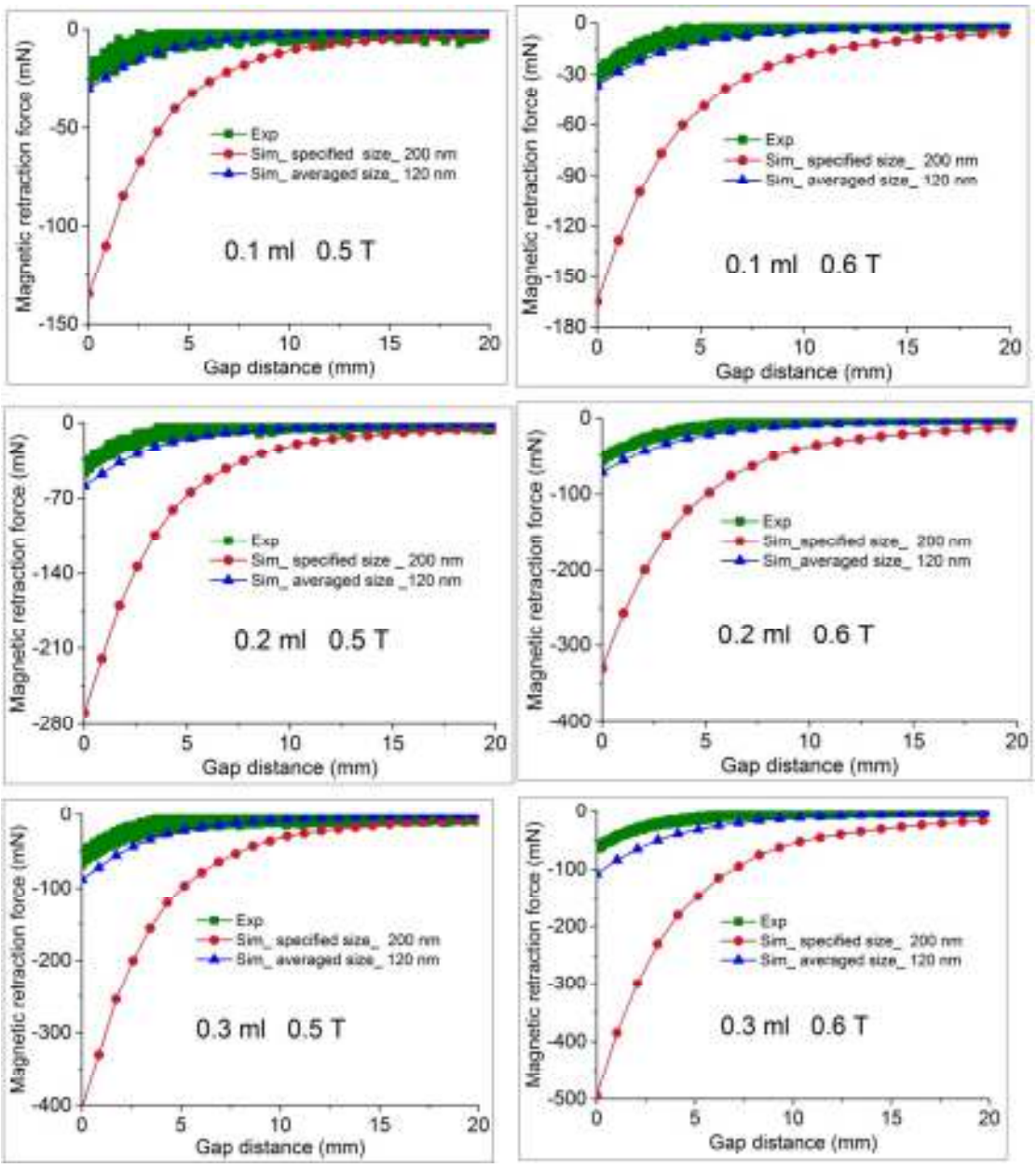

Figure 7.9 The validation of simulation results and experimental results. The simulation showing two different particle sizes: 1) the specified size and 2) the averaged size from the characterising experiment.

It can be seen in the diagrams that the simulations using the specified size of 200 nm are fairly larger than the experimental results. The simulated retraction force of the averaged size is very similar to the experimental results.

Therefore, the averaged size from the characterisation is applied in the following simulation and the model is found to be very similar with the

experimental result, as shown in Figure 7.10. The retraction forces of ferrofluids with two different particle sizes of 10 and 50 nm are compared.

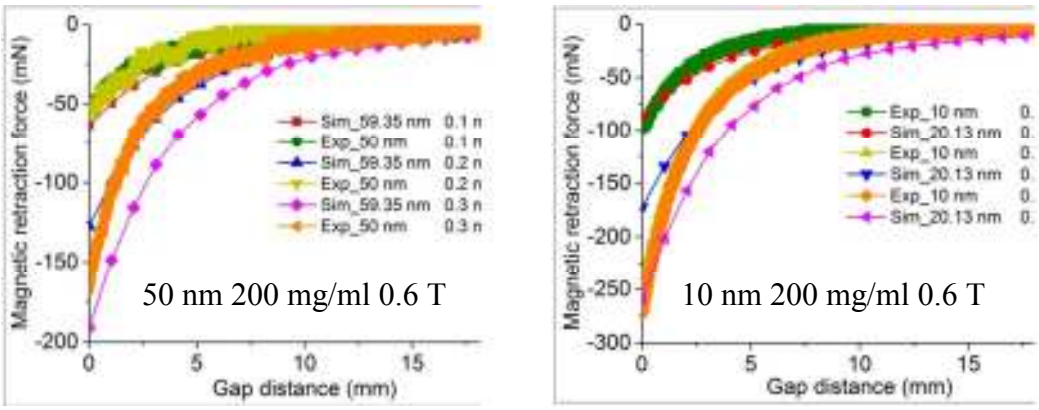

Figure 7.10 The validation of simulation results and experimental results. The parameter is the different particle sizes in the configuration of different volume.

In the most of comparisons, the magnetic retraction force of the experiments is less than the predicted results except the case of 10 nm with the volume of 0.2 ml. The variation could be due to the systematic errors during the experiments or the associated locations of the injections. Table 7.5 summarises the predicted retraction force of ferrofluids with three tested particle size, 10, 50 and 200 nm under the highest magnetic field strength of 0.6 T and the highest concentration of 200 mg/ml.

The governing equation of force model indicates that magnet retraction force supposes to be linear proportional to the volume and concentration of ferrofluids. The magnetic retraction force increases when the concentration and volume of ferrofluids increases. In addition, the retraction force of single particle is predicted in terms of the associated particle size. A larger magnetic particle has a stronger retraction force.

Table 7.5 Numerical results of magnetic response force in terms of different particle size.

Ferrofluids particle size (nm)	10	50	200
Concentration (mg/ml)	200	200	200
Magnetic field strength (T)	0.6	0.6	0.6
1st Quantity (ml)	0.1	0.1	0.1
Predicted maximum magnetic retraction force (mN)*	86.34	63.67	36.51
Predicted maximum magnetic retraction force of single particle (mN)*	3.82e-011	2.45-010	8.30e-009
2nd Quantity (ml)	0.2	0.2	0.2
Predicted maximum magnetic retraction force (mN)*	172.68	127.35	73.01
Predicted maximum magnetic retraction force of single particle (mN)*	3.82e-011	2.45-010	8.30e-009
3rd Quantity (ml)	0.3	0.3	0.3
Predicted maximum magnetic retraction force (mN)*	259.01	191.02	109.52
Predicted maximum magnetic retraction force of single particle (mN)*	3.82e-011	2.45-010	8.30e-009
Coefficient R	0.023	0.047	0.188

It can be seen that the coefficient R was increased with the increased particle size. This coefficient used in different particle size is not changed in terms of other parameters, such as concentration, volume and magnetic field strength.

The last model is to simulate the ferrofluids with coated particles. To characterise the thickness of the coating layer on the particle is difficult, therefore, a

particle model is assumed to separate the particle size uniformly into three intervals so that the diameter of the core of magnetic particle became one-third of the size, as shown in Figure 7.11.

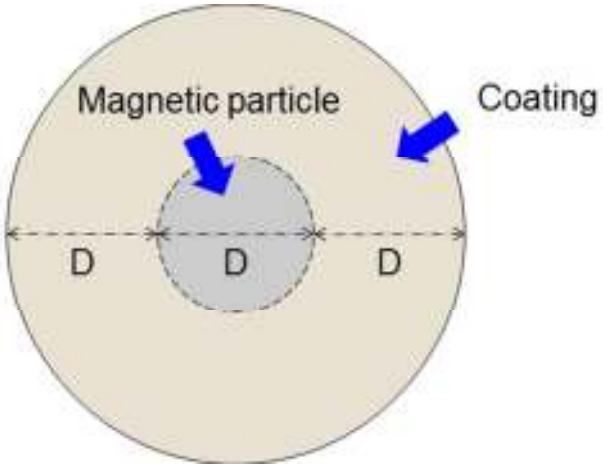

Figure 7.11 An assumed model of the coated particle in the ferrofluid showing the sphere is divided into three intervals. The middle section representing the diameter of the core of a particle.

The simulations of the ferrofluids with coated particles are presented in Figure 7.12. Although the radius of the magnetic particles is not accurate number, it can be seen that the simulated results of retraction using ferrofluids with Amine and DEAE coating were similar to experiments. The properties of the coated particles are summarised in Table 7.6.

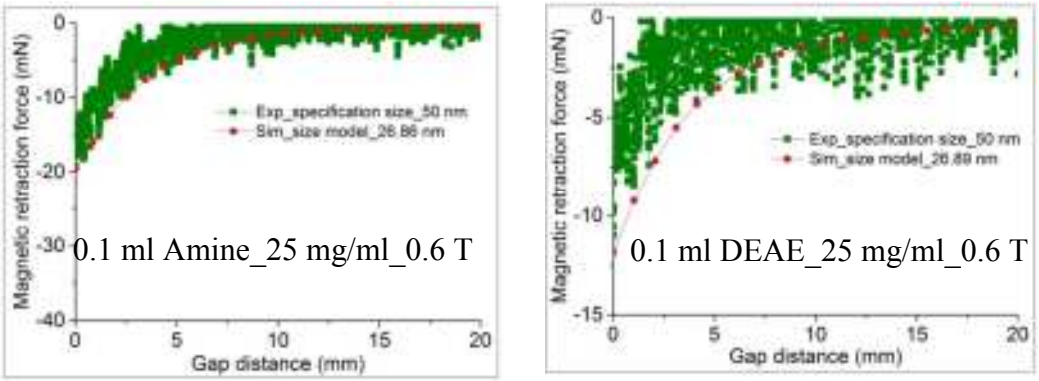

Figure 7.12 The validation of simulation results and experimental results. The parameter is the different particle sizes in the configuration of different volume.

Table 7.6 A table of the properties of the ferrofluids with coated particles.

Ferrofluids	Amine	DEAE
Numbers (/g)	1.3+016	1.3e+016
Size characterisation (nm)	80.59	80.67
Core size (nm)	26.86	26.89
Concentration (mg/ml)	25	25
Magnetic field strength (T)	0.6	0.6
Quantity (ml)	0.1	0.1
Predicted maximum magnetic retraction force (mN)*	23.6	11.84
Predicted maximum magnetic retraction force of single particle (mN)*	7.26e-010	3.64e-010

7.4 Summary

In summary, a numerical study has been established to validate the experimental results in this chapter. Two methods are introduced to simulate the magnetic field strength. The Biot-Savart Law can obtain the ratio of magnetic field strength along the z direction vertical to the magnet surface. The other method of using the FEMM software can obtain the magnetic field strength of a drawing magnet, which can be used in designing the complex magnetic configuration to get stronger field strength. Both of methods can be integrated by the force equation to the magnetic retraction force.

In terms of the retraction force equation, the simulated results are validated by the experiments. Applying the averaged size from experimental characterisation in

the force equation has generated the retraction curve highly similar to the experimental result.

The validation evidences that the force equations can be used to predict the magnetic retraction force. The theoretical model can assist the experimental design effectively and supports the protocol with a physical understanding.

Chapter 8 Discussions

It has been mentioned in the Chapter 2 that there is a concern related to the adverse effects of grip forces applied by conventional graspers resulting in tissue damage during laparoscopic surgery. A sufficient grip force should reside in the range between the pinch force and slippage. However, implementation of conventional graspers is normally blind and often relies on surgeon's experience. An understanding of the applied force and surgeon's training processes are often discussed.

Nowadays, there are also some alternative methods introduced to manipulate tissue during laparoscopic surgery, e.g. MAGS, Vacuum pressure, magnetic fluids and some specific procedure. Instead of using grip forces, these applications use the retraction force to manipulate tissue. In addition to magnetic fluids, the associated retraction has more flexibility and less issues of magnetic collision. This study investigates the feasibility and quantitative forces that are achieved for retraction performance using a nano-particle magnetic fluid, ferrofluid.

Previous chapters have presented systematic investigations of the feasibility of using ferrofluids to manipulate tissue. However, these investigations also bring new questions. This chapter discusses the results, findings and the relevance to other published literature. It is structured as follows. Section 1 discusses how much loading is optimised to indent on tissue. Section 2 discusses how to improve the mechanical design by altering magnetic field strength. Section 3 discusses the required retraction force and a comparison with other developing methods in tissue manipulation.

8.1 Threshold of Loading

The magnetic retraction has demonstrated that a physical contact is made after the retraction. Would the contact affect the performance in tissue retraction?

In the literature review of flat-end indentation, preload has been studied in performance. For example, Roshan et al. (2011) studied the effect of preload on adhesion force of the microfiber pad attached on peritoneum tissue and concluded that the adhesion force reached a plateau after 10 mN. In addition, Greiner et al. (2007) reported that adhesion force was increased beyond hundred μN. However, the adhesion force reached a plateau when the value was more over the range than 1 mN. Besides, Long and Hui (2009) mentioned that the adhesion force is independent of preload if the preload is over a criteria. In the section 5.1.4, preload is investigated that being independent from the magnetic retraction effects.

However, how much loading on tissue is sufficient during the magnetic retraction? Since the greater the applied forces indent the tissue, the greater the damage are perform (Rodrigues et al., 2012). Therefore, a prediction of a sufficient depth of indentation is discussed as following.

A formula of the relationship between the applied force and indentation depth from an indentation by a flat-end cylinder was developed by Sneddon (1965). A compression is made by the indentation, as shown in Figure 8.1.

The formula shown below suggests that the depth of the compression is linear proportional to the applied force. F denotes the preload force, a denotes the radius of the cylinder, E denotes the Young's modulus of the substrate and d denotes the indentation depth.

$$F=2aEd$$

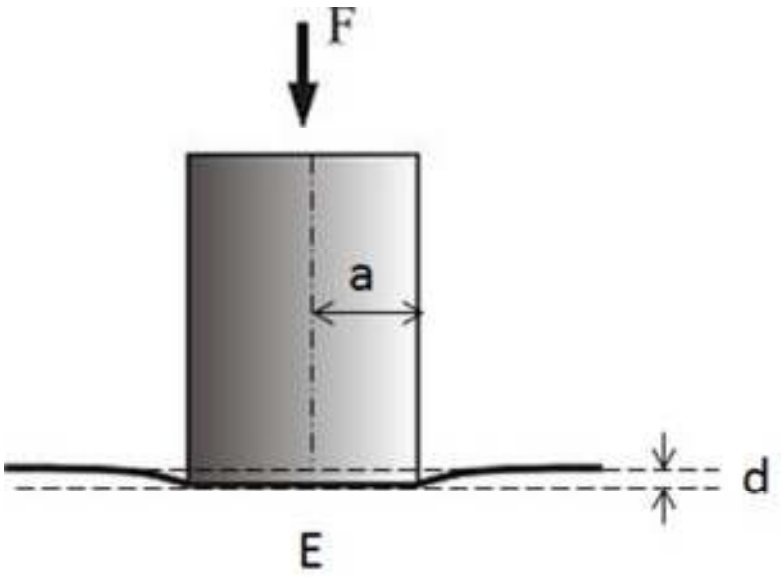

Figure 8.1 A model of the indentation by a flat-end cylinder (Sneddon, 1965).

According to the Sneddon's formula (1965), a desired threshold of loading is predicted with a suggested indentation depth. For example, the ferrofluid is injected at a distance of 1 mm from the tissue surface. A desired threshold of loading is investigated in order to make the indentation depth to 1 mm.

The investigation is also validated with the results in section 5.1.4. When the experimental preload force as 20 and 225 mN, the indentation depths measured are 0.9 and 10.56 mm and the predicted depths are 0.94 and 10.33 mm, respectively. The investigated preload and indentation depth are summarised in Table 8.1. The percentage error is calculated between the experimental and predicted results, and the averaged percentage error is 6.59 %.

In conclusion, at least 20 mN of loading can give to indent on tissue so that the magnet can expose closer to the injection site.

Table 8.1 A summarised relationship between preload and indentation depth of experimental and predicted results.

Preload (mN)	Experimental indentation depth (mm)	Predicted indentation depth (mm)	Percentage error (%)
20	0.9	0.94	4.44
30	1.01	1.41	39.6
50	2.15	2.35	9.30
100	4.97	4.69	5.63
220	10.56	10.33	2.17

8.2 How to Improve the Mechanical Design?

The concentration and injection volume are both the factors of the volume of the magnetic particles suspended in the ferrofluid. However, it is often reported in the literature on the difficulty to manufacture higher concentration due to the particle agglomiration by particles attraction and failure in stability (Lin et al., 2005, Vékás, 2008).

Besides, the leaking issue from the injection site while increasing injection volume has been observed in this study. Tackling the problem in increasing the ferrofluids density has been a big challenge. Therefore, the design of the magnetic probe plays an important role to improve the performance of retraction force from the mechanical engineering perspective.

The restriction of the strength of magnetic field starting to be harmful to human has been regulated. According to Dill's summary (Dill, 2008), the magnetic field strength used for the clinical purposes in the Magnetic Resonance Imaging

(MRI) has been regulated between 0.2 and 3.0 T by the US Food and Drug Administration (FDA). Regarding the safety of human exposed to magnetic field strengths, the research has proved that the magnetic field strength up to 7.0 to 8.0 T is not harmful to the body (Health Protection Agency, 2008). However, the safety regulation is only for the general patients, excluding patients with cardiovascular devices (Levine et al., 2007).

In the literature review of the applications of magnetic retraction, MAGS often used the solid magnet configuration from the size of 3 cm to 5 cm magnets to induce the magnetic retraction (Zeltser et al., 2007, Zeltser and Cadeddu, 2008). The coupling magnetic configurations were often applied but few literature conducted the field strength measurement and prediction of the design (Park et al., 2007, Dominguez et al., 2009, Kume et al., 2008a, Kume et al., 2008b), however, because MAGS used the external magnets to attract the internal magnets, the magnetic interaction between the permanent magnets was fairly strong so that there was not necessary to measure the strength.

In Lin and Valentine's work (2012a, 2012b), they designed a ring-shaped magnetic configuration using the permanent magnets to produce a maximum magnetic field strength of 1.32 T for the DNA separation application. Neuman and Nagy (2008) used a permanent magnet N45 and N50 which also produced a magnetic field strength of 1.3 T. Regarding the magnetic retraction using the magnetic fluid, Wang et al. (2010b) applied a magnetic field strength of 0.5 T produced by the cylinder shaped magnets.

In this study, three configurations of magnets are investigated in the adhesion measurement and the results reveal that the accumulated magnet provides the highest magnetic field strength of 0.6 T.

The magnetic field strength has a lot of space to increase within a safety regulation. To enhance the magnetic field strength, the theoretical method of modelling the magnetic fields, which has been validated by the experimental measurements, can be used to design the magnetic probe in order to make the investigation efficiently.

For example, two models using the accumulated configuration are investigated regarding the strength of magnetic field. The first model is assumed that a third magnet is accumulated on the previous configuration with a larger diameter of 40 mm, as shown in Figure 8.2. And the second model is assumed that the third magnet is accumulated on the previous configuration with a smaller diameter of 5 mm, as shown in Figure 8.3. The associated magnetic fields are simulated using the FEMM software.

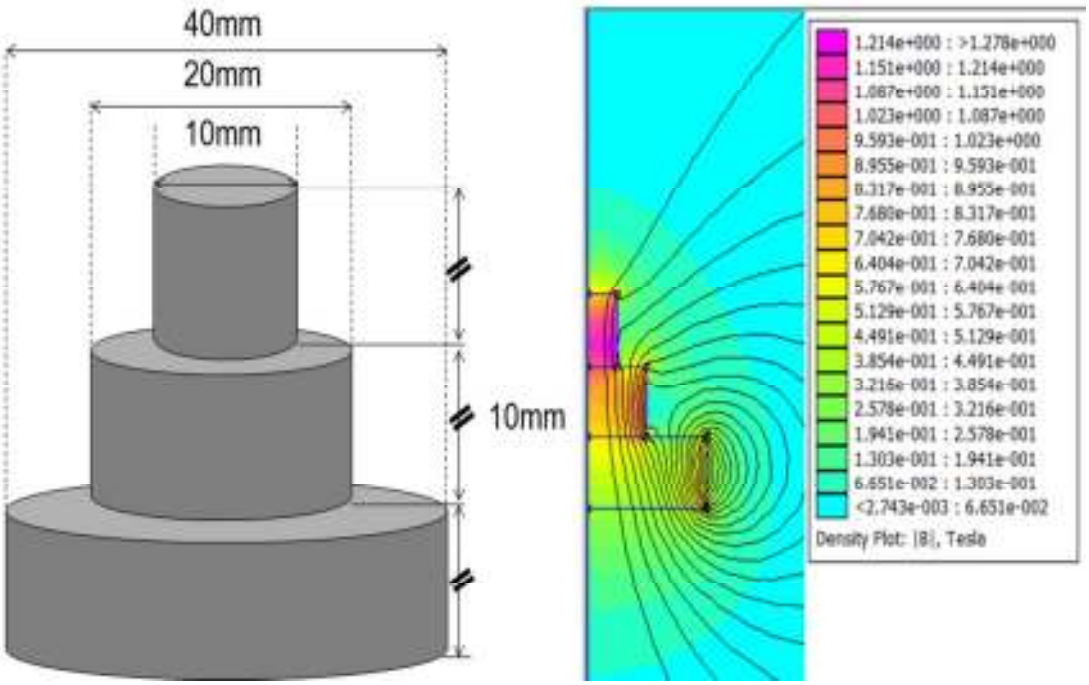

Figure 8.2 The magnetic field of an accumulated configuration of magnetic probe is simulated by the FEMM software.

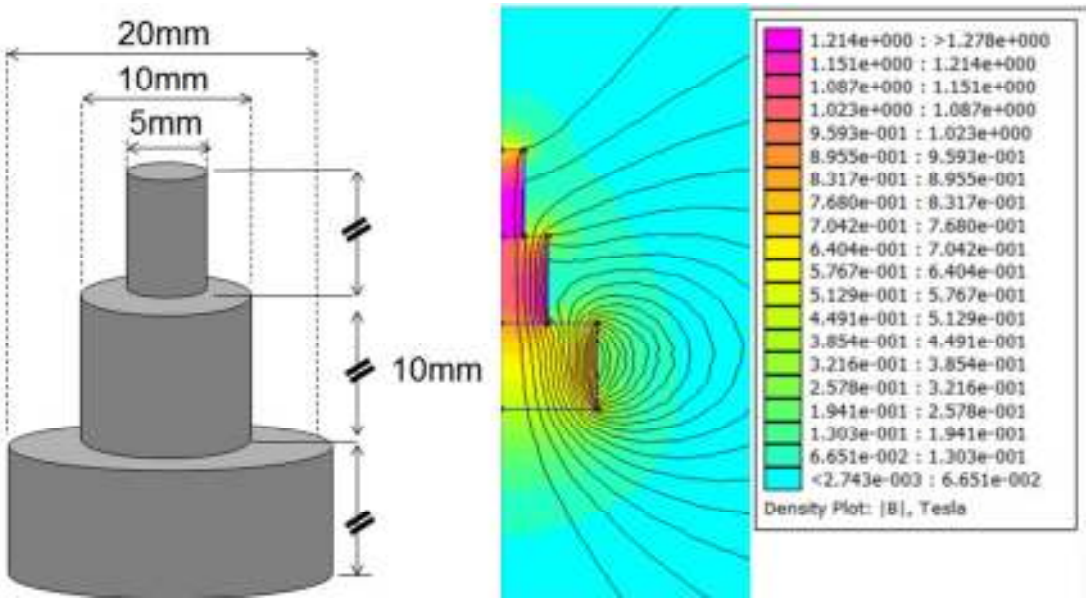

Figure 8.3 The magnetic field of another accumulated configuration of magnetic probe is simulated by the FEMM software

The predicted magnetic field strength along the perpendicular direction to the magnet is presented in Figure 8.4. The simulated results show that the maximum magnetic field strength can be increased to 0.75 - 0.8 T while accumulating another magnet, and accumulating the bigger magnet can generate higher magnetic field strength.

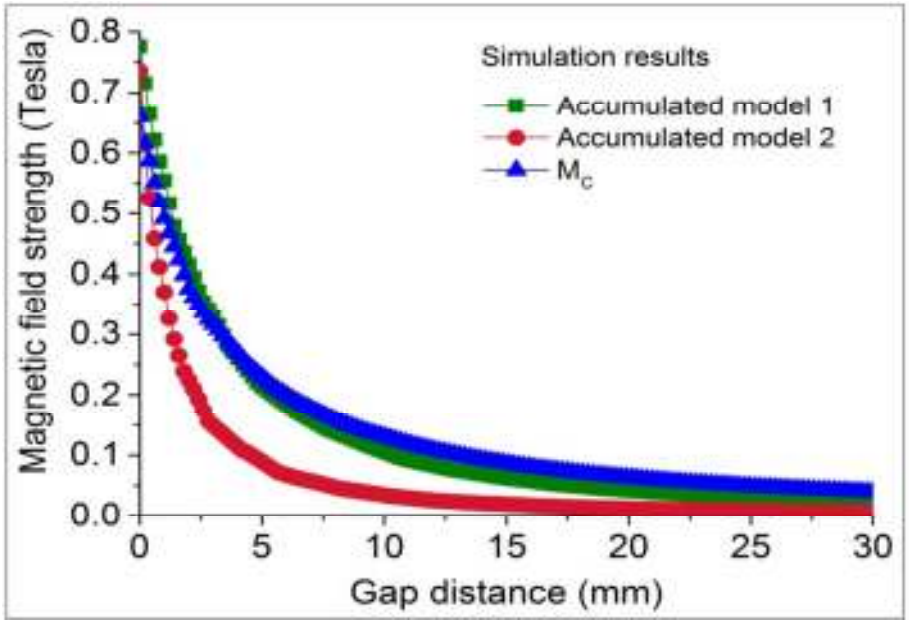

Figure 8.4 A comparison of simulated results of the accumulated magnets.

The simulation of magnetic field benefits on the design of the magnetic probe for the purpose enhancing the force in retraction. The mechanical design is listed on the future work for enhancing the performance in retraction.

8.3 Required Force

In order to establish a protocol of using ferrofluid as a means of tissue manipulation, this section discusses the required force in laparoscopic surgery. The required force for retracting mucosa tissue is reported by Wang et al. (2008) using a tensiometer to measure the applied force for conventional forceps to retract mucosa tissue up to 10 mm. The resultant force of retraction is 0.19±0.09 N and a required force of tissue manipulation for dissection using snares is 0.32±0.15 N. The required force is compared to the adhesion forces obtained in this study, as shown in Figure 8.5. The comparison shows that the non-coated ferrofluid with the particle size of 10 nm and an injection volume of 0.3 ml can be suitable for the application.

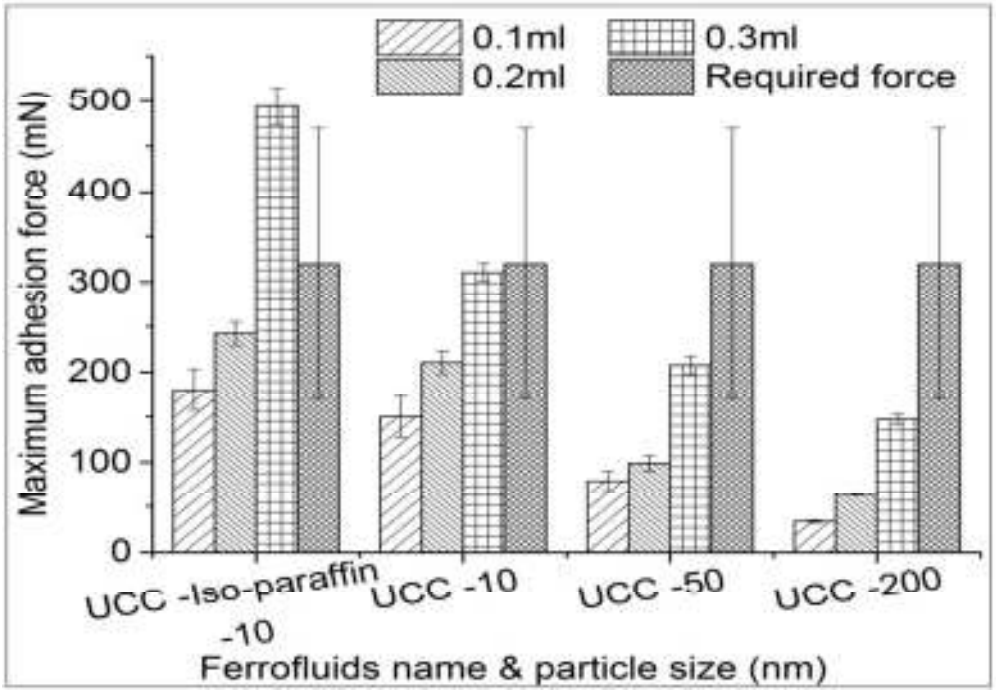

Figure 8.5 A comparison showing the maximum adhesion force of the ferrofluids with the required force for dissecting or retracting tissue for a distance of 10 mm.

Referring to the fluid application in section 2.2.4, Endoscopic Mucosal Resection (EMR) and Endoscopic Submucosal Dissection (ESD) are both the technique developed for lesions and tumours removal by assisting with endoscopic snare resection. The methods are performed with an injection with varies solution (Kantsevoy SV et al., 2008). The volume of injected fluid is from 5 to 50 ml depending on the size of the lesion. The fluid is filled into layers and used to lift up the lesion for resection. The desired solution lifts up the tissue long-lasting and to a sufficiently high elevation (Jung and Park, 2013). Hyun et al. (2006) reported that the height of the mucosal elevation for injecting 1 ml of each solution on a 4×4 cm^2 transverse colon was 6.52±0.26 mm for normal saline, 6.87±0.05 mm for mannitol, 6.92±0.09 mm for sodium hyaluronate, 6.90±0.08 mm for hydroxypropyl methylcellulose and 6.90±0.08 mm for fibrinogen. The height decreases after a while depending on different duration of solutions (Lenz et al., 2010).

Compared EMR and ESD (see section 2.2.4), ferrofluids can provide a sufficient elevation with less quantity. A comparison of distance per injected volume is shown in Figure 8.6. Besides, the duration of the retraction has been studied in session 5.1.6 showing very robust. Therefore, ferrofluids is promising for the purpose.

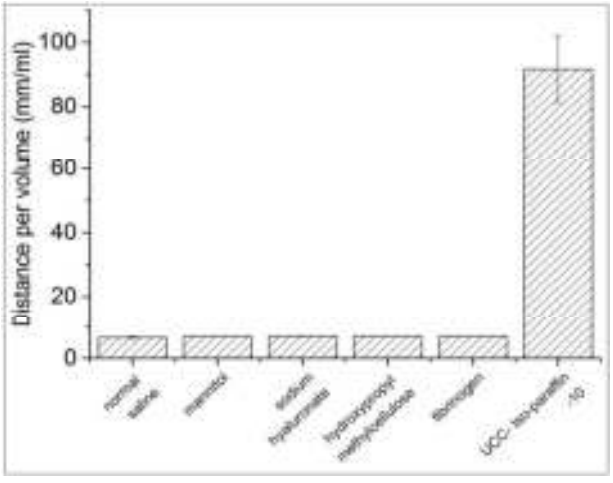

Figure 8.6 A comparison showing an elevation height per volume from the available solutions for ESD, EMR and FF-WHJS.

Chapter 9 Conclusions and Future Work

This project started off to establish a specific protocol of a promising method for tissue manipulation utilising magnetic retraction by nano-scale particles ferrofluids. The existing literature has studied the retraction between solid magnets for example MAGS, and the magnetic fluid with micro-scale stainless steel particles in an external magnetic field. However, few literature has examined ferrofluids as a means of tissue manipulation.

This study has made some progress towards understanding of performance in magnetic retraction. The research achievements refers to the objectives in section 1.2.

- ***To conduct a parameteric study of the ferrofluids in terms of the performance of retraction and adhesion force***

Both ex-vivo and in-vivo measurements have been performed. The ex-vivo experiments have been conducted by using a self-developed tissue tester, as mentioned in Chapter 4. The experimental results have been presented in Chapter 5.

- ***To optimise the retraction and adhesion force and find an appropriate ferrofluid for surgical use***

The multiple parameters have been evaluated by the Taguchi Method in order to optimise the testing environments and to distinguish the significance between parameters.

- ***To identify the mobility of ferrifluids within a tissue and the co-relationship of adhesion force***

A characterisation in particle distribution between the tissue surface and the injection site has been observed by the micro-CT scanner, as described in chapter 6. The method has overcome the difficulty of light microscopy in penetrating an object. The result of each scan has shown a contrast between the particles and the liver tissue, which has been further calculated into an indicator particle density. The particle migration within tissue can be seen in the distribution of particles.

- ***To demonstrate the feasibility of ferrofluids for tissue manipulation in the in-vivo experiment***

The in-vivo result has been presented in Chapter 5 which shows the sucessful retraction and a sufficient height of 80 mm to be applied in MAS procedure.

- ***To analyse the interaction force from a theoretical perspective***

This study has also developed a theoretical model to theorise and validate with the experimental results, as discussed in Chapter 7. The theoretical equation link the applied work with physical theories. The theoretical model not only simulates the magnetic field of the magnetic configurations used in the experiments, but also sheds light on the future design of magnetic configurations. The simulated magnetic retraction force can be integrated into the tissue surface adhesion to become a magnetic adhesion force.

This chapter soon presents the conclusions and future work. It is structured as follows. Section 1 summaries the entire study including methodology, results and discussions. Second 2 presents some recommendations for future work.

9.1 Concluding Remarks

- This project has built a systematic protocol of magnetic tissue retraction. The protocol specifically investigates the retraction performance induced by ferrofluids with nano-scale particles. The evaluation procedure includes a self-developed tissue tester (MagRAT), particles characterisation and a theoretical model. This procedure will need to be completed before the ferrofluids can be applied in in-vivo tests.

Quantitative measurement

- The self-developed tissue tester is aimed to function in a strong magnetic field, and as a result of this every single component has been designed with the non-magnetic material. The tester composes of two modules: the injection module and the adhesion measurement module. The entire experimental procedure has been programmed automatically and systematically controlled with a user-friendly computer interface using LabVIEW®. As a result, the tissue tester can be further used by other project students or researchers. A systematic control also reduces the experimental errors made by operators.
- The injection module innovates the approaches of clamping tissues to avoid tissue deformation during injection. The injection is made perpendicularly to the porcine liver surface. Nevertheless, the injection angle should be altered depending on different tissue or organs. This will be further discussed in the future work.
- The electrical conductivity method developed in the injection module has been proved to work effectively because it controls the injection site with

precision. For example, the contact between the needle and the tissue surface is identified before the needle is pierced into the desired position.

- The adhesion measurement module has illustrated two different concepts of adhesion: 1) the normal adhesion measurement and 2) the shear adhesion force. The methodology for the normal adhesion measurement is a combination of indentation and pull-off test. The shear adhesion is demonstrated by a scratch test using a magnetic probe.
- In the ex-vivo experiments, the raw data have been filtered within ±1 V in order to reduce the systematic errors.
- The parametric study has investigated the effects of different types of ferrofluids, sizes of particles suspended in ferrofluids, concentration of ferrofluids, injection volumes of ferrofluids and magnetic field strengths and operations. The best testing environment observed during this project is the non-coated ferrofluids with small particle size, high concentration, high volume and a strong magnetic field. In this study, the best magnetic adhesion force observed is 512 mN which can retract around 50 g tissue.
- The parameters have been evaluated by the Taguchi orthogonal matrix to distinguish their significances of tissue retraction. The result reveals that the concentration of ferrofluid is the most significant to the retraction force, and the magnetic field strength is the next.
- The result from the parametric study also reveals that the particle size is the most insignificant to the retraction force. The reason of this is because the intensity of the magnetic retraction force depends on the volume of the magnetised matter. Therefore, the retraction force of each single particle has been discussed in Chapter 7. The theoretical model has supported this finding that the larger the size of a particle the more force it can induce. Nevertheless,

particle in smaller sizes spread around and have more numbers suspended in the ferrofluids.

- In terms of the correlation between the coating surface and the volume of a particle, the volume of the magnetic core on a coated particle is smaller than a non-coated particle. Hence, the non-coated ferrofluids have shown better performance in retraction.
- The spatial maps of the retraction force have been established in section 5.1.8. The spatial map has shown the retraction force is being integrated into both the normal adhesion and the shear adhesion. It can be seen that the retraction force has been dramatically decreased when the magnetised tissue is dragged laterally. This interesting finding has been also observed in the in-vivo tests discussed in section 5.4.

Characterisation of particle distribution

- A successful characterisation of particles distribution within tissue is conducted using a micro-CT scanner. An image processing program has been developed using Matlab® program.
- The image processing method developed for particle characterisation converts the scans to the grey images. The contrast between the intensity of the tissue and that of the particles can be clearly distinguished using this method. As such, the density of the particles within each segment of the sample is calculated and the distribution of the particles is formed. A high correlation between the particle density and the distribution can be observed in the following factors: concentration of ferrofluids, volume of ferrofluids and magnetic field strengths. The particles distribute and move towards the tissue

surface in the optimised environments. This interesting finding explains that particle migration is relevant to the magnetic retraction force.

Theoretical model

- The theoretical model developed based on the Biot-Savart law can simulate the magnetic field of a specific magnetic configuration. The simulateion results have been validated by the experimental results. With the support of the theoretical model, the magnetic configurations can be further designed in order to provide higher magnetic field strength, as described in section 8.2.
- In terms of the parameters used in the simulation of magnetic retraction force, it has been found that the simulated force curve using an averaged particle size from the experiment in section 5.2 bears more similarities to the ex-vivo experimental force curve than using the specified size.

In-vivo demonstration in tissue retraction

- The optimised testing environments in light of the Taguchi study have been applied in the in-vivo study, as shown in section 5.4. The result has shown that the porcine bowel is retracted to a height of 80 mm sufficient for the laparoscopic work. The result has demonstrated a robust pull force and less force when dragging the tissue. Besides, the entire bowel section is lifted up by two injection sites.
- In conclusion, the feasibility of using nano-particle ferrofluids to manipulate tissue has been demonstrated in this study with the suggested protocol.

9.2 Suggestions for Future Work

The implementation of ferrofluids as a means of tissue manipulation has not been applied via the laparoscopic procedure. A few suggestions are provided here for future research in these directions:

- *Injection device*

  The injection has been made by a syringe pump. In order to use in a constricted working space, the syringe pump has to be integrated with other laparoscopic tool. The electric conductivity method can still be used to determine the precision of the injection. However, the needle system may need to consider the concept of the blood drawing robot or the procedures of EMR and ESD in order to achieve the injection.

- *Magnetic probe*

  The magnetic field strength is the second most significant factors in the retraction performance. Therefore, it is important to design a magnetic probe to compatible with in the laparoscopic procedure, one that can be integrated into a laparoscopic tool. Future design can further develop the concepts drawing from Wang's permanent magnet study (2012), Lin and Valentine's work about the magnetic tweezers (2012a, 2012b) , Slough and Miller's work about the electromagnet probe (2001). A preliminary design has been established in section 8.2 based on the simulation method provided in Chapter 7.

- *Tissue deformation model*

  Tissue deformation can change the flexibility of tissue retraction. Therefore, in the future it can be expected to use mechanical properties of a specific tissue or organs to predict deformation. In this study, Young's modulus regarding stretch could also be obtained in the pull-off tests or in another tensile

test, but the part was left out of this study due to limited time of study. To build a tissue simulator, the FEM model can be applied.

- *Toxicity of ferrofluids*

Toxicity is decisive if the procedure is to be applied clinically. Although the ferrofluids in this study are almost selected from the existing biomedical applications, the effect of applying them onto human tissue has not been understood completely. The current applications, for example for drug delivery and targeting cancer cells, are suggesting that the particles can be excreted with urine. A few of the particles left on tissue cells can be absorbed by cells uptake (Chomoucka et al., 2010, He et al., 2010). However, how many particles can a unit of tissue absorb to remain innocuous to living creatures has not been studied in the literature. This can be studied through histology (Tietze et al., 2009, Nedosekin et al., 2010, Tietze et al., 2011)

In the in-vivo tests, flexible movement has been observed with regard to the concentration of magnetic effect and dispersion in an absent magnetic field. The injected ferrofluids can be retrieved from the injection site. However, a database of toxicity and an understanding of the limitations of tissue uptake still need to be established.

Reference

ACHANTA, S. C. 2008. *Investigation of Friction from Nano to Macro Force Scale Under Reciprocating Sliding Conditions.* Degree of Doctor, Katholieke Universiteit Leuven.

AL KHABURI, J. A. J. 2010. *Pressure Mapping of Medical Compression Bandages Used for Venous Leg Ulcer Treatment.* PhD, University of Leeds.

ALASWAD, F. D. 2013. Treatment Options of Laparoscopic Complications. *Journal of the American Society of Abdominal Surgeons*.

AOYAMA, K., TAKENAKA I FAU - SATA, T., SATA T FAU - SHIGEMATSU, A. & SHIGEMATSU, A. 1996. Use of the Fibrescope-Video Camera System for Difficult Tracheal Intubation. *British Journal of Anaesthesia,* 77**,** 662-664.

AUSTIN, R. C. 2009. Natural orifice translumenal endoscopic surgery (NOTES) - scar free or scary? *Ann R Coll Surg Engl.,* 91**,** 192-194.

AUTUMN, K. & PEATTIE, A. M. 2002. Mechanisms of Adhesion in Geckos. *Integrative and Comparative Biology,* 42**,** 1081-1090.

BAILEY, L. O., LIPPIATT S FAU - BIANCANELLO, F. S., BIANCANELLO FS FAU - RIDDER, S. D., RIDDER SD FAU - WASHBURN, N. R. & WASHBURN, N. R. 2005. The Quantification of Cellular Viability and Inflammatory Response to Stainless Steel Alloys. *Biomaterials,* 26**,** 5296-5302.

BALLANTYNE, G. H. 2002. The pitfalls of laparoscopic surgery: challenges for robotics and telerobotic surgery. *Surgical Laparoscopy Endoscopy Percutaneous Techniques,* 12**,** 1-5.

BANKS, W. H. & MILL, C. C. 1953. Tacky Adhesion - A Preliminary Study. *Journal of Colloid and Interface Science,* 8**,** 137-147.

BEST, S. L., BERGS, R., GEDEON, M., PARAMO, J., FERNANDEZ, R., CADEDDU, J. A. & SCOTT, D. J. 2011. Maximizing coupling strength of magnetically anchored surgical instruments: how thick can we go? *Surgical Endoscopy,* 25**,** 153-159.

BEST, S. L. & CADEDDU, J. A. 2010. Use of Magnetic Anchoring and Guidance Systems to Facilitate Single Trocar Laparoscopy. *Current Urology Reports,* 11**,** 29-32.

BISHOFF, J. T., ALLAF ME FAU - KIRKELS, W., KIRKELS W FAU - MOORE, R. G., MOORE RG FAU - KAVOUSSI, L. R., KAVOUSSI LR FAU - SCHRODER, F. & SCHRODER, F. 1999a. Laparoscopic bowel injury: incidence and clinical presentation. *The Journal of Urology,* 161**,** 887-890.

BISHOFF, J. T., ALLAF, M. E., KIRKELS, W., MOORE, R. G., KAVOUSSI, L. R. & SCHRODER, F. 1999b. Laparoscopic Bowel Injury: Incidence And Clinical Presentation. *The Journal of Urology,* 161**,** 887-890.

BOROS, M., RŐTH, E., LÁZÁR, G. & GAÁL, C. 2006. *Surgical Techniques Textbook for medical students*, University of Szeged.

BRETTHAUER, M., HOFF GS FAU - THIIS-EVENSEN, E., THIIS-EVENSEN E FAU - HUPPERTZ-HAUSS, G., HUPPERTZ-HAUSS G FAU - SKOVLUND, E. & SKOVLUND, E. 2003. Air and Carbon Dioxide Volumes Insufflated During Colonoscopy. *Gastrointestinal Endoscopy,* 58**,** 203-206.

BRETTHAUER, M., LYNGE AB FAU - THIIS-EVENSEN, E., THIIS-EVENSEN E FAU - HOFF, G., HOFF G FAU - FAUSA, O., FAUSA O FAU - AABAKKEN, L. & AABAKKEN, L. 2005. Carbon Dioxide Insufflation in Colonoscopy: Safe and Effective in Sedated Patients. *Journal of Endoscopy,* 37**,** 706-709.

BRETTHAUER, M., SEIP B FAU - AASEN, S., AASEN S FAU - KORDAL, M., KORDAL M FAU - HOFF, G., HOFF G FAU - AABAKKEN, L. & AABAKKEN, L. 2007. Carbon Dioxide Insufflation for More Comfortable Endoscopic Retrograde Cholangiopancreatography: A Randomized, Controlled, Double-Blind Trial. *Journal of Endoscopy,* 39**,** 58-64.

BROWN, T. H. & IRVING, M. H. 1995. *Introduction to Minimal Access Surgery*, BMJ Publishing Group.

CADEDDU, J., FERNANDEZ, R., DESAI, M., BERGS, R., TRACY, C., TANG, S.-J., RAO, P., DESAI, M. & SCOTT, D. 2009. Novel magnetically guided intra-abdominal camera to facilitate laparoendoscopic single-site surgery: initial human experience. *Surgical Endoscopy,* 23**,** 1894-1899.

CANTILLON, P. J., BRENNAN, P. J., TUGWELL, J., O'DONOGHUE, K. & CAHILL, R. A. Electropermanent Magnets for Transabdominal Anchoring. 21st International Congress of the European Association for Endoscopic Surgery (EAES), 2013 Vienna, Austria.

CARON, J. P. 2012. Equine Laparoscopy: Equipment and Basic Principles. Michigan State University.

CHEMICELL™. 2010. *Ferrofluids* [Online]. Available: http://www.chemicell.com/home/index.html [Accessed 27/09 2010].

CHEUNG, E., KARAGOZLER, M. E., SUKHO, P., BYUNGKYU, K. & SITTI, M. A new endoscopic microcapsule robot using beetle inspired microfibrillar adhesives. Advanced Intelligent Mechatronics. Proceedings, 2005 IEEE/ASME International Conference on, 24-28 July 2005 2005. 551-557.

CHICEA, D., INDREA, E. & CRETU, C. M. 2012. Assesing Fe3O4 nanoparticle size by DLS, XRD and AFM. *JOURNAL OF OPTOELECTRONICS AND ADVANCED MATERIALS,* 14**,** 460-466.

CHOMOUCKA, J., DRBOHLAVOVA J FAU - HUSKA, D., HUSKA D FAU - ADAM, V., ADAM V FAU - KIZEK, R., KIZEK R FAU - HUBALEK, J. & HUBALEK, J. 2010. Magnetic nanoparticles and targeted drug delivering. *Pharmacol Research,* 62**,** 144-149.

CHURCH, J. & DELANEY, C. 2003. Randomized, Controlled Trial of Carbon Dioxide Insufflation During Colonoscopy. *Diseases of the Colon & Rectum,* 46**,** 322-326.

COMAROW, A. 2002. Tiny holes, big surgery. Minimal surgery hurts less and scars less--but is it right for you? *US News World Report,* 133**,** 48-54.

CULMER, P., BARRIE, J., HEWSON, R., LEVESLEY, M., MON-WILLIAMS, M., JAYNE, D. & NEVILLE, A. 2012. Reviewing the technological challenges associated with the development of a laparoscopic palpation device. *The International Journal of Medical Robotics and Computer Assisted Surgery,* 8**,** 146-159.

CULMER PETER, B. J., HEWSON R, LEVESLEY M, MON-WILLIAMS M, JAYNE D, NEVILLE A. 2012. Reviewing the technological challenges associated with the development of a laparoscopic palpation device. *The International Journal of Medical Robotics and Computer Assisted Surgery,* 8**,** 146-159.

CUSCHIERI, A. 1999. Technology for Minimal Access Surgery. *British Medical Journal,* 319**,** 1-6.

CUSCHIERI, A. & BERCI, G. 1990. *Laparoscopic Biliary Surgery,* Oxford, Blackwell Scientific Piblications.

DE, S., ROSEN, J., DAGAN, A., HANNAFORD, B., SWANSON, P. & SINANAN, M. 2007. Assessment of Tissue Damage due to Mechanical Stresses. *The International Journal of Robotics Research,* 26**,** 1159-1171.

DE, S., ROSEN, J., DAGAN, A., SWANSON, P., SINANAN, M. & HANNAFORD, B. Assessment of Tissue Damage due to Mechanical Stresses. Biomedical Robotics and Biomechatronics, 2006. BioRob 2006. The First IEEE/RAS-EMBS International Conference on, 20-22 Feb. 2006 2006. 823-828.

DE VISSER, H. 2003a. *Grasping Safely: Instruments for bowel manipulation investigated.* Delft University of Technology.

DE VISSER, H. 2003b. *Grasping Safety Instruments for Bowel Manipulation Investigated.* PhD thesis, Delft University of Technology.

DERKS, D., LINDNER, A., CRETON, C. & BONN, D. 2003. Cohesive Failure of Thin Layers of Soft Model Adhesives Under Tension. *Journal of Applied Physics,* 93**,** 1557-1566.

DEZIEL, D. J., MILLIKAN KW FAU - ECONOMOU, S. G., ECONOMOU SG FAU - DOOLAS, A., DOOLAS A FAU - KO, S. T., KO ST FAU - AIRAN, M. C. & AIRAN, M. C. 1993. Complications of laparoscopic cholecystectomy: a national survey of 4,292 hospitals and an analysis of 77,604 cases. *American Journal of Surgery,* 165**,** 9-14.

DHUMANE, P. W., DIANA M FAU - LEROY, J., LEROY J FAU - MARESCAUX, J. & MARESCAUX, J. 2011. Minimally Invasive Single-Site Surgery for the Digestive System: A Technological Review. *Journal of Minimal Access Surgery,* 7**,** 40-51.

DILL, T. 2008. Contraindications to Magnetic Resonance Imaging. *Heart,* 94**,** 943-948.

DIODATO JR, M. D., PROSAD, S. M., KLINGENSMITH, M. E. & DAMIANO JR, R. J. 2004. Robotics in Surgery. *Current Problems in Surgery,* 41**,** 752-810.

DOMINGUEZ, G., DURAND, L., ROSA, J. D., DANGUISE, E., AROZAMENA, C. & FERRAINA, P. A. 2009. Retraction and triangulation with neodymium magnetic forceps for single-port laparoscopic cholecystectomy. *Surgical Endoscopy,* 23**,** 1660-1666.

DRILLER, J. & FREI, E. H. 1987. A Review of Medical Applications of Magnet Attraction and Detection. *Journal of Medical Engineering & Technology,* 11**,** 271-277.

EISNER, T. & ANESHANSLEY, D. J. 2000. Defense by foot adhesion in a beetle. *Proceedings of the National Academy of Sciences,* 97**,** 6568-6573.

EMAGNETSUK. 2010. *Neodymium Magnets* [Online]. Available: http://e-magnetsuk.com/magnets/neodymium_magnets/ [Accessed 20. May. 2010.

ESTEY, E. P. 2009. Robotic Prostatectomy: The New Standard of Care or A Marketing Success? *Canadian Urological Association Journal,* 3**,** 488-490.

FALEX TRIBOLOGY. 2014. *Modular Universal Surface Tester* [Online]. FALEX TRIBOLOGY. Available: http://www.falexint.com/en/equipment.

FEDERLE, W., BARNES WJ FAU - BAUMGARTNER, W., BAUMGARTNER W FAU - DRECHSLER, P., DRECHSLER P FAU - SMITH, J. M. & SMITH, J. M. 2006. Wet but not slippery: Boundary friction in tree frog adhesive toe pads. *Journal of the Royal Society of Interface,* 3**,** 689-697.

FILIPPOV, A., POPOV, V. L. & GORB, S. N. 2011. Shear induced adhesion: Contact mechanics of biological spatula-like attachment devices. *Journal of Theoretical Biology,* 276**,** 126-131.

FINE SCIENCE TOOLS GMBH. 2014. *Fine Science Tools GmbH* [Online]. Available: http://www.finescience.de/.

FIRGELLI TECHNOLOGIES INC.® 2011. L12 Linear Actuator.

FRANCIS, B. A. & HORN, R. G. 2001. Apparatus-specific analysis of fluid adhesion measurements. *Journal of Applied Physics,* 89**,** 4167-4174.

GALVAO NETO, M., RAMOS, A. & CAMPOS, J. 2009. Single port laparoscopic access surgery. *Techniques in Gastrointestinal Endoscopy,* 11**,** 84-93.

GAVARA, N. & CHADWICK, R. S. 2010. Noncontact microrheology at acoustic frequencies using frequency-modulated atomic force microscopy. *Nature Methods,* 7**,** 650-654.

GAY, C. 2002. Stickiness - Some Fundamentals of Adhesion. *Integrative and Comparative Biology,* 42**,** 1123-1126.

GEBESHUBER, I. C., STACHELBERGER H FAU - DRACK, M. & DRACK, M. 2005. Diatom bionanotribology--biological surfaces in relative motion: their design, friction, adhesion, lubrication and wear. *Journal of Nanoscience and Nanotechnology,* 5**,** 79-87.

GEIM, A. K., DUBONOS, S. V., GRIGORIEVA, I. V., NOVOSELOV, K. S., ZHUKOV, A. A. & SHAPOVAL, S. Y. 2003. Microfabricated adhesive mimicking gecko foot-hair. *Nature Materials,* 2**,** 461-463.

GRANT, F. S. & WEST, G. F. 1965. *Interpretation Theory in Applied Geophysics*, McGraw-Hill Book Co.

GREINER, C., CAMPO, A. & ARZT, E. 2007. Adhesion of bioinspired micropatterned surfaces: effects of pillar radius, aspect ratio, and preload. *Langmuir,* 7**,** 3495-3502.

GRIEVE, D., BARTON, D., CROLLA, D. & BUCKINGHAM, J. 1998. Design of a lightweight automotive brake disc using finite element and Taguchi techniques. *J Automobile Eng,* 212**,** 245-254.

GUPTA, V., REDDY, N. P. & BATUR, P. Forces in surgical tools: comparison between laparoscopic and surgical forceps. Engineering in Medicine and Biology Society, 1996. Bridging Disciplines for Biomedicine. Proceedings of the 18th Annual International Conference of the IEEE, 31 Oct-3 Nov 1996 1996. 223-224 vol.1.

HASHIZUME, M. & TSUGAWA, K. 2004. Robotic Surgery and Cancer: the Present State, Problems and Future Vision. *Japanese Journal of Clinical Oncology,* 34**,** 227-237.

HATCH, G. P. & STELTER, R. E. 2001. Magnetic design considerations for devices and particles used for biological high-gradient magnetic separation (HGMS) systems. *Journal of Magnetism and Magnetic Materials,* 225**,** 262-276.

HE, C., HU, Y., YIN, L., TANG, C. & YIN, C. 2010. Effects of particle size and surface charge on cellular uptake and biodistribution of polymeric nanoparticles. *Biomaterials,* 31**,** 3657-3666.

HEALTH PROTECTION AGENCY 2008. Static Magnetic Fields - Report of the Independent Advisory Group on Non-ionising Radiation. *In:* DOCUMENTS OF THE HEALTH PROTECTION AGENCY (ed.) *Radiation, Chemical and Environmental Hazards.*

HEIJNSDIJK, E. 2004. *Tissue Manipulation in Laparoscopic Surgery.* PhD thesis, Delft University of Technology.

HIRST MAGNETIC INSTRUMENTS LTD.®. 2004. *Gassmeters* [Online]. Cornwall. Available: http://www.hirst-magnetics.com/instruments/gauss.shtml [Accessed 07.Oct 2013].

HOPKINS, H. H. & KAPANY, N. S. 1954. A Flexible Fibrescope, using Static Scanning. *Nature,* 173**,** 39-41.

HORGAN, S. & VANUNO, D. 2004. Robots in laparoscopic surgery. *Journal of Laparoscopic & Advanced Surgical Techniques,* 11**,** 415-419.

HUBER, G., MANTZ, H., SPOLENAK, R., MECKE, K., JACOBS, K., GORB, S. N. & ARZT, E. 2005. Evidence for capillarity contributions to gecko adhesion from single spatula nanomechanical measurements. *Proceedings of the National Academy of Sciences of the United States of America,* 102**,** 16293-16296.

HYUN, J. J., CHUN, H. R., CHUN, H. J., JEEN, Y. T., WON BAECK, C., KYUN YU, S., SIK KIM, Y., SIK LEE, H., HO UM, S., WOO LEE, S., HYUN CHOI, J., DUCK KIM, C., SANG RYU, H. & HAI HYUN, J. 2006. Comparison of the characteristics of submucosal injection solutions used in endoscopic mucosal resection. *Scandinavian Journal of Gastroenterology,* 41**,** 488-492.

JINDAL, U. C. 2012. *Material Science and Metallurgy*, Dorling Kindersley.

JUNG, Y. S. & PARK, D. I. 2013. Submucosal injection solutions for endoscopic mucosal resection and endoscopic submucosal dissection of gastrointestinal neoplasms. *Gastrointestinal Intervention,* 2**,** 73-77.

KAISER, M., KRUG, J. & ROSE, G. Interventional MRI: Minimal-invasive Surgery under MR guidance. Microwave Symposium Digest (MTT), 2011 IEEE MTT-S International, 5-10 June 2011 2011. 1-4.

KALLOO, A. N., SINGH, V. K., JAGANNATH, S. B., NIIYAMA, H., HILL, S. L., VAUGHN, C. A., MAGEE, C. A. & KANTSEVOY, S. V. 2004. Flexible transgastric peritoneoscopy: a novel approach to diagnostic and therapeutic interventions in the peritoneal cavity. *Gastrointestinal Endoscopy,* 60**,** 114-117.

KANTSEVOY SV, ADLER DG, CONWAY JD, DIEHL DL, FARRAYE FA, KWON R, MAMULA P, RODRIGUEZ S, SHAH RJ, WONG KEE SONG LM & WM., T. 2008. Endoscopic mucosal resection and endoscopic submucosal dissection. *Technology Status Evaluation Report.* American Society for Gastrointestinal Endoscopy.

KEMNER, A. 1999. Experimental evaluation of traumatic properties of laparoscopic dissecting forceps. Delft, The Netherlands: Man-Machine Systems and Control, Delft University of Technology.

KUME, M., MIYAZAWA, H., ABE, F., IWASAKI, W., UCHINAMI, H., SHIBATA, S., SATO, T. & YAMAMOTO, Y. 2008a. A newly designed magnet-retracting forceps for laparoscopic cholecystectomy in a swine model. *Minimally Invasive Therapy,* 17**,** 251-254.

KUME, M., MIYAZAWA, H., IWASAKI, W., ABE, F., UCHINAMI, H. & YAMAMOTO, Y. 2008b. The Use of Magnetic Anchors in the Bowel Lumen for Laparoscopic Anterior Resection of Rectosigmoid Colon in Pigs: with Video. *World Journal of Surgery,* 32**,** 2425-2428.

LACOMBE, R. 2006. *Adhesion measurement methods: theory and practice*, Taylor & Francis Group.

LAM, A., KAUFMAN, Y., KHONG, S. Y., LIEW, A., FORD, S. & CONDOUS, G. 2009. Dealing with Complications in Laparoscopy. *Best Practice & Research Clinical Obstetrics and Gynaecology,* 23**,** 631-646.

LEE, H., LEE, B. P. & MESSERSMITH, P. B. 2007. A reversible wet/dry adhesive inspired by mussels and geckos. *Nature,* 448**,** 338-341.

LENZ, L., DI SENA, V., NAKAO, F. S., ANDRADE, G. P. D., ROHR, M. R. D. S. & FERRARI JR, A. P. 2010. Comparative results of gastric submucosal injection with hydroxypropyl methylcellulose, carboxymethylcellulose and normal saline solution in a porcine model. *Arquivos de Gastroenterologia,* 47**,** 184-187.

LEVINE, G. N., GOMES AS FAU - ARAI, A. E., ARAI AE FAU - BLUEMKE, D. A., BLUEMKE DA FAU - FLAMM, S. D., FLAMM SD FAU - KANAL, E., KANAL E FAU - MANNING, W. J., MANNING WJ FAU - MARTIN, E. T., MARTIN ET FAU - SMITH, J. M., SMITH JM FAU - WILKE, N., WILKE N FAU - SHELLOCK, F. S. & SHELLOCK, F. S. 2007. Safety of Magnetic Resonance Imaging in Patients with Cardiovascular Devices: an American Heart Association scientific statement from the Committee on Diagnostic and Interventional Cardiac Catheterization, Council on Clinical Cardiology, and the Council on Cardiovascular Radiology and Intervention: endorsed by the American College of Cardiology Foundation, the North American Society for Cardiac Imaging, and the Society for Cardiovascular Magnetic Resonance. *Circulation by American Heart Association,* 116**,** 2878-2891.

LIANG, Y. A., AUTUMN, K., HSIEH, S. T., ZESCH, W., CHAN, W. P., FEARING, R. S., FULL, R. J. & KENNY, T. W. Adhesion force measurements on single gecko setae. Solid-State Sensor and Actuator Workshop, June 4-8 2000 Hilton Head Island, South Carolina. 33-38.

LIAO, S.-B., DOURMASHKIN, P. & BELCHER, J. 2004. Introduction to Electricity and Magnetism. MIT OpenCourseWare.

LIEN, H.-H., HUANG, C.-C., TAN, L.-I., WANG, P.-C., LIN, H.-Z. & HUANG, C.-S. 2013. *RE: Review of Cholecystotomy.*

LIN, C.-L., LEE, C.-F. & CHIU, W.-Y. 2005. Preparation and properties of poly(acrylic acid) oligomer stabilized superparamagnetic ferrofluid. *Journal of Colloid and Interface Science,* 291**,** 411-420.

LIN, J. & VALENTINE, M. T. 2012a. High-force NdFeB-based magnetic tweezers device optimized for microrheology experiments. *Review of Scientific Instruments,* 83**,** 053905.

LIN, J. & VALENTINE, M. T. 2012b. Ring-shaped NdFeB-based magnetic tweezers enables oscillatory microrheology measurements. *Applied Physics Letters,* 100**,** 201902-201902-4.

LINDNER, A., DERKS, D. & SHELLEY, M. J. 2005. Stretch flow of thin layers of Newtonian liquids: Fingering patterns and lifting forces. *Physics of Fluids,* 17**,** 072107-072119.

LIPFERT, J., HAO, X. & DEKKER, N. H. 2009. Quantitative Modeling and Optimization of Magnetic Tweezers. *Biophysical journal,* 96**,** 5040-5049.

LIQUIDS RESEARCH LTD. 2014. *Magnetic Fluid* [Online]. Available: http://www.liquidsresearch.com/en-GB/products-46.aspx 2010].

LIRA, S. A. & MIRANDA, J. A. 2009a. Adhesion Properties of Chain-Forming Ferrofluids. *Physical Review E,* 79.

LIRA, S. A. & MIRANDA, J. A. 2009b. Field-Controlled Adhesion in Confined Magnetorheological Fluids. *Physical Review E,* 80**,** 046313-(1-8).

LOBE, T. E. 2003. *Pediatric Laparoscopy*, LeBonbeur Children's Medical Center, University of Tennessee, USA.

LONG, R. & HUI, C.-Y. 2009. The effect of preload on the pull-off force in indentation tests of microfibre arrays. *Proceedings of the Royal Society A: Mathematical, Physical and Engineering Science,* 465**,** 961-981.

LORENZ, B., KRICK BA FAU - MULAKALURI, N., MULAKALURI N FAU - SMOLYAKOVA, M., SMOLYAKOVA M FAU - DIELUWEIT, S., DIELUWEIT S FAU - SAWYER, W. G., SAWYER WG FAU - PERSSON, B. N. J. & PERSSON, B. N. 2013. Adhesion: Role of Bulk Viscoelasticity and Surface Roughness. *Journal of Physics: Condensed Matter,* 25**,** 225004-225020.

MAHLE, S., ILG, P. & LIU, M. 2008. Hydrodynamic theory of polydisperse chain-forming ferrofluids. *Physical Review E,* 77**,** 016305.

MALVERN®. 2014. *Zetasizer Nano* [Online]. Available: http://www.malvern.com/en/products/product-range/zetasizer-range/default.aspx 2012].

MCGEE, M. F., ROSEN, M. J., MARKS, J., ONDERS, R. P., CHAK, A., FAULX, S., CHEN, V. K. & PONSKY, J. 2006. A Primer on Natural Orifice Transluminal Endoscopic Surgery: Building a New Paradigm. *Surgical Innovation,* 13**,** 86-93.

MEEKER, D. 2011. *Finite Element Method Magnetics (FEMM)* [Online]. Available: http://www.femm.info/wiki/HomePage.

MENON, C., MURPHY, M., SITTI, M. & LAN, N. 2007. *Space Exploration - Towards Bio-inspired Climbing Robots,* Vienna, Austria.

MERRIFIELD, B. F., WAGH, M. S. & THOMPSON, C. C. 2006. Peroral transgastric organ resection: a feasibility study in pigs. *Gastrointestinal Endoscopy,* 63**,** 693-697.

MICROMOD PARTIKELTECHNOLOGIE GMBH. 2014. *modular designed particles* [Online]. Available: http://www.micromod.de/ 2010].

MINTZ, Y., HORGAN S FAU - CULLEN, J., CULLEN J FAU - STUART, D., STUART D FAU - FALOR, E., FALOR E FAU - TALAMINI, M. A. & TALAMINI, M. A. 2008. NOTES: a review of the technical problems encountered and their solutions. *Journal of Laparoscopic & Advanced Surgical Techniques,* 18**,** 583-587.

MIRANDA, J. A. & OLIVEIRA, R. M. 2004. Adhesion Phenomena in Ferrofluids. *Physical Review E,* 70**,** 036311-(1-10).

MORSI, H., YONG, K. L. & JEWELL, A. P. 2004. Evaluation of the Taguchi Methods for the Simultaneous Assessment of the Effects of Multiple Variables in the Tumour Microenvironment. *Int Semin Surg Oncol,* 20**,** 1-9.

MULLER, O., HAHN, D. & LIU, M. 2006. Non-Newtonian behaviour in ferrofluids and magnetization relaxation. *Journal of Physics: Condensed Matter,* 18**,** S2623-S2632.

MURPHY, M. P., TSO, W., TANZINI, M. & SITTI, M. Waalbot: An Agile Small-Scale Wall Climbing Robot Utilizing Pressure Sensitive Adhesives. Intelligent Robots and Systems, 2006 IEEE/RSJ International Conference on, 9-15 Oct. 2006 2006. 3411-3416.

NAJMALDIN, A. & GUILLOU, P. 1998. *A Guide to Laparoscopic Surgery,* Leeds.

NASE, J., LINDNER, A. & CRETON, C. 2008. Pattern Formation during Deformation of a Confined Viscoelastic Layer: From a Viscous Liquid to a Soft Elastic Solid. *Physical Review Letters,* 101**,** 074503.

NATIONAL INSTRUMENTS®. 2014. *NI USB-6008 12-Bit, 10 kS/s Low-Cost Multifunction DAQ* [Online]. Available: http://sine.ni.com/nips/cds/view/p/lang/en/nid/201986 [Accessed 28. Sep. 2010.

NEDOSEKIN, D. A., SHASHKOV EV FAU - GALANZHA, E. I., GALANZHA EI FAU - HENNINGS, L., HENNINGS L FAU - ZHAROV, V. P. & ZHAROV, V. P. 2010. Photothermal multispectral image cytometry for quantitative histology of nanoparticles and micrometastasis in intact, stained and selectively burned tissues. *Cytometry Part A,* 77**,** 1049-1058.

NEUMAN, K. C. & NAGY, A. 2008. Single-molecule force spectroscopy: optical tweezers, magnetic tweezers and atomic force microscopy. *Nature Methods,* 5**,** 491-505.

NGUYEN, N. T., ROOT J FAU - ZAINABADI, K., ZAINABADI K FAU - SABIO, A., SABIO A FAU - CHALIFOUX, S., CHALIFOUX S FAU - STEVENS, C. M., STEVENS CM FAU - MAVANDADI, S., MAVANDADI S FAU - LONGORIA, M., LONGORIA M FAU - WILSON, S. E. & WILSON, S. E. 2005. Accelerated growth of bariatric surgery with the introduction of minimally invasive surgery.

NOVEL INSTRUMENTS FOR MINIMALLY INVASIVE TECHNIQUES. 2010. *Novel Instruments For Minimally Invasive Techniques* [Online]. Available: http://www.imdi-nimit.nl/index.php?page=artikel&artikel_id=20.

ODENBACH, S. 2004. Recent progress in magnetic fluid research. *Journal of Physics: Condensed Matter,* 16**,** R1135.

OLYMPUS. 2014. *Polypectomy, EMR & ESD* [Online]. Available: http://www.olympus-europa.com/.

OMEGA®. 2013-2014. *Omega* [Online]. Available: http://www.omega.com/pptst/LCAE.html 2010].

PAI, R. D., FONG, D. G., BUNDGA, M. E., ODZE, R. D., RATTNER, D. W. & THOMPSON, C. C. 2006. Transcolonic endoscopic cholecystectomy: a NOTES survival study in a porcine model (with video). *Gastrointestinal Endoscopy,* 64**,** 428-434.

PAMME, N. 2006. Magnetism and microfluidics. *Lab on a Chip,* 6**,** 24-38.

PAMME, N. & MANZ, A. 2004. On-Chip Free-Flow Magnetophoresis: Continuous Flow Separation of Magnetic Particles and Agglomerates. *Analytical Chemistry,* 76**,** 7250-7256.

PARK, S., BERGS, R. A., EBERHART, R., BAKER, L., FERNANDEZ, R. & CADEDDU, J. A. 2007. Trocar-less Instrumentation for Laparoscopy Magnetic Positioning of Intra-abdominal Camera and Retractor. *Annals of Surgery,* 245**,** 379-384.

PEARL, J. P. & PONSKY, J. L. 2007. Natural orifice transluminal endoscopic surgery: Past, present and future. *J Min Access Surg* 3**,** 43-46.

PETIT, M., LEBOUC, A. K., AVENAS, Y., TAWK, M. & ARTEGA, E. 2011. Calculation and analysis of local magnetic forces in ferrofluids. *Przegląd Elektrotechniczny,* 87**,** 115-119.

PHILOSOPHE, R. 2003. Avoiding Complications of Laparoscopic Surgery. *Sexuality, Reproduction & Menopause,* 1**,** 30-39.

PIZZI, A. & MITTAL, K. L. 2003. *Handbook of Adhesive Technology, Revised and Expanded*, Taylor & Francis.

POCIUS, A. V. 2002. *Adhesion and Adhesives Technology: An Introduction*, Hanser.

POIVET, S. & ET AL. 2003. Cavitation-induced force transition in confined viscous liquids under traction. *EPL (Europhysics Letters),* 62**,** 244.

POIVET, S., NALLET, F., GAY, C., TEISSEIRE, J. & FABRE, P. 2004. Force response of a viscous liquid in a probe-tack geometry: Fingering versus cavitation. *The European Physical Journal E: Soft Matter and Biological Physics,* 15**,** 97-116.

PUANGMALI, P., ALTHOEFER, K., SENEVIRATNE, L. D., MURPHY, D. & DASGUPTA, P. 2008. State-of-the-Art in Force and Tactile Sensing for Minimally Invasive Surgery. *Sensors Journal, IEEE,* 8**,** 371-381.

RABENOROSOA, K., CLEVY, C., LUTZ, P., GAUTHIER, M. & ROUGEOT, P. 2009. Measurement of pull-off force for planar contact at the microscale. *Micro & Nano Letters,* 4.

RAMAN, J. D., SCOTT, D. J. & CADEDDU, J. A. 2009. Role of Magnetic Anchors During Laparoendoscopic Single Site Surgery and NOTES. *JOURNAL OF ENDOUROLOGY,* 23**,** 781-786.

RAMARAJ, R., SUGUMARAN, A., KHAN, H., MATHIALAHAN, T. & GEORGE, P. 2011. Comparison of carbon dioxide (CO2) to air insufflation in colonoscopy. *Gut,* 60**,** A200.

RENTSCHLER, M., DUMPERT, J., PLATT, S., FARRITOR, S. & OLEYNIKOV, D. 2007. Natural orifice surgery with an endoluminal mobile robot. *Surgical Endoscopy,* 21**,** 1212-1215.

RENTSCHLER, M. E., DUMPERT, J., PLATT, S. R., OLEYNIKOV, D., FARRITOR, S. M. & IAGNEMMA, K. Mobile in vivo biopsy robot. Robotics and Automation, 2006. ICRA 2006. Proceedings 2006 IEEE International Conference on, 15-19 May 2006 2006. 4155-4160.

RODRIGUES, S. P., HOREMAN T FAU - DANKELMAN, J., DANKELMAN J FAU - VAN DEN DOBBELSTEEN, J. J., VAN DEN DOBBELSTEEN JJ FAU - JANSEN, F.-W. & JANSEN, F. W. 2012. Suturing Intraabdominal Organs: When Do We Cause Tissue Damage? *Surgical Endoscopy,* 26**,** 1005-1009.

ROSHAN, R., JAYNE, D. G., LISKIEWICZ, T., TAYLOR, G. W., GASKELL, P. H., CHEN, L., MONTELLANO-LOPEZ, A., MORINA, A. & NEVILLE, A. 2011. Effect of tribological factors on wet adhesion of a microstructured surface to peritoneal tissue. *Acta Biomaterialia,* 7**,** 4007-4017.

RYOU, M. & THOMPSON, C. 2009. Magnetic retraction in natural-orifice transluminal endoscopic surgery (NOTES): addressing the problem of traction and countertraction. *Endoscopy,* 41**,** 143-148.

SANGBAE, K., SPENKO, M., TRUJILLO, S., HEYNEMAN, B., SANTOS, D. & CUTKOSKY, M. R. 2008. Smooth Vertical Surface Climbing With Directional Adhesion. *Robotics, IEEE Transactions on,* 24**,** 65-74.

SCHLAGER, A., KHALAILEH, A., SHUSSMAN, N., ELAZARY, R., KEIDAR, A., PIKARSKY, A., BEN-SHUSHAN, A., SHIBOLET, O., HORGAN, S., TALAMINI, M., ZAMIR, G., RIVKIND, A. & MINTZ, Y. 2010. Providing more through less: current methods of retraction in SIMIS and NOTES cholecystectomy. *Surgical Endoscopy,* 24**,** 1542-1546.

SCHLIEMANN, H. & GOODMAN, S. M. 2011. A new study on the structure and function of the adhesive organs of the Old World sucker-footed bat (Myzopoda: Myzopodidae) of Madagascar. *Verhandlungen des Naturwissenschaftlichen Vereins in Hamburg,* 46**,** 313-330.

SCOTT, D. J., TANG, S.-J., FERNANDEZ, R., BERGS, R., GOOVA, M. T., ZELTSER, I., KEHDY, F. J. & CADEDDU, J. A. 2007. Completely transvaginal NOTES cholecystectomy using magnetically anchored instruments. *Surgical Endoscopy,* 21**,** 2308-2316.

SHAIKH, S. N. & THOMPSON, C. 2010a. Natural Orifice Translumenal Surgery: Flexible Platform Review. *World Journal of Gastrointestinal Surgery,* 2**,** 210-216.

SHAIKH, S. N. & THOMPSON, C. C. 2010b. Natural orifice translumenal surgery: Flexible platform review. *World Journal of Gastrointestinal Surgery,* 2**,** 210-216.

SHANG, J., PAYNE, C. J., CLARK, J., NOONAN, D. P., KWOK, K. W., DARZI, A. & YANG, G. Z. 2012. Design of a Multitasking Robotic Platform with Flexible Arms and Articulated Head for Minimally Invasive Surgery. *2012 IEEE/RSJ International Conference on Intelligent Robots and Systems.*

SHAO, H., BACHUS, K. N. & STEWART, R. J. 2009. A Water-Borne Adhesive Modeled after the Sandcastle Glue of P. californica. *Journal of Macromolecular Bioscience,* 9**,** 464-471.

SHAO, H. & STEWART, R. J. 2010. Biomimetic Underwater Adhesives with Environmentally Triggered Setting Mechanisms. *Advanced Materials,* 22**,** 729-733.

SHINKAI, M. 2002. Functional magnetic particles for medical application. *Journal of Bioscience and Bioengineering,* 94**,** 606-613.

SHLIOMIS, M. 2003. Ferrohydrodynamics: Retrospective and Issues. *In:* ODENBACH, S. (ed.) *Ferrofluids.* Springer Berlin Heidelberg.

SILVA, A., SILVA-FREITAS, É., CARVALHO, J., PONTES, T., ARAÚJO-NETO, R., SILVA, K., CARRIÇO, A. & EGITO, E. 2012. *Magnetic Particles in Biotechnology: From Drug Targeting to Tissue Engineering*.

SLOUGH, J. T. & MILLER, K. E. 2001. Small, high frequency probe for internal magnetic field measurements in high temperature plasmas. *Review of Scientific Instruments,* 72**,** 417-420.

SNEDDON, I. N. 1965. The relation between load and penetration in the axisymmetric boussinesq problem for a punch of arbitrary profile. *International Journal of Engineering Science,* 3**,** 47-57.

SOETIKNO, R. M., GOTODA, T., NAKANISHI, Y. & SOEHENDRA, N. 2003. Endoscopic mucosal resection. *Gastrointestinal Endoscopy,* 57**,** 567-579.

SOUZA, G. R., MOLINA, J. R., RAPHAEL, R. M., OZAWA, M. G., STARK, D. J., LEVIN, C. S., BRONK, L. F., ANANTA, J. S., MANDELIN, J., GEORGESCU, M.-M., BANKSON, J. A., GELOVANI, J. G., KILLIAN, T. C., ARAP, W. & PASQUALINI, R. 2010. Three-dimensional tissue culture based on magnetic cell levitation. *Nat Nano,* 5**,** 291-296.

STARK, A. Y., BADGE, I., WUCINICH, N. A., SULLIVAN, T. W., NIEWIAROWSKI, P. H. & DHINOJWALA, A. 2013. Surface wettability plays a significant role in gecko adhesion underwater. *Proceedings of the National Academy of Sciences,* 110**,** 6340-6345.

STYLE, R. W., HYLAND, C., BOLTYANSKIY, R., WETTLAUFER, J. S. & DUFRESNE, E. R. 2013. Surface Tension and Contact with Soft Elastic Solids. *Nat Commun,* 4**,** 2728.

SUMIYAMA, K., GOSTOUT, C. J., RAJAN, E., BAKKEN, T. A., DETERS, J. L., KNIPSCHIELD, M. A., HAWES, R. H., KALLOO, A. N., PASRICHA, P. J., CHUNG, S., KANTSEVOY, S. V. & COTTON, P. B. 2006. Pilot study of the porcine uterine horn as an in vivo appendicitis model for development of endoscopic transgastric appendectomy. *Gastrointestinal Endoscopy,* 64**,** 808-812.

TAGUCHI, G. 1993. *Taguchi on Robust Technology Development: Bringing Quality Engineering Upstream*, ASME Press.

TAYLOR, G., LISKIEWICZ, T., NEVILLE, A., MORINA, A. & GASKELL, P. H. 2009. Providing Adhesion for a Miniature Mobile Intra-Abdominal Device Based on Biomimetic Principles. *3rd Vienna International Conference NANO-TECHNOLOGY.* Vienna.

TAYLOR, G. W. & JAYNE, D. G. 2007. Robotic Applications in Abdominal Surgery: Their Limitations and Future Developments. *The International Journal of Medical Robotics and Computer Assisted Surgery,* 3**,** 3-9.

TAYLOR, G. W., NEVILLE, A., JAYNE, D. G., ROSHAN, R., LISKIEWICZ, T., MORINA, A. & GASKELL, P. H. 2010. Wet adhesion for a miniature mobile intra-abdominal device based on biomimetic principles. *Proceedings of the Institution of Mechanical Engineers, Part C: Journal of Mechanical Engineering Science,* 224**,** 1473-1485.

THE HEALTH AND SOCIAL CARE INFORMATION CENTRE 2012. National Bowel Cancer Audit (NBCA) Annual Report. NBCA.

THE HEALTH AND SOCIAL CARE INFORMATION CENTRE 2013. National Bowel Cancer Audit (NBCA) Annual Report.

TIETZE, R., JURGONS, R., LYER, S., SCHREIBER, E., WIEKHORST, F., EBERBECK, D., RICHTER, H., STEINHOFF, U., TRAHMS, L. & ALEXIOU, C. 2009. Quantification of drug-loaded magnetic nanoparticles in rabbit liver and tumor after in vivo administration. *Journal of Magnetism and Magnetic Materials,* 321**,** 1465-1468.

TIETZE, R., RAHN H FAU - LYER, S., LYER S FAU - SCHREIBER, E., SCHREIBER E FAU - MANN, J., MANN J FAU - ODENBACH, S., ODENBACH S FAU - ALEXIOU, C. & ALEXIOU, C. 2011. Visualization of superparamagnetic nanoparticles in vascular tissue using XmuCT and histology. *Histochen and Cell Biology,* 135**,** 153-158.

TOLEDO, L., GOSSOT D FAU - FRITSCH, S., FRITSCH S FAU - REVILLON, Y., REVILLON Y FAU - REBOULET, C. & REBOULET, C. 1999. Study of Sustained Forces and The Working Space of Endoscopic Surgery Instruments. *Annales de Chirurgie,* 53**,** 587-897.

TORTORA, G., SALERNO, M., RANZANI, T., TOGNARELLI, S., DARIO, P. & MENCIASSI, A. A modular magnetic platform for natural orifice transluminal endoscopic surgery. Annual International Conference of the IEEE EMBS, 3 - 7 July 2013 2013 Osaka, Japan. 6265-6268.

TRAN CAO, H. S., LOPEZ, N., CHANG, D. C. & ET AL. 2014. Improved perioperative outcomes with minimally invasive distal pancreatectomy: Results from a population-based analysis. *JAMA Surgery,* 149**,** 237-243.

TRIEF & OLK. 2013. *Schematic of Laparoscopic Cholecystectomic Surgery* [Online]. Available: http://www.laparoscopicsurgeryinfo.com/images/laparoscopic1.jpg 2013].

UEMATSU, D., AKIYAMA, G., MAGISHI, A., NAKAMURA, J. & HOTTA, K. 2010. Single-Access Laparoscopic Left and Right Hemicolectomy Combined With Extracorporeal Magnetic Retraction. *Diseases of the Colon & Rectum,* 53**,** 944-948.

VAN DER VOORT, M., HEIJNSDIJK, E. A. M. & GOUMA, D. J. 2004. Bowel Injury as a Complication of Laparoscopy. *British Journal of Surgery,* 91**,** 1253-1258.

VÉKÁS, L. 2008. Ferrofluids and Magnetorheological Fluids. *Advances in Science and Technology,* 54**,** 127-136.

VIGNAUD, A., MAÎTRE, X., GUILLOT, G., DURAND, E., DE ROCHEFORT, L., ROBERT, P., VIVÈS, V., SANTUS, R. & DARRASSE, L. 2005. Magnetic susceptibility matching at the air–tissue interface in rat lung by using a superparamagnetic intravascular contrast agent: Influence on transverse relaxation time of hyperpolarized helium-3. *Magnetic Resonance in Medicine,* 54**,** 28-33.

VONCK, D. 2013a. *The Feasibility of Vacuum Technique in Minimal Invasive Surgery*. PhD Thesis, Delft University of Technology.

VONCK, D. 2013b. *The feasibility of vacuum technique in minimal invasive surgery: Improving the patient safety through instrument design*. Delft University of Technology.

VONCK, D., GOOSSENS, R. H. M., EIJK, D. J., HINGH, I. H. J. T. & JAKIMOWICZ, J. J. 2010. Vacuum grasping as a manipulation technique for minimally invasive surgery. *Surgical Endoscopy,* 24**,** 2418-2423.

VONCK, D., JAKIMOWICZ, J. J., LOPUHAÄ, H. P. & GOOSSENS, R. 2011. Grasping soft tissue by means of vacuum technique. *Medical Engineering & Physics*.

VONCK, D., JAKIMOWICZ, J. J., LOPUHAÄ, H. P. & GOOSSENS, R. H. M. 2012. Grasping soft tissue by means of vacuum technique. *Medical Engineering & Physics,* 34**,** 1088-1094.

WAGH, M. S., MERRIFIELD, B. F. & THOMPSON, C. C. 2006. Survival studies after endoscopic transgastric oophorectomy and tubectomy in a porcine model. *Gastrointestinal Endoscopy,* 63**,** 473-478.

WANG, Y., WERTHEIM, D. F., JONES, A. S. & COOMBES, A. G. A. 2010a. Micro-CT in drug delivery. *European Journal of Pharmaceutics and Biopharmaceutics,* 74**,** 41-49.

WANG, Z., BROWN, A. W., BROWN, S. I., WANG, L., ANDRE, P., FLORENCE, G. J. & CUSCHIERI, A. Intra-luminal injection of ferro-fluid for magnetic bowel retraction in minimal access surgery. Mechatronics and Embedded Systems and Applications (MESA), 2010 IEEE/ASME International Conference on, 15-17 July 2010 2010b. 168-173.

WANG, Z., SCHMIDT, A., BROWN, S. I., BROWN, A., MCLEAN, D., FLORENCE, G. J., ANDRE, P. & CUSCHIERI, A. 2012. Design and Evaluation of Permanent Magnet-Based Probe Having Adjustable Magnetic Force for Bowel Retraction in Laparoscopic Surgery. *Society of American Gastrointestinal and Endoscopic Surgeons (SAGES).* San Diego, The USA.

WANG, Z., WANG, L., BROWN, S. I., FRANK, T. G. & CUSCHIERI, A. 2009. Ferromagnetization of Target Tissues by Interstitial Injection of Ferrofluid: Formulation and Evidence of Efficacy for Magnetic Retraction. *IEEE Transactions on Biomedical Engineering,* 56**,** 2244-2252.

WANG, Z., WANG, L., TANG, B., FRANK, T., BROWN, S. & CUSCHIERI, A. 2008. Retraction by Surface Ferromagnetisation of Target Tissues: Preliminary Studies on Feasibility of Magnetic Retraction for Endoscopic Surgery. *Surgical Endoscopy,* 22**,** 1838-1844.

WÉBER, G., LANTOS, J., BORSICZKY, B., FERENCZ, A., JANCSÓ, G., FERENCZ, S., HORVÁTH, S., BAHRI, H. H., TAKÁCS, I. & BALATONYI, B. 2008. *Basic Surgical Techniques*, University of Pécs, Medical School.

WESTEBRING-VAN DER PUTTEN, E. P. 2011. *A Sense of Touch in Laparoscopy: Using Augmented Haptic Feedback to Improve Grasp Control.* PhD Thesis, Delft University of Technology.

YAMAUCHI, Y., YAMASHITA, J., MORIKAWA, O., HASHIMOTO, R., MOCHIMARU, M., FUKUI, Y., UNO, H. & YOKOYAMA, K. 2002. Surgical Skill Evaluation by Force Data for Endoscopic Sinus Surgery Training System. *In:* DOHI, T. & KIKINIS, R. (eds.) *Medical Image Computing and Computer-Assisted Intervention — MICCAI 2002.* Springer Berlin Heidelberg.

ZABER TECHNOLOGIES INC.®. 2014. *Zaber Technologies Inc.* [Online]. Available: http://www.zaber.com/products/product_detail.php?detail=T-LSR075B#tabs 2013].

ZELTSER, I. S., BERGS, R., FERNANDEZ, R., BAKER, L., EBERHART, R. & CADEDDU, J. A. 2007. Single Trocar Laparoscopic Nephrectomy Using Magnetic Anchoring and Guidance System in the Porcine Model. *The Journal of Urology,* 178**,** 288-291.

ZELTSER, I. S. & CADEDDU, J. A. 2008. A Novel Magnetic Anchoring and Guidance System to Facilitate Single Trocar Laparoscopic Nephrectomy. *Current Urology Reports,* 9**,** 62-64.